University of Central Florida
STARS

Electronic Theses and Dissertations | Doctoral Dissertation (Open Access)

Dynamic Behavior and Performance of Different Types of Multi-Effect Desalination Plants

2019

Mohamed Abdelkareem
University of Central Florida

Find similar works at: https://stars.library.ucf.edu/etd

University of Central Florida Libraries http://library.ucf.edu

 Part of the Energy Systems Commons

STARS Citation

Abdelkareem, Mohamed, "Dynamic Behavior and Performance of Different Types of Multi-Effect Desalination Plants" (2019). *Electronic Theses and Dissertations*. 6336.
https://stars.library.ucf.edu/etd/6336

This Doctoral Dissertation (Open Access) is brought to you for free and open access by STARS. It has been accepted for inclusion in Electronic Theses and Dissertations by an authorized administrator of STARS. For more information, please contact lee.dotson@ucf.edu.

DYNAMIC BEHAVIOR AND PERFORMANCE OF DIFFERENT TYPES OF MULTI-EFFECT DESALINATION PLANTS

by

MOHAMED LOTFY ELSAYED ABDELKAREEM

B.S. Zagazig University, Egypt, 2008
M.S. Zagazig University, Egypt, 2012
M.S. University of Central Florida, 2017

A dissertation submitted in partial fulfillment of the requirements
for the degree of Doctor of Philosophy
in the Department of Mechanical and Aerospace Engineering
in the College of Engineering and Computer Science
at the University of Central Florida
Orlando, Florida

Spring Term

2019

Major Professor: Louis Chow

© 2019 Mohamed Abdelkareem

ABSTRACT

Water and energy are two of the most vital resources for the socio-economic development and sustenance of humanity on earth. Desalination of seawater has been practiced for some decades and is a well-established means of water supply. However, this process consumes large amounts of energy and the global energy supply is also faced with some challenges. In this research, multi-effect desalination (MED) has been selected due to lower cost, lower operating temperature and efficient in terms of primary energy and electricity consumption compared to other thermal desalination systems. The motivation for this research is to address thermo-economics and dynamic behavior of different MED feed configurations with/without vapor compression (VC). A new formulation for the steady-state models was developed to simulate different MED systems. Adding a thermal vapor compressor (TVC) or mechanical vapor compression (MVC) unit to the MED system is also studied to show the advantage of this type of integration. For MED-TVC systems, results indicate that the parallel cross feed (PCF) configuration has better performance characteristics than other configurations. A similar study of MED-MVC systems indicates that the PCF and forward feed (FF) configurations require less work to achieve equal distillate production. Reducing the steam temperature supplied by the MVC unit leads to an increase in second law efficiency and a decrease in specific power consumption (SPC) and total water price.

Following the fact that the MED may be exposed to fluctuations (disturbances) in input parameters during operation. Therefore, there is a requirement to analyze their transient behavior. In the current study, the dynamic model is developed based on solving the basic conservation equations of mass, energy, and salt. In the case of heat source disturbance, MED plants operating in the backward feed (BF) may be exposed to shut down due to flooding in the first effect. For all applied

disturbances, the change in the brine level is the slowest compared to the changes in vapor temperature, and brine and vapor flow rates. For MED-TVC, it is recommended to limit the seawater cooling flow rate reduction to under 12% of the steady-state value to avoid dryout in the evaporators. A reduction in the motive steam flow rate and cooling seawater temperature of more than 20% and 35% of steady-state values, respectively, may lead to flooding in evaporators and plant shutdown. Simultaneous combinations of two different disturbances with opposing effects have only a modest effect on plant operation and they can be used to control and mitigate the flooding/drying effects caused by the disturbances. For the MED-MVC, the compressor work reduction could lead to plant shutdown, while a reduction in the seawater temperature will lead to a reduction in plant production and an increase in SPC.

DEDICATION

To my mother, my father, my wife and my three little kids.

ACKNOWLEDGMENTS

I would like to express my deepest appreciation to my advisor, Professor Louis Chow, for his guidance, encouragement, and patience rendered throughout my years of study at the University of Central Florida (UCF). I'm extremely indebted for his suggestions and daily discussions; he continually and convincingly conveyed a spirit of adventure regarding both basic research level and industrial applications. Without his guidance and persistent help, this dissertation would not have been possible.

I would like to thank my Ph.D. committee members, Professor **Steven Duranceau**, Professor **Hansen Mansy** and Professor **Tuhin Das** for their suggestions and continuous instruction in regard to my research. I am extending my thanks for Professor **Osama Mesalhy**, for his never-ending generous advice, a wealth of knowledge and his efforts to make this dissertation more meaningful. Furthermore, I would like to express my appreciation to my friends in the Lab for their limitless help and support and in particular my very close friend Ramy Abdelhady for all daily consultations.

I am grateful for this opportunity to acknowledge all of my family members – especially my parents, my brother and my sister – for their appreciation, encouragement, and prayers.

Special thanks are to be to my beloved wife Nada; her tolerance of my many hours researching in the lab is proof in itself of her unyielding devotion and love. To my adorable little kids Khadeejah, Yahiya, and Salsabella, thanks for making my life full of happiness and fun.

I gratefully acknowledge the financial support of the Ministry of Education in the Arab Republic of Egypt through the Egyptian Cultural Bureau in Washington, D.C.

TABLE OF CONTENTS

LIST OF FIGURES

LIST OF TABLES

CHAPTER 1 INTRODUCTION

1.1 Introductory Background

Energy and water are two of the most vital resources for the socio-economic development and sustenance of humanity on earth. However, despite progress towards the UN millennium development goal, about 768 million people in the world still lack access to improved (safe) drinking water, and over 2 billion people suffer inadequate supply [1]. Salinity in water resources (both surface/sea and groundwater) contributes greatly to the freshwater shortfall and affects agricultural yields. Desalination of saline water to recover fresh water has been practiced for several decades and is a well-established means of water supply in many countries, most notably Saudi Arabia, United Arab Emirates and Kuwait in the Middle East [2]. The global capacity of desalination plants has been increasing steadily since the early 1970's, and was over 25 million m^3/day by the year 2000 [3], and is now over 90 million m^3/day [4]. Although seawater desalination projects seem to have attracted much attention, the number of brackish desalination projects is increasing at a more rapid rate. Desalination processes consume large amounts of energy; however, the global energy supply is also faced with a number of challenges.

Virtually all work done by humans on the planet requires some form of energy, and in most cases involves the conversion of the available form of energy into the desired form. Presently, fossil fuel is the primary source of energy on the planet, accounting for about 82% (Oil 31.5%, Gas 21.3%, and Coal 28.8%) of the global energy demand, with other sources including Nuclear and Renewables accounting for the remaining fraction. Humanity's strong dependence on fossil fuels for energy has eventually given rise to a global energy challenge which stands to threaten the future of the global energy supply. These challenges include rising energy cost, increasing demand, energy security and concerns for climate change due to energy-related pollutions. The Earth is said

to have a finite quantity of fossil fuels which will eventually be depleted at some point; analysts have predicted a depletion time of about 35 to 110 years [5]. Yet, about 1.3 billion people (a quarter of the world's population) have no access to electricity, and another 1 billion only have unreliable and intermittent supply [6].

1.2 Thermodynamics of Desalination

Desalination requires a minimum amount of work, intrinsic to saline solution properties and not specific desalination methods [7]. Desalination can be thought of as physically separating pure water from dissolved ions in solution (water being the solvent). Minimum work required to separate pure water from solution is the reversible portion of energy exerted to overcome chemical potential between dissolved ions and water. Desalination minimum work is a theoretical lower limit, unachievable by real-world processes. However, by examining desalination thermodynamics and establishing theoretical limits, the following conclusions can be made: (1) Desalination requires thermodynamic work, (2) Minimum required work is a function of salinity and temperature, unrelated to particular desalination methods, and unachievable: some loss will occur and (3) Help in selection of the best desalination method [7].

A generalized equation (1) for the least energy of separation assuming reversible behavior is proposed by Mistry and Lienhard [8] based on arbitrary desalination technologies as shown in Figure 1. The right-hand side (RHS) of the equation represents the least amount of exergy required to separate the input process streams into output streams of different chemical compositions. For a desalination process, a feed stream is divided into a low salinity product and a high salinity concentrate.

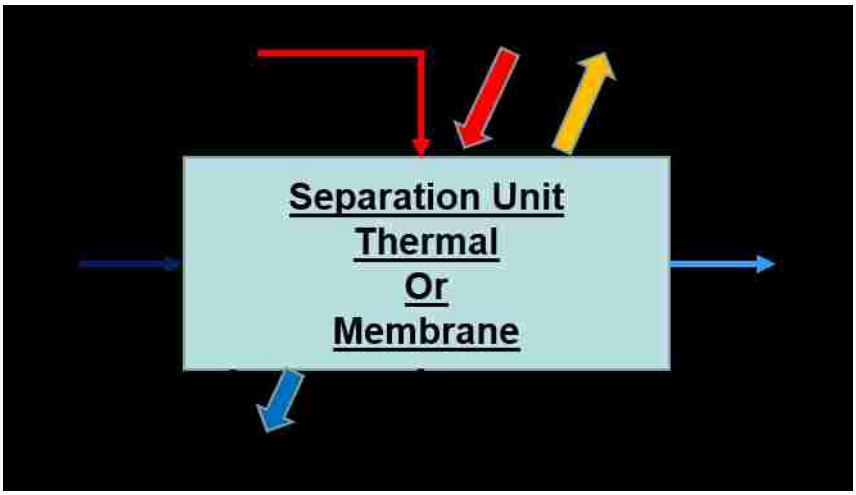

Figure 1 Generic model for desalination.

$$\dot{W} + \sum_{l=1}^{P} \left(1 - \frac{T_0}{T}\right) \dot{Q}_l + \sum_{in-out} \dot{m}\, \bar{\xi}(T, P, N_i) = \sum_{out-in} \dot{m} \bar{g}\,(T_0, P_0, N_i) \tag{1}$$

Some chemical separation processes are powered by work only. Examples of work-driven desalination systems include RO, mechanical vapor compression (MVC), and electrodialysis (ED). Simplifying Equation (1), with only work input and heat transfer from the environment, yields the definition of the least work of separation Equation (2):

$$\frac{\dot{W}_{min}}{\dot{m}_p} = \left(g_{p-}g_c\right) - \frac{1}{\alpha}\left(g_{f-}g_c\right) \tag{2}$$

Where the subscripts *c*, *p* and *f* represent rejected concentrate brine, produced fresh water and feed seawater (35,000 ppm), and g is the specific Gibbs energy and α is the recovery rate. Minimum work for separation for various feed salinities and recovery ratios at a constant temperature of 25 ºC, shows in Figure 2 that higher salt concentration and higher recovery rate require higher energy consumption. Based on the above equations, at standard seawater (35,000 ppm) with 50% recovery, the reversible process requires 3.93 kJ/kg. The current well designed seawater Reverse Osmosis (RO) systems or controlled pilot scale plants energy consumption can be as low as ~7.92

kJ/kg, which is two times the minimum required theoretical value. Considering pretreatment, posttreatment or other factors such as membrane fouling, pipe friction losses, pump efficiency, there is only about a 20% improvement possible [9]. The least work of separation is a strong function of feed salinity and recovery ratio, and a weak function of the product salinity (for typically low product salinities).

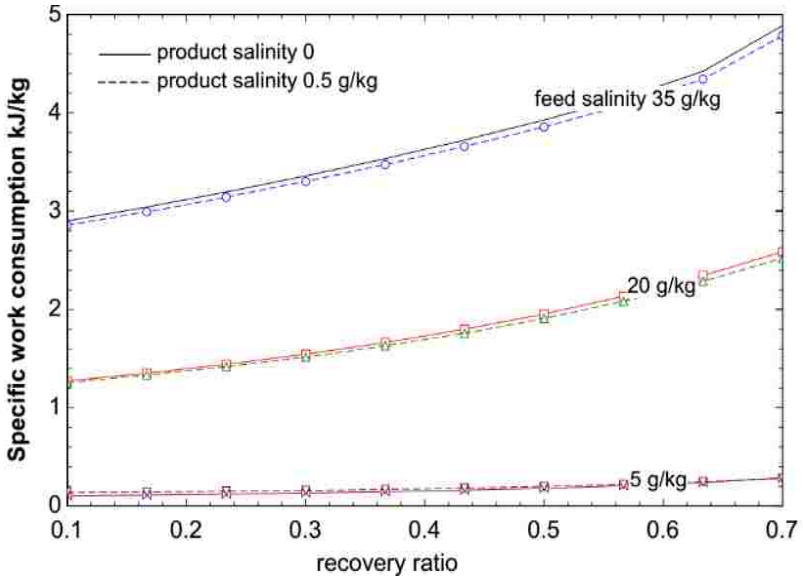

Figure 2 Least work of separation as a function of feed salinity and recovery ratio.

Let us consider a phase-change desalination process to explain the advantage of low-temperature desalination. Using generic phase-change desalination process shown in Figure 1 and based on the first law of thermodynamics, the recovery rate of this process could be expressed by Equation (3):

$$\frac{m_p}{m_f} = \frac{\frac{Q_i - Q_L}{m_f} + (h_f - h_c)}{h_{L(T_e)} + h_p - h_c} \tag{3}$$

where h_p, h_c, h_f are the specific enthalpy of fresh water vapor, concentrated brine and feed seawater respectively, and $h_{L(T_e)}$ is the latent heat at the evaporation temperature. Heat losses $Q_L = UA(T_{evap} - T_{amb})$ and rejected heat transfer $Q_o = m_c h_{L(T_e)}$ If we define the specific energy consumption for a general desalination process as Q_i/m_p , assume the feed seawater is at 25°C

and the final products have the same temperature for a given energy input, Q_i. The results shown in Figure 3a, for a Q_i of 1,000 kJ/hr and UA = 0.8 J/s.K indicate that for a given feed rate, higher production rate is possible at lower temperature. The relationship between the recovery rate α and the specific energy consumption (kJ/kg of freshwater produced) at various evaporation temperatures is shown in Figure 3b assuming ambient temperature of 25 °C. This plot shows that lower the evaporation temperature, lower is the specific energy requirement for a desired recovery.

The thermodynamic benefits of low-temperature desalination using low-grade heat source can be recognized from Figure 3 as it offers higher productivity and lowers energy consumption. Thus, phase change desalination has to be done at the lowest temperature possible to maximize the recovery and minimize the specific energy requirement. Apart from the above thermodynamic advantages, low-temperature desalination systems can benefit from the following practical considerations [10]: Low energy costs, Low corrosion rates, Flexibility, Minimal scaling rates, and High-purity distillate.

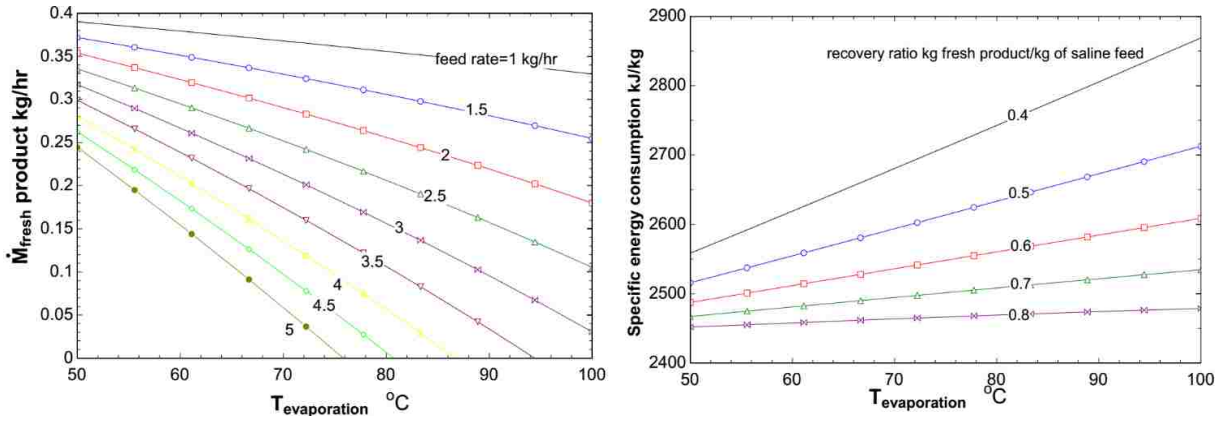

Figure 3 a) Product as a function of feed rate and evaporation temperature at fixed heat input, b) Specific energy as a function of recovery rate and evaporation temperature.

1.3 Aim and Objectives

The aim of the research reported here was to investigate the impact of operational and design parameters on the performance of multi-effect desalination (MED) and draw conclusions on its economic viability. This aim was achieved by meeting the following objectives:

1 Develop a validated steady-state thermodynamic cycle model that allows rapid estimation of performance for MED operating under different configurations as a function of the process heat source temperatures, heat source flow rate, seawater feed concentration, and cooling seawater flow rate.

2 Develop a validated dynamic model that allows performance prediction of different types and configurations of MED as a function of process conditions, including operating times and plant location.

3 Use the models developed above to elucidate the effect of input process parameters on the performance of MED and draw conclusions on the range of conditions where MED is likely to be economically viable.

1.4 Details of the Publications

Up to now, the outcomes of the current dissertation have been reported in the form of six papers published in international journals. In addition, two peer reviewed conference papers have also been published. In this section, the aims and objectives of each individual journal paper and how they link together with the global objectives of this dissertation are described.

The current research is divided into four main stages: 1. Steady state model development and detailed thermodynamic analysis for the performance of MED (for objectives 1 and 3), 2. Possible thermodynamic and economic comparison between different MED configurations (objective 3),

3. Steady-state model validation and possible MED system combined with vapor compression (VC) units (for objectives 1 and 3), and 4. Dynamic model development and validation of MED systems (for objectives 2 and 3). The papers included in this dissertation (in the final publication format) have been chosen to best describe the progression of the research, which includes both steady-state and dynamic model development of conventional MED and MED integrated to VC units, and the elucidation of the effect of process parameters on the performance of MED using validated models. In addition, summaries of the aims and approach for each article are provided below.

1.4.1. Exergy and thermo-economic analysis for MED systems

Ch.3 Exergy and thermo-economic analysis for MED-TVC systems

(Published in *Desalination Journal* Vol. 447, pp. 29-42, 2018)

The aim of this paper was to study the factors that influence the performance of MED-TVC systems using thermodynamic and exergo-economic models. This aim was achieved by meeting the following objectives:

- to develop a model that contribute on process design, performance analysis, and exergo-economic studies with different feed configuration of the MED systems integrated to the TVC unit.
- to estimate the fresh water productivity cost based on exergy analysis and to identify the cost concentrated components.
- to elucidate the effect of operational parameters on the proposed system performance.

Ch.4 Process performance modeling for MED-MVC systems: Exergy and thermo-economic analysis approach

(Published in *Energy Journal* Vol. 166, pp. 552-568, 2019)

The aim of this paper was to enumerate all possible configurations of MED-MVC, analyze and compare their performance using thermodynamic and exergo-economic models. This aim was achieved by meeting the following objectives:

- to enumerate all possible thermodynamic cycles of MED-MVC at various operational and design conditions and describe their operational processes in details,
- to determine and compare the relative performance of various types of MED-MVC systems in terms of specific energy consumption and fresh water productivity cost using mathematical model.

1.4.2. Dynamic model development and validation for MED systems

Ch.5 Transient Performance of MED Processes with Different Feed Configurations

(Published in *Desalination Journal* Vol. 438, pp. 37-53, 2018)

The aim of this paper was to develop a validated dynamic model that allows prediction of MED performance and transient behavior as a function of process conditions. This aim was achieved by meeting the following objectives:

- to develop a general multi-system dynamic mathematical model, which incorporates transient mass, salt and energy transfer processes in evaporators units.
- to understand their transient behavior under changes or fluctuations in three main input parameters, namely the motive steam flow rate, cooling seawater flow rate and cooling seawater temperature.

- to pinpoint the most reliable configuration in terms of steady-state operation and dynamic response.

Ch.6 Effect of disturbances on MED-TVC plant characteristics: Dynamic modeling and simulation
(Published in *Desalination Journal* Vol. 443, pp. 99-109, 2018)

The aim of this paper was to further improve and apply the dynamic model developed in Ch.5 to study the behavior of a parallel/cross feed of MED-TVC system. This aim was achieved by meeting the following objectives:

- to explain the physics behind the transient behavior of a MED-TVC system subject to external disturbances.
- to define the sensitivivity of MED-TVC system to the applied disturbances and fluctuations in the input parameters compared to stand alone MED.
- to determine the effect of change in feed seawater salinity on plant operation.

Ch.7 Effect of Input Parameters Intensity and Duration on Dynamic Performance of MED-TVC Plant
(Published in *Applied Thermal Engineering Journal* Vol. 139, pp. 210-221, 2018)

The aim of this paper was to define the critical limits for the fluctuations of the input parameters to avoid plant shutdown due to flooding or dry out of MED-TVC system. This aim was achieved by meeting the following objectives:

- to investigate the plant behavior and performance under various intensity and duration of disturbances introduced in the main operational parameters

- to study the effects of simultaneous combinations of two different disturbances in assisting and opposing effects direction.

Ch.8 Transient and Thermo-Economic Analysis of MED-MVC Desalination Process

(Published in *Energy Journal* Vol. 167, pp. 283-269, 2019)

The aim of this paper was to further extend the model developed in Ch.5 to study the transient behavior of MED-MVC desalination system. Also, to enumerate all possible configurations of MED-MVC, analyze and compare their performance using thermodynamic and exergo-economic models. This aim was achieved by meeting the following objectives:

- to modify and customize the previous model to track the behavior of four effects, two preheaters and a mechanical compressor unit.
- enumerate all possible thermodynamic cycles of MED-MVC at various operational and design conditions and describe their operational processes in details,
- to determine and compare the relative performance parameters of MED-MVC system under changes in the input operating parameters.

The remaining three chapters in the dissertation are explained as follow; Chapter 1; expresses an introduction and the generic energy requirement for desalination method followed by motivations and objectives of the research. Chapter 2; an extended introduction review of the different commercial available desalination methods and current research desalination method selection criteria. Finally, chapter 9 shows the comprehensive Ph.D. research conclusion and the suggested future work. The contents of each chapter are summarized as follows.

CHAPTER 2 DESALINATION SYSTEMS

The purpose of this chapter is to provide a general overview into issues relating to energy and freshwater production using desalination to identify the gaps in the knowledge. Furthermore, the chapter address the different available desalination methods and the define the most common one. Detailed explanation about the major three commercial desalination methods are provided and method for the preferred desalination method (MED) is discussed. More detailed investigations into specific area of MED are contained in the introduction section of each of the journal publications that make up the subsequent chapters.

2.1 Global water availability challenges

The total amount of water on Earth composed of 97.5% as seawater and the remaining 2.5% as freshwater. A remarkable 80% of the freshwater is frozen in glaciers so that only 0.5% of the total amount available is found in lakes, rivers and aquifers. Freshwater differs substantially from seawater by the salt content. The salinity of water is usually expressed in terms of its total dissolved solids (TDS). Based on the salt concentration, Figure 4 shows a very simple classification of natural water based on its saline content. Typical seawater compositions (average salinity 35, 000 ppm) are given in Figure 4. According to the WHO, water is considered good for drinking at a TDS level of less than 500 ppm [11].

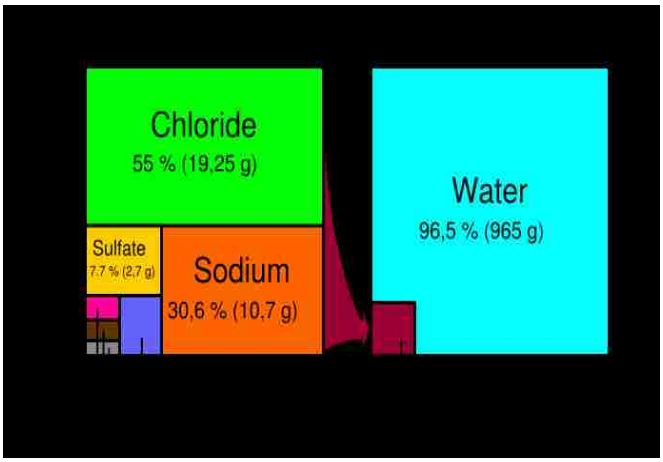

Figure 4 . Standard seawater composition.

Table 1 Water classification based on salinity content

Type	Total dissolved solids (TDS)	Note
Freshwater	< 1,500	Variable composition
Brackish water	1,500 – 10,000	Variable composition
Saltwater	> 10,000	Variable composition
Seawater	10,000 – 45,000	Fixed composition
Standard seawater	35,000	Fixed composition

2.2 Alternative energy source(s)

The energy challenges have fostered growing interest in sustainable alternatives or renewable energy sources such as wind, solar, geothermal, biomass and waste heat [12]. Presently, renewable energy sources account for less than 15% of the global energy supply, of which biomass is a significant contributor. However, solar has recorded the fastest growth, and have been projected to possibly become the world's second-largest source of power generation [13].

Studies have already shown that renewable heat sources have the potential of meeting the global energy demand several times over [14]. For instance, of these energy sources, biomass is an old and well-known energy source; it has the advantage of continuity over the intermittence of other energy sources like solar[15]. On the other hand, solar energy has the highest capacity [16]. It stands out as a potential solution for meeting the global energy demand, the annual fraction of the

sun's energy striking the earth is about $3.9*10^6$ exajoules (EJ), but considering technical constraints (including conversion efficiencies), only about 1600 EJ can be harvested [14] which is still over 3 times the global energy need. Thus, the solar energy resource is abundant and could meet the global energy demand, but its widespread adoption is not yet economically competitive. Nevertheless, it is viable and most suited for decentralized applications in remote or isolated regions of the world with high solar insolation.

Besides the natural renewable thermal sources, the potential of exploiting waste heat from existing thermal processes (including industrial processes and internal combustion engines) that would otherwise be wasted have also been considered promising [17]. This is achievable, as between 20 to 50% of the energy input to these processes are discharged (lost) as waste heat [18]. For example, in the US industries, this equates to about 5 – 13 EJ of waste heat, according to the US Department of Energy (DOE). In the face of the global energy challenges, waste heat recovery offers a viable means of reducing the effect of the energy challenges for industrial facilities by increasing energy production.

2.3 Renewable energy powered desalination

Water is essential to life and the importance of supplying potable water can hardly be overstressed. Man has been dependent on rivers, lakes and underground water reservoirs for fresh water requirements in domestic life, agriculture and industry. However, rapid industrial growth and the population explosion all over the world have resulted in a large escalation of demand for fresh water. Added to this is the problem of pollution of rivers and lakes by industrial wastes and the large amounts of sewage discharged. The only nearly inexhaustible sources of water are the oceans.

Their main drawback, however, is their high salinity. It would be attractive to tackle the water-shortage problem with desalination of this water.

Over the years, there have been a number of studies on alternative energy (especially solar) driven desalination technologies [19]. Desalination can be achieved by using several techniques which may be classified based on what is extracted from seawater, as well as the type of separation process adopted as shown in Figure 5a. The processes are further grouped as follows, phase-change or thermal processes; and membrane or single-phase processes. Another classification based on renewable energy type is shown in Figure 5b. A membrane process (reverse osmosis (RO) and forward-osmosis (FO)) involves passing water through a barrier (a membrane) to remove certain substances. Thermal processes (multi-stage flash (MSF); multi-effect distillation (MED); solar still (ST); humidification-dehumidification (HDH); passive vacuum desalination (PVD); membrane distillation (MD); freezing-melting (FM); thermal vapor compressor (TVC); mechanical vapor compressor (MVC); absorption vapor compression desalination (ABVC); and adsorption vapor compression desalination (ADVC)) produce pure water by bringing a saltwater solution to its saturation temperature, further heated to form water vapor, which can be condensed and collected as clean, salt-free liquid water.

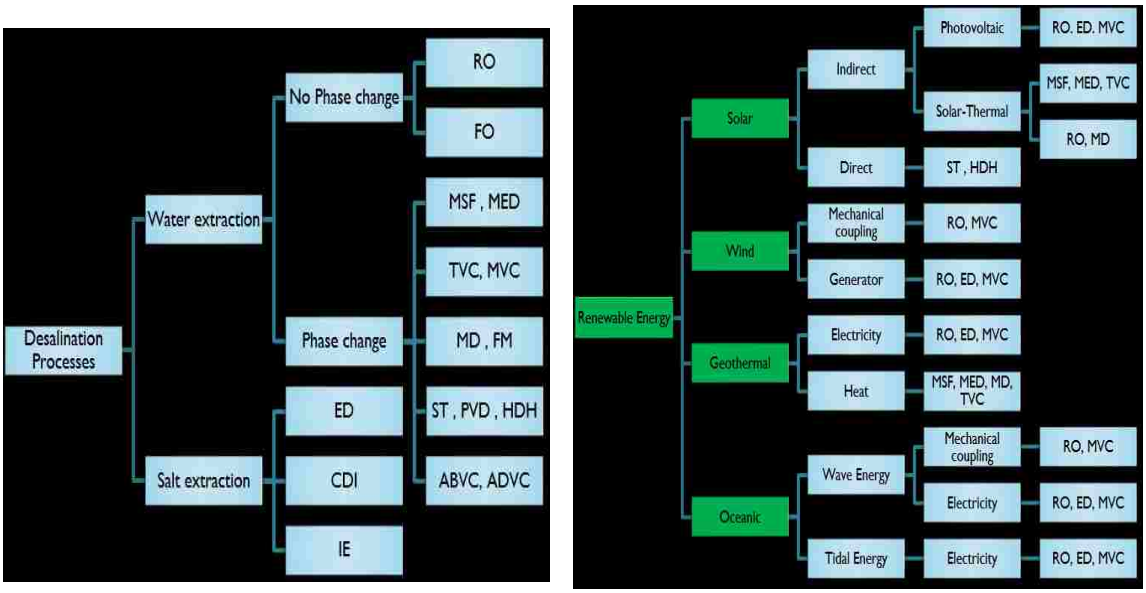

Figure 5 Desalination process grouped by a) extracted substance b) renewable energy used.

Processes for extracting salt such as electrodialysis (ED), ion exchange (IE) and capacitive deionization (CDI) are normally used in brackish water desalination but not seawater desalination. Among all of the above-mentioned desalination processes, MSF, MED, RO and ED account for about 95% of the global desalination capacity, as shown in Figure 6 [4].

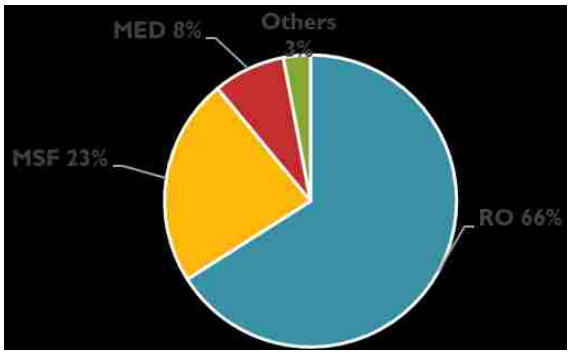

Figure 6 Worldwide desalination capacities.

2.4 Desalination method selection

Cost-effective desalination, especially solar-powered desalination technology, can play an important role in helping to solve the water supply problems of many regions of the world. As

illustrated in Figure 7a, RO, which is the biggest desalination process internationally in terms of capacity, requires only electricity from PV or mechanical energy from a solar pond or collector through a heat engine such as a sterling engine or a Rankine engine, [20]. RO requires extensive water pretreatment but is energy efficient compared to phase change thermal processes, and part of the consumed mechanical energy can be reclaimed from the rejected concentrated brine with a suitable energy recovery device such as a pressure exchanger. Osmosis is a natural phenomenon in which water passes through a membrane from the lower salt concentration side to the higher salt concentration side. To reverse the flow of water, a pressure larger than the osmotic pressure must be applied. Seawater pressure must be higher than the natural osmotic pressure, typically 2500 kPa, but is kept below the membrane tolerance pressure, typically between 6000 and 8000 kPa, forcing pure water molecules through the RO membrane pores to the freshwater side. Freshwater is collected while the concentrated brine is rejected. Among the reported solar assisted RO, PV driven RO and solar thermal heat engine driven RO is the most widely studied.

Solar thermal assisted RO System differs from PV-RO plants which are almost commercially available in small-scale and compact plants. Some researchers have studied the application of solar thermal energy for desalination coupled with the reverse seawater osmosis through power cycle such as organic Rankine cycle (ORC) [21, 22]. The advantage of combining an ORC with a desalination system is that the seawater provides a heat sink for the ORC condenser while at the same time it is preheated to increase the RO membrane permeability, leading to reduced power consumption. A single ORC with R245fa as the working fluid was pointed out by [23]to have a higher efficiency than the cascade system studied by Kosmadakis et al. [22] when operating between the same two temperatures. In addition to that, Tchanche et al. [24] pointed out that the

integration of different devices is not significantly rewarded with an efficiency gain; therefore, it is preferable to keep the configuration of the ORC simple when designing an ORC-RO system.

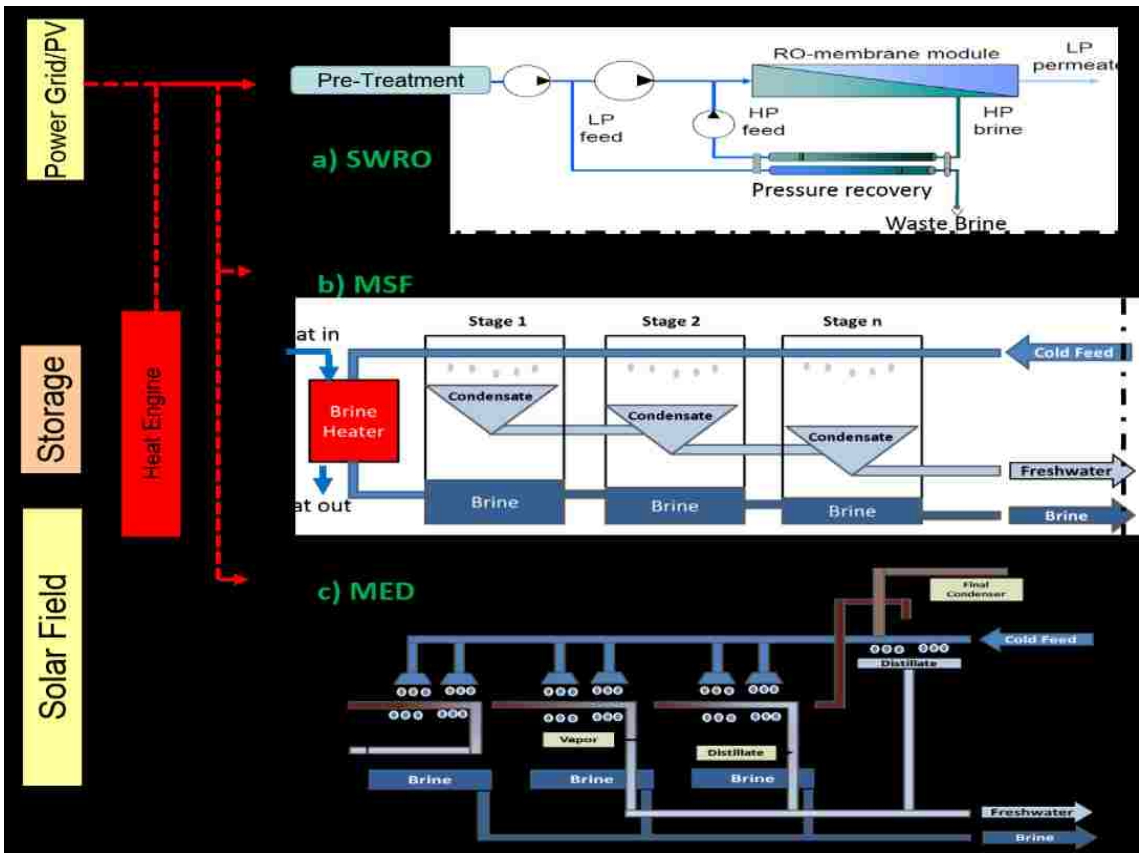

Figure 7 Schematic of solar-assisted RO, MSF and MED systems

In an MSF process, as shown in Figure 7b seawater moves through a sequence of vacuumed reactors called stages that are held at successively lower pressures where seawater is preheated. External heat is supplied to heat the preheated seawater above its saturation temperature. Seawater is then successively passed from one stage to the next in which a small amount of water flashes to steam in each stage and the remaining brine flows to the next stage for further flashing. The flashed steam is condensed and collected as fresh water after removing the latent heat of condensation, to preheat the entering seawater at each stage. MSF is used in large-scale cogeneration power plants

because it can use low-quality steam rejected from power cycles as the heat source [25, 26]. Some researchers claim that MSF is not as thermally efficient as MED [27]. Others do not see any clear advantages in the thermodynamics between the MED and MSF processes, except that thermal losses are higher in the MSF than in the MED, due to its higher operating temperature [28]. In general, MSF series-connected stages require precise pressure and temperature control and some transient time is needed to establish the normal running operation of the plant. Since the solar heat source is intermittent, an effective thermal storage system (i.e. a storage tank), can be used for thermal buffering [28]. MSF uses the seawater feed as the coolant which means that MSF uses sensible heat to recover the latent heat from the distilled water. Therefore MSF requires large amounts of seawater recirculating within the system and consumes more electricity than a MED process which is a thermal process has a lower energy consumption compared to MSF (half of MSF pumping power) [29].

MED may be operated in four configurations: forward-feed FF, backward feed BF, parallel feed and parallel/cross feed PF. Figure 7c shows the schematic of parallel feed MED, in which seawater is delivered to a sequence of successively low-pressure vessels, called effects. The external heat is supplied to the first effect and the generated vapor of the previous effect supplies its latent heat of condensation to the next effect. Unlike MSF which recovers latent heat from the vapor by the sensible heating of the seawater, MED systems reuse latent heat to vaporize the seawater. The specific heat capacity of water is approximately 4 kJ/kg·K while the latent heat of vaporization is approximately 2300 kJ/kg. Therefore MED systems normally have 2-14 effects while MSF systems have more than 20 stages. MED systems use falling film horizontal tube evaporator/condensers for high heat transfer efficiency [30]; operate with a relatively low top brine temperature (usually lower than 75°C) to reduce scale formation and corrosion [31]; and can be

combined with vapor compressors to improve the overall efficiency [32, 33]. The combination of economic costs and low energy consumption, together with the inherent durability of the low-temperature MED, avoid the necessity of comprehensive seawater pretreatment (such as with RO plants) and make the MED process one of the best candidates for safe and durable large capacity desalination [34]. Compared to MSF, MED has high overall efficiency, high heat transfer coefficient, relative independent stages and less water recycling [35]. However, to lower the energy consumption, MED needs a large surface area of evaporators to reduce the temperature difference of adjacent stages, some research has shown that when operating with high-pressure steam, MED consumed more energy than MSF [28].

Vapor Compression (VC) Desalination units are generally used for small or medium scale [36, 37] applications and they are normally combined with other thermal processes [32, 33, 38]. There are four basic types of vapor compression applications in desalination processes [37]. These include thermal vapor compressor (TVC), mechanical vapor compressor (MVC), adsorption (ADVC) and absorption (ABVC) [32] as shown in Figure 8. TVC could be used with MED or MSF in different sizes of commercial desalination plants [39, 40], in which the steam compression is carried out by an ejector and the vapor from the last effect of the MED process is carried by a motive stream back to the first effect. MVC is widely studied and used because of its simplicity and relatively low energy consumption [41, 42]. The bottoming condenser is eliminated because the entire vapor formed in the last stage is routed to the mechanical vapor compressor, where it is compressed to the desired temperature and pressure to recover heat in the rejected brine and distillate product streams[43]. ABVC [44, 45] absorbs the last effect vapor through LiBr-water and discharges steam for use by the first effect; while ADVC [46, 47] uses zeolite-water or other pairs to recover vapor from the last effect MED and generate high-temperature steam through a desorber bed. ABVC and

ADVC are regarded to have a higher potential for applications in desalination than TVC and MVC [32, 47-50]; however, at present there are no commercial applications. For instance, adsorption-based desalination technology can handle feed water with high salinity (up to 67,000ppm) and produce low salinity water (10ppm) with minimum running cost (0.2$/m3) as reported in [51].

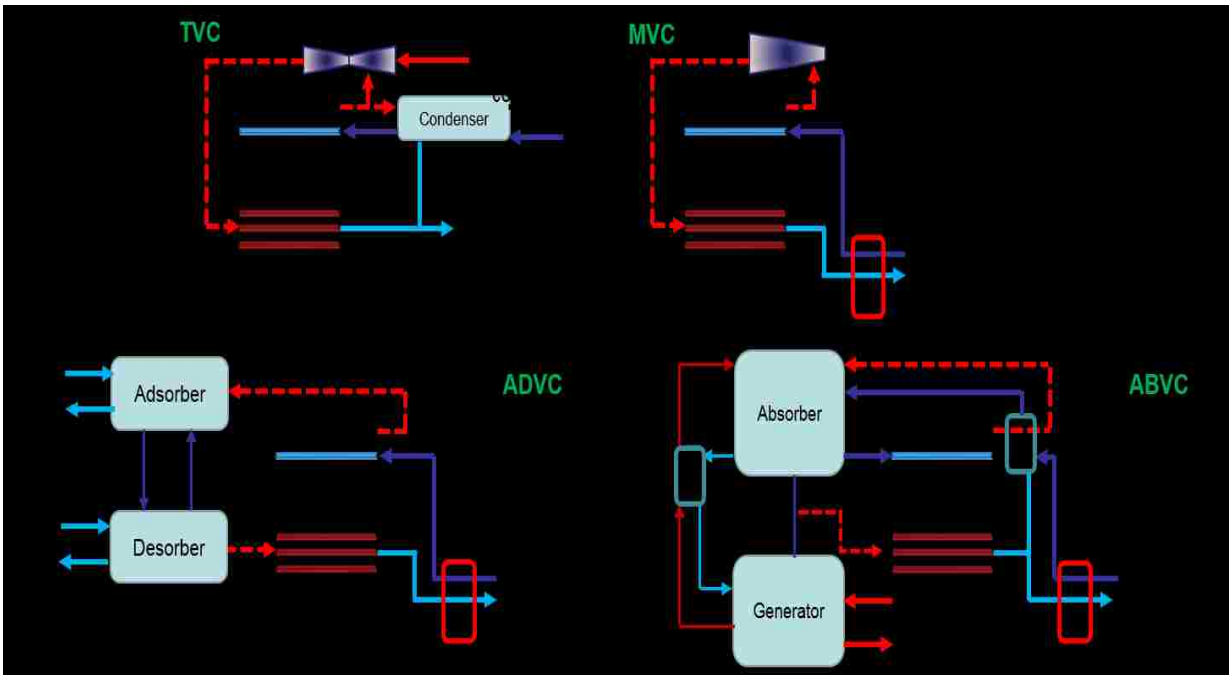

Figure 8 Schematic of different vapor compression process used in desalination.

All vapor compression-combined thermal desalination systems recover the low-temperature vapor from certain parts of the MED/MSF system and convert it to higher temperature vapor to improve the system efficiency [32]. Furthermore, since low-temperature vapor could be recovered, the whole desalination system needs less cooling water and consumes less electricity. The differences among various VC based systems are that (1) MVCs use electricity as energy source (Figure 9) and could be used as stand-alone desalination systems; (2) TVCs use higher temperature and pressure (>200kPa) steam; (3) ABVC and ADVC use either higher temperature steam or other heat sources in the absorption/adsorption cycles [52-57]. Solar assisted VC combined with other

desalination processes could be used as shown in Figure 9. MVC must be driven by mechanical energy, therefore, a photovoltaic (PV) system or a heat engine are used; TVC/ABVC/ADVCs use steam therefore they are connected between the solar thermal process and the thermal desalination process. PV can be employed independently or jointly with other sources to generate the electricity needed to power desalination systems. Some of the characteristics of the five leading desalination technologies are shown in Table 2 [58]. The purpose of this comparison was to select the most appropriate thermal and mechanical desalination method for the combination of solar energy.

Over recent years, improved membrane technologies and better energy recovery systems have yielded RO systems to have specific energy consumption between 2.5 and 3.5 kWh/m^3 [59]. Despite the low energy consumption, the drawbacks of RO systems are the product water quality associating with residuals of boron, chlorides, and bromides, as well as the high maintenance of the mechanical equipment and membrane life-span. In addition to that, in countries where the seawater feed is subjected changing feed quality, arising from the water salinity, silt, and the harmful algae blooms (HABs), the dominant method employed in these sites is usually the thermally-driven methods such as the MSF and the MED. The seawater feed in the Gulf has salinity more than 45,000 ppm while the rest of the world is less than 30,000 ppm. Also, the Gulf is fed with rivers from countries where wastewater treatment is lacking and the amount of nutrients fed into the Gulf water promotes HABs. It has been reported that during a HAB, RO plants in Oman and UAE were shut down for 6-8 weeks, a period on no water supply in Gulf co-operation countries (GCC) economies is unthinkable as their potable water storage in some countries are less than 5 days. For these reasons, the desalination plants sited in the GCC are usually the MSF and MED processes where their production capacity shares are 80% while the RO plants are found far away from the coast or inland and they are employed for the treatment of ground or re-use water

[60]. In addition to the suspended pollutants, the main cause of concern emanates from the release of toxins by algae microbes in the seawater feed, such as neuro, paralytic, and diarrheic-toxins. Such microbial-based toxins are of the same molecular sizes and they posed health hazards to humans when traces of toxins are ingested. When water vapor is evaporated by thermally-driven processes, the toxins are separated from the distillate product of MED or MSF plants [61].

Table 2 : Characteristics of different desalination technologies processes.

	MSF	MED	TVC	MVC	RO
Operating range (°C)	35-120	35-75	35-120	35-70	20-45
Pretreatment requirement	Low	Low	Low	Low	High
Scale problem	High	Medium	Medium	Medium	Low
Freshwater quality (ppm)	<10	<10	<10	<10	350-500
Heat consumption (kJ/kg of product)	90-567	108-432	-	-	-
Electricity consumption (kWh/m^3)	3-5	1.5-2.5	-	8-15	2.5-7
Production capacity m^3/d	<76000	<36000	<50000	<5000	<20000
Recovery ratio %	10-25	23-33	23-33	23-41	20-50
Energy recovery	Sensible to latent	Latent to latent	Recovery low Tvap	Recovery low Tvap	Pressure recovery
Maintenance/year	0.5-1	1-2	1-2	1-2	Several times
Plant cost ($\$/m^3/d$)	1500-2000	900-1200	900-1700	1500-2000	900-1500

Comparing MSF and MED, it becomes clear that MED is more efficient in terms of primary energy and electricity consumption and has a lower cost. Moreover, the operating temperature of MED is lower, thus requiring steam at lower pressure if connected in co-generation to a steam cycle power plant. Thus, the combination of solar energy with MED will be more effective than a combination with MSF desalination. Comparing the mechanically driven desalination options, reverse osmosis has a lower electricity consumption and cost per unit product water than the mechanical vapor compression method. The much lower primary energy consumption of RO and the slightly lower

cost compared to MED suggests that RO might be the preferred desalination technology anyway. However, if MED is coupled to a power plant, it replaces the cost of the condensation unit of the steam cycle and partially uses waste heat from power generation for the desalination process. In this case, not all the primary energy used must be accounted for the desalination process, but only the portion that is equivalent to a reduction of the amount of electricity generated in the plant when compared to conventional cooling at a lower temperature, and of course the direct power consumption of the MED process. Processes combining thermal and mechanical desalination may lead to more efficient future desalination systems [58].

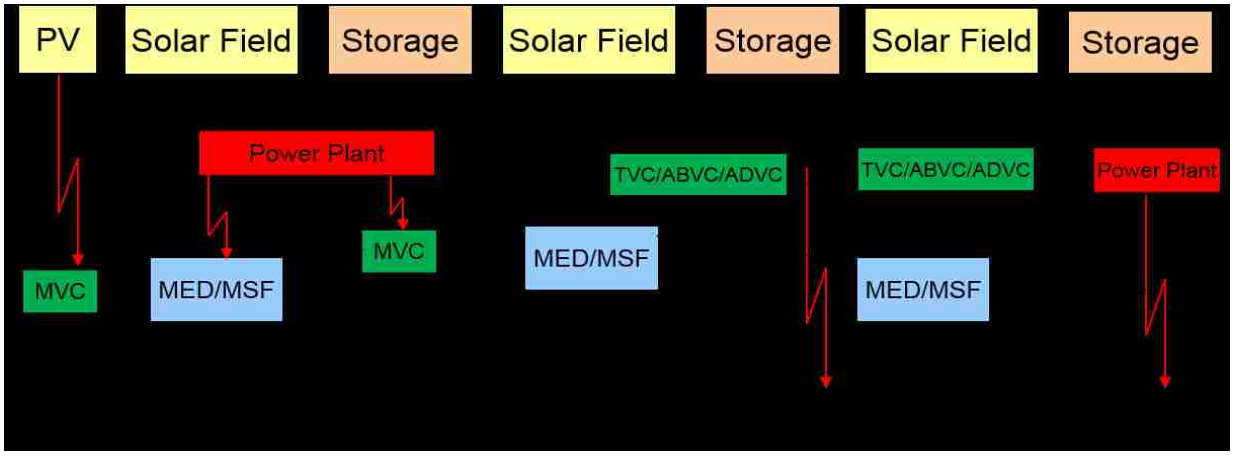

Figure 9 Possible configuration for the solar-assisted VC and combinations.

CHAPTER 3 EXERGY AND THERMO-ECONOMIC ANALYSIS FOR MED-TVC DESALINATION SYSTEMS[**]

3.1 Abstract

An exergo-economic model is used to simulate four different feed configurations of multi-effect desalination with thermal vapor compressor (MED-TVC) system. The feed configurations considered are backward feed (BF), forward feed (FF), parallel feed (PF) and parallel cross feed (PCF). The model results indicate that the PCF configuration has better performance characteristics than the other feed configurations regarding gain output ratio (GOR) and specific heat consumption (SHC), but it has the highest specific cooling seawater flow rate (sM_{cw}). On the other hand, the BF configuration has the lowest sM_{cw}. The highest exergy destruction (58%) occurs within the TVC unit and this can be reduced by lowering the supplied motive steam pressure. The exergy destructions in the condenser and pumps account for 4 to 6.7 % of the total exergy destruction for all feed configurations. The MED-TVC under consideration has a second law efficiency between 3.9 to 4.6 %. Lowering the motive steam pressure for the PCF from 2300 to 300 kPa results in a 7.5% reduction in GOR and a 25.4% increase in the second law efficiency. Reducing the exergy destruction in the TVC unit is cost-effective for the entire system even with the increase in capital investment costs. The specific exergy cost flow method is used to estimate the total water price for BF, FF, PF and PCF as 2.12, 2.30, 2.16 and 2.09 \$/m^3, respectively.

[**] **Mohamed L. Elsayed**, Osama Mesalhy, Ramy H. Mohammed, Louis C. Chow, "Exergy and thermo-economic analysis for MED-TVC systems." Desalination, volume 447, December 2018, Pages 29-42.

3.2 Introduction

Thermally-driven seawater desalination methods such as Multi-effect-desalination (MED) and multistage flash (MSF) are used to provide the required potable water and water for industrial used. They are preferred in Gulf co-operation countries (GCC) and the Middle East and North Africa (MENA) regions due to the abundant source of available oil [62]. In addition to that, the quality of the feed seawater may change due to salinity, silt and harmful algae blooms (HABs). The current share of GCC in the worldwide desalination market is about 41% of which nearly 56% is based on the thermal desalination methods [63]. The MED systems provide better performance compared to reverse osmosis (RO) or MSF using a newly proposed figure of merit, called the universal performance ratio (UPR), which represents the ratio of evaporative energy to the primary energy and not the derived energy. The reported values of UPR for RO, MED and MSF are 86.0, 88.0 and 60.0, respectively [64, 65]. The hybridization of MSF/MED with reverse osmosis (RO) can improve system performance, but the overall recovery is controlled by operational temperatures of MED/MSF [66]. Moreover, the hybridization MED method with the adsorption desalination (AD) cycles almost doubles the water production compared to conventional MED system [56, 67-69].

Recently, MED system with thermal vapor compression (TVC) unit has gained more interest in large scale-desalination projects especially in GCC than other thermal systems such as MSF. The main advantages of MED-TVC desalination systems include high thermal efficiency with lower energy consumption compared to MSF. The MED-TVC systems could also result in small condenser size, smooth operation and maintenance, low scale formation, reasonable production costs and high gained output ratio (GOR) which represents the distillate product per amount of heat source supplied. MED-TVC can operate at low top brine temperature (TBT) (<70°C) and requires

less pumping power. Frequent and increasingly larger installations for MED-TVC systems are proliferating in capacity worldwide. For instance, Yanbu II expansion in Saudi Arabia is the world's largest installed MED-TVC desalination plant with capacity reaching 146,160 m^3/day [70]. The TVC unit works as a heat pump to recover the latent heat of condensation in the product vapor from MED system at a specific location to induce evaporation of seawater when the temperature level of produced vapor is not sufficient for stable evaporation. High-pressure motive steam is used to compress a portion of the last effect generated vapor to the first effect in the TVC unit.

Developing an accurate simulation program that can model the operating performance of thermal desalination systems enables the designers to select the best components and determine the optimal operating conditions to improve desalination plants performance, reduce energy consumption and save money. For that purpose, several studies have been carried out in this area during the last two decades. The studies available in the literature include different conceptual designs, simulations codes to examine the influence of the desalination system physical characteristics and internal operational conditions (TBT, fluid flow configuration, number of effects, etc.) on the design performance (water production capacity, heat or power consumption, components sizing, etc.). However, most of these analyses are based on the first law of thermodynamics [28, 39, 71-75] with little attention on the second law analysis (exergy) point of view since the middle of the last decade [76]. The first law is an essential tool for evaluating the performance of thermal desalination systems, but it does not consider the quality of energy transferred and cannot show where the maximum loss of available energy takes place. On the other hand, the second law analysis enables the identification of the locations, reasons and magnitudes of energy degradation in the system [77]. Such information is useful to show which components in the system have room for improvement to increase the overall exergy efficiency and help improve and optimize designs [78]. For example,

The combined exergy destruction of the TVC and evaporator units was estimated by Alasfour et al. [79], Choi et al. [80] and Binamer [76] as 92, 70 and 84 % of the total exergy destruction in the MED-TVC systems, respectively. Many researchers have attempted to improve the operation and performance of MED-TVC desalination system and thus increase the overall production. Darwish and A1-Najem [81] performed exergy analysis on MED-TVC and concluded that the system could be more efficient if the heat content of the brine and distillate streams leaving the MED-TVC is recovered and utilized in heating the feed to the system. However, the additional cost of adding preheaters for the feed should be considered against the reduction of steam cost obtained by increasing the system efficiency. Han et al. [82] experimentally tested a new method to improve the entrainment performance of the TVC unit by preheating entrained vapor. Their results showed that the TVC entrainment ratio increases with the entrained vapor superheat. Sayyaadi et al. [83] optimized the thermal and economic aspects of MED-TVC desalination system to minimize the cost of the system product (freshwater). Sharaf et al. [84] proposed mathematical and economic models for MED-TVC processes powered by a solar thermal cycle. Esfahani et al. [85] presented exergetic analysis using a multi-objective optimization incorporating genetic algorithm (GA) based on neural network model to optimize the MED-TVC system.

Other groups of researchers have recently dealt with the integration of desalination systems with various thermal systems (diesel engines, gas turbines, solar energy systems, etc.). For example, Shakib et al. [86] performed a thermo-economic analysis and an optimization to minimize the product cost for a combination of the gas turbine power plant, heat recovery steam generator (HRSG) and MED-TVC system. They concluded that the optimal design with high productivity required higher capital investment and resulted in a higher product cost. Catrini et al. [87] conducted an exergo-economic analysis to determine the electricity and water production price of a combined

steam power cycle integrated with MED-TVC system. Also, the integration of the MED-TVC system into the Linear Fresnel Rankine Cycle (LFRC) was investigated using exergy and exergo-economic analysis in [88]. Salimi and Amidpour [89], performed an economic assessment for a reciprocating internal combustion engine coupled to HRSG and MED-TVC desalination system.

Although there have been many simple modeling studies on the steady-state nature of MED-TVC systems, to the best of the authors' knowledge, there have been very few, or no satisfactory contributions on the process design, performance analysis, and exergo-economic studies with different feed configuration of the MED systems integrated to the TVC unit. Thus, a comprehensive thermo-economic study of the MED-TVC process is needed to get a better understanding of the different feed configurations of MED-TVC system performance and the cost of flow streams to or from the thermal systems. The effect of changing the feed configurations for better unit performance regarding first and second law analysis is the aim of this study and to pinpoint the deficiencies in each configuration. Further, a comprehensive thermo-economic analysis is applied to evaluate the final product cost based on exergy and to identify the cost concentrated components. A sensitivity analysis is conducted to study the impact of motive steam pressure on the system's performance including GOR, second law efficiency, total system exergy destruction and specific cooling seawater flow rate (sM_{cw}). The effects of variation of the economic parameters such as cost index factor (C_{index}), interest rate (i), specific steam cost (SSC) and electricity cost (C_e) on the total water price (TWP) for different feed configurations of MED-TVC system are investigated as well.

3.3 Configuration of MED-TVC systems

Figure 10 shows a schematic diagram of MED-TVC systems with the major elements of (N) effects, thermal vapor compression unit, condenser, and pumps for brine/distillate and cooling

seawater. Vapor flows from the first effect through inter-effects and leaves the bottom condenser unit, while the feed and brine flow may have different flow directions depending on the MED configuration. The different feed configurations of MED integrated with TVC unit considered in this study include backward feed (BF), forward feed (FF), parallel feed (PF) and parallel/cross feed (PCF). Each evaporation effect is composed of tube bundles of horizontal falling film tubes, demister for droplets separation and spray nozzles housed inside the shell that has space for the saturated vapor and the brine concentrate pool. Droplets of the feed/brine are sprayed on the tubes forming a thin liquid film and causing evaporation to occur. The heat source (steam) introduced to the first effect condenses to distillate inside the effects tubes by transferring its latent heat to the continuous thin film of the sprayed feed. The temperature of the feed seawater around the tubes in the 1st effect is raised to its boiling temperature which is also known as the top brine temperature (TBT). A fraction of the feed in the first effect evaporates, and the vapor flows as a heat source into the tubes of the second effect which is at a lower pressure and temperature than the first effect. In all effects, condensation and evaporation occur inside and outside the tubes for vapor and thin sprayed seawater film respectively. Adding the TVC unit to the MED system helps to recover part of the latent heat of the vapor generated in the last effect and increases the system GOR through decreasing the required amount of heat source in the first effect as shown in Figure 10. Part of the vapor generated in the last effect is used to preheat the feed seawater, and the remaining part is entrained to the TVC unit using high-pressure motive steam extracted from a boiler or a power plant steam turbine. The ratio of the motive steam flow rate to the entrained vapor flow rate is called the entrainment ratio (R_a). For a MED-TVC system, electricity is the only required to operate the pumps to deliver the feed to the effects and to discharge brine and distillate.

In the BF configuration, while cooling seawater passing through the bottom condenser it exchanges heat with the last effect vapor and a significant portion is rejected back to the sea. The remaining part of the cooling seawater (feed) enters the last effect with lowest vapor temperature and sprays outside walls of horizontally installed tubes forming a thin liquid film that exchanges heat with the vapor from the previous effect. Part of the feed is evaporated while the temperature and concentration of the remaining part temperature increased forming concentrated brine leaving the last effect. This brine is cascaded sequentially through effects in backward direction till it reaches as a feed for the first effect and then leaves as a rejected high concentrated brine blown down back to the sea. In the BF configuration feed and vapor flow has reverse flow (counter-current) directions. One of the significant drawbacks of BF is exposure of heat transfer tubes of the first effect with TBT to the high concentrated brine which increases the chances for scaling in the evaporator system. Also, the BF configuration requires higher pumping powers to overcome the inter-pressure differences between effects which increases the complexity and operational power consumption of the system.

In the FF arrangement, the preheated feed water is directed all the way to the first effect with the highest TBT. Again, a portion of the sprayed feed is evaporated over the tubes of the first effect while the remaining unevaporated brine part with high TBT is directed as a feed to the next effect and this process is cascaded in a forward direction towards the last effect. Feed (brine) and vapor flow have the same direction (co-current). The main advantage of the FF configuration is its adequacy to operate at high TBTs. It is preferred if the Multi-effect stack configuration is used where the gravity provides the required the brine pumping between the effects. Figure 10 also shows the PF process in which the preheated feed is divided and distributed to a sequence of successively low-pressure effects at the same time. The feed stream to the first effect exchange

heat with the heat source steam and form the brine while the other feed stream exchanges heat with the vapor from the previous effects. Crossing the hot brine leaving from an effect with high pressure in the PF configuration to a lower effect pressure causes the brine to flash which enhance the effect vapor production rate, and the configuration called parallel/cross feed. The choice of between these feed arrangements depends on the application and affects the design and performance of the MED desalination system. These criteria include the heat transfer areas required in each effect, the heat transfer area of the condenser unit, the vapor generated in each effect, the vapor generated by boiling and by flashing, the pumping energy and the specific cooling seawater (cooling seawater to distillate ratio) [84, 90].

3.4 MED-TVC systems mathematical model

The four different feed arrangements for MED-TVC systems are considered and compared to pinpoint the most reliable configuration regarding steady state and exergo-economic operation. The steady state models used to solve mass, energy and salt equation in the different feed configurations MED systems with the assumptions listed as follows:

1. Non-condensable gases effect on evaporator performance is not considered.
2. Thermophysical properties of the brine and vapor are temperature and salinity dependent. Appropriate correlations are selected from [73].
3. The temperature difference between the brine pool and vapor generated in effect was due to the following temperature losses; (i) Boiling Point Elevation (BPE), (ii) non-equilibrium allowance (NEA) [73].
4. The vapor and distillate are salt-free.
5. Pressure losses of vapor in the connections are ignored.
6. Sprayed seawater thoroughly wets evaporator tubes, no dry patches exist.

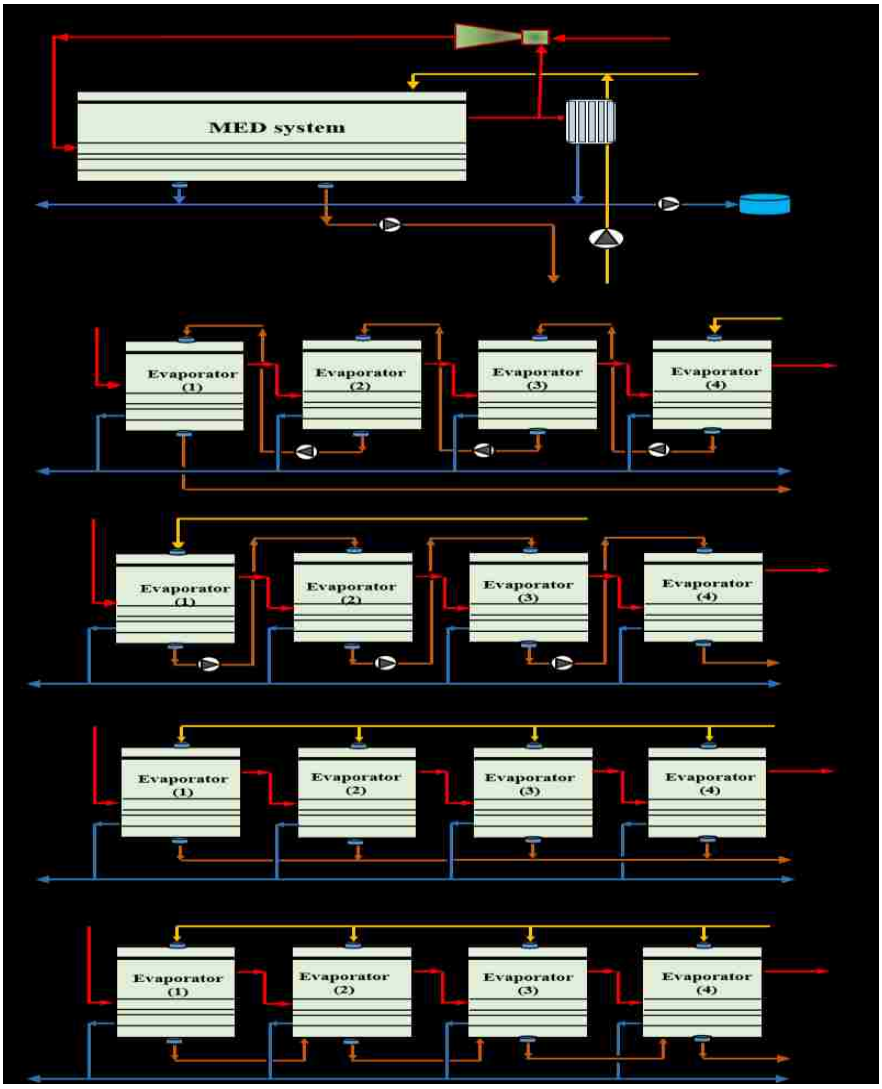

Figure 10 Schematic diagram of MED-TVC desalination system with different feed configurations.

The solution is carried out iteratively to adjust the temperature drop across the effects to obtain equal evaporators heat transfer area. The model solution flow is presented in Figure 11 for the conservation equations for all MED-TVC configurations components. The maximum difference in effect areas is calculated and with assuming error criteria ε =0.01 m^2 is required. Therefore, a new iteration sequence is initiated. The second iteration starts with calculations of the new heat transfer area. A new profile for the temperature drop across the effects is then calculated. A new iteration is then taken, which starts with temperature profiles and continues to the convergence

criteria part. The details of the mass, energy, and salt balance for BF, FF, PF, and PCF configurations are presented in Table 3. To estimate the performance of TVC, quasi-steady correlations for the entrainment ratio that relates expansion ratio and a compression ratio of the ejector are extracted from the Power's graphical data chart [91] by Hassan and Darwish [92], which are suitable for the range of typical MED operation conditions. To unify operational conditions of the different feed configuration, the specifications and design limits considered for MED-TVC with different configurations are compared to an actual plant operated in Tripoli, Libya [72] with 5000 m^3/day operation capacity. In the steady state solution, the vapor/brine temperature, feed flow rate, brine flow rate, vapor flow rate and salinity at each effect are calculated in addition to the effects heat transfer surface areas. The motive steam flow rate, compression ratio and expansion ratio determine the entrainment ratio which in turn define the amount of vapor entrained to the TVC unit.

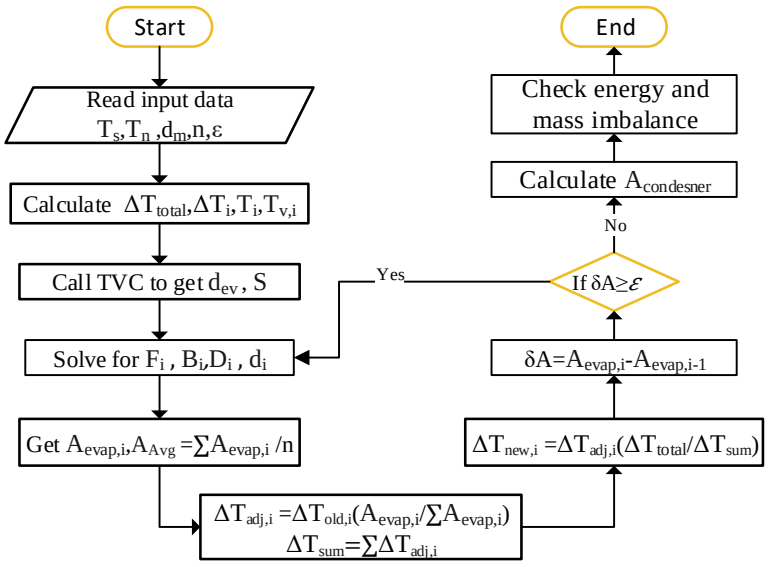

Figure 11 Solution flow chart for the steady state model to adjust evaporators area in MED-TVC.

Table 3 Balance of the governing equations for different MED feed configurations.

Configuration		1st effect	2 to n-1	Last effect (n)	F	B	D
BF	Mass	$B_i = B_{i+1} - D_i$		$B_i = F - D_i$	F_n	B_1	$\sum_{i=1}^{n} D_i$
	Salt	$B_i.X_i = B_{i+1}.X_{i+1}$		$B_i.X_i = F.X_f$			
	Energy	$D_1 = \frac{S.\lambda_s - B_1(h_1 -$ $(\lambda_1 + (h_1 - h_2$	$D_i = \frac{D_{i-1}.\lambda_{i-1} - B_i(h_i -$ $(\lambda_1 + (h_i - h_{i+1})$	$D_i = \frac{D_{i-1}.\lambda_{i-1} - B_i(h_i -$ $(\lambda_i + (h_i - h_f)$			
FF	Mass	$B_1 = F - D_1$	$B_i = B_{i-1} - (D_i + d_i)$		F_1	B_n	$\sum_{i=1}^{n} D_i + d_i$
	Salt	$F.X_f = B_1.X_1$	$B_i.X_i = B_{i-1}.X_{i-1}$				
	Energy	$D_1 = \frac{S.\lambda_s - F(h_1 - h}{\lambda_1}$ $d_1 = 0$	$D_i = \frac{(D_{i-1} + d_{i-1}).\lambda_{i-1}}{\lambda_i}$, $d_i = \frac{B_{i-1}(h_{i-1} - h_i)}{\lambda_i}$				
PF	Mass	$B_1 = F_1 - D_1$	$B_i = F_i - D_i$		$\sum_{i=1}^{n} F_i$	$\sum_{i=1}^{n} B_i$	$\sum_{i=1}^{n} D_i$
	Salt	$F_1.X_f = B_1.X_1$	$B_i.X_i = F_i.X_f$				
	Energy	$D_1 = \frac{S.\lambda_s - F_1(h_1 -$ (λ_1)	$D_i = \frac{D_{i-1}.\lambda_{i-1}}{\lambda_i} - \frac{F_i(h_i - h_f)}{\lambda_i}$				
PCF	Mass	$B_1 = F_1 - D_1$	$B_i = F_i - D_i + B_{i-1} - d_i$		$\sum_{i=1}^{n} F_i$	B_n	$\sum_{i=1}^{n} D_i + d_i$
	Salt	$F_1.X_f = B_1.X_1$	$B_i.X_i = B_{i-1}.X_{i-1} + F_i.X_f$				
	Energy	$D_1 = \frac{S.\lambda_s - F_1(h_1 -$ λ_1 $d_1 = 0$	$D_i = \frac{(D_{i-1} + d_{i-1}).\lambda_{i-1}}{\lambda_i} - \frac{F_i(h_i - h_f)}{\lambda_i}$, $d_i = \frac{B_{i-1}(h_{i-1} - h_i)}{\lambda_i}$				
Overall mass balance $F = B + D$ Overall salt balance $F.X_f = B.X_n$							
d_i , represents the amount of vapor generated from hot brine flashing when exposed to lower pressure.							

1.4.3. Exergy modeling

The exergy is defined as the maximum available work obtainable when a stream of substance is brought from its initial state to the environmental state. Energy is conserved in any process according to the first law of thermodynamics, but exergy is destroyed due to irreversibilities taking place due to entropy generation [80]. For an open system operating under steady state condition, the appropriate exergy rate balance is established including the loss of exergy or loss of work in the following form:

$$\sum_j \left(1 - \frac{T_o}{T_j}\right) \dot{Q}_i + \sum_i \dot{m}_i \, e_i - \sum_e \dot{m}_e \, e_e - \dot{W} - \dot{E}_D = 0.0 \quad (4)$$

where, $\dot{E}_D$ (kW) is the exergy destruction of the system. The specific exergy transfer terms e_i and e_e can be expressed as the summation of physical, chemical, potential and kinetic exergy [77]. The last two terms are neglected in the current simulation, so the flow exergy takes the following form,

$$e = \overbrace{h - h^* - T_o(s - s^*)}^{physical} + \underbrace{\sum_{i=1}^{n} x_i(\mu_i^* - \mu_i^o)}_{chemical} \quad (5)$$

Where h, s, x and μ are specific enthalpy, specific entropy, salt mass fraction and chemical potential, respectively. Subscript i represent number of species in the mixture. Superscript '0' is for the ambient conditions. Superscript '*' is for the ambient pressure and temperature, and initial concentration of the system conditions.

At steady state, the total exergy transported into the system equals the total exergy brought out of system and exergy destruction in the system. The total exergy destruction in the system $\dot{E}_{D,total}$ is known as exergy consumption and can be expressed as the subsystem exergy destructions summation. The input exergy in MED-TVC system $\dot{E}_{in,total}$ is expressed by summation of the exergy input from the high-pressure motive steam, from the pump work and through the incoming cooling water stream. The output exergy $\dot{E}_{out\ total}$ represents the exergy of the product distillate, condensate back to the boiler, brine blow down and the exergy of the seawater rejected to the sea. The second law exergetic efficiency for the MED-TVC systems is used as a performance criterion and represents the ratio of the minimum exergy input required (which is equal to the minimum heat of separation) to the total actual exergy input.

$$\eta_{II} = 1 - \frac{\dot{E}_{D,total}}{\dot{E}_{in,total}} = \frac{\dot{E}_{out,total}}{\dot{E}_{in,total}} \quad (6)$$

The second law analysis becomes more evident when the analysis is performed at the component level for the different feed configurations of MED-TVC, and the locations of maximum exergy destruction are identified. Also, the fraction of exergy destruction within each component is determined to quantify the percentage of exergy destruction in all components for the different feed configurations. The exergy balance equation for each component is discussed in detail in next section.

1.4.4. Exergy-economic model

In the assessment and cost optimization of energy systems, it is required to obtain the annual values of capital-related charges, fuel costs, and the operating and maintenance expenses. These cost components may vary considerably within the operation life of the system. Thus, levelized annual values should be used in the cost assessment process [83]. The production cost is divided into the direct/indirect cost and annual operating cost. The direct capital costs (DCCs) represent the expenses that are directly associated with the construction of the MED plant; value afforded for the process equipment purchasing [93]. Table 4 presents the existing equations in the literature that are used to determine the purchase price of some of the MED components [94]. Other components (such as TVC unit) are apportioned according to their contribution to the overall plant costs. Maintenance and operational costs are taken as a subset of the DCCs [93]. The operating costs include all expenses afforded after plant commissioning and during real operation and are categorized as variable and fixed. The changeable operating expenses are those related to the purchase of electrical power, heating steam, chemicals for pre/post-treatment and other requirements that are dependable on the plant capacity of fresh water production and standards.

Fixed operating costs represent expenses that are needed for the operation of the plant but are independent of the plant capacity. In many cases, these costs are related to the capacity of the plant or taken as a factor of the direct capital cost (DCCs). Cost index C_{index} =1.2 was used to accommodate the equipment price change to fit the current time calculations [74]. Also, the indirect capital cost (IDCC: freight, insurance, construction overhead, owner's costs and contingency costs), is assumed to be IDCC=0.15DCC according to [95]. Operating cost categories are estimated based on available data from the literature [73] with maintenance costs taken as a proper subset of the fixed operating cost such as 2%.

Table 4 Purchase cost of MED-TVC system components.

Instrument	Capital cost of instrument ($)	Comments					Ref.
MED effect	$\mathbf{201.67 \times UA_{evaporator} dp_t^{0.15} dp_s^{-0.15}}$	**S for shell side and t for tube side dp (kPa), A (m^2), U ($kW/m^2.k$)**					[94]
MED condenser	$\mathbf{430 \times 0.582\ UA_{condenser} dp_t^{-0.01} dp_s^{-0.1}}$						
Water pump	$\mathbf{32 \times 0.435} \times \dot{m}_{water}^{0.55} \Delta P^{0.55} \left(\frac{\eta}{\eta-1}\right)^{1.05}$	$\boldsymbol{\eta = 0.9}$, $\boldsymbol{\Delta P}$ (kPa)					
			BF	**FF**	**PF**	**PCF**	
		Number of pumps	**6**	**6**	**3**	**3**	

The hourly capital investment (CI) cost and operation and maintenance costs (OM) for each component is calculated using an amortization factor $A_f = \frac{i.(1+i)^{nt}}{(1+i)^{nt}-1}$ (1/year), plant availability (LF) 0.9, plant lifetime (nt) =30 year and interest rate i=5% as:

$$\dot{Z}_{component}^{CI+OM}(\$/h) = \frac{Z_{component}^{CI+OM} \cdot A_f}{LF \times 24 \times 365} \quad (7)$$

In the current work, the specific exergy costing (SPECO) approach was used in which the exergo-economic analysis is used to calculate the cost rate of the product streams of the system [96]. The cost balance expresses the variable $\dot{C}$ that denotes a cost rate associated with a flow exergy stream: stream of matter, power, or heat transfer. According to the conservative nature of costs [97], the

cost rate associated with the system product $\dot{C}_P \left(\frac{\$}{h}\right)$ is equal to the total rate of expenditure used to generate this product in a component, namely the fuel expenditures cost resulting from the cost associated with the exergy flows $\dot{C}_F \left(\frac{\$}{h}\right)$ and the cost rates associated with the capital investment (CI) and operating and maintenance (OM) taking the general form as:

$$\dot{C}_P = \sum \dot{C}_F + \dot{Z}^{CI+OM}_{component} \tag{8}$$

The above cost balance equation is applied to the MED-TVC system components to obtain the product stream cost. Typically the number of unknown cost parameters is higher than the number of cost balance equations for the component; additional auxiliary equations are used to accommodate this difference. Usually, the auxiliary equation represents the equality of the average cost of the inlet and exit for the same stream, and they are formulated based on different principles (exergy extraction, multiple outputs, and external assessment) [98]. The cost balance equations and the auxiliary equations for each component are presented in Table 5. Also, the exergy and cost balance equation for the inter-effects pumps in case of FF and PF are presented in Table 6. For the mixing points, the product cost is considered the summation of cost rate for the inlet points and while for the splitting points the outlet cost rate streams are equally divided.

To include non-exergy related costs such as the specific labor cost ($SLC = 0.05 \frac{\$}{m^3}$), and specific chemical cost ($SCC = 0.025 \frac{\$}{m^3}$) in the exergo-economic analysis, the inlet feed stream to the feed pump was considered as $\dot{C}_1(\$/h) = (SLC + SCC)(\$/m^3) \times D(m^3/h)$. Also, the specific steam cost ($SSC = 1.28 \frac{\$}{m^3}$) [74] is used to obtain inlet heating stream cost for the TVC unit calculated from $\dot{C}_5(\$/h) = (SHC)(\$/m^3) \times D(m^3/h)$. The summation of the outlet stream flow rate cost must be equal to the sum of the carrying charges, fuel cost rate and the operating and maintenance costs

calculated on a per hour basis to satisfy the cost rate balance for the total system [98]. Finally, the total water price ($TWP_{exerg-economic}$) ($\$/m^3$) from the exergo-economic analysis is calculated by dividing the cost rate of all the outlet streams (distillate, brine and rejected cooling seawater) ($\$/h$) from the MED-TVC unit by the total production rate (D) of the plant (m^3/h).The linear system of algebraic equations are solved by consideration of the cost of the electrical energy used for the pumps as $C_e = 0.08\ \frac{\$}{kWh}$ [99].

The results from the cost exergy model are sufficient for (a) providing more details from an economic standpoint that enables the calculation of the product stream cost separately at any intermediate state in the system, (b) Understanding the cost formation process and the flow of costs in the system that highlights the involvement of the component in the final cost, and (c) identifying the cost concentrated components that need attention to achieve a lower product cost [98]. Three important parameters for evaluating the exergo-economic analysis of the thermal energy systems are calculated using the component exergetic efficiency (ϵ_k) and average cost per unit fuel exergy$c_{F,k}$. The variables include: the exergy destruction cost rate ($\dot{C}_{D,k}$), relative cost difference (r_k), and the exergoeconomic factor (f_k) which are given by Eqs. (9)–(11) [98].

$$\dot{C}_{D,k} = c_{F,k}\dot{E}_{D,k} \tag{9}$$

$$r_k = \frac{1-\epsilon_k}{\epsilon_k} + \frac{\dot{Z}_k^{CI+OM}}{c_{F,k}\dot{E}_{P,k}} \tag{10}$$

$$f_k = \frac{\dot{Z}_k}{\dot{Z}_k + \dot{C}_{D,k}} \tag{11}$$

Table 5 Fuel and product cost rates of the MED-TVC system components.

Component		Fuel ($\dot{C}_F$)	Product ($\dot{C}_P$)	Capital and investment	Auxiliary equation
Feed pump (FP)		$C_e.\dot{W}_{FP} + \dot{C}_1$	$\dot{C}_2$	$\dot{Z}_{FP}$	--
Brine pump (BP)		$C_e.\dot{W}_{BP} + \dot{C}_{10}$	$\dot{C}_{11}$	$\dot{Z}_{BP}$	--
Distillate pump (DP)		$C_e.\dot{W}_{DP} + \dot{C}_8$	$\dot{C}_9$	$\dot{Z}_{DP}$	--
TVC unit		$\dot{C}_5 + \dot{C}_{20}$	$\dot{C}_{14}$	$\dot{Z}_{TVC}$	--
Condenser		$\dot{C}_2 + \dot{C}_{21}$	$\dot{C}_3 + \dot{C}_{22}$	$\dot{Z}_{con}$	$\frac{\dot{C}_{21}}{\dot{E}_{21}} = \frac{\dot{C}_{22}}{\dot{E}_{22}}$
1st effect	BF	$\dot{C}_{19} + \dot{C}_{14}$	$\dot{C}_{15} + \dot{C}_{16} + \dot{C}_{10}$	$\dot{Z}_{Ev,1}$	$\frac{\dot{C}_{14}}{\dot{E}_{14}} = \frac{\dot{C}_{15}}{\dot{E}_{15}}$ & $\frac{\dot{C}_{19}}{\dot{E}_{19}} = \frac{\dot{C}_{10}}{\dot{E}_{10}}$
	FF	$\dot{C}_6 + \dot{C}_{14}$	$\dot{C}_{15} + \dot{C}_{16} + \dot{C}_{18}$		$\frac{\dot{C}_{14}}{\dot{E}_{14}} = \frac{\dot{C}_{15}}{\dot{E}_{15}}$ & $\frac{\dot{C}_6}{\dot{E}_6} = \frac{\dot{C}_{18}}{\dot{E}_{18}}$
	PF	$\dot{C}_{\acute{6}} + \dot{C}_{14}$			$\frac{\dot{C}_{14}}{\dot{E}_{14}} = \frac{\dot{C}_{15}}{\dot{E}_{15}}$ & $\frac{\dot{C}_{\acute{6}}}{\dot{E}_{\acute{6}}} = \frac{\dot{C}_{18}}{\dot{E}_{18}}$
	PCF				
2nd effect	BF	$\dot{C}_{16} + \dot{C}_{23}$	$\dot{C}_{17} + \dot{C}_{18} + \dot{C}_{20}$	$\dot{Z}_{Ev,2}$	$\frac{\dot{C}_{16}}{\dot{E}_{16}} = \frac{\dot{C}_{17}}{\dot{E}_{17}}$ & $\frac{\dot{C}_{23}}{\dot{E}_{23}} = \frac{\dot{C}_{18}}{\dot{E}_{18}}$
	FF	$\dot{C}_{16} + \dot{C}_{19}$	$\dot{C}_{17} + \dot{C}_{20} + \dot{C}_{22}$		$\frac{\dot{C}_{16}}{\dot{E}_{16}} = \frac{\dot{C}_{17}}{\dot{E}_{17}}$ & $\frac{\dot{C}_{19}}{\dot{E}_{19}} = \frac{\dot{C}_{22}}{\dot{E}_{22}}$
	PF	$\dot{C}_{\acute{6}} + \dot{C}_{16}$	$\dot{C}_{17} + \dot{C}_{19} + \dot{C}_{21}$		$\frac{\dot{C}_{16}}{\dot{E}_{16}} = \frac{\dot{C}_{17}}{\dot{E}_{17}}$ & $\frac{\dot{C}_{\acute{6}}}{\dot{E}_{\acute{6}}} = \frac{\dot{C}_{21}}{\dot{E}_{21}}$
	PCF	$\dot{C}_{\acute{6}} + \dot{C}_{16} + \dot{C}_{18}$			
3rd effect	BF	$\dot{C}_{20} + \dot{C}_{27}$	$\dot{C}_{21} + \dot{C}_{24} + \dot{C}_{22}$	$\dot{Z}_{Ev,3}$	$\frac{\dot{C}_{20}}{\dot{E}_{20}} = \frac{\dot{C}_{21}}{\dot{E}_{21}}$ & $\frac{\dot{C}_{22}}{\dot{E}_{22}} = \frac{\dot{C}_{27}}{\dot{E}_{27}}$
	FF	$\dot{C}_{20} + \dot{C}_{23}$	$\dot{C}_{21} + \dot{C}_{24} + \dot{C}_{26}$		$\frac{\dot{C}_{20}}{\dot{E}_{20}} = \frac{\dot{C}_{21}}{\dot{E}_{21}}$ & $\frac{\dot{C}_{23}}{\dot{E}_{23}} = \frac{\dot{C}_{26}}{\dot{E}_{26}}$
	PF	$\dot{C}_{\acute{6}} + \dot{C}_{19}$	$\dot{C}_{20} + \dot{C}_{22} + \dot{C}_{24}$		$\frac{\dot{C}_{19}}{\dot{E}_{19}} = \frac{\dot{C}_{20}}{\dot{E}_{20}}$ & $\frac{\dot{C}_{\acute{6}}}{\dot{E}_{\acute{6}}} = \frac{\dot{C}_{24}}{\dot{E}_{24}}$
	PCF	$\dot{C}_{\acute{6}} + \dot{C}_{19} + \dot{C}_{21}$			
4th effect	BF	$\dot{C}_6 + \dot{C}_{24}$	$\dot{C}_{13} + \dot{C}_{25} + \dot{C}_{26}$	$\dot{Z}_{Ev,4}$	$\frac{\dot{C}_{24}}{\dot{E}_{24}} = \frac{\dot{C}_{25}}{\dot{E}_{25}}$ & $\frac{\dot{C}_6}{\dot{E}_6} = \frac{\dot{C}_{26}}{\dot{E}_{26}}$
	FF	$\dot{C}_{24} + \dot{C}_{27}$	$\dot{C}_{13} + \dot{C}_{10} + \dot{C}_{25}$		$\frac{\dot{C}_{24}}{\dot{E}_{24}} = \frac{\dot{C}_{25}}{\dot{E}_{25}}$ & $\frac{\dot{C}_{27}}{\dot{E}_{27}} = \frac{\dot{C}_{10}}{\dot{E}_{10}}$
	PF	$\dot{C}_{\acute{6}} + \dot{C}_{22}$	$\dot{C}_{23} + \dot{C}_{13} + \dot{C}_{25}$		$\frac{\dot{C}_{22}}{\dot{E}_{22}} = \frac{\dot{C}_{23}}{\dot{E}_{23}}$ & $\frac{\dot{C}_{\acute{6}}}{\dot{E}_{\acute{6}}} = \frac{\dot{C}_{25}}{\dot{E}_{25}}$
	PCF	$\dot{C}_{\acute{6}} + \dot{C}_{22} + \dot{C}_{24}$	$\dot{C}_{23} + \dot{C}_{13} + \dot{C}_{10}$		$\frac{\dot{C}_{22}}{\dot{E}_{22}} = \frac{\dot{C}_{23}}{\dot{E}_{23}}$ & $\frac{\dot{C}_{\acute{6}}}{\dot{E}_{\acute{6}}} = \frac{\dot{C}_{10}}{\dot{E}_{10}}$

Table 6 Cost and exergy balance equations for inter-effects pumps for BF and FF systems

Component	Exergy balance	Cost rate balance
Pump1	$\dot{E}_{D,P1} = \dot{E}_{18} + \dot{W}_{P1} - \dot{E}_{19}$	$\dot{C}_{19} = \dot{C}_{18} + C_e.\dot{W}_{P1} + \dot{Z}_{P1}$
Pump2	$\dot{E}_{D,P2} = \dot{E}_{22} + \dot{W}_{P2} - \dot{E}_{23}$	$\dot{C}_{23} = \dot{C}_{22} + C_e.\dot{W}_{P2} + \dot{Z}_{P2}$
Pump3	$\dot{E}_{D,P3} = \dot{E}_{26} + \dot{W}_{P3} - \dot{E}_{27}$	$\dot{C}_{27} = \dot{C}_{26} + C_e.\dot{W}_{P3} + \dot{Z}_{P3}$

3.5 Model validation

The developed energy model using Engineering Equation Solver (EES) software is validated by comparing to results with data reported from a model developed by El-Dessouky and Ettouney [73] for forward feed MED-TVC system. In addition to that, actual date reported for MED-TVC plant located in Kish Iceland, Iran [100] that operates in parallel/crossfeed arrangement was compared to the current developed model as shown in Table 7. The validity of the currently used models shows perfect agreement with data in the literature, where the maximum deviation does not exceed 6.0%.

Table 7 Validation of MED-PCF model with actual data.

Parameter	PCF-TVC	Kish Iceland [72]	% error	FF-TVC	El-Dessouky [73]	% error
Inlet feed salinity, g/kg	45		--	42		--
Outlet brine salinity, g/kg	70		--	70		--
Top brine temperature (TBT), °C	68		--	56.67		--
last brine temperature T_n, °C	47		--	40		--
Feed temperature T_f, °C	44		--	35		--
Motive steam flow rate kg/s	2.89		--	0.19		--
Gain output ratio (GOR)	7.72	8.0	3.5	5.09	5.26	3.2
Distillate production kg/s	22.311	23.148	3.6	0.967	1	3.3
Brine flow kg/s	51.326	54.629	6.0	1.453	1.5	3.1
Feed flow kg/s	73.637	77.778	5.3	2.42	2.5	3.2
Steam flow rate to the first effect	5.31	NA	--	0.2804	0.2754	1.82
Entrained vapor kg/s	2.42	NA	--	0.0904	0.08532	5.95
Entrainment Ratio for TVC	1.194	NA	--	2.1	2.228	5.7

3.6 Results and Discussion

3.6.1. Steady-state analysis

The steady-state input operating conditions adopted for all configurations are shown in Table 8. Changing the feed configuration and keeping the rate of fresh water production unchanged lead to a variation in the required motive steam flow rate. The motive steam changes from 8.9 kg/s for PCF to 9.28, 9.7 and 9.22 kg/s for PF, FF, and BF feed configurations, respectively. The PCF configuration has the highest GOR and the lowest specific heat consumption (SHC) compared to other configurations. However, it has a relatively high specific cooling water flow rate which depends on the condenser load where the remaining portion of vapor leaving the last effect condenses. In the BF configuration, the vapor leaving the last effect to the condenser is lower compared to other configurations. This leads to smaller condenser size and lower cooling water flow rate. Table 8 shows that nearly the same specific heat transfer area (S_A) for all feed configurations. The electrical energy needed to operate the feed, brine, distillate pumps as well as the inter-effects pumps is calculated for the FF and BF configurations. The results show that FF has the highest electric power consumption, and this is attributed to the high pump work needed to drive the required cooling seawater in the condenser. The total power consumption (TPC) for the MED-TVC desalination processes is estimated by considering the conversion efficiency of the thermal energy to work is 0.35 and the steam boiler efficiency equals 0.94 [67]. The data show that the total power consumption is the lowest for the PCF configuration due to the relatively lower motive steam mass flow rate through the TVC compared to the other feed configurations. Just calculating the energy required to drive the system is not sufficient to evaluate its performance because this does not consider the effect of the availability of the thermal energy. Other meaningful criteria can be considered such as the second law efficiency and exergo-economic analysis factors.

Table 8 Steady-state operation parameters for different MED process configurations.

Configuration	BF	FF	PF	PCF
Number of effects	4			
Motive steam pressure, kPa	2300			
Top brine temperature T_1, °C	60.1			
last brine temperature T_n, °C	45.4			
Seawater temperature T_{cw}, °C	31.5			
Feed temperature T_f, °C	41.5			
Feed content, g/kg	35			
Brine content, g/kg	53			
Distillate production (D)kg/s	56.12			
Motive steam flow rate kg/s	9.22	9.71	9.28	8.89
Gain output ratio (GOR)	6.08	5.778	6.05	6.31
Specific cooling seawater flow ($sM_{cw} = \dot{m}_{cw}$/D)	3.9	7.6	5.3	6.7
Specific heat transfer area (S_A) m^2/kg/s	124.3	124.6	125.3	124.5
Specific heat consumption [101] (SHC=2330/GOR) kJ/kg	383.0	403.3	385.1	369.3
Pump power consumption ($\dot{W}_{pumps}$/D) kWh/m^3	0.24	0.35	0.21	0.24
Total power consumption kWh/m^3 (TPC=$\left(\frac{\dot{Q}_{thermal}}{\eta_{boiler}=0.94} + \frac{\dot{W}_{pumps}}{\eta_{thermal}=0.35}\right)$/D)	136.7	144.3	137.4	131.8

3.6.2. Exergy analysis

Exergy analysis helps to determine the location of highest entropy generation and thus the analysis identify the components that have the most considerable losses in the system [78] and where there is room for improvement to increase overall exergy efficiency and improve and optimize designs. Component exergy destructions and their percentages for MED-TVC system with different feed configurations are shown in Figure 12. In each component, exergy destruction is caused by irreversibility due to energy conversion processes such as heat transfer, pressure drop, heat loss of fluid in the pump, and effluent streams. The exergy destruction calculations show that the exergy

destructions in the TVC unit and evaporators represent the highest share. Together, they are responsible for about 80 % of the total exergy destruction for different feed configurations. This is attributed mainly to the high motive steam pressure and temperature difference across the TVC unit and the heat transfer process in the effects that are associated with phase change. Other components such as condenser and pumps have the lowest share in the exergy destruction, ranging between 4 to 6.7% for all feed configurations. Figure 12 also indicates that pumps have the highest exergetic efficiencies (lowest exergy destructions and losses). The others exergy destruction represents the exergy destruction in the outlet streams of brine, distillate, and cooling water when they are rejected to the environment. The second law efficiency for all feed configurations of MED-TVC system is found to be in the range of 4 to 4.4%, which is comparable with the results for MED-TVC desalination system found in the literature. The thermal desalination process necessarily comprises evaporation/condensation, and this is the main cause for its low second-law efficiency [102]. The data show that PCF has the highest value of second law efficiency followed by the FF, while the PF has the lowest value among all configurations.

Furthermore, the performance of the MED–TVC system is compared to those of a conventional MED system with the similar capacity. The considered MED system is operating with BF configuration with a bottom condenser and is modeled using models developed by El-Dessouky et al. [73] under the similar constraints for the same freshwater production (56.12 kg/s) and rejected brine salinity (53 ppt). The simulation shows that the required steam mass flow rate for the conventional MED is 17.29 kg/s compared to 9.22 kg/s for the case of MED-TVC operating with BF configuration. The calculated value of GOR for generation of 4848 m^3/d is 6.087 for MED–TVC and 3.25 for conventional MED. MED-TVC reduces the amount of steam used to produce 1 m^3 of freshwater by 46% as compared to traditional MED system operating in BF configuration.

However, from the exergy point of view, the exergy efficiency of MED–TVC (4.11%) is about 30% of the corresponding value of conventional MED (11.84%). This is expected as the MED-TVC systems are inefficient in energy utilization due to the use of high-pressure motive steam. Adding TVC to the MED systems increases the exergy costs to produce the same amount of the fresh water.

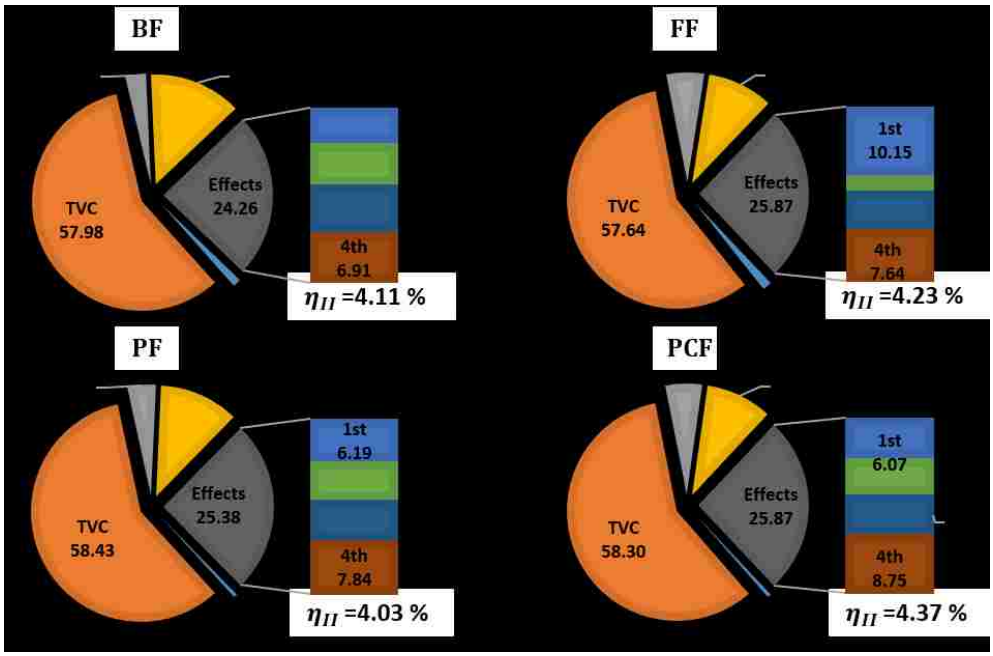

Figure 12 Percentage exergy destruction for main component of various feed MED-TVC system.

TVC systems operate with the pressure of motive steam ranging from 20 to 30 bars supplied directly from a steam boiler, or with a pressure close to 3 bars extracted from a steam power plant turbine [79]. Figure 13 shows the effect of reducing the motive steam pressure on the GOR, exergetic efficiency, total exergy destruction of the system (TVC, evaporators, condenser and leaving streams) and specific cooling water per plant capacity (sM_{cw}). For instance, the decrease of the motive steam pressure from 2300 to 300 kPa results in approximately 10% reduction in GOR while the second law efficiency increases by 35% for the PCF configuration. The

improvement in the second law efficiency results from the reduction in exergy destruction in the TVC unit as the motive pressure decreases. Lowering the motive steam pressure reduces the entrained vapor from the last effect which lowers the GOR and increases the required cooling seawater for the condenser. For the PCF configuration, Figure 13 shows that as the motive steam pressure decreases from 2300 to 300 kPa, the total exergy destruction reduces significantly by approximately 31.7%. The decrease in GOR is apparent for motive steam pressure below 1500 kPa since the entrainment ratio is larger at this pressure [103].

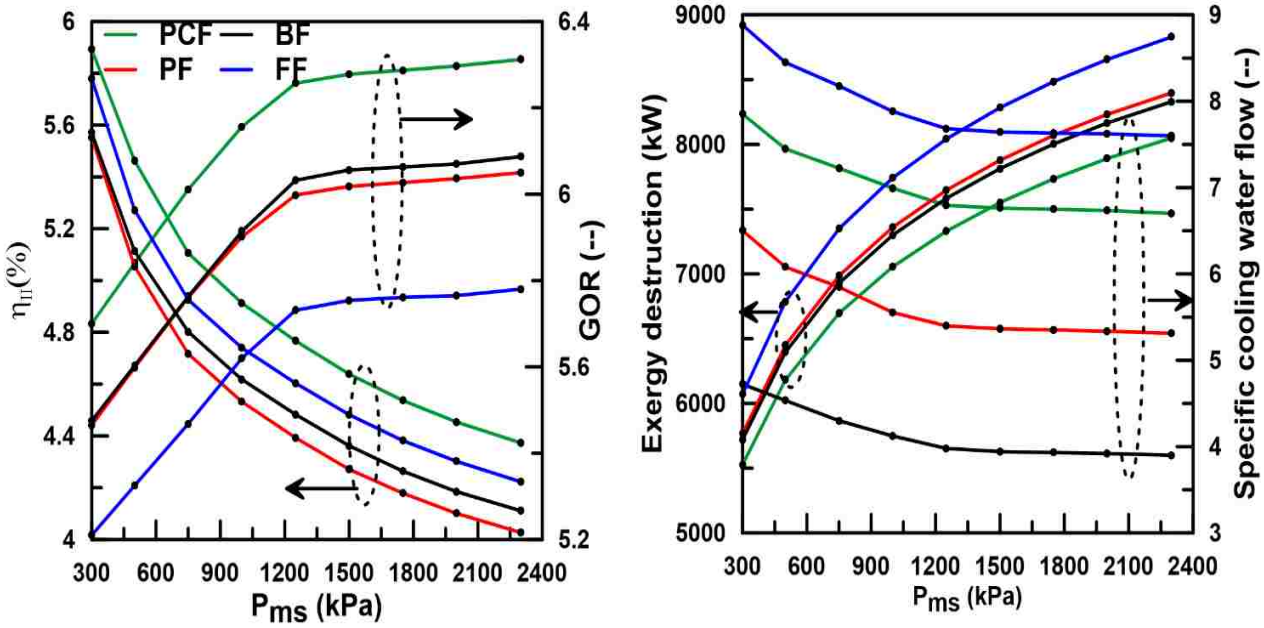

Figure 13 Effect of motive steam pressure on GOR, η_{II} , $\dot{E}_{D,total}$, sM_{cw}, for different feed configurations.

3.6.3. Exergo-economic analysis

Simple conventional economic models treat the MED-TVC plant as a whole unit. These models are introduced in the literature to obtain a reasonable estimation of the total water price for the MED systems. For example, El-Dessouky et al. [73] calculated the annualized cost of the plant directly and eventually estimated the total water price for MED-TVC systems. However, to

indicate the contribution of each flow stream and each component in the final product cost, the exergo-economic analysis is applied to all MED-TVC components and flow streams. When conducting a thermoeconomic analysis for the current MED-TVC system, a cost balance equation is used to correlate the exergy instead of the energy of the flow stream with the pricing value of the component. Exergy-based costs are more reasonably split among outputs since costs units based on exergy are more significative than energy-based ones. This cost balance incorporated with suitable auxiliary thermo-economic relations, resulting in a system of linear algebraic equations which are solved for the unknown values of cost rates or of cost per exergy unit. As mentioned before, non-exergy related costs represented by heating cost, chemical cost, and labor cost are added to the exergo-economic model as input stream in the TVC unit inlet and feed seawater respectively. By solving the exergy-cost balance equations, the costs for various streams at different locations in the MED-TVC plant are obtained, and the final product cost is estimated.

The most expensive component is the evaporator unit (due to large heat transfer area needed), and the cheapest equipments are the TVC unit, pumps and the condenser as shown in Figure 14. For the BF the price of the condenser is the lowest due to its relatively smaller size. The total fixed cost for the FF (13.15 $/h) is the highest due to (i) the high motive steam flow rate, (ii) the high pumping power for inter-effects pumps, and (iii) the required large condenser area. Exergo-economic variables are shown for both PCF and BF feed configurations because they have higher GOR and lower SHC compared to the FF and PF feed configurations.

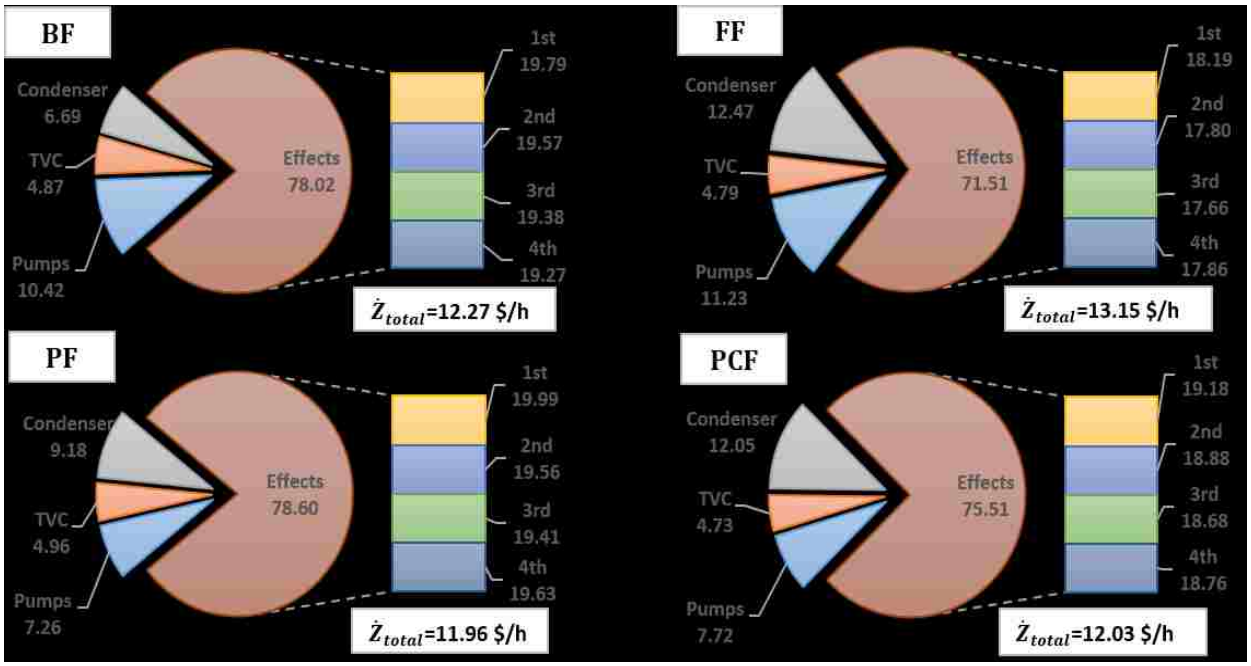

Figure 14 Percentage of fixed cost rate for main components in BF and PCF configurations.

Table 9 summarizes the essential thermo-economic variables calculated for the components of MED-TVC systems of BF and PCF feed configurations. The variables include the second law (exergetic) efficiency of system components ϵ_k, the components rate of exergy destruction $\dot{E}_{D,k}$, the average cost per unit fuel exergy $c_{F,k}$, the product exergy $c_{P,k}$, the cost rate of exergy destruction (exergetic inefficiency) $\dot{C}_{D,k}$, the investment and O&M cost rate $\dot{Z}_k$, the relative cost difference factor r_k, and the exergo-economic factor f_k. The relative cost difference (r_k) for a component represents the average cost per exergy unit between fuel and product and it is useful to evaluate and optimize a system component [98]. The higher value of the total operating cost $\dot{C}_{D,k} + \dot{Z}_k$ indicates the higher influence of the component on the overall system performance, therefore in designing of a new system, the first design changes must initially be applied to that component. The exergo-economic factor (f_k) is used to identify the relative significance of non-exergy related costs (CI&OM) to the sum of owning and operating of exergetic inefficiency costs, $\dot{Z}_k + \dot{C}_{D,k}$. A

low value of f_k for major components suggests that the cost saving for the system could be accomplished by improving the components efficiency (reduction of exergy destruction) even if the capital cost investment increases.

For the PCF configuration, the last effect has highest values of the sum $\dot{Z}_k + \dot{C}_{D,k}$ among evaporators (due to high exergy destruction) following the TVC unit which has the lowest exergetic efficiency. Similar situation occurs for the BF but with the highest value of $\dot{Z}_k + \dot{C}_{D,k}$ in the TVC unit. Therefore, the TVC unit is the most important component from the thermo-economic point of view in the MED-TVC systems. The lower value of the variable f_k for the TVC unit shows that the cost associated with the TVC unit is dominated by the exergy destruction while the remaining part is caused by $\dot{Z}_k$ value of the component as indicated for both feed configurations. So, it can be concluded that, reducing the exergy destruction in the TVC unit could be cost effective for the entire system even if this would increase the investment costs associated with this component. Part of the exergy destruction in the TVC unit can be avoided by reducing the motive steam pressure without affecting the flow rate of the motive steam. So, TVC motive steam pressure is a key design variable because it affects the exergy associated with the inlet stream as well as the performance and investment cost of the TVC unit. In actual practice, a change in motive steam pressure is associated with a proportional change in the motive steam mass flow rate [91, 104]. Reducing the motive steam pressure reduces the $\dot{C}_{D,k}$ value for the TVC unit but increases the capital investment (CI) cost to achieve the designed value of the steam flow rate.

Turning next to the evaporators assembly, which has the second highest value of $\dot{Z}_k + \dot{C}_{D,k}$, the relatively small value of the factor f_k suggests also that the exergy destruction cost dominates the investment and O&M cost. According to the cost model assumption, the capital investment costs

for the evaporators depend on the evaporator areas and the overall heat transfer coefficients. Therefore, modifications and improvements to the heat transfer process must be considered. For both feed configurations, the last effect and condenser have the lowestf_k, which indicate that the exergy destruction costs are controlling even with a relatively high exergetic efficiency of the component. Table 9 indicates that the highest exergetic efficiency belongs to the pumps, especially the distillate pump. However, the lower value for the f_k factor for the brine pumps and inter-effects pumps for BF configuration suggests that the exergy destruction costs still dominate the total cost of these components. One important conclusion which can be drawn from the results presented in Table 9 is that thermo-economic analysis aims at identifying the possible reduction of sub-components total costs. This reduction can be either for the cost of inefficiencies or the cost of owning and operating of components, whichever is dominant. Therefore, for components such as pumps, improvement is achieved by reducing the ownership and operating cost of the sub-system under consideration at a cost of a reduction in the thermodynamic efficiencies. For components like TVC where component inefficiency is the dominant cost, improvement to reduce inefficiency costs can be obtained by improving the thermodynamic efficiency or the operating condition.

Table 9 Exergo-economic variables for MED-TVC systems with BF and PCF configurations.

	Component	$\dot{E}_{D,k}(kW)$	$\epsilon_k(\%)$	$c_{F,k}(\$\ MJ^{-1})$	$c_{P,k}(\$\ MJ^{-1})$	$\dot{C}_{D,k} + \dot{Z}_k(\$/h)$	$r_k(\%)$	$f_k(\%)$
BF	TVC unit	4835	50.72	0.0075	0.0244	131.66	194.78	0.45
	Condenser	241.1	60.62	0.0731	0.0678	66.86	130.7	1.23
	1st effect	369.3	92.85	0.0244	0.0271	38.8	15.9	6.26
	2nd effect	436.8	90.30	0.0271	0.0299	49.1	22.01	4.89
	3rd effect	517.3	85.82	0.0298	0.0336	62.13	33.69	3.82
	4th effect	542.8	79.96	0.0336	0.0443	72.08	50.96	3.28
	Feed pump	12.72	76.03	0.0480	0.102	2.56	68.38	14.5
	distillate pump	3.402	99.15	0.0226	0.0300	0.46	2.23	38.9
	Brine pump	24.61	97.29	0.0595	0.1052	5.45	5.64	3.59
	P1	17.08	96.09	0.0539	0.0957	3.51	8.31	5.36
	P2	20.4	96.94	0.0562	0.0992	4.31	6.41	4.15
	P3	20.64	97.49	0.0533	0.1022	4.13	5.22	4.05
PCF	TVC unit	4697	50.14	0.0078	0.0333	132.57	199.24	0.43
	Condenser	415.9	60.6	0.0730	0.1084	115.15	130.79	1.26
	1st effect	447.5	89.8	0.0334	0.0356	61.08	23.15	3.78
	2nd effect	400	89.6	0.0356	0.0401	58.36	23.69	3.90
	3rd effect	434.6	87.34	0.0401	0.0509	70.15	29.47	3.21
	4th effect	670.6	78.09	0.0507	0.0792	130.86	56.59	1.73
	Feed pump	21.97	75.99	0.0313	0.0668	2.98	57.09	16.8
	distillate pump	3.4	99.12	0.0291	0.043	0.54	2.189	33.1
	Brine pump	17.78	94.23	0.0768	0.1449	5.17	12.36	4.84

Using average values of the economic parameters such as cost index factor (C_{index}=1.2), interest rate (i=5%,), specific steam cost (SSC=1.28 \$/m^3) and electricity cost (C_e =0.08 \$/kWh), the cost rate pricing for the PCF and BF configurations for all flow streams through the MED-TVC system is shown in Figure 15. The estimated total water price for PCF and BF is 2.09 and 2.12 \$/m^3, respectively. Besides showing the cost flow rate at each stream point, the figure shows the exergy, temperature and flow rate with the exergy destruction (kW) for the main components of MED-TVC system as well. For the FF and PF configurations, the total water price is 2.30 and 2.16 \$/m^3, respectively.

The effects of variation of the economic parameters on the total water price (TWP) for different feed configurations of MED-TVC system are presented in Figure 16. Cost index and interest rate affect the fixed cost and the capital investment of the plant while specific steam cost and electricity cost affect the plant operating cost. Increasing the cost index from 1 to 2 has a smaller effect than interest rate change. At the higher value of interest rate (15%), the total water price of PCF and BF configurations are equal. Increasing the interest rate from 2 to 15% translates to a total water price increase in the range of 7 to 9%.

Fuel cost to operate the plant (steam cost and electricity cost) depends on the plant location associated with different steam or electricity production prices. The main energy consumption of the MED-TVC desalination system is represented by the steam requirement which is required to operate the TVC unit, while the electricity is used to operate the installed pumps. Increasing the electricity cost has a smaller effect than changing the steam heating cost. For the lower values of SSC, different configurations have nearly the same TWP (~1 $\$/m^3$), while for the higher values, FF configuration has the highest TWP. This is attributed the high amount of steam required to produce 5000 m^3/day of fresh water for FF configuration compared to the other configurations. Moreover, if the MED-TVC with PCF configuration is installed in two regions with the different price of SSC 1 and 2 $\$/m^3$, the TWP will be 1.69 and 3.11 $\$/m^3$, respectively. An increase in the SSC of 100% increases the TWP by 84%. This sensitivity study results reveal that the most important parameter that cannot be neglected while comparing different installation areas for MED-TVC systems is the specific steam cost.

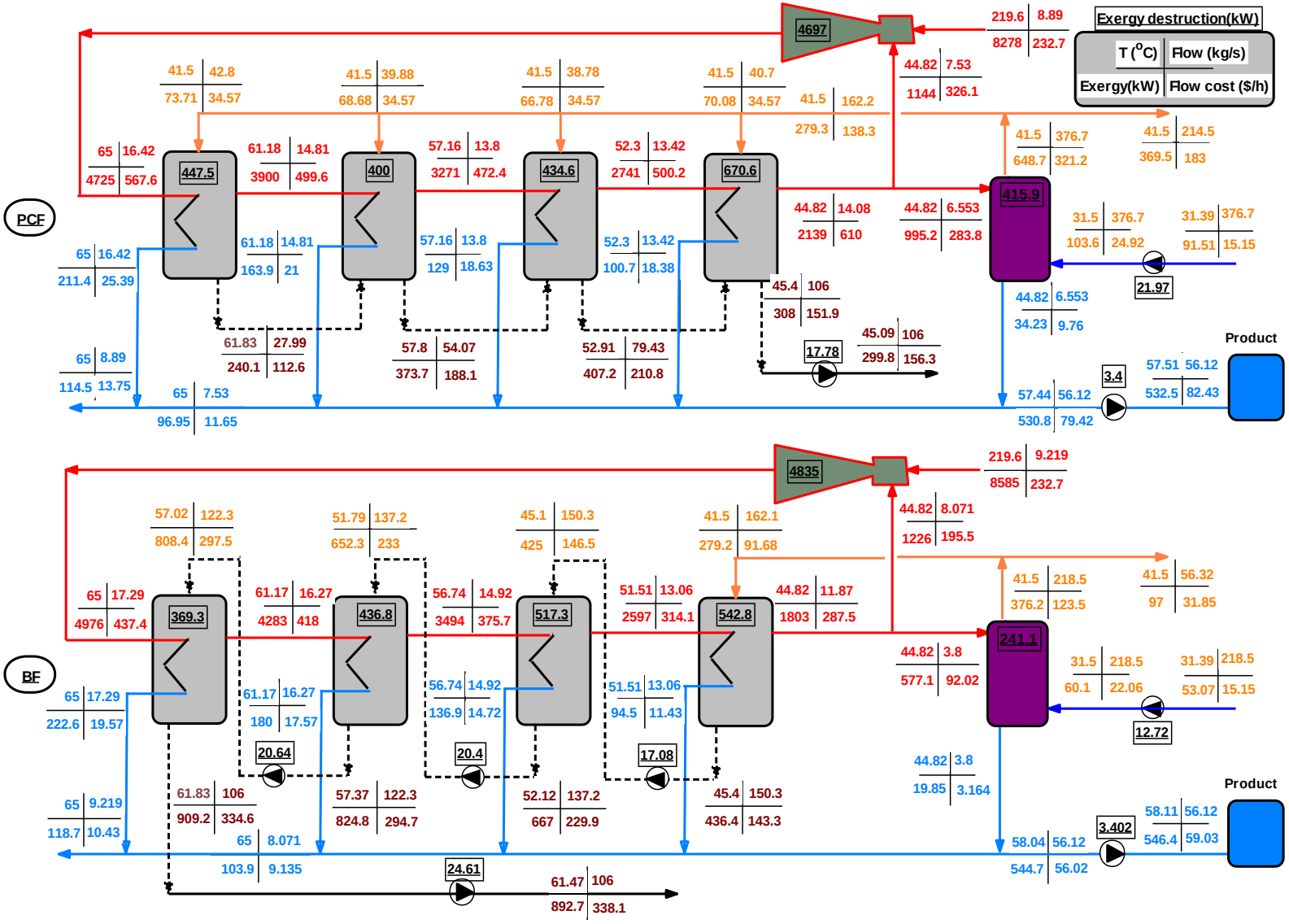

Figure 15 Cost flow diagram for MED-TVC system with PCF and BF configurations.

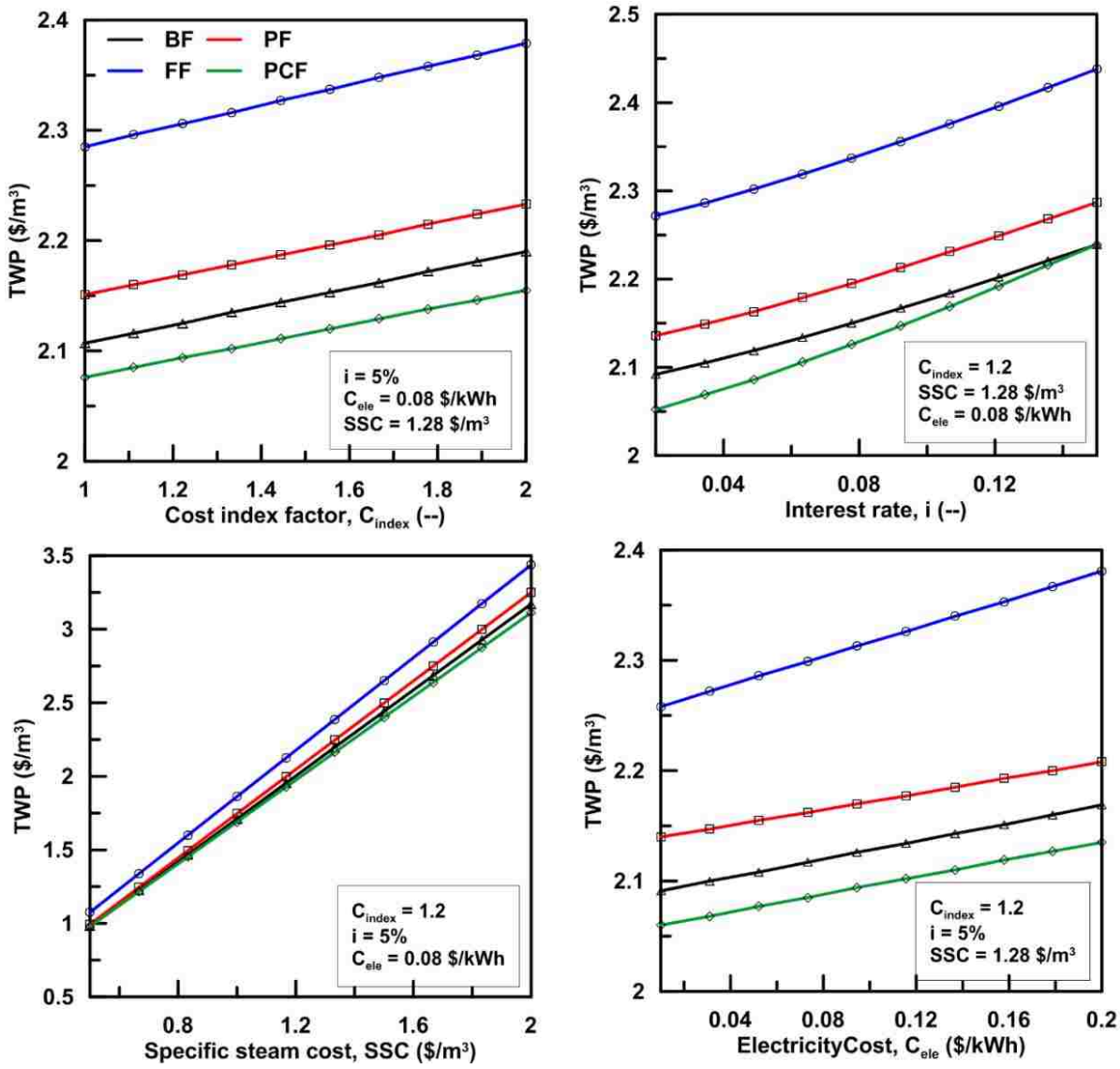

Figure 16 Total water price for different feed configuration and economic parameters.

3.7 Conclusions

The effects of employing four different feed configurations (BF, FF, PF, and PCF) for MED-TVC desalination system on the total water price and plant performance are investigated. The MED-TVC systems considered with a fixed daily water production rate of 5000 m^3/day. The calculated gain output ratio (GOR) is 6.08, 5.78, 6.05 and 6.31 for BF, FF, PF and PCF,

respectively. The PCF configuration shows the lowest specific heat consumption (SHC) and the lowest total power consumption (TPC) compared to the other configurations, but it has a high specific cooling water flow rate. On the other hand, the BF configuration has a smaller specific cooling seawater flow rate. The electric power consumption is higher for the FF configuration due to the required high pumping power. Also, the exergy destruction of the MED-TVC systems is calculated. The study reveals that the exergy destruction in the TVC unit (58%) and evaporator units (24%), represent the highest share of the total exergy destruction in the system. The second law efficiency is the highest for PCF configuration (4.37%), while the PF has the lowest value (4.03%). A reduction in the motive steam pressure for the current system from 2300 to 300 kPa results in a 10% reduction in GOR and a 35% increase in the second law efficiency.

A detailed thermo-economic analysis of the BF and PCF configurations of MED-TVC are presented covering both thermodynamic and economic aspects of the system design and their components. The results show that for the PCF configuration, the most expensive (highest investment cost) components are the evaporator units. The lower value of the variable f_k for the TVC unit shows that the cost associated with the TVC unit is dominated by the exergy destruction while the remaining part is determined by the $\dot{Z}_k$value of the component as indicated for PCF and BF configurations. Reducing the exergy destruction in the TVC unit could be cost effective for the entire system even if this would increase the capital investment costs associated with this component. Part of the exergy destruction in the TVC unit can be avoided by reducing the motive steam pressure without affecting the flow rate of the motive steam. So, TVC motive steam pressure is a key design variable because it affects the exergy

associated with the inlet stream as well as the performance and investment cost of the TVC unit.

Finally, a specific exergy cost flow method is used to estimate the production cost for BF, FF, PF and PCF as 2.12, 2.30, 2.16 and 2.09 $/m^3, respectively using average values of the economic parameters. Changes in cost index, interest rate and electricity cost have a minimal effect on the total water price. On the other hand, changing the specific steam cost has a significant effect on the TWP, especially for the FF configuration.

CHAPTER 4 PERFORMANCE MODELING OF MED-MVC SYSTEMS: EXERGY-ECONOMIC ANALYSIS[**]

Abstract

In this study, exergy analysis of four different feed configurations of a multi-effect desalination with mechanical vapor compressor (MED-MVC) system is initially studied to identify the area of exergy destruction within system components and followed by an exergo-economic study. The feed configurations considered are forward feed (FF), backward feed (BF), parallel feed (PF) and parallel/cross feed (PCF). From the 1st law energy analysis, the PCF and FF configurations require less work to achieve equal distillate production compared to other two configurations. For instance, the specific power consumption (SPC) values are 30.1, 13.7, 23 and 13.9 kWh/m^3 for the BF, FF, PF and PCF configurations, respectively. Changing the feed arrangement from BF to FF and PF to PCF at a constant compression ratio, the total fixed cost for the MED-MVC plant can be reduced by ~30% and 17%, respectively. Second law efficiency (η_{II}) calculations show that the PCF (2.9%) has the highest value followed by the FF (2.7%), while the BF (2.4%) exhibits the lowest value among all configurations. The highest exergy destruction (35-50%) occurs within the MVC unit. This can be reduced by limiting the design plant operation to a lower temperature range or increasing the number of effects. Increasing the number of effects for PCF from 1 to 6 results in a 39% reduction in the SPC and a 70% increase in the second law efficiency. Operating at lower steam temperature results in an increase in the $\eta_{II,}$and a decrease in the SPC and total water price (TWP) of the MED-MVC system. Reducing the exergy destruction in the preheaters and the MVC

[**] **Mohamed L. Elsayed**, Osama Mesalhy, Ramy H. Mohammed, Louis C. Chow, "Performance modeling of MED-MVC systems: Exergy and thermo-economic analysis" Energy volume 166, January 2019, pages 552-568.

unit is cost-effective for the entire system even with an increase in capital investment costs. Three different cost models are used to estimate the average TWPs for the BF, FF, PF and PCF configurations, and the TWPs are found to be 3.0, 1.7, 2.4 and 1.7 $/m^3, respectively.

Introduction

Multi-effect desalination with mechanical vapor compressor (MED-MVC) systems are widely applied as a common solution for medium-scale (100-5000 m^3/day) water reclamation desalination and solution concentration for high-salinity wastewater treatment (salt recovery) [105]. Several advantages associated with MVC systems include high-quality water recovered, compact equipment, low-temperature design and long-term stable operation. Corrosion and scale formation are minimal which lead to high plant operation availabilities [106, 107]. The main limitation of the MED-MVC systems is the low capacity of the available mechanical vapor compressors (MVC). The low volumetric flow and pressure head limit the production capacity to 5000 m^3/day [108]. The MVC units are typically radial centrifugal or axial flow compressors due to their high suction flow rates and low maintenance requirements and could be single stage or multistage with intercoolers [109, 110].

Various studies for MVC systems available in the literature include steady-state model development, simplified design methods, experimental research and performance prediction. Some of these studies, as well as a few others of interest, are presented in the following paragraphs. There are more experimental studies on the MVC systems than theoretical investigations [111]. For example, Veza [112] and Lucas and Tabourier [113] described a MVC seawater desalination unit producing 500 and 1500 m^3/day of distilled water at a specific power consumption (SPC) of 11.5 and 11 kWh/m^3, respectively when operating at 40% water recovery. Bahar [42] tested a

MVC pilot plant with two vertical double fluted tubes evaporators with one m^3/day capacity and a top brine temperature (TBT) of 103°C. The highest performance ratio (ratio of kg of distillate output to 2326 kJ of heat input) obtained was 2.52. A single-effect MVC system with a 5 m^3/day capacity was experimentally tested by Aly and Fiqi [36] with mathematical modeling included. Two immersion electrical heaters were used to provide the steam needed to start the desalination process. The amount of steam was based on the supplied feed seawater temperature and the compressor power. There were several efforts made to operate MVC systems with renewable energy resources, since they are more tolerant to intermittent operation compared to the reverse osmosis (RO) process. For instance, Plantikow [114] presented a wind-powered MVC desalination plant installed in Germany which was capable of producing 360 m^3/day of freshwater with a SPC of 16.7 kWh/m^3.

The process performance of MVC units varies slightly, depending on the application. Beyond seawater treatment, MVC has been used to produce water from heavy oil fields and high salinity wastewater treatment in recent years. The MVC process presents some advantages compared to other technologies [115]. 0 capacity of 600 m^3/day at a SPC of 13.6 kWh/m^3 of distillate [116]. To improve the environmental performance and save energy, MVC systems are used as zero-emission desalination (ZED) systems. Han et al. [117] proposed ZED based on a MVC model and showed that the multi-effect ZEDS design is beneficial to reduce the required compressor power compared to the single-effect system. To achieve a salt crystallization concentration of 28.9% from the initial salt mass concentration of seawater of 3%, the required compression work was 760.8 and 604 kJ/kg for single stage and three stages, respectively. Wu et al. [118] presented a novel MVC system with a capacity rated at 1.44 m^3/day. This MVC system separates the evaporator and condenser to

overcome the traditional MVC deficiencies such as descaling, anti-scaling and heat transfer conditions for sewage water treatment. Shen et al. [119, 120] revealed that an injection of 5% or less mass fraction of water in a twin-screw compressor with high isentropic efficiency and high-pressure ratio could substantially reduce the SPC, but they recommended its use only for a capacity less than 600 m^3/day. The commercial and experimental pilot plants found in the literature for different applications are presented in Figure 17 and Table 10, showing the SPC, total water price (TWP) and heat source temperature. For single effect, the SPC has various values which are the highest for desalting of wastewater, oil recovery, and crystallization while in desalination it is in the moderate range.

Steady-state mathematical models of the MVC system are found in many studies. For instance, Aybar [121] and Aussenac et al. [122] developed a model of a single-effect MVC system and analyzed the system performance with variations in the primary parameters. Aly [123] analyzed and compared MVC systems with single, two and three effects. Their results showed that the TWP and the SPC range between 1.3 to 1.7 \$/m^3 and 8 to 24 kWh/m^3, respectively. Nafey et al. [38] showed that the MED-MVC system performance decreased by 8% if external steam is used to initiate the evaporation compared to the MVC without external steam. A single-effect MVC for brine crystallization coupled with a wind farm was investigated by Fernández-López [124]. The total capacity is 2400 m^3/day and the SPC is 30.31 kWh/m^3. Helal and Al-Malek [125] presented a hybrid diesel/solar photovoltaic (PV) assisted MVC desalination system. The system was to supply small communities in remote areas with drinkable water at a production capacity of 120 m^3/day. A diesel engine was used to overcome the uncertainty in the availability of solar energy. Henderson et al. [126] proposed a wind/diesel hybrid driven MVC desalination system for off

electric grid locations in the USA. Optimization of a similar plant driven by wind/PV hybrid has been carried out by Zejli et al. [127] for a water production capacity of 120 m^3/day. Mounir et al. [128] presented the effect of the temperature difference across the effect on the system cost of a MVC used in pollutant concentration. The results showed that the optimum cost is when the temperature difference is between 2 and 3^{o}C.

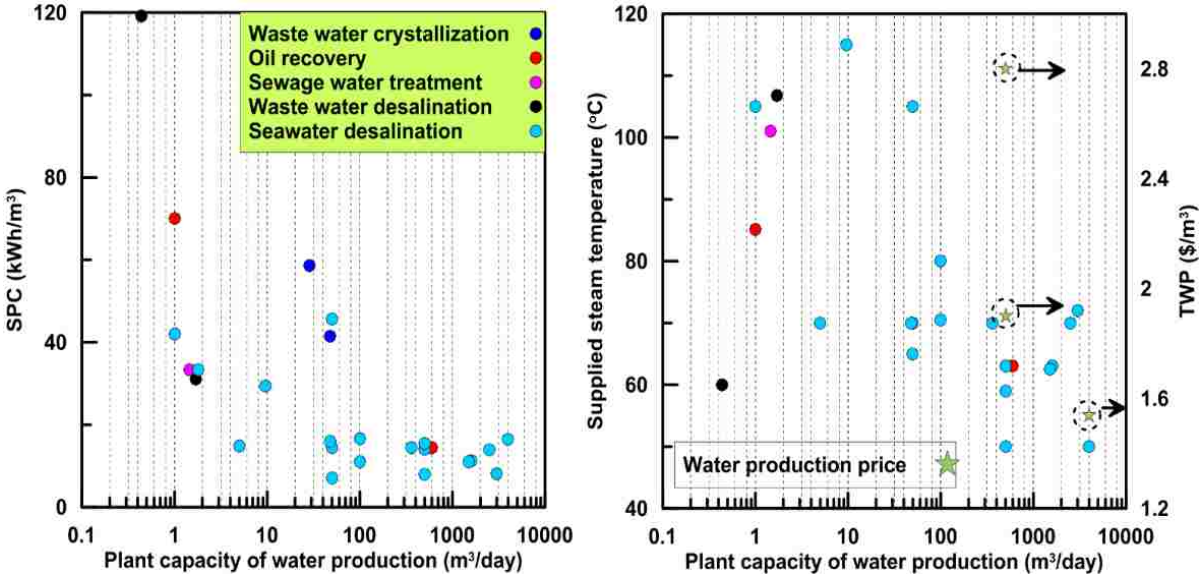

Figure 17 The influence MVC plant application on the SPC, TWP and steam supplied temperature.

Exergy analysis studies are utilized to identify the components with the highest thermodynamic irreversibility rate [77]. For example, Alasfour and Abdulrahim [129] applied steady-state model based on the second law of thermodynamics on a single stage MVC unit. They found that if the temperature difference across the effect increases, the exergy destruction of the unit increases. Nafey et al. [38] analyzed a MED-MVC system with a two-effect forward feed configuration and showed that the plant SPC, second law exergetic efficiency (η_{II}) and the unit product cost are 9.4 kWh/m^3, 5.7% and 1.7 $/m3, respectively. Ahmadi et al. [111] compared single and double effect

mechanical vapor recompression (MVR) and showed that energy saving is achieved by using the double-effect MVR instead of the single-effect. Recently, Jamil and Zubair [130] presented an exergo-economic analysis for a MED-MVC system with a forward feed configuration. The second law efficiency, SPC and product cost range from 7 to 10.96%, 7.67 to 11.36 kWh/m^3 and 0.862 to 1.186 \$/m^3, respectively when the number of evaporation effects increases from 2 to 6. Their results showed that the percentage of exergy destruction in the MVC unit ranges from 0.03 to 0.05% which is far lower compared to available data in the literature [111, 129, 131, 132]. Moreover, the calculated TWP in their study was much lower than the values reported in the literature [38, 112, 123, 133].

Although there have been many simple modeling studies on the steady-state nature of single-effect MVC [32, 129, 134], there have been little or no adequate contributions on the process design, performance analysis, and economic studies when different feed configurations of MED systems are integrated to a MVC unit. Thus, a comprehensive thermo-economic study of the MED-MVC process is carried out and described in this paper to provide a thorough understanding of the performance of different MED-MVC feed configurations. Steady-state energy and exergo-economic models for different feed configurations of MED-MVC process are used to identify the advantages and deficiencies in each configuration. Three different cost methods (simple conventional economic model, exergy-based component cost model and exergy aggregation model) are used to compare the final price of the freshwater production. The exergo-economic cost model is used to identify the cost concentrated components besides the highest cost flow streams in the system. A sensitivity analysis is conducted to study the impact of the number of effects on the system's performance including the SPC, second law efficiency and TWP. The effects of

varying the economic parameters such as cost index factor (C_{index}), interest rate (i) and electricity cost (C_e) on the TWP for different feed configurations of MED-MVC system are investigated as well.

Table 10 Actual installed MED-MVC systems with different industrial applications.

Steam Temp. ^oC	Application	Capacity m^3/day	# of effect	SPC kWh/m^3	Energy Source	Location
70	Desalination SW	50	1	14.4	Wind	Gran Canaria, Spain [135]
70	Desalination SW	48	1	16	Wind	Borkum Island, Germany [114]
70	Desalination SW	360	1	16.7	Wind	Rügen Island, Germany [114]
NA	Crystallization WW	28.8	1	58.6	EM	Jiangsu, China [136]
NA	Crystallization WW	48	2	41.5	EM	
63.0	Desalination SW	1600	4	11.25	EM	Porto Empedocle, Italy [137]
72	Desalination SW	3000	3	8.1	EM	Sardinia, Italy [10]
50	Desalination SW	500:4000	1	8:16.5	EM	Installed plant by IDE [133]
60	Desalination WW	0.437	1	120.87	EM	Beihang University, China [138]
106.8		1.7		31.07		
70.5	Desalination SW	100	1	16.578	EM	Kuwait [139]
62.5	Desalination SW	1500	4	11	EM	Flamanville, France [113]
67	Oil recovery	600	1	14.48	EM	Germany [116]
85.1	Oil recovery	1	1	70	EM	São Paulo State, Brazil [140]
65	Desalination SW	50	2	13.6	EM	Trombay, India [141]
105	Desalination SW	1	2	42	EM	National University of Singapore [42]
80	Desalination SW	100	1	11	EM	Copenhagen, Denmark **[142]**
70	Desalination SW	5	1	14.8	EM	Egypt **[36]**
105	Desalination SW	50	2	45.6	EM	Tianjin, China **[119]**
59	Desalination SW	500	1	14.0	EM	Las Palmas, Spain **[112]**
--	Desalination SW	1.8	1	33.29	EM	Beijing, China **[143]**
101	Sewage treatment	1.45	1	33.3	EM	Beijing, China **[118]**
115	Desalination SW	9.6	1	29.4	EM	Beijing, China **[144]**
63	Desalination SW	500		15.504	Diesel engine	Palma de Mallorca, Spain [145]
70		2500	1	13.92		

SW: Seawater, WW: Wastewater, EM: Electrical motor

Configuration of MED-MVC

Mechanical vapor compression in a MED is a cyclic process. The entire vapor generated in the last effect is routed to the MVC unit through a wire mesh mist eliminator (demister) to separate water droplets from the vapor. The vapor is compressed to the desired target condition of temperature and pressure before directing it as supply steam to the inside of the first effect tubes bundles. The supply steam from the MVC unit condenses to distillate on the tube-side of the first effect by transferring its latent heat to a thin film of feed seawater sprayed around the tubes. A fraction of the sprayed feed evaporates and flows as a heat source to the tubes of the second effect which is at a lower pressure and temperature than the first effect. In MVC desalination systems, the end condenser in a conventional MED is absent as the entire vapor produced in the end effect is sucked out by the mechanical compressor, where it is compressed to increase its enthalpy and used as a heating vapor for supplied feed.

In a MED-MVC, two multi-flow plate-type heat exchangers (pre-heaters) are needed to recuperate the heat coming from both the fresh water product and brine blowdown streams. The product and concentrated brine are drawn off the preheaters by pumps at a temperature slightly above the ambient seawater temperature. Cooling seawater is split up into two portions, and its temperature is elevated to the feed temperature by passing through the pre-heaters and then directed to the MED. Usually, MED-MVC systems are installed where electrical power for operation is available from the grid or through wind energy or other sources of renewable energy. However, for start-up purpose and maintaining standard operating conditions without compressor surges, external steam (make-up steam) extracted from a steam boiler or a power plant steam turbine is used to raise the 1^{st} effect temperature to the TBT [36, 113]. The mechanical energy required for the vapor compressor can be shaft driven if such power is available in a steam power plant. Also, a MVC

can be driven with power provided from the electricity grid, wind power plant, geothermal power plant [146], photovoltaic modules or electric generators if electricity services are not available [127]. The MED-MVC system is suitable for use in remote off-public electric grid locations in which water transport is expensive [114]. This energy is used to activate the MVC unit, pumps, vacuum system and any other control components. It is worth noting that the MVC unit represents the central power consuming component in a MED-MVC system. The power required depends on the pressure difference, on the thermodynamic efficiency of the polytropic process and the efficiency of the electric motor [129, 147].

Multi-effect desalination systems may be represented as some streams exchanging thermal energy among them for achieving the required evaporation [148]. Different configurations differ in the flow directions of the heating steam and the evaporating feed/concentrate or feed water supply. These configurations include forward feed (FF), parallel feed (PF), backward feed (BF) and parallel/cross feed (PCF). Schematic diagrams of different MED configurations are shown in Figure 18. In each configuration, MVC provides high-temperature steam that enters the tubes side of the first effect as a heating medium to heat and evaporate the feed seawater/brine. In the BF configuration, the entire seawater feed passing through the preheaters is directed to the last effect where it is sprayed onto the tubes, forming a thin liquid film that exchanges heat with the vapor from the previous effect. Part of the feed is evaporated while the temperature and concentration of the remaining portion increase, forming concentrated brine leaving the last effect. In the BF, both seawater feed and steam/vapor have counter-current flow directions. The brine is consecutively cascaded in backward direction through the effects till it approaches the first effect as a feed. In the FF, the entire seawater feed is supplied to the first effect at the highest TBT. The unevaporated brine with high TBT is consecutively cascaded in the forward direction (co-current with the

steam/vapor flow) towards the last effect. In the PF, the preheated feed is distributed to all the evaporator effects at the same time. The feed stream to the first effect exchanges heat with the heat source steam and forms brine while the other feed streams exchange heat with the vapor from the previous effects. Here the brine extracted from each effect is at relatively high temperature, so it is directly rejected back to the sea after exchanging heat with the cooling seawater in the brine pre-heater. In the PCF configuration, brine from the first effect is directed to the following effect to utilize its energy by flashing due to an abrupt decrease in pressure. The brine flow process continues to the last effect as shown in Figure 18.

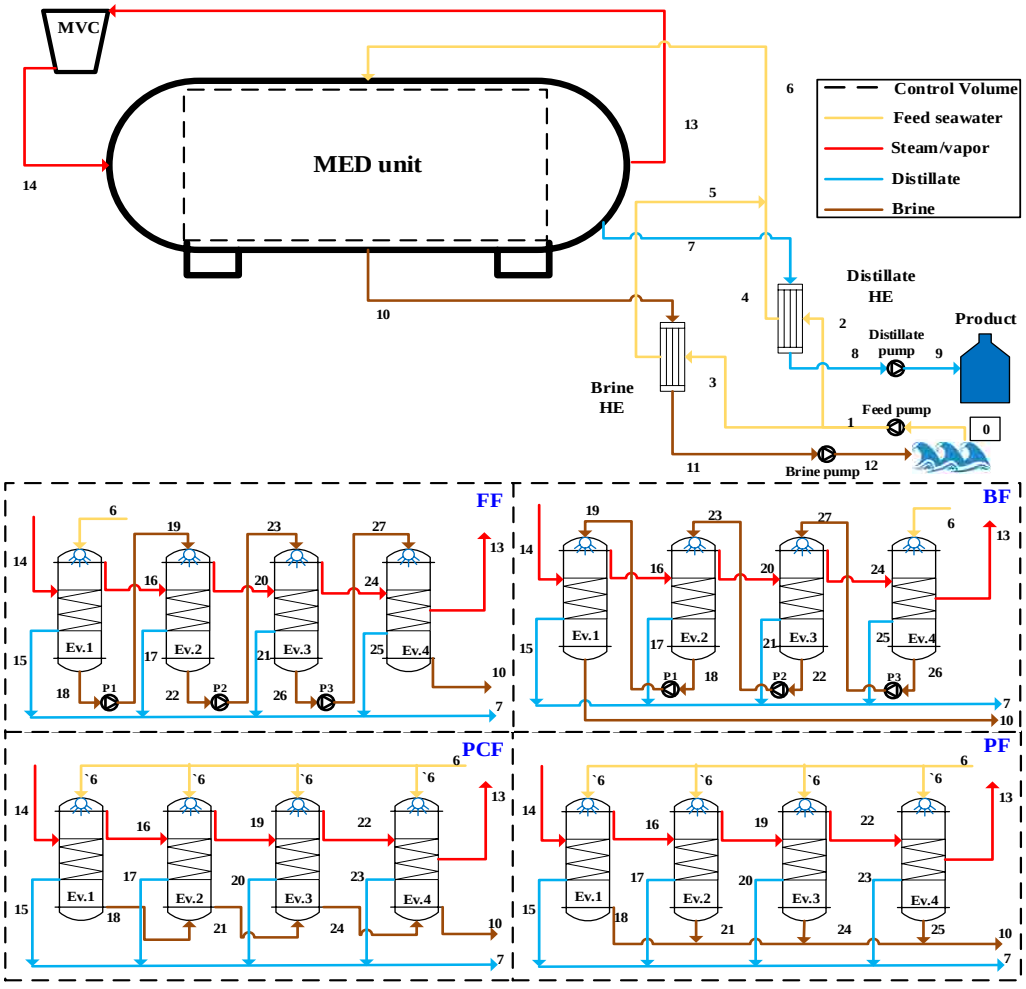

Figure 18 Flow path of different feed configurations of MED-MVC desalination system.

MVC system mathematical model

4.4.1. Energy and Exergy modeling

In this study, the steady-state operation of MED-MVC system of different feed arrangements is analyzed to pinpoint the most favorable feed arrangement from the viewpoint of exergo-economic operation. The steady-state conservation equations are solved, and iterative solution method is used to adjust the compressor power that is required to drive the evaporation process in the first effect. The steady state flow rates of the feed, brine and vapor for each evaporator effect are calculated in addition to the heat transfer surface area and brine salinity. The assumptions used to develop the steady-state model for MED-MVC system are as follows:

7. Thermophysical properties for the brine and vapor are temperature and salinity dependent. Appropriate correlations are selected from [73].
8. Temperature losses between the brine pool and vapor in the effect are; (i) Boiling Point Elevation (BPE), (ii) non-equilibrium allowance (NEA) [73].
9. The vapor and distillate are salt-free [149].
10. Pressure losses of vapor in the connections are ignored.

The mass, energy, and salt balance for BF, FF, PF, and PCF are shown in Table 11. The primary contributor to the power consumption for a MED-MVC system is the power required for the compressor which is a function of inlet vapor specific volume, compression ratio and isentropic compressor efficiency. The secondary consumptions are due to liquid pumps, vacuum pumps and steam boiler during startup [112]. Due to the fixed production capacity of different feed configurations, the amount of vapor in the last effect changes. To ensure balance in all conservation equations, the required thermal energy for the first effect is compensated by the equivalent

electricity consumption from the MVC unit. As shown in Figure 19, the energy supplied to the first effect is defined as:

$$Q_{s,1} = \dot{m}_s.\lambda_s + E_{SH} \tag{12}$$

where $\dot{m}_s\lambda_s$ represents the heat of condensation at T_s of the vapor generated in the last effect and E_{SH} represents enthalpy gained by compression above the energy at saturation condition. The enthalpy of the compressed superheated vapor at the compressor exit ($h_{v,\acute{T}_s}$) is expressed in terms of the saturation enthalpy of the compressed vapor (h_{v,T_s}), and enthalpy gained by compression as shown in Figure 19b:

$$h_{v,\acute{T}_s} = h_{v,T_s} + E_{SH}/\dot{m}_s \tag{13}$$

Hence, the actual compressor work can be calculated from:

$$\dot{W}_c = \dot{m}_s.\left(h_{v,\acute{T}_s} - h_{v,T_n}\right) \tag{14}$$

where, h_{v,T_n} is the saturated vapor enthalpy at the compressor inlet.

Specific power consumption due to the MVC unit and the installed pumps are calculated from:

$$\mathrm{SPC}(kWh/\mathrm{m}^3) = \frac{\dot{W}_{\mathrm{compressor}} + \sum \dot{W}_{\mathrm{pumps}}}{\mathrm{D}\ (\mathrm{m}^3/h)} \tag{15}$$

The performance ratio (PR) is calculated by the following relation suggested by Nafey [38] which was modified to accommodate the actual work converted to the primary fuel energy [67].

$$\mathrm{PR} = \frac{D\lambda_{distillate}}{\dot{m}_{steam}.\lambda_s + \frac{\dot{W}_{\mathrm{compressor}}}{\eta_{thermal}=0.35}} \tag{16}$$

Two multi-flow direction plate type heat exchangers with effectiveness $\varepsilon = 0.8$ are used in the current simulation to preheat seawater inlet feed by recuperating thermal energy from the distillate and the rejected brine from the MED system. The total feed is divided into two portions to flow in both the brine and distillate heat exchangers. All streams are assumed to be in a liquid phase. The heat transfer area for each heat exchanger can be calculated as follows:

$$A_{HEx} = \frac{\dot{m}_{B,D}\left(h_{10,7} - h_{11,8}\right)}{U_{B,D}.LMTD_{HEx(B,D)}} \tag{17}$$

where h is the enthalpy of the flow stream at a specified temperature as shown in Figure 18. The log mean temperature differences in the brine and distillate preheaters $LMTD_{HEx(B,D)}$ are evaluated by using the following equation:

$$LMTD_{HEx(B,D)} = \frac{\left(T_{10,7-}T_{5,4}\right) - \left(T_{11,8-}T_{cw}\right)}{ln\left[\frac{T_{10,7-}T_{5,4}}{T_{11,8-}T_{cw}}\right]} \tag{18}$$

The overall heat transfer coefficient for the plate type heat exchangers is calculated by using:

$$U_{B,D} = \left[\frac{1}{h_o} + \frac{1}{h_o} + R_{f,o} + R_{f,o} + \frac{\delta_{plate}}{K_{wall}}\right]^{-1} \tag{19}$$

where K_{wall} is the thermal conductivity of the stainless steel plates, and the inner/outer convective heat transfer coefficients (h_i, h_o) are calculated by using the following correlations [150]:

$$h_{o,i} = 0.2536Re^{0.65}Pr^{0.4}\left(\frac{K_{wall}}{D_{eq}}\right),\ Re = \frac{\rho V D_{eq}}{\mu},\ D_{eq} = \frac{4(w.t_{plate})}{2(w+t_{plate})} \sim 2t_{plate} \tag{20}$$

where w is the plate width, δ_{plate} is the plate thickness and t_{plate} is the plate spacing. The velocity of each stream is V(m/s) and Re is the stream flow Reynolds number.

As shown in Figure 19a, the solution procedure starts by assuming the brine temperature in all effects and the energy supplied to the first effect. Then, the equations in Table 11 are solved to determine the feed and brine flow rates as well as the vapor generated in each effect. The mass flow rate imbalance between the vapor generated in the last effect and the required steam for the first effect is minimized iteratively by modifying the term, E_{SH}. This calculation continues till a satisfactory specified accuracy criterion is achieved (ε=10^{-4}). The mixing temperature of the brine and distillate is used to calculate the actual feed temperature by solving the equations of the brine and distillate feed preheaters. The whole calculations are repeated till the specified feed temperature is reached.

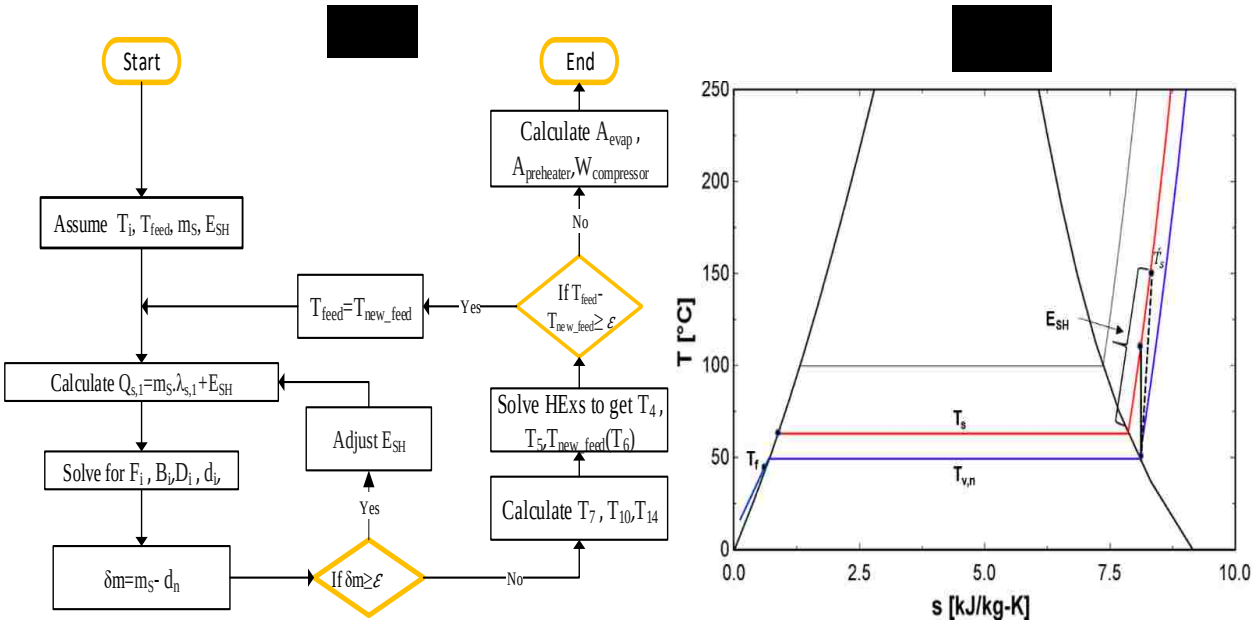

Figure 19 (a) Flow chart for solution for the steady state model, (b) T-S diagram for MED-MVC system operation.

Table 11 Steady-state balance equations for MED-MVC systems.

Configurations/Equations		First effect	Second to n-1	Last effect (n)	F	B	D
BF	Mass	$B_i = B_{i+1} - D_i$		$B_i = F - D_i$	F_n	B_1	$\sum_{i=1}^{n} D_i$
	Salt	$B_i.X_i = B_{i+1}.X_{i+1}$		$B_i.X_i = F.X_f$			
	Energy	$D_1 = \frac{Q_{s,1} - B_1(h_1 -$	$D_i = \frac{D_{i-1}.\lambda_{i-1} - B_i(h_i -$	$D_i = \frac{D_{i-1}.\lambda_{i-1} - B_i(h_i}{(\lambda_i + (h_i - h_f$			
FF	Mass	$B_1 = F - D_1$	$B_i = B_{i-1} - (D_i + d_i)$		F_1	B_n	$\sum_{i=1}^{n} D_i + d_i$
	Salt	$F.X_f = B_1.X_1$	$B_i.X_i = B_{i-1}.X_{i-1}$				
	Energy	$D_1 = \frac{Q_{s,1} - F(h_1 -}{\lambda_1}$, $d_1 = 0$	$D_i = \frac{(D_{i-1} + d_{i-1}).\lambda_{i-1}}{\lambda_i}$, $d_i = \frac{B_{i-1}(h_{i-1} - h_i)}{\lambda_i}$				
PF	Mass	$B_1 = F_1 - D_1$	$B_i = F_i - D_i$		$\sum_{i=1}^{n} F_i$	$\sum_{i=1}^{n} B_i$	$\sum_{i=1}^{n} D_i$
	Salt	$F_1.X_f = B_1.X_1$	$B_i.X_i = F_i.X_f$				
	Energy	$D_1 = \frac{Q_{s,1} - F_1(h_1 -}{(\lambda_1)}$	$D_i = \frac{D_{i-1}.\lambda_{i-1}}{\lambda_i} - \frac{F_i(h_i - h_f)}{\lambda_i}$				
PCF	Mass	$B_1 = F_1 - D_1$	$B_i = F_i - D_i + B_{i-1} - d_i$		$\sum_{i=1}^{n} F_i$	B_n	$\sum_{i=1}^{n} D_i + d_i$
	Salt	$F_1.X_f = B_1.X_1$	$B_i.X_i = B_{i-1}.X_{i-1} + F_i.X_f$				
	Energy	$D_1 = \frac{Q_{s,1} - F_1(h_1 -}{\lambda_1}$, $d_1 = 0$	$D_i = \frac{(D_{i-1} + d_{i-1}).\lambda_{i-1}}{\lambda_i} - \frac{F_i(h_i - h_f)}{\lambda_i}$, $d_i = \frac{B_{i-1}(h_{i-1} - h_i)}{\lambda_i}$				

Total mass balance $F = B + D$
Total salt balance $F.X_f = B.X_n$
d_i , Vapor produced by brine flashing.
D, Total distillate flow rate.
F, Total feed flow rate.
B, Total brine flow rate.

The exergy is known as the maximum available work obtainable when a stream of substance is brought from its initial state to the environmental state. Energy is conserved in any process according to the first law of thermodynamics, but exergy is destroyed due to irreversibilities taking place in entropy creation [80]. For an open system operating under steady state condition, the appropriate exergy rate balance is established including the loss of exergy or loss of work in the following form:

$$\sum_j \left(1 - \frac{T_o}{T_j}\right) \dot{Q}_i + \sum_i \dot{m}_i \, e_i - \sum_e \dot{m}_e \, e_e - \dot{W} - \dot{E}_D = 0 \tag{21}$$

where, $\dot{E}_D$ (kW) is the exergy destruction of the system. The specific exergy transfer terms e_i and e_e can be expressed as the summation of physical, chemical, potential and kinetic exergy [77]. The last two terms are neglected in the current simulation, so the flow exergy takes the following form,

$$e = \overbrace{h - h^* - T_o(s - s^*)}^{physical} + \underbrace{\sum_{i=1}^{n} x_i(\mu_i^* - \mu_i^o)}_{chemical} \tag{22}$$

where h, s, x and μ are specific enthalpy, specific entropy, salt mass fraction and chemical potential, respectively; subscript i represents the species in the mixture; superscript 'o' is for the ambient conditions; and superscript '*' is for the ambient pressure and temperature, and initial concentration of the system conditions. The second law exergetic efficiency for the MED-MVC systems is the ratio of the minimum exergy input required (which is equivalent to the minimum work of separation) to the total actual exergy input. Second law efficiency is used as a criterion of system performance and is calculated considering the exergy loss from the process to the environment as:

$$\eta_{II} = 1 - \frac{\dot{E}_{D,total}}{\dot{E}_{in,total}} = \frac{\dot{W}_{min}}{\dot{E}_{in,total}} \tag{23}$$

where, $\dot{E}_{in,total}$ is the total exergy at the various inlet fluid streams and work provided to the compressor and installed pumps; and $\dot{W}_{min}$ is the minimum work input for the separation of a certain amount of seawater feed at 25°C, 1 atm and a salinity of 36 ppt into fresh water with zero salinity and the rejection of a certain amount of saline water at the same temperature and pressure. The minimum work is equal to the difference between the exergies of the outgoing and incoming

streams as well as the exergy difference due to salinity change. The exergy of the supplied feed seawater is approximately zero as its state is considered as the reference state for exergy calculations [151].

$$\dot{W}_{min} = \dot{E}_9 + \dot{E}_{12} - \dot{E}_0 \quad (24)$$

The exergy analysis is more revealing when the analysis is performed at the component level of different MED-MVC feed configurations. The sites of maximum exergy destruction can be identified. Also, the fraction of exergy destruction within the components is determined to quantify the percentage of exergy destruction in all components for different feed configurations. The exergy balance equation for each component is discussed in detail in the exergo-economic section.

4.4.2. Economic models

a) Simple model

The production cost is divided into the direct/indirect cost and annual operating cost. The direct capital cost (DCC) represents the expenses that are directly associated with the construction of the MED plant and the equipment purchasing expenses [93]. Table 12 presents the existing equations in the literature that are used to determine the purchase price of the MED-MVC system components. The other direct cost (land, well construction, auxiliary equipment and building construction) is calculated from [95] for the fixed capacity of 1500 m^3/day to be ~ 80k $. The DCC is equal to the summation of the purchased equipment for the MED-MVC system in Table 12 plus the other costs. Also, the indirect capital cost (freight, insurance, construction overhead, owner's costs and contingency costs) is expressed as a percentage of the total direct capital cost and is assumed as ID_{CC}=0.15DCC [95].

Table 12 Purchase cost of MED-MVC system components.

Instrument	Capital cost of instrument (Z_k) ($)	Comments	Ref.
Preheater (heat exchanger)	$\mathbf{Z}_{preheater} = \mathbf{1000}(\mathbf{12.82} + \boldsymbol{A}_{Hex}^{\mathbf{0.8}})$	S for shell side and t for tube side $\boldsymbol{dp}$ (kPa), A (m^2), $\boldsymbol{U}$ $(\boldsymbol{kW/m^2.k})$	[74]
MED effect (evaporator)	$\mathbf{Z}_{effect} = \mathbf{250.26} \times \boldsymbol{UA}_{evaporator}\boldsymbol{dp}_t^{-0.01}\boldsymbol{dp}_s^{-0.1}$		[94]
Water pump	$\mathbf{Z}_{pump} = \mathbf{13.92} \times \dot{\boldsymbol{m}}_{water}{}^{0.55}\Delta\boldsymbol{P}^{0.55}\left(\frac{\eta_p}{1-\eta_p}\right)^{1.05}$	$\boldsymbol{\eta_p} = \mathbf{0.9}$, $\Delta\boldsymbol{P}$ $(\boldsymbol{kPa})$	
		BF FF PF PCF	
		Number of pumps 6 6 3 3	
Compressor (MVC)	$\mathbf{Z}_{MVC} = \mathbf{794.68} \times \dot{\boldsymbol{W}}_{compressor} + \mathbf{66.11}$	$\dot{\boldsymbol{W}}_{compressor}$ (Watt)	[95]
Other direct costs	$\mathbf{Z}_{rest} = \mathbf{21635.4} \times \boldsymbol{D}^{\mathbf{0.1773}}$	$\boldsymbol{D}$ (m^3/day)	

The operating cost includes all expenses needed after plant commissioning and during plant operation. These expenses can be categorized as variable and fixed costs. The variable operating expenses are those related to the purchase of electrical power, heating steam, chemicals for pre/post-treatment and other requirements that are dependent on the plant capacity of fresh water production and standards. The fixed operating costs represent expenses that are needed for the operation of the plant but are independent of the plant capacity. In many cases, these costs are related to the designed capacity of the plant or taken as a factor of the direct capital cost (DCC). A cost index C_{index} =1.2 is used to accommodate the equipment price change to fit the current reference year calculations. A linearly dependent correlation for the compressor cost of the compressor power is used based on the work done by Lukic et al. [95]. Both operating cost categories are determined based on published data from the literature [73] with maintenance costs taken as a proper subset of the fixed operating cost. Investment and operating & maintenance costs analyses are performed for each configuration using an interest rate set at 5%. The annualized cost method is used to estimate the annual capital cost of system components in this study for 20 years

plant lifetime and plant maintenance factor (ϕ) of 1.06. Table 13 illustrates the equations used to calculate the annual capital and operating costs using the amortization cost.

Table 13 Cost parameters for MED desalination plant.

Parameter	Equation	Comments	Ref.
Capital recovery factor, 1/y	$\boldsymbol{CRF = \frac{i.(1+i)^{nt}}{(1+i)^{nt}-1}}$	i is the interest rate 5%, nt (20 year)	[152]
Annual fixed charges, $/y	$\boldsymbol{AFC = (1.38 \times DCC) \times CRF}$		[73]
Annual electric power cost, $/y	$\boldsymbol{AEPC = C_e \times SPC \times \phi \times D \times 365}$	Specific electricity cost $\boldsymbol{C_e = 0.08 \frac{\$}{kWh}}$	
Annual chemical cost, $/y	$\boldsymbol{ACC = SCC \times \phi \times D \times 365}$	Specific chemical cost $\boldsymbol{SCC = 0.025 \frac{\$}{m^3}}$	
Annual labor cost, $/y	$\boldsymbol{ALC = SLC \times \phi \times D \times 365}$	Specific labor cost $\boldsymbol{SLC = 0.1 \frac{\$}{m^3}}$	
Operating and maintenance annual cost, $	$\boldsymbol{OMC = 0.02 \times CRF \times DCC}$		
Total annual cost, $/y	$\boldsymbol{TAC = AFC + AEPC + ACC + ALC + OMC}$		
Total water price $/m^3	$\boldsymbol{TWP_{simple} = \frac{TAC.\phi}{D \times 365}}$		

b) Exergy-economic model

In the estimation and cost analysis of an energy system, it is essential to obtain and compare the annualized values of fuel costs, capital or carrying charges, and the operating and maintenance (O&M) expenditures. Within the system economic operating life, the component costs may vary significantly. Therefore, annualized values for all cost components should be used in the estimation and cost analysis optimization for proper economic analysis [83]. In this regard, the hourly capital investment (CI) cost for each component based on the actual annual number of operating hours (N) is calculated as:

$$\dot{Z}_k^{CI}(\$/h) = \frac{Z_k.CRF.\phi}{N} \quad (25)$$

The exergo-economic analysis is used to calculate the cost rate of the product streams of the system. The cost balance expresses the variable $\dot{C}$ that indicates a cost rate associated with an exergy stream: a stream of matter, power, or heat transfer. According to the conservative nature of

costs [97], the cost rate associated with the system product $\dot{C}_P \left(\frac{\$}{h}\right)$ is equal to the total rate of expenditure used to generate this product in a component, namely the fuel cost resulting from the cost associated with the exergy flows $\dot{C}_F \left(\frac{\$}{h}\right)$ and the cost rates associated with the CI and OM as:

$$\dot{C}_P = \sum \dot{\mathrm{C}}_F + \dot{Z}_k^{CI+OM} \tag{26}$$

The above cost balance equation is applied to the MED-MVC system components to obtain the product stream cost. Typically, the number of unknown cost parameters is higher than the number of cost balance equations for the component, so additional auxiliary thermodynamic equations are used to accommodate this difference. Usually, the auxiliary equations represent the equality of the average cost of the inlet and exit for the same stream, and they are formulated based on different principles (exergy extraction, multiple outputs, and external assessment) as shown in Table 14. To obtain the exergy definition equations for fuel and product for the MED-MVC components, all $\dot{C}$ in the fuel and product columns in Table 14 are replaced by $\dot{E}$ and linear system of equations are used to solve the exergy balance equation to obtain the component exergy destruction. For the mixing points, the product cost is considered as the summation of cost rate for the inlet points while for splitting points the outlet cost rate streams are equally divided. The exergy and cost balance equations for the inter-effects pumps in the cases of FF and PF are presented in Table 15.

To include the labor and chemical cost (non-exergy related costs) in the exergo-economic analysis, inlet feed stream to the feed pump is considered as $\dot{C}_o(\$/h) = (SLC + SCC)(\$/m^3) \times D(m^3/h)$. Also, the summation of the outlet stream flow rate cost must be equal to the sum of the carrying charges, fuel cost rate and the operating and maintenance calculated on a per hour basis to satisfy the cost rate balance for the total system [98]. Finally, the total water price ($\mathrm{TWP}_{exergo-economic}$)

($\$/m^3$) from the exergo-economic analysis is calculated by dividing the cost rate of the product ($\$/h$) from the distillate pump by the total production rate of the plant (m^3/h). The linear system of algebraic equations presented in Table 11 to Table 15 are solved by consideration of the cost of the electrical energy used for the pump and compressor as 0.08 $/kWh [99]. The results from the cost exergy model are sufficient for (a) providing more details from an economic standpoint to enable the calculation separately of the product stream cost at any intermediate state in the system; (b) understanding the cost formation process and the flow of costs in the system to highlight the involvement of each component in the final cost and offer an opportunity to identify the cost concentrated components that need attention to achieve a lower product cost [98]. Three important parameters for evaluating the exergo-economic analysis of the thermal energy systems are calculated using the component exergetic efficiency (ϵ_k) and average cost per unit fuel exergy $c_{F,k}$. The variables include: the exergy destruction cost rate ($\dot{C}_{D,k}$), relative cost difference (r_k) and the exergo-economic factor (f_k) which are given by Eqs. (16)–(18) [98].

$$\dot{C}_{D,k} = c_{F,k}\dot{E}_{D,k} \tag{27}$$

$$r_k = \frac{1-\epsilon_k}{\epsilon_k} + \frac{\dot{Z}_k^{CI+OM}}{c_{F,k}\dot{E}_{P,k}} \tag{28}$$

$$f_k = \frac{\dot{Z}_k}{\dot{Z}_k + \dot{C}_{D,k}} \tag{29}$$

The r_k for a component represents the average cost per exergy unit between fuel and product and it is useful to evaluate and optimize a system component. The higher value of the total operating cost $\dot{C}_{D,k} + \dot{Z}_k$ indicates the higher influence of the component on the overall system performance, therefore in designing a new system, the first design changes must initially be applied to that component. The f_k is used to identify the relative significance of non-exergy related costs (CI&OM) to the sum of CI, O$M and the exergy destruction cost rate. A low value of f_k for major

components suggests that the cost saving for the system could be accomplished by improving the components efficiency (reduction of exergy destruction) even if the capital cost investment increases [98].

Table 14 Fuel and product cost rates of the MED-MVC system components.

		Fuel	Product	Capital and investment	Auxiliary equation
Feed pump		$C_e.\dot{W}_{FP} + \dot{C}_o$	$\dot{C}_1$	$\dot{Z}_{FP}$	--
Brine pump		$C_e.\dot{W}_{BP} + \dot{C}_{11}$	$\dot{C}_{12}$	$\dot{Z}_{BP}$	--
Distillate pump		$C_e.\dot{W}_{DP} + \dot{C}_8$	$\dot{C}_9$	$\dot{Z}_{DP}$	--
MVC unit		$C_e.\dot{W}_{compressor} + \dot{C}_{13}$	$\dot{C}_{14}$	$\dot{Z}_{compressor}$	--
Brine heater		$\dot{C}_3 + \dot{C}_{10}$	$\dot{C}_5 + \dot{C}_{11}$	$\dot{Z}_{F/B}$	$\frac{\dot{C}_{10}}{\dot{E}_{10}} = \frac{\dot{C}_{11}}{\dot{E}_{11}}$
distillate heater		$\dot{C}_2 + \dot{C}_7$	$\dot{C}_4 + \dot{C}_8$	$\dot{Z}_{F/D}$	$\frac{\dot{C}_7}{\dot{E}_7} = \frac{\dot{C}_8}{\dot{E}_8}$
1st effect	BF	$\dot{C}_{19} + \dot{C}_{14}$	$\dot{C}_{15} + \dot{C}_{16} + \dot{C}_{10}$	$\dot{Z}_{Ev,1}$	$\frac{\dot{C}_{14}}{\dot{E}_{14}} = \frac{\dot{C}_{15}}{\dot{E}_{15}}$ & $\frac{\dot{C}_{19}}{\dot{E}_{19}} = \frac{\dot{C}_{10}}{\dot{E}_{10}}$
	FF	$\dot{C}_6 + \dot{C}_{14}$	$\dot{C}_{15} + \dot{C}_{16} + \dot{C}_{18}$		$\frac{\dot{C}_{14}}{\dot{E}_{14}} = \frac{\dot{C}_{15}}{\dot{E}_{15}}$ & $\frac{\dot{C}_6}{\dot{E}_6} = \frac{\dot{C}_{18}}{\dot{E}_{18}}$
	PF	$\dot{C}_{\acute{6}} + \dot{C}_{14}$			$\frac{\dot{C}_{14}}{\dot{E}_{14}} = \frac{\dot{C}_{15}}{\dot{E}_{15}}$ & $\frac{\dot{C}_{\acute{6}}}{\dot{E}_{\acute{6}}} = \frac{\dot{C}_{18}}{\dot{E}_{18}}$
	PCF				
2nd effect	BF	$\dot{C}_{16} + \dot{C}_{23}$	$\dot{C}_{17} + \dot{C}_{18} + \dot{C}_{20}$	$\dot{Z}_{Ev,2}$	$\frac{\dot{C}_{16}}{\dot{E}_{16}} = \frac{\dot{C}_{17}}{\dot{E}_{17}}$ & $\frac{\dot{C}_{23}}{\dot{E}_{23}} = \frac{\dot{C}_{18}}{\dot{E}_{18}}$
	FF	$\dot{C}_{16} + \dot{C}_{19}$	$\dot{C}_{17} + \dot{C}_{20} + \dot{C}_{22}$		$\frac{\dot{C}_{16}}{\dot{E}_{16}} = \frac{\dot{C}_{17}}{\dot{E}_{17}}$ & $\frac{\dot{C}_{19}}{\dot{E}_{19}} = \frac{\dot{C}_{22}}{\dot{E}_{22}}$
	PF	$\dot{C}_{\acute{6}} + \dot{C}_{16}$	$\dot{C}_{17} + \dot{C}_{19} + \dot{C}_{21}$		$\frac{\dot{C}_{16}}{\dot{E}_{16}} = \frac{\dot{C}_{17}}{\dot{E}_{17}}$ & $\frac{\dot{C}_{\acute{6}}}{\dot{E}_{\acute{6}}} = \frac{\dot{C}_{21}}{\dot{E}_{21}}$
	PCF	$\dot{C}_{\acute{6}} + \dot{C}_{16} + \dot{C}_{18}$			
3rd effect	BF	$\dot{C}_{20} + \dot{C}_{27}$	$\dot{C}_{21} + \dot{C}_{24} + \dot{C}_{22}$	$\dot{Z}_{Ev,3}$	$\frac{\dot{C}_{20}}{\dot{E}_{20}} = \frac{\dot{C}_{21}}{\dot{E}_{21}}$ & $\frac{\dot{C}_{22}}{\dot{E}_{22}} = \frac{\dot{C}_{27}}{\dot{E}_{27}}$
	FF	$\dot{C}_{20} + \dot{C}_{23}$	$\dot{C}_{21} + \dot{C}_{24} + \dot{C}_{26}$		$\frac{\dot{C}_{20}}{\dot{E}_{20}} = \frac{\dot{C}_{21}}{\dot{E}_{21}}$ & $\frac{\dot{C}_{23}}{\dot{E}_{23}} = \frac{\dot{C}_{26}}{\dot{E}_{26}}$
	PF	$\dot{C}_{\acute{6}} + \dot{C}_{19}$	$\dot{C}_{20} + \dot{C}_{22} + \dot{C}_{24}$		$\frac{\dot{C}_{19}}{\dot{E}_{19}} = \frac{\dot{C}_{20}}{\dot{E}_{20}}$ & $\frac{\dot{C}_{\acute{6}}}{\dot{E}_{\acute{6}}} = \frac{\dot{C}_{24}}{\dot{E}_{24}}$
	PCF	$\dot{C}_{\acute{6}} + \dot{C}_{19} + \dot{C}_{21}$			
4th effect	BF	$\dot{C}_6 + \dot{C}_{24}$	$\dot{C}_{13} + \dot{C}_{25} + \dot{C}_{26}$	$\dot{Z}_{Ev,4}$	$\frac{\dot{C}_{24}}{\dot{E}_{24}} = \frac{\dot{C}_{25}}{\dot{E}_{25}}$ & $\frac{\dot{C}_6}{\dot{E}_6} = \frac{\dot{C}_{26}}{\dot{E}_{26}}$

	Fuel	Product	Capital and investment	Auxiliary equation
FF	$\dot{C}_{24} + \dot{C}_{27}$	$\dot{C}_{13} + \dot{C}_{10} + \dot{C}_{25}$		$\frac{\dot{C}_{24}}{\dot{E}_{24}} = \frac{\dot{C}_{25}}{\dot{E}_{25}}$ & $\frac{\dot{C}_{27}}{\dot{E}_{27}} = \frac{\dot{C}_{10}}{\dot{E}_{10}}$
PF	$\dot{C}_{6'} + \dot{C}_{22}$	$\dot{C}_{23} + \dot{C}_{13} + \dot{C}_{25}$		$\frac{\dot{C}_{22}}{\dot{E}_{22}} = \frac{\dot{C}_{23}}{\dot{E}_{23}}$ & $\frac{\dot{C}_{6'}}{\dot{E}_{6'}} = \frac{\dot{C}_{25}}{\dot{E}_{25}}$
PCF	$\dot{C}_{6'} + \dot{C}_{22} + \dot{C}_{24}$	$\dot{C}_{23} + \dot{C}_{13} + \dot{C}_{10}$		$\frac{\dot{C}_{22}}{\dot{E}_{22}} = \frac{\dot{C}_{23}}{\dot{E}_{23}}$ & $\frac{\dot{C}_{6'}}{\dot{E}_{6'}} = \frac{\dot{C}_{10}}{\dot{E}_{10}}$

Table 15 Cost and exergy balance equations for inter-effects pumps for BF and FF MED-MVC systems

Configuration	Exergy balance	Cost rate balance
Pump$_1$	$\dot{E}_{D,P1} = \dot{E}_{18} + \dot{W}_{P1} - \dot{E}_{19}$	$\dot{C}_{19} = \dot{C}_{18} + C_e.\dot{W}_{P1} + \dot{Z}_{P1}$
Pump$_2$	$\dot{E}_{D,P2} = \dot{E}_{22} + \dot{W}_{P2} - \dot{E}_{23}$	$\dot{C}_{23} = \dot{C}_{22} + C_e.\dot{W}_{P2} + \dot{Z}_{P2}$
Pump$_3$	$\dot{E}_{D,P3} = \dot{E}_{26} + \dot{W}_{P3} - \dot{E}_{27}$	$\dot{C}_{27} = \dot{C}_{26} + C_e.\dot{W}_{P3} + \dot{Z}_{P3}$

c) Aggregation level exergy cost model

Exergy cost model can be applied considering only the overall system as a group of components (MED-MVC plant as a whole unit) [98]. To study the effect of the aggregation level on the cost estimation, consider an overall system as shown in Figure 20 for the MED-MVC system. The cost rate balance for the MED-MVC system using the aggregation level is as follows:

$$\dot{C}_9 = \dot{C}_0 + \dot{Z}_{total}^{CI+O\&M} + C_e.\left(\dot{W}_{\text{compressor}} + \dot{W}_{pumps}\right) - \dot{C}_{12} \quad (30)$$

where $\dot{Z}_{total}^{CI+O\&M}$ represents the hourly CI cost and OM for all MED-MVC components.

The previous equation involves two unknowns: the cost per exergy unit associated with brine and distillate streams. Therefore, one auxiliary relation is required before these unknowns can be determined. For simplicity the auxiliary equation for this aggregated system is considered as: $\frac{\dot{C}_{12}}{\dot{E}_{12}} = \frac{\dot{C}_9}{\dot{E}_9}$. The total water price from aggregation method ($\text{TWP}_{aggregation}$) $(\$/m^3)$ is calculated by dividing the cost rate of all the outlet streams (distillate and brine) $(\$/h)$ by the total production

rate (D) of the plant (m^3/h). Equation (19) could represent any desalination system that uses electricity to produce fresh water.

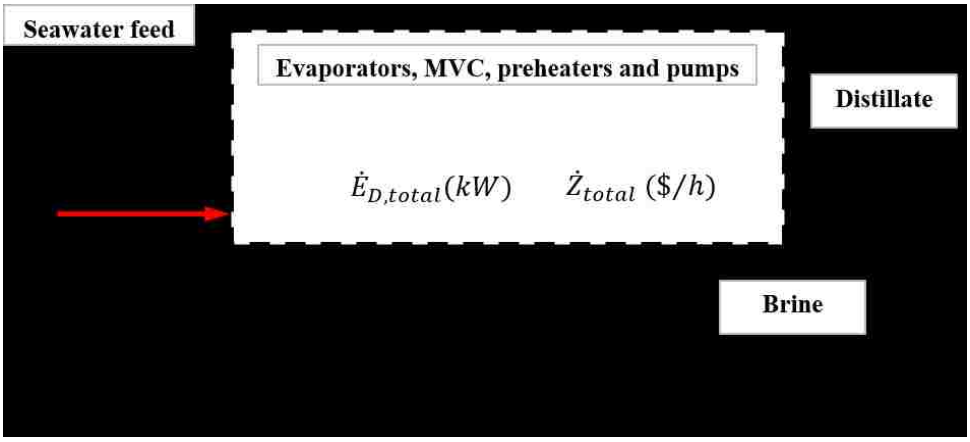

Figure 20 Aggregation level for exergy costing for MED-MVC system

Results and discussion

4.5.1. Model validation

As a first step to validate the developed model using the Engineering Equation Solver (EES) software, a comparison is made between the calculated and actual parameters of two MVC systems available in the literature. As shown in Table 16, the single-effect MVC model provides predictions very close to the actual data reported for a MVC plant located in Spain [112]. Furthermore, the results from the MED-MVC model compare very well with the actual operational parameters of a two-effect MED-MVC plant located in India operating in the PCF configuration [141]. The current models are therefore validated because the maximum deviation between the model predictions and the actual data is under 7%.

Table 16 Validation of the single-effect MVC and MED-MVC with PCF models.

Parameter	1-effect MVC	Veza [112]	% error	2-effect MVC	Kishore et al. [141]	% error
Inlet feed salinity, g/kg	38		-	35		-
Outlet brine salinity, g/kg	65		-	70		-
Steam temperature T_s, °C	61.1		-	65.0		-
last brine temperature T_n, °C	-		-	60.0		-
Pressure ratio	1.1			1.26		
Distillate production, (D)m^3/h	20.92	20.8	0.6	2.03	2.09	2.9
Feed flow (F), m^3/h	50.37	50	0.75	4.06	4.16	2.4
Brine flow (B), m^3/h	29.45	29	1.6	2.03	2.08	2.4
Feed temperature T_f, °C	53.7	55	2.4	56.0	NA	-
Compressor work ($\dot{W}_{comp}$), kW	228	240	5	29.59	28.41	4.2
Performance ratio PR	0.89	NA	-	1.83	NA	-
heat transfer area, $m^2/kg/s$	469.9	448.9	4.7	371.1	349.8	6.1
Total SPC, kWh/m^3	13.25	14	5.4	14.57	13.64	6.8
Total water price (TWP), $\$/m^3$	2.69	2.8	3.9	2.34	NA	-

4.5.2. Energetic and exergetic analysis

The current work is focused on modeling of MED-MVC systems operating with four different feed configurations using the first and second law of thermodynamics accompanied with exergo-economic analysis. The developed model is applied to a MED-MVC system with four effects. The different feed arrangements are compared to identify the most reliable configuration considering energetic and exergo-economic analysis for cost flow rate for each component. The steady-state input operating conditions (base case) adopted for all configurations are shown in Table 17. These conditions are obtained from an actual MED-MVC plant located in France [113]. From the 1st law energy analysis, the PCF and FF configurations require less work to produce the same amount of distillate. The PR also compares favorably to the other configurations as shown in Table 17. The calculated SPC values are 30.1, 13.7, 23 and 13.9 kWh/m^3 for the BF, FF, PF and PCF

configuration, respectively. The required compressor work for the BF configuration is the highest which is due to the increase in the E_{SH} term to compensate for the small value of vapor flow rate recovered from the last effect. On the other hand, the FF requires the lowest work to achieve the same production capacity. Changing the feed arrangement from BF to FF and PF to PCF at a constant compression ratio, the SPC is reduced by 54% and 39%, respectively. The FF configuration has the highest electric power needed to operate the feed, brine, distillate pumps as well as the inter-effects pumps. The performances of the MED-MVC operating in the PCF and FF configurations are comparable and are higher than those in the BF and PF configurations. This is primarily due to the decrease in compressor work consumption and the more efficient reuse of the hot brine. In the FF and PCF configurations, the hot brine passes in the forward direction where the pressure decreases from one effect to the next which allows brine flashing to occur.

Table 17 Steady-state specifications of MED-MVC different process configurations.

Configuration	BF	FF	PF	PCF
Number of effects (N)	4			
Inlet feed content, g/kg	36			
Outlet brine content, g/kg	65			
Inlet steam temperature T_s, °C	62.5			
last brine temperature T_n, °C	50.3			
Feed temperature T_f, °C	49			
Pressure ratio	1.852			
Distillate production, (D)m^3/h	63.36			
Feed flow (F), m^3/h	141.98			
Brine flow (B), m^3/h	78.66			
Heat source flow rate (S), kg/s	4.12	4.6	4.27	4.35
Performance ratio PR	2.89	3.19	3.02	3.33
Specific heat transfer area (S_A), $m^2/kg/s$	288.9	260.2	211	227.2
Compressor actual work (W_a), kW	1873	845.1	1430	862
Pumps work, kW	10.4	13.1	7.5	7.5

The first step in any improvement or enhancement project is diagnostics, and the most powerful diagnostics tool in thermodynamics is second law analysis. Exergy analysis overcomes many of

the shortcomings of energy analysis and identifies the causes, locations and actual magnitudes of waste due to thermodynamic inefficiency. Starting with the minimum work of separation $\dot{W}_{min}$ for the separation of 39.4 kg/s of seawater into 17.6 kg/s of fresh water and 21.8 kg/s of brine with a salinity of 65 ppt at the same temperature and pressure. The value of $\dot{W}_{min}$ was determined independently using the relation developed by Cerci [153] as 28.2 kW for recovery ratio of ~40%. For the BF, FF, PF and PCF configurations, the value of $\dot{W}_{min}$ obtained from equation (13) is 44.8, 22.4, 34.6 and 23.7 kW, respectively. The exergy analysis was carried out to estimate the component irreversibilities to obtain the rates of exergy destruction and the percentage of each component so that the locations with the highest exergy destruction can easily be identified for the MED-MVC system with different feed configurations as shown in Figure 21.

Generally, there are two causes of exergy destruction in the MED-MVC systems. The first is heat transfer across the temperature difference between hot and cold streams in each evaporator effect and the preheaters, resulting in process irreversibility. In addition, exergy destructions in the pumps and compressor are due to irreversibilities in the compression process. The second is the exergy discharge, through brine and distillate, into the environment. The MVC unit and evaporators are significant sources of exergy destruction in the MED-MVC systems which range between 86 and 90% for all configurations. These high levels can be attributed to the thermodynamic inefficiency of the MVC unit and the heat transfer in the effects that are associated with phase change process. MVC has the highest exergy destruction percentages for the BF and PF configurations while the percentages are lower at the evaporators. The reverse is true for the FF and PCF configurations. For all configurations, the first effect has the highest exergy destruction among the four effects. The high exergy destructions in the evaporators indicate that

the evaporation process itself is highly inefficient. Therefore, modifications and improvements to the process should be considered. The exergy destruction can be reduced by increasing the number of effects, though the number is limited by the compression ratio of MVC units currently available. Also, if the temperature difference within each effect is lowered to reduce exergy destruction, economic consideration due to increasing the heat transfer surface needed to achieve evaporation and condensation processes should be accounted. Other components such as brine and distillate feed heaters have the second lowest share in the exergy destruction of the systems that range between 7.6 and 10.9% for all configurations. The exergy destruction for both feed heaters changes slightly with feed configuration due to the constant flow rates and the small differences in the hot and cold side flow stream temperatures. Moreover, Figure 21 shows that the exergy destruction in the pumps accounts for a negligible share of the total exergy destruction for the PCF and PF configurations. However, due to inter-effects pumps in BF and FF configurations, exergy destruction percentage due to pumps increases to 1.63 and 3.76%, respectively, compared to the PF and PCF configurations without inter-effects pumps.

By calculating the second law efficiency for all configurations, the results show that the PCF configuration has the highest value followed by the FF configuration, while the BF configuration exhibits the lowest value among all configurations. This indicates how crossing the hot brine between effects to acquire its energy through flashing is beneficial in both increasing the evaporation amount in each effect and in improving the total system performance. Furthermore, it should be noted that the calculated exergetic efficiency is quite low as 2.38, 2.73, 2.4 and 2.92% for the BF, FF, PF and PCF configurations, respectively. These values are close to the exergetic efficiency presented in Refs. [38, 154, 155] for similar plants. The performance and economics of

the MED–MVC system are compared to those of conventional MED and MED-TVC systems with a similar capacity. The considered MED and MED-TVC systems operated in the PCF configuration with a bottom condenser and were investigated using a model developed by El-Dessouky and Ettouney [73] under the similar constraints for the same freshwater production (17.6 kg/s) and rejected brine salinity (65 ppt). The simulation shows that the required mass flow rate of the steam supplied to the 1st effect is 5.13 and 2.7 kg/s for MED and MED-TVC, respectively compared to 4.4 kg/s in case of MED-MVC. To account for the difference in input energy of MED (steam) and MED-MVC (electrical), the input exergy definition for MED-MVC is modified by assuming the thermal efficiency for the power plant supplying the electrical energy to the MVC unit is equal to 40%. The calculated values of gained output ratio (GOR=fresh water per steam required) and TWP for fresh water generation of 1500 m^3/d are 3.99[-] and 1.6 \$/m^3 for MED–MVC, 3.43[-] and 3.1 \$/m^3 for conventional MED and 6.4[-] and 2.6 \$/m^3 for MED-TVC as reported in [90, 156]. The MED-MVC saves approximately 50% in the cost of freshwater production compared to the conventional MED system. Furthermore, no condenser is required for heat rejection as in the conventional MED or MED-TVC systems. However, from the exergy point of view, the exergy efficiency of MED–MVC (2.9%) is much lower than the conventional MED (11.9%) or MED-TVC (4.6%). The low exergy efficiency is due to the fact that the MED-MVC systems are inefficient as they convert electrical energy into thermal energy.

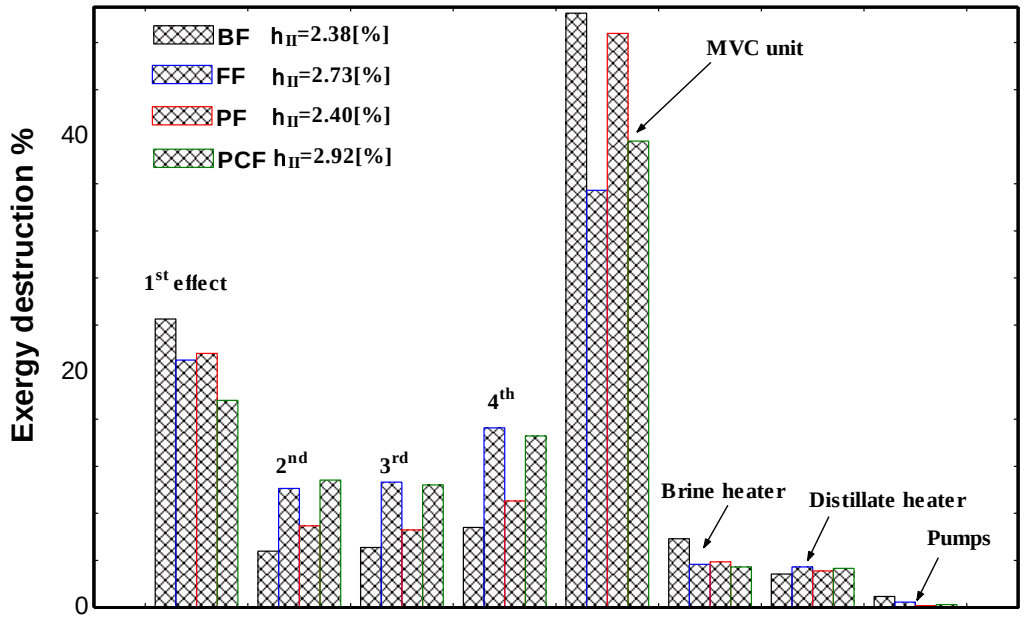

Figure 21 Percentage of exergy destruction for main component of various feed MED-MVC systems.

4.5.3. Economic and exergo-economic analysis

The component costs on the hourly basis for different feed configurations are presented in Table 18. The most expensive components are the evaporators and compressor, and the cheapest equipment is the pumps. For the BF and PF arrangements, the price of the MVC unit is high due to the high actual work required to achieve the given fresh water production. The fixed cost for the BF is the highest compared to other configurations. Also, Table 18 illustrates that by changing the feed arrangement from BF to FF and PF to PCF at a constant compression ratio, the total fixed cost for the MED-MVC plant is reduced by ~ 30% and 17%, respectively.

Table 18 Fixed cost rate per hour for different feed MED-MVC system components.

Component	BF	FF	PF	PCF
Feed pump	0.17			
Brine pump	0.13			
Distillate pump	0.11			
MVC unit	20.9	9.7	15.9	10.0
Brine heater	0.5	0.75	0.6	0.75
Distillate heater	0.54	1.0	0.67	1.0
1st effect	7.63	4.13	3.7	3.6
2nd effect	4.8	4.31	3.1	3.0
3rd effect	3.8	4.48	3.5	3.5
4th effect	3.5	4.67	3.8	3.8
Inter-effects pumps	0.25	0.27	--	--
Total ($/h)	42.4	29.7	31.7	26.2

A simple conventional economic model treating the MED-MVC plant as a whole unit is used to calculate the annualized cost of the plant and to estimate the total water price for a MED-MVC system. The model shows that changing the plant layout by moving from BF to FF or from PF to PCF will reduce the TWP estimated from the economic model by 45% or 31%, respectively as shown in Table 19. However, to indicate the share of each flow stream and each component in the total cost of the product, the economic analysis based on exergy is applied to all MED-MVC configurations. When conducting a thermoeconomic analysis for the current MED-MVC system, a cost balance equation is used to correlate the exergy instead of the energy of the flow stream with the pricing value of a component. This cost balance, combined with appropriate auxiliary thermo-economic relations, result in a system of linear algebraic equations, which can be solved for the unknown values of cost rates or of cost per exergy unit. As mentioned before, non-exergy related costs including chemical cost and labor cost are added to the exergo-economic model as input stream in the feed seawater. Further, it should be mentioned that there is no additional information to appropriately apportion the value of other cost and indirect cost between the product streams (distillate and brine) in the cost exergy equations. The other cost (80k $) and indirect cost

(0.15DCC) are calculated on a per hour basis, and a value of 3.59 $/h is obtained. For simplicity, these costs are divided equally between the distillate and brine streams to adjust the final distillate stream price. Solving the exergy-cost balance equations, the cost rates for the various stream at different locations in the MED-MVC plant are obtained.

The effects of variation of the economic parameters such as cost index factor (C_{index}), interest rate (i), and electricity cost (C_e) on the TWP for different feed configurations of a MED-MVC system are presented in Figure 22. The cost index and interest rate affect the fixed cost and the capital investment of the plant while electricity cost affects the plant operating cost. Increasing the cost index from 1 to 2 has a smaller effect than a change in interest rate. Increasing the interest rate from 2 to 15% translates to a total water price increase in the range of 22 to 28%. The fuel cost to operate a MED-MVC plant (electricity cost) depends on the plant location associated with different electricity production prices. The main energy consumption of a MED-MVC desalination system is represented by the electricity requirement which is required to operate the MVC unit and the installed pumps. Increasing the electricity cost has a significant effect on the TWP compared to other economic parameters. For low values of C_e, the PF and FF configurations have a TWP of ~1 \$/m^3 and PCF has a TWP of 0.77 \$/m^3. On the other hand, for high values of C_e, the FF and PCF configurations have nearly the same TWP. This could be explained as follows, for low price of electricity, the cost of evaporator installation (heat transfer area) dominates the water production price; while for high price of electricity, the cost of the MVC unit dominates the TWP for the same plant capacity. If the MED-MVC with the PCF configuration is integrated to a power generation cycle in two regions with a different price of $C_e = 0.03$ and 0.09 \$/kWh, the TWP will be 0.92 and 1.85 \$/m^3, respectively. A 200% increase in C_e increases the TWP by approximately 100%. These

results reveal that the most important parameter that cannot be neglected while comparing different installation areas for MVC systems is the electricity cost.

Using average values of the economic parameters (C_{index} =1.2, i=5% and C_e=0.08 \$/kWh), the cost rate pricing for the FF, PF and PCF configurations for all flow streams through the MED-MVC system are shown in Figure 23. Also, Table 19 shows the final estimated total water price using the three methods (simple conventional economic model, exergy-based component cost model and exergy aggregation model). These estimates are consistent with the results for thermal desalination units found in the literature [38, 95, 157, 158]. Besides showing the cost flow rate at each stream point, Figure 22 shows the flow exergy, temperature and stream flow rate as well. To some extent, the three economic models yield similar estimates for the TWP. However, it is preferable to apply exergy costing on the component level rather than only components grouping. Also, the aggregation formulation does not consider the essential information related to how the actual processes occur and the actual cost formation process in the system. Furthermore, the differences between exergy-based component cost and simple cost model are directly attributed to the assumptions used such as auxiliary equations and the uncertainty associated with the cost due to round-off [98].

Table 19 Total water price for different MED-MVC process configurations and different cost models.

Configuration	BF	FF	PF	PCF
TWP using simple method, \$/m^3	3.19	1.73	2.46	1.7
$TWP_{exergo-economic}$, \$/m^3	3.08	1.81	2.53	1.77
$TWP_{aggregation}$, \$/m^3	2.85	1.53	2.15	1.62

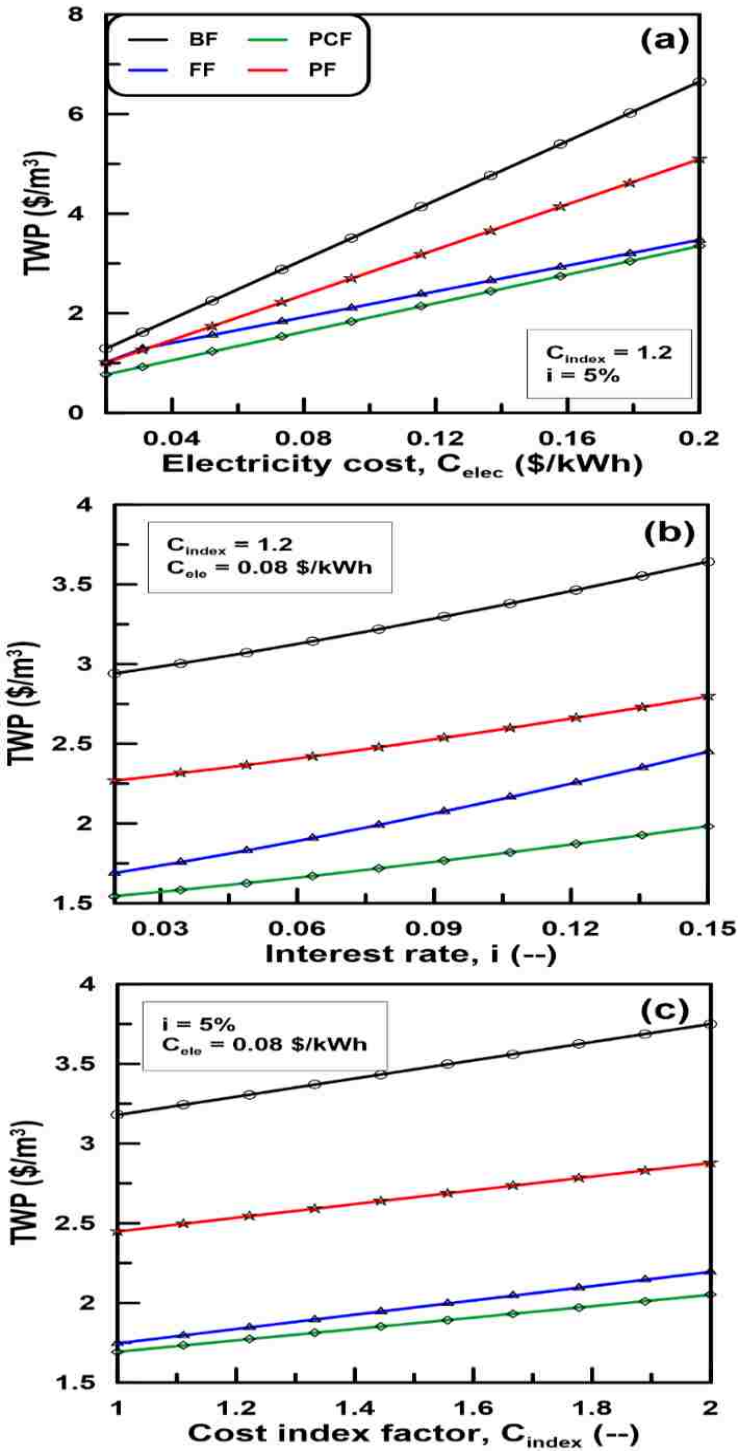

Figure 22 Effect of economic parameters on TWP for different feed configurations of MED-MVC system.

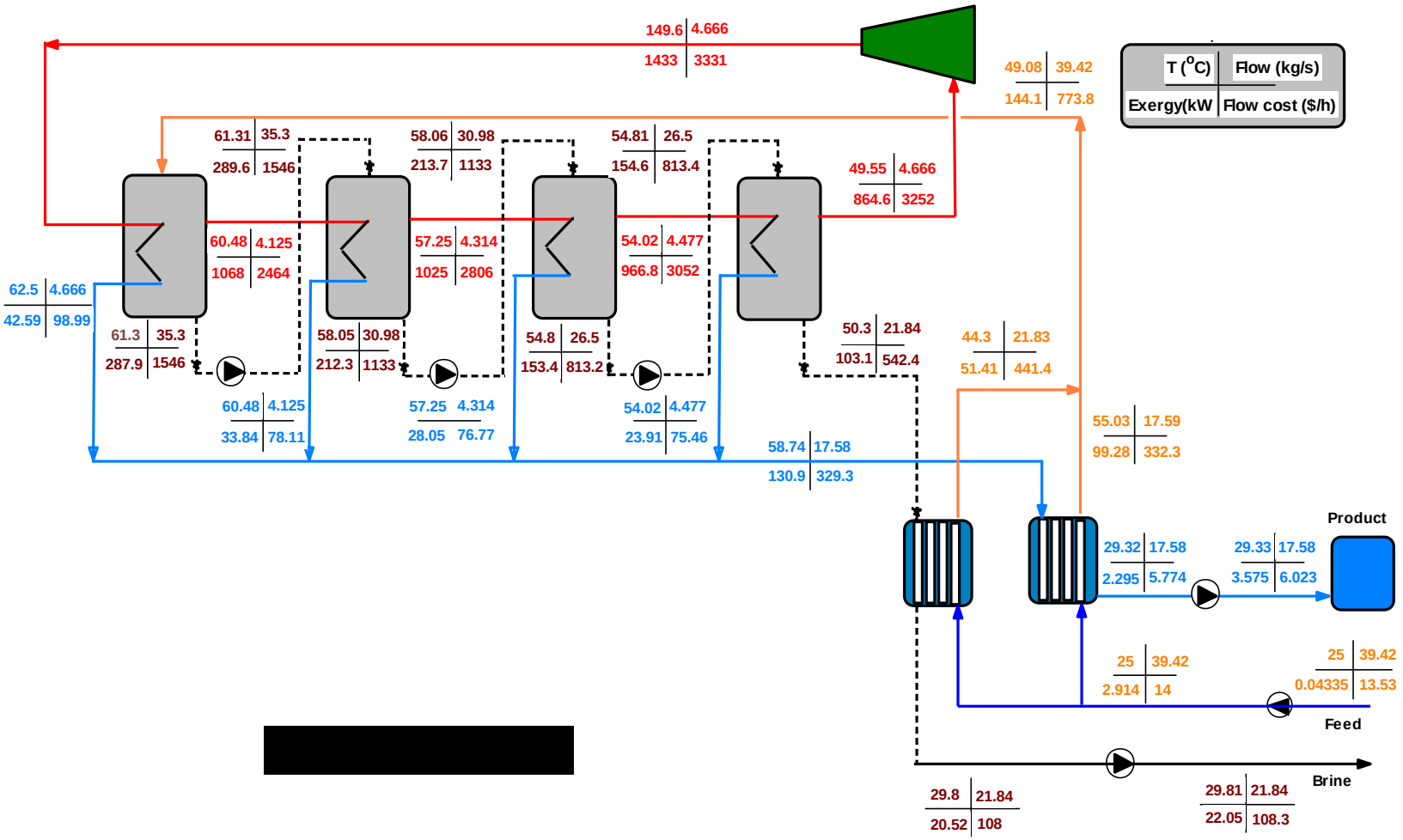

Figure 23 Cost flow diagram for MED-MVC system with (a) FF, (b) PF and (c) PCF configurations.

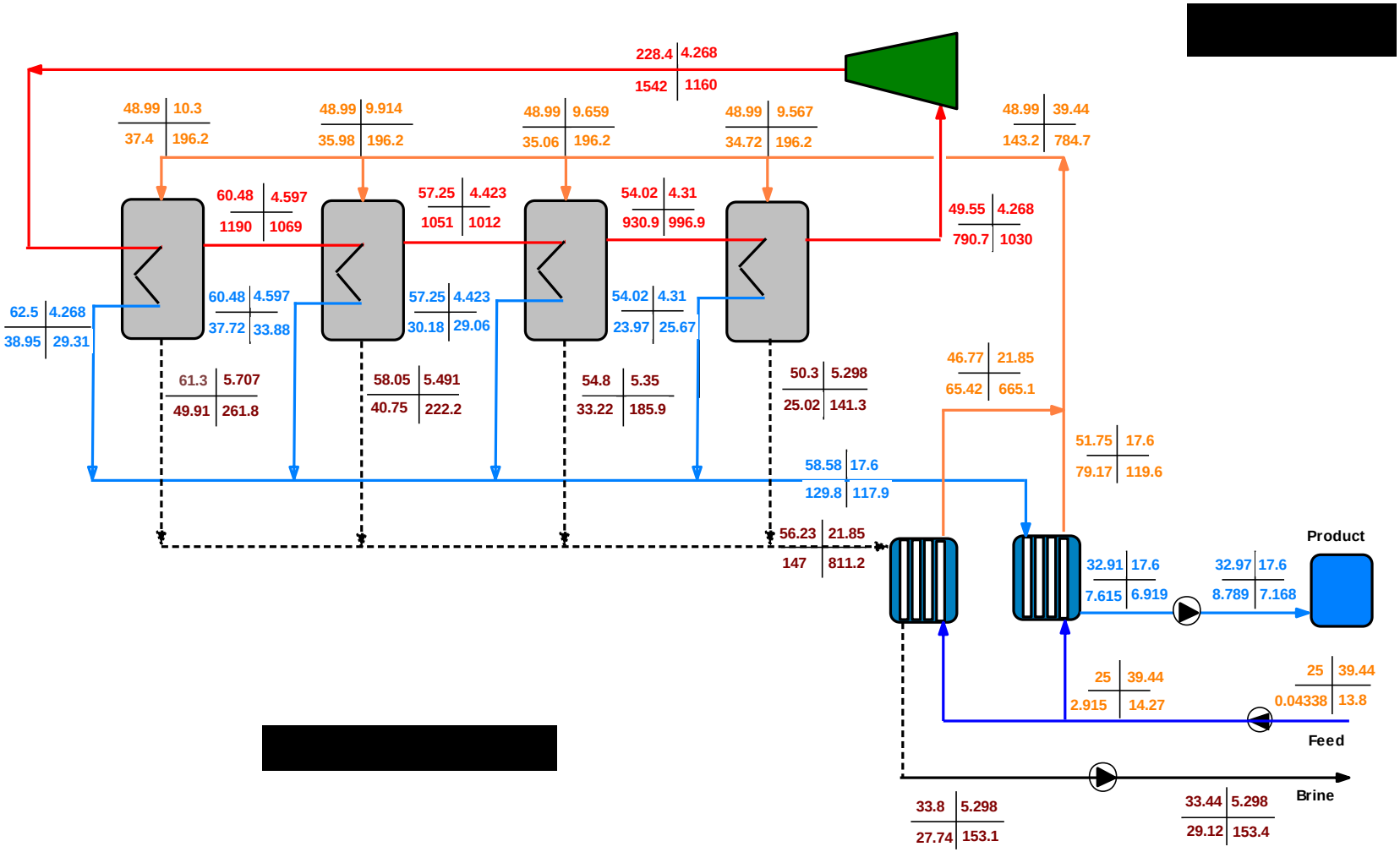
228.4 4.268
1542 1160
48.99 10.3
37.4 196.2
48.99 9.914
35.98 196.2
48.99 9.659
35.06 196.2
48.99 9.567
34.72 196.2
48.99 39.44
143.2 784.7
60.48 4.597
1190 1069
57.25 4.423
1051 1012
54.02 4.31
930.9 996.9
49.55 4.268
790.7 1030
62.5 4.268
38.95 29.31
60.48 4.597
37.72 33.88
57.25 4.423
30.18 29.06
54.02 4.31
23.97 25.67
61.3 5.707
49.91 261.8
58.05 5.491
40.75 222.2
54.8 5.35
33.22 185.9
50.3 5.298
25.02 141.3
46.77 21.85
65.42 665.1
51.75 17.6
79.17 119.6
58.58 17.6
129.8 117.9
56.23 21.85
147 811.2
32.91 17.6
7.615 6.919
32.97 17.6
8.789 7.168
Product
25 39.44
2.915 14.27
25 39.44
0.04338 13.8
Feed
Brine
33.8 5.298
27.74 153.1
33.44 5.298
29.12 153.4

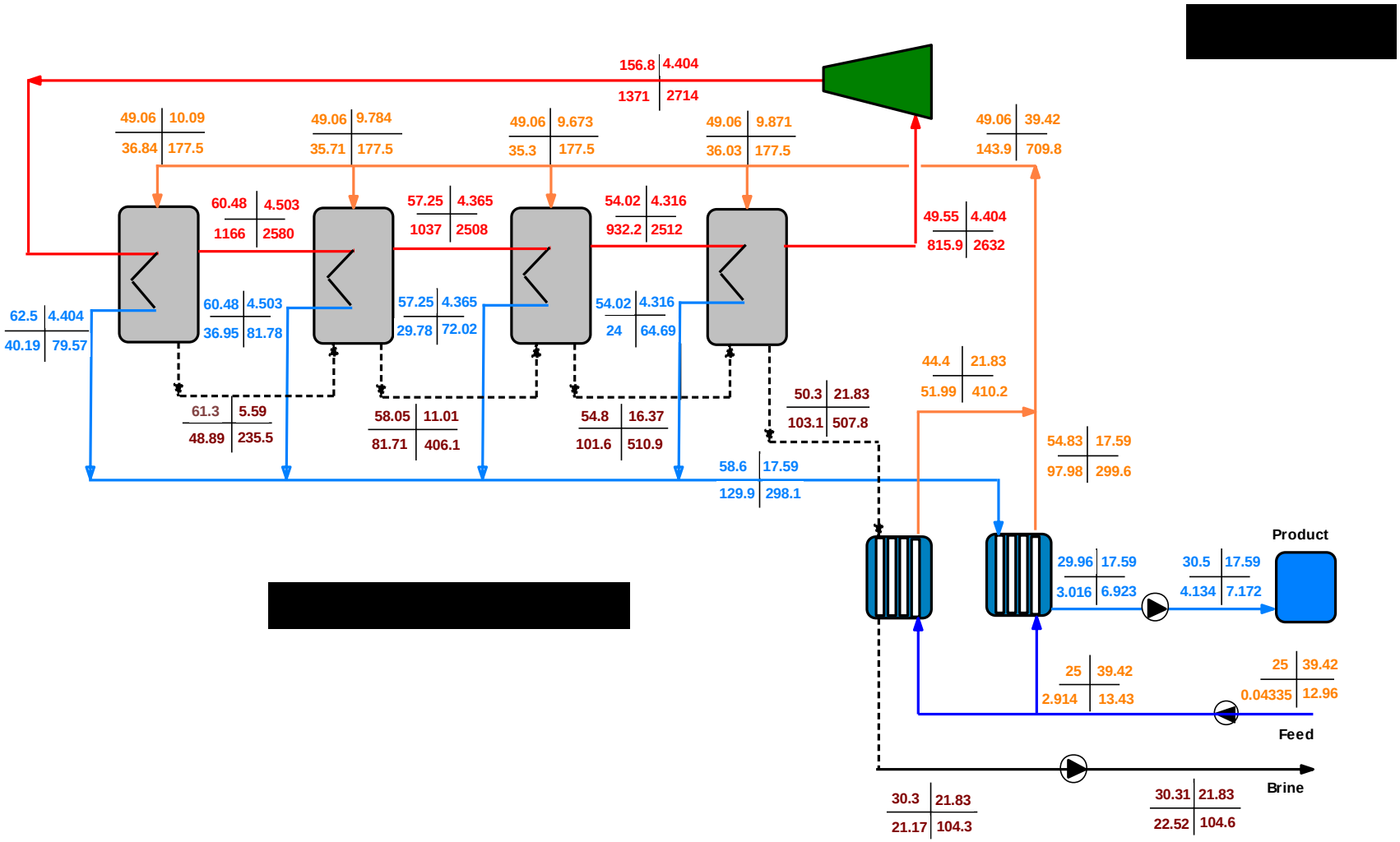
156.8 4.404
1371 2714
49.06 10.09
36.84 177.5
49.06 9.784
35.71 177.5
49.06 9.673
35.3 177.5
49.06 9.871
36.03 177.5
49.06 39.42
143.9 709.8
60.48 4.503
1166 2580
57.25 4.365
1037 2508
54.02 4.316
932.2 2512
49.55 4.404
815.9 2632
62.5 4.404
40.19 79.57
60.48 4.503
36.95 81.78
57.25 4.365
29.78 72.02
54.02 4.316
24 64.69
44.4 21.83
51.99 410.2
61.3 5.59
48.89 235.5
58.05 11.01
81.71 406.1
54.8 16.37
101.6 510.9
50.3 21.83
103.1 507.8
54.83 17.59
97.98 299.6
58.6 17.59
129.9 298.1
Product
29.96 17.59
3.016 6.923
30.5 17.59
4.134 7.172
25 39.42
2.914 13.43
25 39.42
0.04335 12.96
Feed
Brine
30.3 21.83
21.17 104.3
30.31 21.83
22.52 104.6

The exergo-economic parameters of the MED-MVC system operating in PCF and FF configurations are calculated for the base case as shown in Table 20. The calculated parameters for each component include the component second law efficiency ϵ_k, exergy destruction $\dot{E}_{D,k}$, cost per unit fuel exergy $c_{F,k}$, cost per unit product exergy $c_{P,k}$, exergy destruction cost rate $\dot{C}_{D,k}$, investment and O&M cost rate $\dot{Z}_k$, relative cost difference factor r_k, and exergo-economic factor f_k. For the PCF configuration, the last effect has highest values of the sum $\dot{Z}_k + \dot{C}_{D,k}$ among the evaporators while for the FF configuration it is the first effect. For both configurations, MVC unit has the highest values of $\dot{Z}_k + \dot{C}_{D,k}$ which is considered the most important component from the thermo-economic point of view in the MED-MVC systems. The lower values of the variable f_k for the MVC unit, brine preheater and distillate preheater show that the cost associated with these components is dominated by the exergy destruction. The remaining part is caused by $\dot{Z}_k$value of the component as indicated for both feed configurations. So, it can be concluded that, reducing the exergy destruction in these components could be cost effective for the complete system even if this would increase the investment costs associated with these components. For the evaporator units, the high values of $\dot{Z}_k + \dot{C}_{D,k}$ and the relatively small values of factor f_k suggest that the exergy destruction cost dominates the investment and O&M cost. According to the cost model assumption, the capital investment costs for the evaporators depend on the evaporator areas and the overall heat transfer coefficients. Therefore, modifications and improvements to the heat transfer process should be considered. For the FF configuration, the inter-effect pumps have highexergetic efficiency but also it has the lowest f_k, which indicate that the exergy destruction costs are controlling even with a relatively high exergetic efficiency of the component. One important conclusion which can be drawn from the results presented in Table 20 is that thermo-economic analysis aims at identifying the possible reduction of sub-components total costs. This

reduction can be either for the components inefficiency cost or the cost of components operating, whichever is controlling. Therefore, for components such as pumps, improvement is achieved by reducing the owning and operating cost of the sub-system under consideration at a cost of reduction in the thermodynamic efficiencies. For components such as MVC, brine/distillate preheaters where component inefficiency is the dominant cost, improvement to reduce inefficiency costs can be obtained by improving the thermodynamic efficiency or the operating condition. Finally, it is noted that the values obtained for f_k and r_k parameters are close the values reported in [155].

Table 20 Exergo-economic variables for MED-MVC systems with FF and PCF feed configurations.

	Component	$\dot{E}_{D,k}(kW)$	$\epsilon_k(\%)$	$c_{F,k}(\$\ MJ^{-1})$	$c_{P,k}(\$\ MJ^{-1})$	$\dot{C}_{D,k} + \dot{Z}_k(\$/h)$	$r_k(\%)$	$f_k(\%)$
FF	MVC unit	301.9	65.3	0.42	0.5	460.9	21.5	2.1
	Distillate heater	29.3	77.2	1.03	1.05	114.7	30.5	0.89
	Brine heater	31.2	62.2	1.2	1.9	145.0	45.9	0.52
	1st effect	179	87.1	0.50	0.55	328.2	13.0	1.26
	2nd effect	86.1	91.7	0.55	0.57	157.7	6.2	2.74
	3rd effect	90.6	91	0.57	0.67	176.6	7.5	2.54
	4th effect	130	86.2	0.67	0.81	304.5	12.7	1.53
	Feed pump	0.87	76.7	0.64	1.2	1.6	21.6	11.0
	Distillate pump	0.44	74.6	0.28	0.54	1.7	58.6	6.42
	Brine pump	0.51	75.1	0.74	1.4	4.8	8.8	2.6
	P1	0.75	69.2	0.68	1.37	23.9	3.5	0.41
	P2	0.65	69.6	0.7	1.41	19.7	3.8	0.46
	P3	0.59	67.8	0.72	1.45	15.8	4.12	0.53
PCF	MVC unit	345	61.7	0.46	0.55	580.3	25.6	1.73
	Distillate heater	28.9	77.2	1.06	1.1	117.2	30.2	0.86
	Brine heater	30.0	63.4	1.17	1.78	134.0	43.5	0.56
	1st effect	153.1	88.5	0.55	0.61	306.7	12.3	1.18
	2nd effect	94.25	91.7	0.61	0.6	211.7	8.2	1.5
	3rd effect	90.64	91.0	0.67	0.75	222.7	8.6	1.5
	4th effect	126.8	86.0	0.75	0.89	345.5	13.6	1.1
	Feed pump	0.87	76.7	0.64	1.2	1.8	24.8	9.9
	Distillate pump	0.6	65.1	0.33	0.53	1.3	30.2	8.4
	Brine pump	0.68	66.4	0.7	1.3	3.4	6.2	3.7

4.5.4. Sensitivity analysis

The primary goal in the analysis of the MED-MVC desalination system is to reduce the operation and capital costs. The operation cost can be reduced by increasing the performance ratio or decreasing the SPC. The primary contributor to the SPC in a MED-MVC system is the power consumed by the MVC unit which depends on the compressor efficiency, compression ratio and inlet vapor specific volume. Therefore, efforts are made to reduce the cost associated with the MVC. This can be done by reducing the vapor flow rate through the MVC unit by installing more effects N while keeping a constant overall temperature difference. On the other hand, capital cost can be reduced by reducing the required specific heat transfer area for evaporators and pre-heaters units. For MED-MVC, to decrease the S_A, the TBT must be increased. The increase in TBT will increase specific chemical pre-treatment costs and may add cost over the tube material and maintenance. Increasing N has its limits as this increases the required S_A for evaporation due to the decrease in the temperature difference between effects. Consequently, the capital costs savings would be overcome by the operating cost increase. It is essential to determine the optimal balance design parameters of N and TBT that achieve the optimum economic operation. The decrease in the SPC with increasing the number of effects N has its limit as shown in Figure 24 for both FF and PCF configurations.

A single-effect MVC has the maximum SPC due to the amount of vapor flow (displacement volume) through the MVC unit, leading to a high TWP of 2.4 $\$/m^3$. Adding another effect for the same overall temperature difference increases the second law efficiency for both feed configurations by around 61% and reduces the SPC by 39%. Although this increases the specific heat transfer area by 67%, the TWP reduces to ~ 1.6 $\$/m^3$ which is due to the decrease in the operating cost of the MVC unit. Further increase in the number of effects between 2 to 6 brings

little increase in the η_{II} , especially for the PCF configuration. In addition, there is no significant change in the SPC for both feed configurations. On the other hand, the value of TWP price keeps increasing with the increase in N which is due to the continuous increase in the required heat transfer area (capital cost). Increasing N beyond 6 leads to an increase in the SPC and η_{II} for both the FF and PCF configurations at a given production capacity. This is attributed to the large decrease in the volumetric vapor flow rate through the MVC unit which may not be sufficient to generate the required amount of vapor in the first effect. This low amount of vapor routed in the MVC unit from the last effect has to be compensated partially by adding extra energy E_{SH} by superheating the vapor through the MVC unit. Increasing the number of effects from 2 to 10 causes an increase in the TWP by 16% and 63% for the PCF and FF configurations, respectively. The use of more than 2 effects in the MED-MVC system does not improve the SPC compared to conventional MED. The main reason for not using multiple effects beyond 6 in MVC systems is the practical limitation of the displacement volume of the commercially available compressors [159]. In the literature, there is no report for the actual installation of MED-MVC systems with more than 6 effects [113].

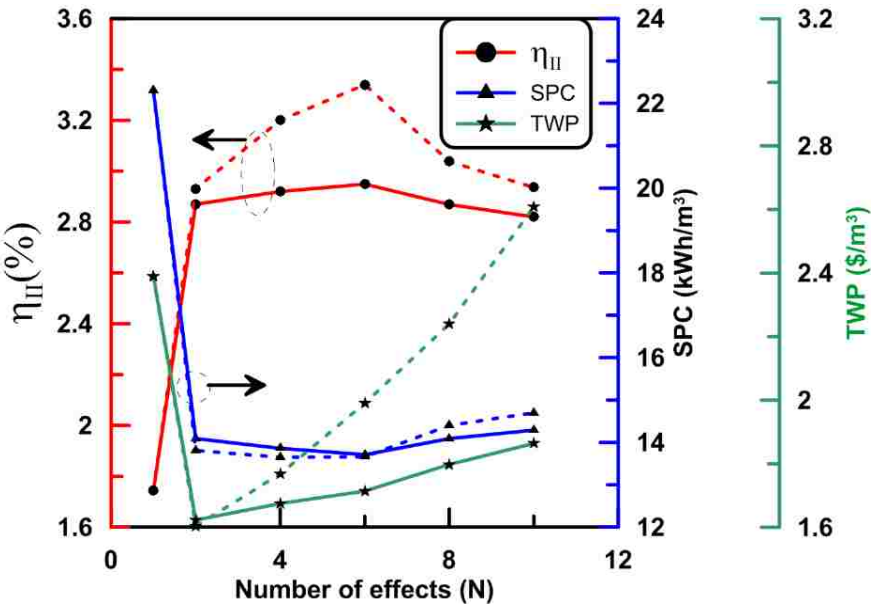

Figure 24 Effect of number of effects on SPC, η_{II} and, TWP(Dash line FF, Solid line PCF).

Another critical factor addressed in the current study is the effect of the compressor pressure head on the plant operating performance and economic parameters. Figure 25 shows the effect of variation of the compressed vapor temperature (55 to 110^{o}C) on the SPC, η_{II} and TWP for a 4-effect MED-MVC system operating in a PCF configuration. At the low-temperature difference between the compressed vapor and the last effect vapor, the compression ratio decreases which decreases the SPC power consumed through the compression process and the highest η_{II} is obtained. Although the required specific heat transfer area is large, the TWP shows the lowest value (1.6 \$/m^3) for steam temperature around 60^{o}C. On the other hand, at the high-temperature difference, the specific heat transfer area decreases but the TWP continues to increase significantly. This is attributed to the increase in the operating cost of the MVC unit with the increase of the SPC. Lowering the steam temperature from 110 to 55^{o}C results in 100% increase in the η_{II}, and 20 and 40% decrease in the SPC and TWP, respectively. Finally, it should be mentioned that the values of SPC and TWP at the operating temperatures simulated are consistent with the data available in the literature [38, 95, 133, 155, 157].

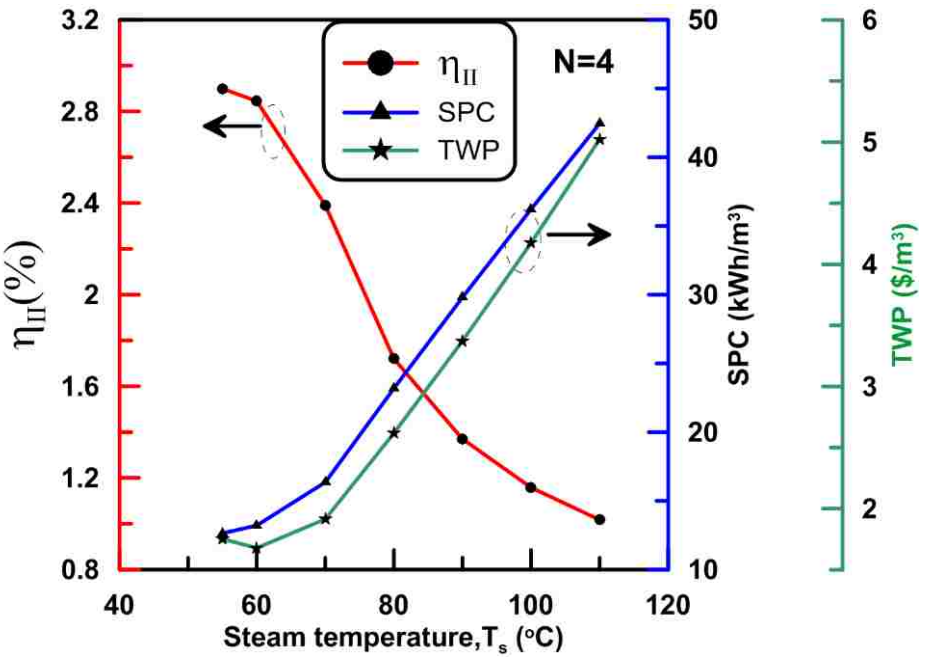

Figure 25 Effect of steam temperature on SPC, η_{II} and TWP for PCF feed configuration.

Conclusions

In the current study a new formulation for the steady-state thermodynamic model of MED-MVC desalination systems operating in different feed configurations has been presented. The effects of using different feed configurations for a MED-MVC desalination system on the total water price and plant performance are investigated. The calculated performance ratio (PR) is 2.89, 3.19, 3.0 and 3.33 for BF, FF, PF and PCF, respectively. Of the four configurations, the FF configuration yields the lowest specific power consumption (13.7 kWh/m^3), followed by the PCF configuration. The study reveals that the exergy destructions in the MVC unit (~35 to 50%) and evaporator units (~34 to 50%) represent the highest share of the total exergy destruction in the system. Other components, such as the brine and distillate feed heaters, have much lower shares in the exergy destruction which range between 7.6 to 10.9 % for all configurations. The second law efficiency is the highest for the PCF configuration (2.9%), while the BF has the lowest value (2.38%). The fixed cost for the BF configuration is the highest compared to the other configurations.

Results from the present economic models show that the most expensive (highest investment cost) components are the evaporator units. For the PF and FF configurations, the low values of the variable f_k for the MVC unit, evaporator units and the two preheaters show that the costs associated with these components are dominated by exergy destruction with the remaining costs determined by the $\dot{Z}_k$value. Reducing the exergy destruction in these units could be cost effective for the entire system even if this would increase the associated capital investment costs. Sensitivity analysis show that the MED-MVC system is superior to the single-effect MVC system, but there is a limit on the number of effects N that can be implemented. Increasing the number of effects from 2 to 6 results in no significant increase in the SPC or η_{II} for both the PF and FF configurations. On the contrary, the value of TWP increases by 15 and 63% as the number of effects increases from 2 to 10 for the FF and PCF configurations, respectively. Also, lowering the steam temperature supplied by the MVC unit from 110 to 55^{o}C results in 100% increase in the η_{II} , and 20 and 40 % decrease in the SPC and TWP, respectively. By using average values for the economic parameters, different cost models are used to estimate the average total water price for the BF, FF, PF and PCF configurations as 3.0, 1.69, 2.4 and 1.7 \$/m^3, respectively. Changes in the cost index and interest rate have a minimal effect on the total water price. On the other hand, changing the electricity cost has a significant effect on the TWP. The TWP for the PCF configuration could reach 0.92 \$/m^3 if the electricity cost is 0.03 \$/kWh.

CHAPTER 5 TRANSIENT PERFORMANCE OF MED PROCESSES WITH DIFFERENT FEED CONFIGURATIONS[**]

5.1 Abstract

Four different configurations of Multi-Effect-Desalination (MED): backward feed (BF), forward feed (FF), parallel feed (PF) and parallel/cross feed (PCF) are modeled in steady and dynamic operation to examine the behavior of these configurations under transient operation. Adding thermal vapor compressor (TVC) unit with the last effect of parallel/cross configuration is also studied and compared to the other configurations to show the advantage of this type of integration. The transient operation is achieved by applying ramp changes (disturbances) in the main input parameters that include steam flow rate at the heat source and cooling seawater temperature and flow rate at the heat sink. Steady state results indicate that parallel/cross feed has a relatively better performance characteristic than the other feed configurations regarding Gain Output Ratio (GOR) and specific heat consumption (SHC). Adding TVC unit to the parallel/cross feed achieves the lowest water production cost. Dynamic results show that MED-TVC with parallel/cross feed has the fastest response while backward feed and forward feed have the slower response to the applied disturbances. In the case of heat source disturbance, MED plants operating in the backward feed arrangement may be exposed to shut down due to the significant increase in brine level for the first effect. The MED-TVC process is susceptible to the heat sink disturbances compared to the PCF and other configurations. Also, changes in input parameters lead to the highest reduction in GOR for the MED-TVC process compared to the different configurations, especially for cooling

[**] **Mohamed L. Elsayed**, Osama Mesalhy, Ramy H. Mohammed, Louis C. Chow, "Transient Performance of MED Processes with Different Feed Configurations." Desalination, volume 438, July 2018, Pages 37-53.

seawater temperature. The highest reduction in brine level occurs in MED-TVC for a disturbance in the cooling seawater flow rate and may lead to MED-TVC evaporator drying condition. Hence, MED-TVC will require a reliable control system to avoid this type of plant operational disturbance.

5.2 Introduction

Much research has been done to compare the merits of various desalination processes integrated with renewable energy systems [160, 161], including multi-effect-desalination (MED), multistage flash (MSF) and reverse osmosis (RO) [162-165]. Moreover, The hybridization of MSF/MED with RO can improve system performance, but the overall recovery is controlled by operational temperatures of MED/MSF [66]. Significant advantages have been demonstrated in several scenarios for RO over MED and MSF; however, there has been rapidly increasing interest to use MED in countries near the Persian Gulf, and the Arabian Sea. In these countries, ambient conditions are challenging with seasonal high air and seawater temperatures and saline concentrations, but the resource of solar energy is abundant [166]. Also, the MED process requires less comprehensive seawater pretreatment compared to RO [73].

The integration of thermal desalination systems such as MED and a solar field as the heat source is one of the most promising options to connect a seawater desalination system with a solar power plant [63, 167]. Due to the intermittent nature of solar-powered systems, the MED systems may be exposed to fluctuations (disturbances) in input parameters during operation. These disturbances could be changes due to the environment such as cooling seawater swings with the weather or the time of day, and heat source swings. Another type of disturbances is called “turndown” which represents the changes in gross plant throughput and this is done intentionally to handle for example power demand swings [168]. Therefore, it is essential to analyze the transient behavior of MED

output based on the changes of the input with time to get a better understanding of the desalination process performance and behavior. Dynamic simulation predicts the system behavior from the start up to shut down and can be used to establish advanced control strategies, test operating scenarios, address potential problems related to unexpected transient events, and produce a comparatively stable output during the production period. Also, it helps engineers to understand better and develop optimal control strategies, prevent significant damages caused by malfunction, and troubleshoot disorders [169].

The MED is formed from a series of evaporators (or called effects), where the vapor generated in one effect is used in the next effect till it reaches the bottom condenser. This allows the MED to operate in different configurations that differ in the vapor flow (heating vapor) and feed directions. The published data reveal slight attention to comprehend the detailed dynamic modeling and in-depth analyses of various feed configurations of the MED processes. For example, El-Dessouky et al. [170] conducted a steady state performance analysis on two operating modes of MED, which includes the parallel (PF) and the parallel/cross (PCF) flow systems. The study concluded that better performance is obtained for the parallel/cross flow system. However, the PF system has similar characteristics and more straightforward design and operation procedures. Sharaf et al. [84] reported that parallel feed configuration is chosen over the forward and backward ones for solar collectors driven MED systems. Also, it was proven that the configuration of parallel/cross feed with equal feed flow rate is most efficient as compared to backward and forward feed configurations regarding distillate production and specific heat consumption by Al-Mutaz and Wazeer [171]. Sharan, P. and S. Bandyopadhyay [172] presented a comparison between four different configurations regarding scaling problem and pumping power requirement and operating temperature. They concluded that parallel feed has the lowest gain output ratio (GOR) which

represents the distillate product per amount of heat source supplied. Also, the backward has highest pumping requirement and scaling problem while the forward feed is the least in comparison with other two configurations. Mistry et al. [173] developed a MED modular model for studying various feed configurations with minimum code duplication. However, the model did not investigate the thermal performance or conduct a comparison between different feed configurations. In case of Multi-effect stack-type (MES). The forward feed configuration is preferred due to its simplicity and operation efficient with no pumping requirement to deliver feed to the next effect. Forward feed configuration is experimentally tested for medium scale freshwater production of 72 and 60 m^3/day in Spain [174] and China [175], respectively.

Transient modeling for different feed multi-effect evaporator (MEE) was investigated by a few researchers. For example, Miranda and Simpson [176] described a stationary and dynamic lumped model of backward feed MEE for tomato concentration. Tonelli et al. [177] presented an open-loop dynamic response model of triple effect evaporators for apple juice concentrators with backward feed configuration. Kumar et al. [178] modeled transient characteristics of mixed feed MEE system for paper industry based on the work in [179]. Their results show that the effects temperature has a faster response compared to the solid concentration. The dynamic behavior of four effects parallel/cross MED systems was done by Aly and Marwan [179] which allowed the study of system start-up, shutdown and load changes using lumped model of mass, energy and salt balance equations. El-Nashar and Qamhiyeh [180] developed a simulation lumped model for predicting the dynamic behavior of MES evaporators with forwarding feed configuration. The model yielded a reasonable agreement with data taken during plant start-up of the under-operation plant at Abu Dhabi. A dynamic representation of 14-effect with forward configuration was experimentally validated for MES desalination system in [181, 182]. Mazini et al. [183] extended

the procedure of [179] for parallel/cross configuration integrated with thermal vapor compressor (TVC). Their model was validated by actual data of an operating plant. Medhat Bojnourd et al. [184] presented lumped and distributed models for four-MEEs with forward feed to concentrate whole milk. Cipollina et al. [185] developed a dynamic model for a 12-effect parallel/cross MED-TVC based on available data from the Trapani plant in Italy using the equation-based process simulator gPROMS®.

There is a lack of comprehensive and in-depth analysis of the transient performance of the different configurations of MED systems. It is important to understand their transient behavior under changes or fluctuations in three main input parameters, namely the motive steam flow rate, cooling seawater flow rate and cooling seawater temperature. In this study, four different feed arrangements for MED systems are considered and compared to pinpoint the most reliable configuration in terms of steady-state operation and dynamic response. To accomplish this, the steady-state mass, energy, and salt balance equations are solved to determine the steady-state operation of the different feed arrangements. Then, a general set of three nonlinear ordinary differential equations (ODEs) that govern the variations of brine level, brine salinity and vapor temperature with time is developed. Also, a detailed model for the condenser which can predict the dynamic variations of the condenser pressure, condenser liquid level and the feed temperature with time is developed. The current model is developed in a general way so that it can be used to predict the dynamic behavior under disturbances in the three main input parameters for all feed configurations.

5.3 MED process configurations

A Multi-Effect-Evaporation (MEE) system is formed by a sequence of standing separate effect evaporators, and the vapor generated in one effect is used in the following effect till it reaches the bottom condenser. Vapor reuse in the MEE prevents the rejection of a large amount of thermal energy to the surrounding, which is the main drawback of the single effect system. Freshwater is obtained in a MEE system due to the evaporation of water at the horizontal heat transfer tube bundle in each effect or due to brine/feed flashing. Different MEE configurations differ in the directions of the vapor flow or supplied feed/concentrate to the evaporators. These configurations include parallel feed (PF), parallel/cross feed (PCF), backward feed (BF) and forward feed (FF).

Selection among these configurations depends on the application and relies on variation in the solid composition as a function of the top brine temperature (TBT) and the maximum allowable composition in the rejected brine. At higher temperatures or higher concentrations, scale formation takes place inside and outside the tube surfaces, which in turn causes evaporator performance degradation with time. For example, an FF (co-current) system can operate at high TBT. However, it is not found on a commercial scale for the desalination industry [73] because it has more complex layout than the simple parallel feed configuration. Yet, it is widely used in the sugar, dairy industries and recently is preferred in MES medium scale desalination systems. In the BF (counter-current) type, more pumping power is needed (to pump the feed from each effect to the preceding one which is at higher pressure), and there is more possibility for air leakage through the points of pump connections. However, in juice concentration applications where the viscosity of fruit juice increases rapidly with its concentration [186], there is a need to avoid highly viscous fluids at low temperatures. So, the BF configuration is more preferred than the other arrangements [187] and is widely used in the food, pulp, and paper industries as well. Schematic diagrams of different MED

configurations are shown in Figure 26. In each configuration except for the MED-TVC configuration, an external heat source such as solar heat can use a boiler to provide saturated steam that enters the tubes of the first effect as a heating medium to heat and evaporate the feed seawater [84].

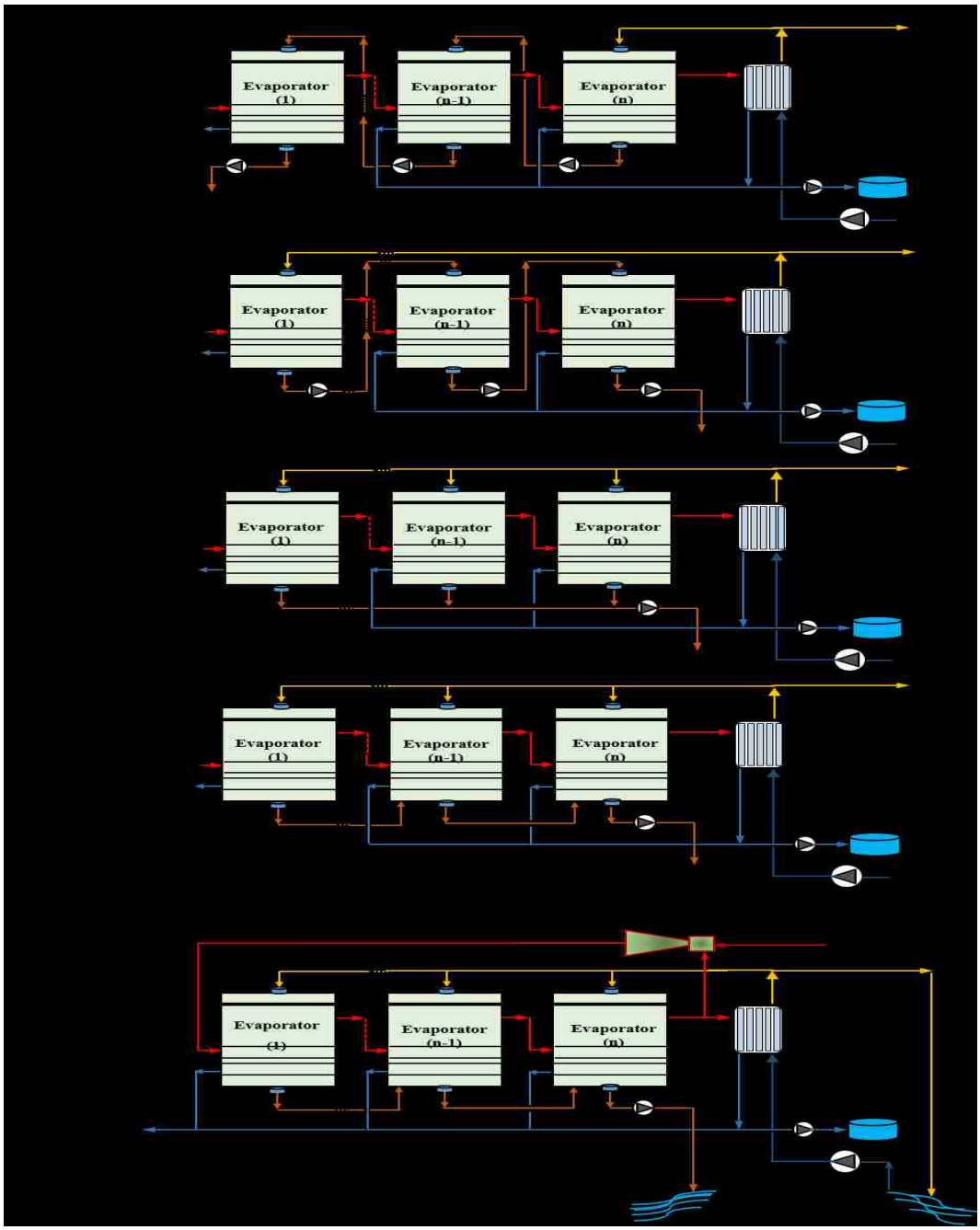

Figure 26 Schematic diagram MED systems with different feed configurations.

In the BF configuration, the feed passing through the condenser is directed to the last effect where it is sprayed on the outside walls of the horizontal tube bundle, forming a thin liquid film. A portion of this liquid film is evaporated by absorbing heat from the vapor coming from the previous effect and condensing inside the tube bundle. The brine from the last effect is passed to the previous effect. The feed and vapor flow in BF has reverse flow (counter-current) directions, so the brine is cascaded sequentially through effects in backward direction till it reaches as a feed for the first effect. In the FF arrangement, the preheated feed water is directed all the way to the first effect with the highest TBT. Again, a part of the feed is evaporated in the first effect while the remaining unevaporated brine with high TBT is directed as a feed to the next effect. This process is cascaded in a forward direction (co-current) towards the last effect.

In the PF and PCF configurations, the feed leaving the condenser is divided among all effects, and both the vapor and the brine streams flow in the same direction. For PCF arrangement, the unevaporated brine crosses between effects. At industrial scale desalination, the PF configuration is commonly used due to its simplicity compared to other previously mentioned configurations. Adding thermal vapor compressor (TVC) to the last effect in the PCF configuration forms a typical MED-TVC as shown in Figure 26. High-pressure motive steam is extracted from a boiler or a power plant steam turbine enters through the TVC. The motive steam entrains a portion of the vapor generated in the last effect of the MED system. The remaining vapor is used to preheat the cooling seawater in the condenser. The ratio of the motive steam to the entrained vapor flow rate is called the entrainment ratio (R_a). Adding TVC unit to MED systems improves the GOR and decreases the cost of input energy by recompressing the entrained vapor with the motive steam to form hot compressed steam that is recycled to the first effect as a heating medium[188]. The choice between these feed configurations changes the design and performance of the MED desalination

system, e.g. the required effects heat transfer area, the amount of vapor formed in each effect by boiling or feed/brine flashing, the required pumping power, the GOR, and the cooling seawater to distillate ratio [84].

5.4 Dynamic Model Development

Before solving the dynamic model, the steady state conservation equations of mass, energy, and salt are solved to obtain the steady-state values of all the parameters in the plant. The solution is carried out iteratively to adjust the temperature drop across the effects to yield the same evaporator area for all the effects. The details of the steady-state model for different configurations is presented in Appendix A. In order to estimate the performance of TVC, a quasi-steady correlations for the entrainment ratio that relates expansion ratio and compression ratio of the ejector are extracted from the Power's graphical data chart [91] by Hassan and Darwish [92], which are suitable for the range of typical MED operation conditions. The solution of the steady-state model is considered as the initial condition for the dynamic model. Figure 27 shows schematic diagrams for the first and i^{th} effect evaporators and the condenser. A comprehensive dynamic model for different feed configurations is developed. Each evaporator is divided into three lumps: brine, vapor, and tube lump. For each lump, energy, mass, and salt balance are written. The assumptions used in generating these dynamic models are listed as follows [179, 189]:

11. The accumulation of mass and energy in the evaporator tubes is taken to be negligible compared to the accumulation of mass and energy in the brine pool inside an effect.
12. Non-condensable gases effect on evaporator operation is taken to be insignificant.
13. For FF and PCF, the brine stream from the *i-1* effect is assumed to flash adiabatically upon entering the i effect.

14. Thermophysical properties for the brine and vapor are considered to be temperature and salinity dependent. Appropriate correlations for overall heat transfer coefficients for evaporators and condenser units are given in Table 21 .
15. Thermodynamic penalty representing the temperature difference between the brine pool and the vapor generated in effect is taken as the Boiling Point Elevation (BPE).

$$T_{v,i} = T_{b,i} - BPE\left(T_{v,i}, X_{b,i}\right) \tag{31}$$

16. For MED-TVC, the thermo-compressor has quick dynamic response compared to other components [183]. It is considered to be in a quasi-steady state condition and is modeled by the correlations from [92].
17. Heating steam temperature is maintained constant at a value comparable to the values used in industrial scale [190].
18. The vapor and distillate are salt-free.

Table 21 Thermophysical properties of seawater, saturated steam, and condensate [73]

Properties	Appropriate relation	Notes
Boiling point elevation (BPE), ℃	$BPE = AX + BX^2 + CX^3$ $A = (8.325x10^{-2} + 1.883x10^{-4}T + 4.02x10^{-6}T^2)$ $B = (-7.625x10^{-4} + 9.02x10^{-5}T - 5.2x10^{-7}T^2)$ $C = (1.522x10^{-4} - 3x10^{-6}T - 3x10^{-8}T^2)$	0< X < 160 ppt 10 < T < 180 °C
Seawater density, kg/m^3	$\rho = 10^3[A_1F_1 + A_2F_2 + A_3F_3 + A_4F_4]$ $A_1 = 4.032G_1 + 0.115G_2 + 3.26x10^{-4}G_3$ $A_2 = -0.108G_1 + 1.57x10^{-3}G_2 - 4.23x10^{-4}G_3$ $A_3 = -0.012G_1 + 1.74x10^{-3}G_2 - 9x10^{-6}G_3$ $A_4 = 6.92x10^{-4}G_1 - 8.7x10^{-5}G_2 - 5.3x10^{-5}G_3$ $G_1 = 0.5$ $G_2 = B$ $G_3 = 2B^2 - 1$ $B = \frac{2X - 150}{150}$ $F_1 = 0.5$ $F_2 = A$ $F_3 = 2A^2 - 1$ $F_4 = 4A^3 - 3A$ $A = \frac{2T - 200}{160}$	0< X < 160 ppt 10 < T < 180 °C
Water vapor density, kg/m^3	$\rho_v = 0.0051 + 0.00024T_v + 1.8x10^{-5}{T_v}^2 - 4.33x10^{-8}{T_v}^3 + 4.34x10^{-9}{T_v}^4$	
Specific heat capacity at constant pressure, kJ/kg ℃	$C_p = 10^{-3}[C_0 + C_1T + C_2T^2 + C_3T^3]$ $C_0 = (4206.8 - 6.62X + 1.23x10^{-2}X^2)$ $C_1 = (-1.13 + 5.4x10^{-2}X - 2.27x10^{-4}X^2)$ $C_2 = (1.2x10^{-2} - 5.36x10^{-4}X + 1.89x10^{-6}X^2)$ $C_3 = (6.88x10^{-7} + 1.51x10^{-6}X - 4.43x10^{-9}X^2)$	20< X < 160 ppt 10 < T < 180 °C
Enthalpy of saturated Water vapor, kJ/kg	$h_v = 2501.69 + 1.81T + 5.88x10^{-4}T^2 - 1.22x10^{-5}T^3$	
Latent heat of evaporation, kJ/kg	$h_{fg} = 2501.897 - 2.41T + 1.19x10^{-3}T^2 - 1.59x10^{-5}T^3$	
Enthalpy of water, kJ/kg	$h_b = -0.0336 + 4.208T - 6.2x10^{-4}T^2 + 4.46x10^{-6}T^3$	
U of condenser kW/m^2.k	$U_{con} = 1.72 + 3.21x10^{-3}T_v - 1.6x10^{-5}{T_v}^2 - 1.99x10^{-7}{T_v}^3$	U is the overall heat transfer coefficient
U of evaporator kW/m^2.k	$U_E = 1.97 + 1.2x10^{-3}T_b - 8.598x10^{-5}{T_b}^2 + 2.57x10^{-7}{T_b}^3$	
Saturated temperature:	$T_{sat} = \left(42.6776 - \frac{3892.7}{(ln(P/1000) - 9.48654)}\right) - 273.15$	T_{sat} in °C and P in kPa.
Saturated pressure:	$ln(P_{sat}/P_c) = \left(\frac{T_c}{T + 273.15} - 1\right)\sum_{i=1}^{8} f_i\left(0.01(T + 273.15 - 338.15)\right)^{(i-1)}$, $T_c = 647.286\ K$ and $P_c = 22089\ kPa$ f_1 = -7.416242; f_2 = 0.29721; f_3 = -0.1155286; f_4 = 0.008685635 f_5 = 0.001094098; f_6 = -0.00439993; f_7 = 0.002520658; f_8 = -0.000521868	where T in °C and P_{sat} in kPa.

5.4.1. Evaporator model

Based on the above assumptions, the transient mass, energy, and salt balance equations for the ith effect evaporator considering, for example, PCF configuration can be written as,

- Brine and vapor lumps mass balance for *ith* effect are given by,

$$\frac{dM_{bi}}{dt} = m_{f,i} + m_{b,i-1} - m_{vg,i} - m_{b,i} \tag{32}$$

$$\frac{dM_{vi}}{dt} = m_{vg,i} - m_{v,i} \tag{33}$$

- Brine, vapor, and tube lump energy balance for *ith* effect are given as:

$$\frac{dM_{bi}h_{bi}}{dt} = m_{f,i}h_{f,i} + m_{b,i-1}h_{b,i-1} - m_{vg,i}h_{v,i} - m_{b,i}h_{b,i} + Q_{E,i} \tag{34}$$

$$\frac{dM_{vi}h_{v,i}}{dt} = m_{vg,i}h_{v,i} - m_{v,i}h_{v,i} \tag{35}$$

$$M_T \frac{dh_{T,i}}{dt} = m_{v,i-1}\left[h_{v,i-1} - h_{d,i}\right] - Q_{E,i} \quad , \tag{36}$$

$$Q_{E,i} = U_{e,i}A_{e,i}\frac{\left(T_{v,i-1} - T_f\right) - \left(T_{v,i-1} - T_{b,i}\right)}{ln\left[\frac{T_{v,i-1} - T_f}{T_{v,i-1} - T_{b,i}}\right]}$$

- Since vapor lump is salt-free, salt balance on the *ith* effect brine lump is:

$$\frac{dM_{bi}X_{bi}}{dt} = m_{f,i}X_{f,i} + m_{b,i-1}X_{b,i-1} - m_{b,i}X_{b,i} \tag{37}$$

The evaporator is supposed to have a cross-sectional area $A_{ce,i}$ and a total height H_E. The brine pool height $L_{b,i}$ and vapor height $H_E - L_{b,i}$ are shown in Figure 27b. After some manipulations, equations 8, 9 and 10 can be derived from the combined lumps mass, energy and salt balances for i^{th} effect. The coefficients of these equations are presented in Table 22:

$$C_{11}\frac{dL_{b,i}}{dt} + C_{12}\frac{dT_{v,i}}{dt} + C_{13}\frac{\partial X_{b,i}}{\partial t} = C_{14} \tag{38}$$

$$C_{21}\frac{dL_{b,i}}{dt} + C_{22}\frac{dT_{v,i}}{dt} + C_{23}\frac{\partial X_{b,i}}{\partial t} = C_{24} \tag{39}$$

$$C_{31}\frac{dL_{b,i}}{dt} + C_{32}\frac{dT_{v,i}}{dt} + C_{33}\frac{\partial X_{b,i}}{\partial t} = C_{34} \tag{40}$$

Table 22 Dynamic rate coefficients from i[th] effect balance equations for different feed configurations.

C_{11}	C_{12}	C_{13}
$A_{ce,i}(\rho_{b,i} - \rho_{v,i})$	$\left[A_{ce,i}L_{b,i}\frac{d\rho_{b,i}}{dT_{b,i}}\left(1+\frac{\partial BPE}{\partial T_{v,i}}\right)+(H_E-L_{b,i})A_{ce,i}\frac{d\rho_{v,i}}{dT_{v,i}}\right]$	$\left[A_{ce,i}L_{b,i}\left\{\frac{d\rho_{b,i}}{dT_{b,i}}\frac{\partial BPE}{\partial X_{b,i}}+\frac{d\rho_{b,i}}{dX}\right\}\right]$
C_{21}	C_{22}	C_{23}
$A_{ce,i}(\rho_{b,i}h_{b,i} - \rho_{v,i}h_{vi})$	$\left[A_{ce,i}L_{b,i}\left\{\rho_{b,i}\frac{dh_{b,i}}{dT_{b,i}}+h_{b,i}\frac{d\rho_{b,i}}{dT_{b,i}}\right\}\left(1+\frac{\partial BPE}{\partial T_{v,i}}\right)+(H_E-L_{b,i})A_{ce,i}\left\{\rho_{v,i}\frac{dh_{v,i}}{dT_{v,i}}+h_{v,i}\frac{d\rho_{v,i}}{dT_{v,i}}\right\}\right]$	$\left[A_{ce,i}L_{b,i}h_{b,i}\left(\frac{d\rho_{b,i}}{dT_{b,i}}\frac{\partial BPE}{\partial X_{b,i}}+\frac{d\rho_{b,i}}{dX}\right)+A_{ce,i}L_{b,i}\rho_{b,i}\frac{dh_{b,i}}{dT_{b,i}}\frac{\partial BPE}{\partial X_{b,i}}\right]$
C_{31}	C_{32}	C_{33}
$A_{ce,i}\rho_{b,i}X_{b,i}$	$\left[A_{ce,i}L_{b,i}X_{b,i}\frac{d\rho_{b,i}}{dT_{b,i}}\left(1+\frac{\partial BPE}{\partial T_{v,i}}\right)\right]$	$\left[A_{ce,i}L_{b,i}\left\{X_{b,i}\frac{d\rho_{b,i}}{dT_{b,i}}\frac{\partial BPE}{\partial X_{b,i}}+\rho_{b,i}+X_{b,i}\frac{d\rho_{b,i}}{dX}\right\}\right]$

	BF	FF	PF	PCF
C_{14}	$m_{b,i+1}-m_{b,i}-m_{v,i}$	$m_{b,i-1}-m_{b,i}-m_{v,i}$	$m_{f,i}-m_{b,i}-m_{v,i}$	$m_{f,i}+m_{b,i-1}-m_{b,i}-m_{v,i}$
C_{24}	$m_{b,i+1}h_{b,i+1}-m_{b,i}h_{b,i}+Q_{E,i}$	$m_{b,i-1}h_{b,i-1}-m_{b,i}h_{b,i}+Q_{E,i}$	$m_{f,i}h_{f,i}-m_{b,i}h_{b,i}+Q_{E,i}$	$m_{f,i}h_{f,i}+m_{b,i-1}h_{b,i-1}-m_{b,i}h_{b,i}+Q_{E,i}$
C_{34}	$m_{b,i+1}X_{b,i+1}-m_{b,i}X_{b,i}$	$m_{b,i-1}X_{b,i-1}-m_{b,i}X_{b,i}$	$m_{f,i}X_{f,i}-m_{b,i}X_{b,i}$	$m_{f,i}X_{f,i}+m_{b,i-1}X_{b,i-1}-m_{b,i}X_{b,i}$

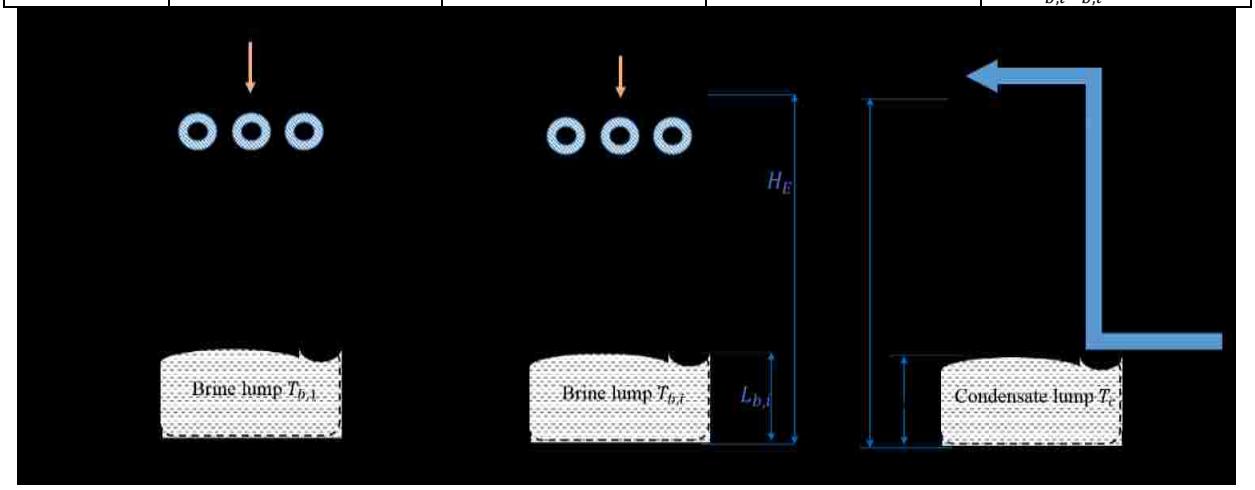

Figure 27 Control volume with different terms for (a) first effect, (b) i[th] effect and (c) condenser.

Brine flow rate between effects is represented by $m_{b,i} = C_{b,i}\sqrt{\Delta P_{b,i}}$ where $\Delta P_{b,i} = P_{i-1} - P_i + \rho_b g\left(L_{b,i} - L_{b,i-1}\right)$ for the PCF configuration and the vapor flow from an effect to the next is calculated from $m_{v,i} = C_{vi}\sqrt{\Delta P_{vi}}$ where $\Delta P_{vi} = P_i - P_{i-1}$. In the BF and FF configurations, a pressure jump equal to the hydrostatic pressure of the evaporator height H_E is considered to deliver the feed/brine to the previous/next effect.

5.4.2. Condenser model

To predict the dynamic variation of condenser temperature, condenser liquid level, and the preheated feed temperature from condenser with time accurately, a detailed model for the condenser is developed. The condenser is used to condense the total vapor generated in the last effect for all configurations or fraction of the vapor not entrained by the TVC unit in case of MED-TVC system which raises the cooling seawater to the required feed temperature. The condenser is sectioned into three lumps; condensate liquid, vapor, and tube as shown in Figure 27c. As shown the condenser assumed to have a cross-sectional area A_{cc} and a total height of H_{con} while the condensate pool height is L_{con} and vapor height is $H_{con} - L_{con}$. Mass balance of the liquid and vapor lumps can be written as:

$$\frac{dM_{con}}{dt} = m_{con} - m_{con,O} \tag{41}$$

$$\frac{dM_v}{dt} = \left(m_{v,n} - D_{ev}\right) - m_{con} \tag{42}$$

Energy balance for condensate liquid, vapor and tube lumps is applied as follow:

$$\frac{dM_{con}h_{con}}{dt} = m_{con}h_{con} - m_{con,O}h_{con,O} \tag{43}$$

$$\frac{dM_v h_v}{dt} = \left(m_{v,n} - D_{ev}\right)h_{v,n} - m_{con}h_{con} - Q_{con} \tag{44}$$

$$M_{T,con}\frac{dh_{T,con}}{dt} = m_{cw}h_{cw} - m_{cw}h_f + Q_{con}\ , \qquad M_{T,con} = \rho_{Tube,c}\forall_{Tube,con} \tag{45}$$

Combined mass and energy for vapor and condensate lumps are given by equations 16, and 17 respectively.

$$D_{11}\frac{dL_{con}}{dt} + D_{12}\frac{dT_{con}}{dt} = D_{13} \tag{46}$$

$$D_{21}\frac{dL_{con}}{dt} + D_{22}\frac{dT_{con}}{dt} = D_{23} \tag{47}$$

where the coefficients from the previous equations are presented in Table 23:

Table 23 Dynamic rate coefficients from mass, and energy balance for end condenser.

$\boldsymbol{D_{11}}$	$\boldsymbol{D_{12}}$	$\boldsymbol{D_{13}}$
$A_{cc}(\rho_{L,con} - \rho_{v,con})$	$\left[A_{cc}L_{con}\frac{d\rho_{L,con}}{dT} + (H_{con} - L_{con})A_{cc}\frac{d\rho_{v,con}}{dT}\right]$	For all configurations $m_{v,n} - m_{con,O}$ For MED-TVC$(m_{v,n} - D_{ev}) - m_{con,O}$
$\boldsymbol{D_{21}}$	$\boldsymbol{D_{22}}$	$\boldsymbol{D_{23}}$
$A_{cc}(\rho_{L,con}h_{con} - \rho_{v,con}h_v)$	$\left[A_{cc}L_{con}h_{con}\frac{d\rho_{L,con}}{dT} + (H_{con} - L_{con})h_vA_{cc}\frac{d\rho_{v,con}}{dT} + A_{cc}L_{con}\rho_{L,con}\frac{dh_{con}}{dT} + (H_{con} - L_{con})\rho_{L,con}A_{cc}\frac{dh_v}{dT}\right]$	For all configurations $m_{v,n}h_{v,n} - m_{con,O}h_{con,O} - Q_{con}$ MED-TVC $(m_{v,n} - D_{ev})h_{v,n} - m_{con,O}h_{con,O} - Q_{con}$

To obtain the transient nature of feed seawater temperature, the condenser tube enthalpy is assumed to be the average of the feed and cooling seawater enthalpies and is given as, $h_{T,con} = \frac{h_f + h_{cw}}{2}$. Using the energy balance for the condenser tube lump, the rate of change of feed water temperature can be written as:

$$\frac{dT_{feed}}{dt} = \frac{2\left(Q_{con} + m_{cw}h_{cw} - m_{cw}h_f\right)}{\rho_{tube,c}\forall_{tube,c}\frac{dh_f}{dT}} \tag{48}$$

$$\text{where } Q_{con} = U_{con}A_{con}\frac{(T_{v,n} - T_f) - (T_{con} - T_{cw})}{ln\left[\frac{T_{v,n} - T_f}{T_{con} - T_{cw}}\right]} \tag{49}$$

By solving Eqs. (20-31), the brine level, vapor temperature, salinity from each effect, condenser liquid level, condenser vapor temperature and feed temperature can be calculated at each time step. The condenser pressure is assumed to be equal to the saturation pressure at the condenser temperature.

5.4.3. Numerical solution

A FORTRAN code is developed to solve both the steady-state and dynamic models equations. The first-order nonlinear ODEs of the dynamic model for the condenser and evaporators are solved using the Runge-Kutta fourth order method. In the steady state solution, the vapor and brine

temperatures, feed flow rate, brine flow rate, vapor flow rate and salinity at each effect are calculated in addition to the evaporator and condenser surface areas. Then, the steady-state solution is used as the initial condition for the dynamic response calculations. At each time step, the temperature, liquid level, and salinity are computed in each effect. The condenser temperature, condenser distillate level and feed temperature are also calculated. The brine and vapor flow rates among the effects are calculated based on the liquid level and the saturation pressure in each effect. In case of MED-TVC, an accurate model for steam jet ejectors is considered to evaluate its performance where the entrainment ratio of the TVC is updated at every time step using the correlations given in [92] and the values of the pressure at the last effect and the pressure of the motive steam. A time step was chosen to be 0.1 s to eliminate the instability in the solution [179]. The model solution flow chart is presented in Figure 28. Any parameter can be changed (or disturbed) with various intensity from its steady state value abruptly or in a ramp form for a specified period. The operating conditions of the MED systems are expected to deviate from the steady state condition upon the introduction of disturbances. Behavior indicator parameters such as brine level, effect temperature and vapor flow between effects are obtained in addition to the performance indicator parameters such as GOR as a function of time while the disturbances are applied or removed from the dynamic model solution.

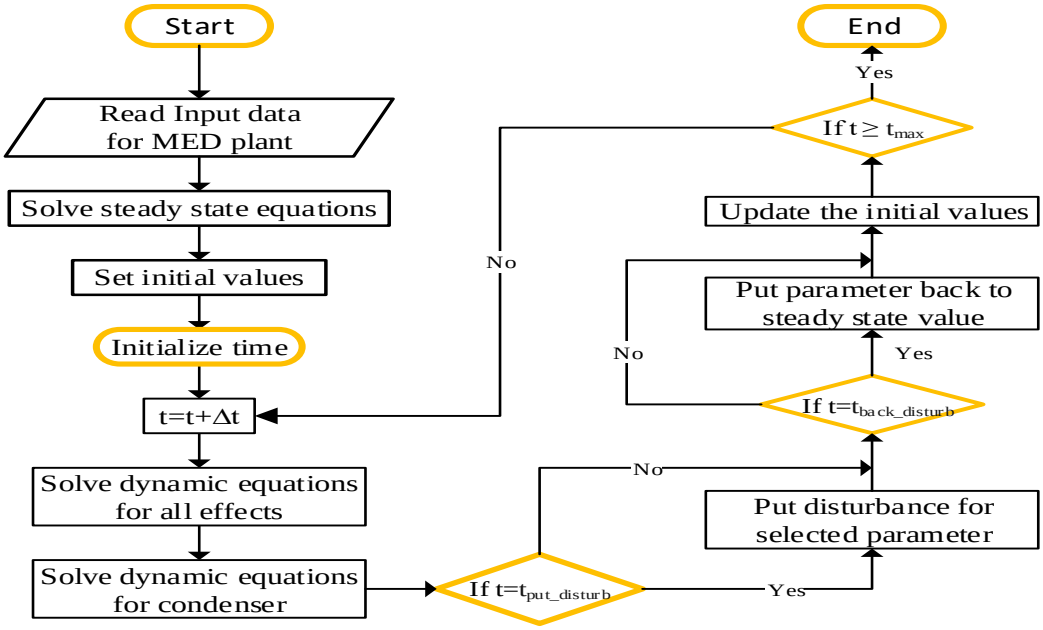

Figure 28 Flow chart for the solution procedure of the dynamic model of MED systems.

5.5 Results and Discussion

Steady-state and dynamic models were developed for the four different conventional configurations of MED process. In addition to that MED with PCF configuration was integrated into TVC unit and its dynamic behavior is investigated as well. First, the steady-state and dynamic model results are validated with a lab-controlled three-effect MED plant of shell and tube evaporators with a total freshwater production of 3 m^3/day shown in Figure 29a. [191]. The operational parameters of the 3-effects plant are shown in Table 24 with the steady state solution results. The heat transfer areas for the first effect, second and third effects and condenser are 1.2, 1.6 and 1.44 m^2, respectively. The heat source used in this plant is a hot water stream that is introduced to the first effect. The vapor temperature in each effect is measured when the hot water heat source is shut off for a specified time interval. To investigate the validity of the dynamic model under experimentally similar conditions, the heat supplied to the first effect is set as the disturbance in the numerical model. Due to the small value of the sensible heat of the hot water,

the heat supplied to the first effect is set to zero at the time of hot water shutdown and is returned to its steady-state value at the end of the disturbance period. Figure 29b shows a comparison between the vapor temperature in each effect obtained from the dynamic model and the data published in [191]. The average absolute error between the actual and simulated data for each effect is 2% which indicates good agreement between the simulation and the measured experimental data.

The developed models are applied to an industrial scale plant located in Tripoli, Libya [72] in steady state operation or when it is subjected to perturbations from the design steady-state values of the main input parameters. This plant is a four effect MED-TVC plant working with PCF arrangement. The number of effects is set at 4 to ensure a reasonable temperature drop between effects [192]. A comparison between the results calculated by the present model and the corresponding available values of actual data from this commercial plant in Tripoli is also used for model validation as in Table 25. Then, to unify operational conditions for a different configuration, the actual operating conditions of Tripoli plant was used to obtain the steady state operation for the other MED process arrangements.

Table 24 Validation with design data for three MED unit operating in PF configuration [191].

State #	Temperature ^{o}C	Flow rate kg/s (model)	Flow rate kg/s [191]	Note
1,2	22	1.0159	1.0599	Cooling water
3	29	0.087	0.0916	Total Feedwater
4	29	0.032	0.0334	Feed 1st effect
5	29	0.028	0.03	Feed 2nd effect
6	29	0.026	0.028	Feed 3rd effect
7	60.08	0.016	0.0167	Brine 1st effect
8	55.28	0.014	0.015	Brine 2nd effect
9	48.55	0.013	0.014165	Brine 3rd effect
10	75	0.91888		Hot fluid in
11	65			Hot fluid out
12	60.08	0.016	0.01667	vapor 1st effect
13	55.28	0.014	0.015	vapor 2nd effect
14	48.55	0.013	0.014165	vapor 3rd effect

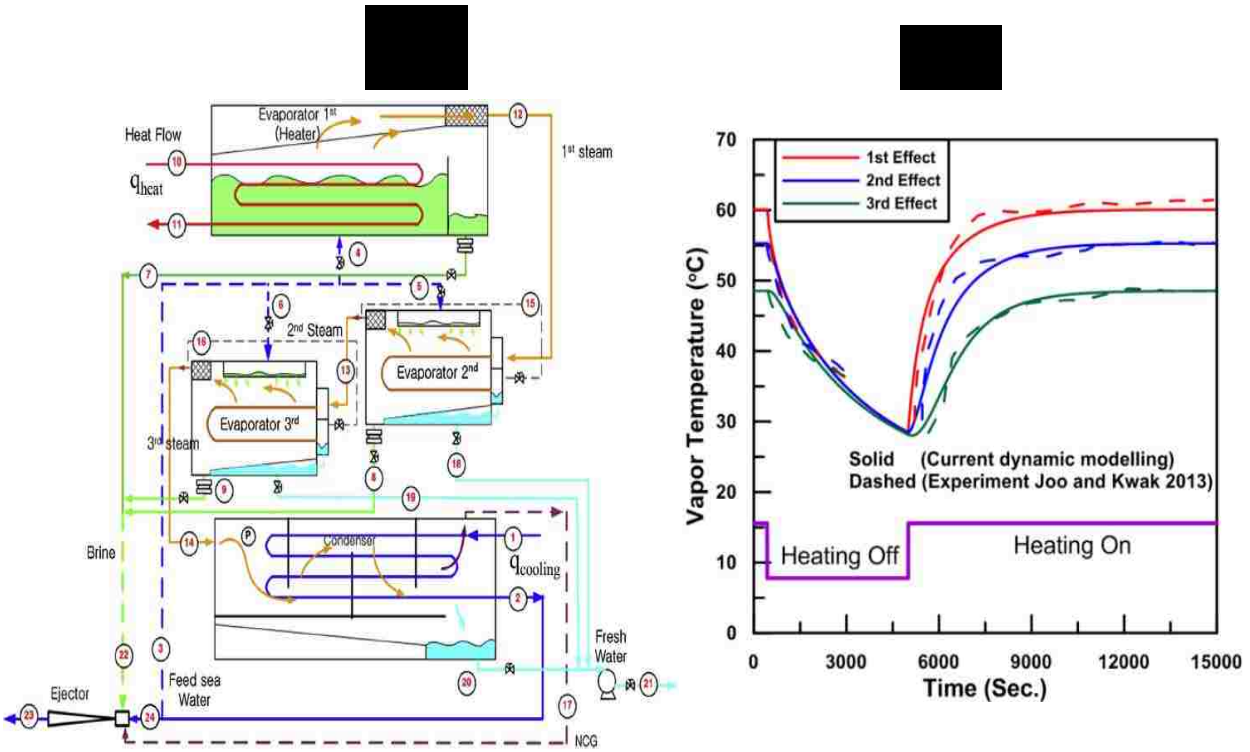

Figure 29 (a) Distribution diagram of an evaporative multi-effect distiller [191].

(b) Vapor temperature in each evaporator for simulated model experiment.

Table 25 shows the results of the steady state operating parameters of different feed configurations of MED process. Among the four different feed configurations, PCF scheme has the best performance with the highest GOR followed by the PF while the BF system has a likely higher

GOR than the FF configuration. However, the BF system is not used on the industrial scale for the desalination due to the salinity increase in the direction of high brine temperatures towards the first effect. Regarding the specific heat transfer area (S_A) which represents the heat transfer area summation of all effects plus condenser area divided by the total distillate production, PCF has the lowest value while PF has the highest value among the four configurations. The comparison of the specific heat consumption (SHC) among the different feed configurations shows that the FF system has the highest SHC and the lowest belongs to the PCF feed arrangement. For the current fixed number of effects (n=4), MED-PCF feed configuration is considered the most reliable among the other configurations based on many terms and merit criteria such as TWP, S_A, condenser size, SHC, and GOR. Adding TVC to the MED-PCF boosts the GOR of the MED from 3.878 to 6.342 which is apparently due to the reduction in the amount of the required heat source to the plant. Another benefit of adding TVC unit is the lower amount of cooling seawater necessary for the condenser compared to other configurations which indicate that a smaller condenser size is needed. Also, MED-TVC has the least S_A, SHC and total water price (TWP) compared to the other standing alone MED configurations. The results of TWP obtained are consistent with the results for thermal desalination units found in the literature [73, 74]. For the PCF-TVC configuration, if the considered interest rate is varied from 3 to 12 %, the TWP will increase from 2.04 to 2.18 $/m^3.

Table 25 Comparison between steady-state operation for different MED configurations.

Configuration	BF	FF	PF	PCF	PCF-TVC	Tripoli [72]
Number of effects	4					
Inlet feed salinity, g/kg	35					
Outlet brine salinity, g/kg	53					
Inlet steam temperature T_s, °C	65					
last brine temperature T_n, °C	45.4					
Feed temperature T_f, °C	31.5					
Heat source flow rate (S), kg/s	14.4				8.89	
Motive steam pressure, kPa	--				2300	
Entrained vapor, kg/s	--				5.83	5.55
Distillate production (D), kg/s	53.133	50.49	53.628	56.006	56.38	57.861
Gain output ratio (GOR=D/S)	3.67	3.5	3.724	3.878	6.342	6.508
Brine flow (B), kg/s	103.346	98.006	104.187	108.901	108.906	109.21
Feed flow (F), kg/s	156	148.5	157.906	164.907	165.286	167
Cooling seawater flow, kg/s	644.475	824.726	715.771	808.848	375.81	NA
Specific heat transfer area (S_A), $m^2/kg/s$	141.38	143.86	145.751	137.17	123.685	NA
Specific heat consumption [101] (SHC=2330/GOR), kJ/kg	634.8	665.71	625.67	600.8	367.39	NA
Total water price, $\$/m^3$	2.626	2.7645	2.5974	2.506	2.088	NA

In real operation, the operating parameters may not be maintained constant due to the fluctuations in weather conditions and the rate of the supplied heat source to the plant. These changes in operating parameters away from the design steady state values may lead the plant to i) reach another steady state condition with different performance; ii) disrupt the plant operation by changing the amount of product; or iii) in some instances, cause the plant to approach drying or flooding in one or more of the effects. The behavior of the four feed configurations and the MED-TVC is determined under differently applied disturbances. Three disturbances are selected as a step ramp decrease from the steady state values of the operational parameters. These disturbed parameters include - steam flow rate (heat source disturbance), cooling seawater temperature, and cooling seawater flow rate (heat sink disturbances) which are denoted as m_{ms}, T_{cw}, and m_{cw} disturbances, respectively. A ramped type disturbance with a linear variation in the main input parameters is considered in the current study and the magnitude of reduction and applied duration

of ramp disturbances are fixed. A ramp time of 500 s is considered which represents the time that the designed value of input parameter takes to reach the value of the reduction at the beginning of disturbance application. On the other hand, before the end of the disturbance, it represents the time needed to reach the steady state designed values of the input parameter. The outlet condition for brine discharge from the plant is the same in all configurations while a pressure jump condition is considered for inter-effects pumps in the FF and BF configurations.

5.5.1. Effect of Heat Source Disturbance

The disturbance in a supplied heat source (steam) considered is a 10% ramp stepwise reduction in the steady-state value (14.4 kg/s for BF, FF, PF, and PCF), and (6.36 kg/sec for MED-TVC) starting at 1,000 secs, and this reduction lasts for 14,000 sec. Considering that the heating steam is supplied from a boiler with its pressure regulated, the heating steam temperature is kept constant, and the energy swings cause a disturbance in steam mass flow rate. The dynamic response of the brine level and vapor temperature for this reduction in the amount of supplied steam to the four-different configurations and the MED-TVC unit as well are shown in Figure 30. It is clear from the figure that the vapor temperature response is faster than the brine level response due to the higher thermal capacity of the liquid lump compared to the vapor lump. Also, in general, the temperature drop in the effects decreases gradually from the first effect towards the last effect because the first effect is impacted first by the reduction in steam mass flow rate. In addition, the first effect is impacted by pressure change. This pressure change originates from changes in both the brine level and the vapor temperature, which have contradicting effects. Based on the calculations, the maximum pressure change for BF configuration in the first effect is only 9 kPa.

For the BF configuration, the reduction in the vapor temperature and consequently pressure in the effects in the upstream direction of brine flow produces a higher brine mass flow rate (from the last effect towards the first effect). This can be observed by noticing the increase in the brine level and brine mass flow rate in the first effects as shown in Figure 30 and Figure 31. The highest increase in the brine level in all configurations is reached in BF. This increase for the currently used plant dimensions and effects heights may lead to first effect flooding. The flooding condition, in the thermal desalination plant, causes the plant shutdown because the effect's tubes bundles will be fully submerged with concentrated brine which in turn will drastically reduce the evaporation rate. For FF configuration, the brine level increases faster in the effects in the downstream direction of the brine flow at the beginning of disturbance application due to their pressure drop that is associated with the disturbance. However, later on, the generated hydrostatic head helps to push the brine in the forward direction which causes the brine level and brine mass flow rate to increase in the last effects as shown in Figure 30 and Figure 31. The vapor flow rate shows a slight decrease from the first to last effect for both BF and FF arrangements as shown in Figure 31. Since the feed in parallel flow arrangements is divided among all effects, the brine level response is faster comparing with BF and FF arrangements. The MED-TVC configuration shows a slightly higher increase in the brine level against both PF and PCF configuration, and this could be attributed to the higher reduction in the evaporation that the MED-TVC be exposed to upon reducing the motive stream by 10% as shown in Figure 31. For all configurations, the 10% reduction in the heat source flow rate causes a nearly 10% reduction in the vapor flow rate from each effect except in the case of MED-TVC where it reaches ~13%.

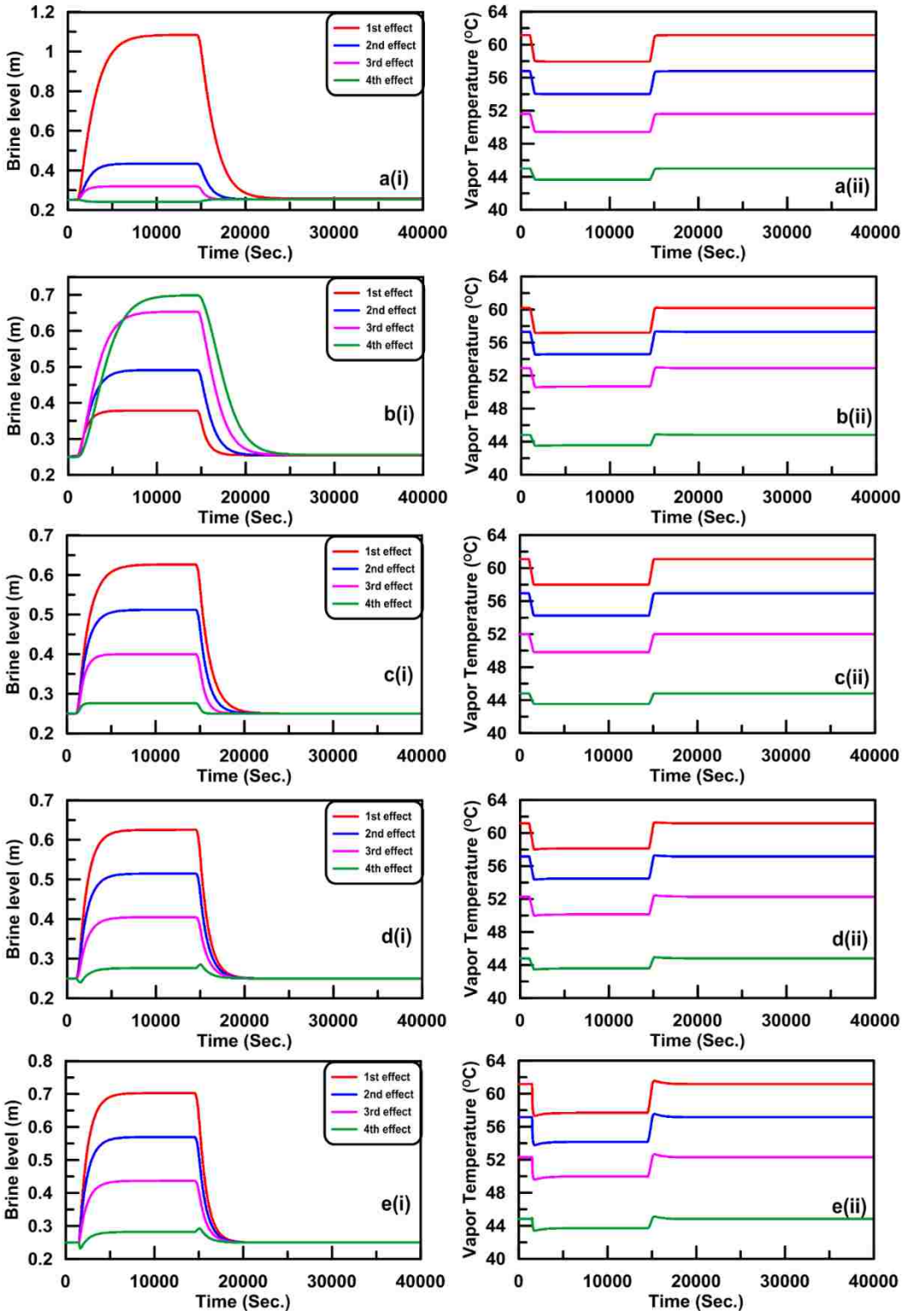

Figure 30 Variation for brine level and vapor temperature for different feed configurations and reduction in heat source flow. (a)BF, (b) FF, (c) PF, (d) PCF, (e) PCF-TVC.

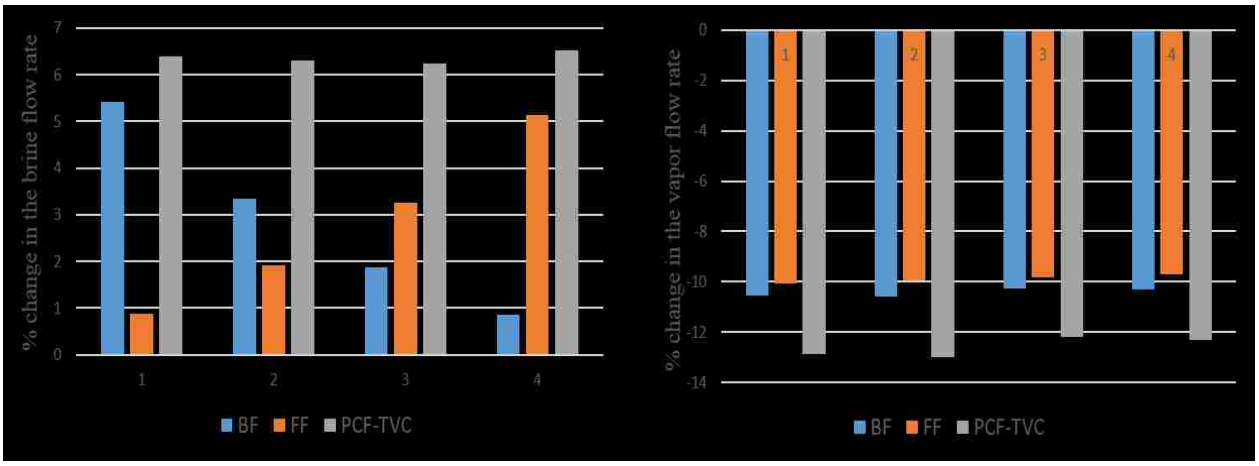

Figure 31 Percentage change in brine and vapor flow rate with 10% reduction in the heat source flow rate.

5.5.2. Effect of Heat Sink Disturbances

The second type of applied disturbance is related to the heat sink of the plant which is the cooling seawater that is introduced into the condenser. The disturbance could be a reduction in the cooling seawater temperature or the cooling seawater mass flow rate. First, a 10% reduction in the cooling seawater temperature from the steady state value is applied to the different feed configurations. Starting with the BF where the total feed is directed to the last effect, the results show that the drop-in vapor temperature of the last effect is relatively high. Also, the brine level and mass flow rate for all effects increases as shown in Figure 32 and Figure 33. As the brine moves from the last effect towards the first effect, the increase in the brine mass flow rate in each effect due to cooling seawater temperature drop adds up sequentially and produces more mass flow rate and brine level in the backward direction. The brine level in the first effect increases by 63% of its original steady-state value. The FF configuration has the opposite trend where the brine level and brine mass flow rate increase in the forward direction. Increasing the brine flow rate in the forward direction causes the reduction in vapor temperature to increase from the first effect towards the

last effect. The maximum vapor temperature drop occurs at the last effect. Also, the reduction in vapor flow rate due to cooling seawater temperature drop has the opposite trend for BF and PF as shown in Figure 33.

In the PF and PCF configuration, all effects are exposed to lower feed temperature at the same time due to the drop-in cooling seawater temperature. Accordingly, the evaporation rate decreases in all effects and this reduction becomes more significant in the first effect where the brine temperature is the highest. This produces an increase in brine level in the first effect which transmits sequentially in the forward direction to the last effect as in Figure 32. Both the configurations have similarities in response to the applied cooling seawater temperature reduction. However, it is noticed that the PF needs longer time to reach steady state condition than PCF configuration. Adding TVC unit to the PCF reduces the size of the back condenser, which makes the condenser more sensitive to the cooling seawater temperature. Reducing the cooling seawater temperature results in a considerable drop in condenser pressure which drive more vapor in the forward direction and generates adverse pressure gradient to the brine flow. This increases the vapor temperature drop and the brine level in the first effect as shown in Figure 32 for PCF-TVC configuration.

The second disturbance in the heat sink considered is a 10% reduction in cooling seawater flow rate. The data show that lowering the cooling seawater flow rate has the reverse effect of decreasing the cooling seawater temperature regarding increasing vapor temperature and reducing the brine level in all effects as shown in Figure 34. The highest reduction in brine level is reached in MED-TVC. So, if a condition for evaporator drying is assigned, MED-TVC will be the most candidate arrangement that may violate this situation and hence will require a reliable control system to avoid plant operational disturbance. The increase in the feed and vapor temperatures

causes a reduction in the brine flow rate which travels in the backward and forward directions for BF and FF, respectively as shown in Figure 35. In PF and PCF, similar patterns for the process response with the reduction in cooling seawater flow rate, but still PF needs more time to reach new steady state compared to PCF. With the addition of the TVC unit to the PCF, the increase in the vapor flow rate reaches ~ 3 to 4 folds in the PF or PCF, and this again could be attributed to the smaller size of the condenser. The enhancement in vapor flow rate shows opposite trend in the forward direction for BF and FF as shown in Figure 35. However, for PCF-TVC, this improvement does not follow a specific pattern because the vapor flow rate depends on both the cooling seawater flow rate and the TVC entrainment ratio.

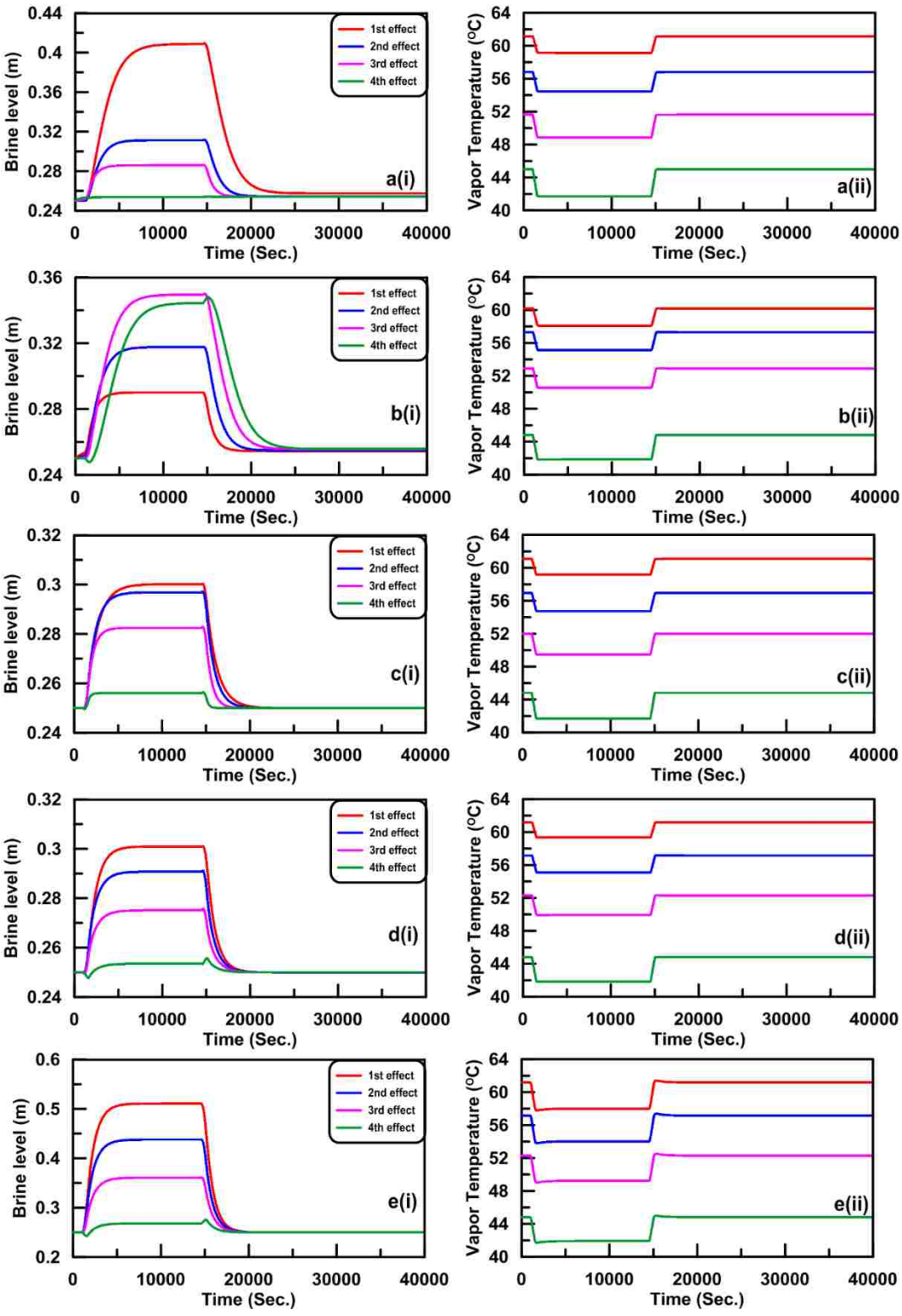

Figure 32 Variation for brine level and vapor temperature for different feed configurations and reduction in cooling seawater temperature. (a)BF, (b) FF, (c) PF, (d) PCF, (e) PCF-TVC.

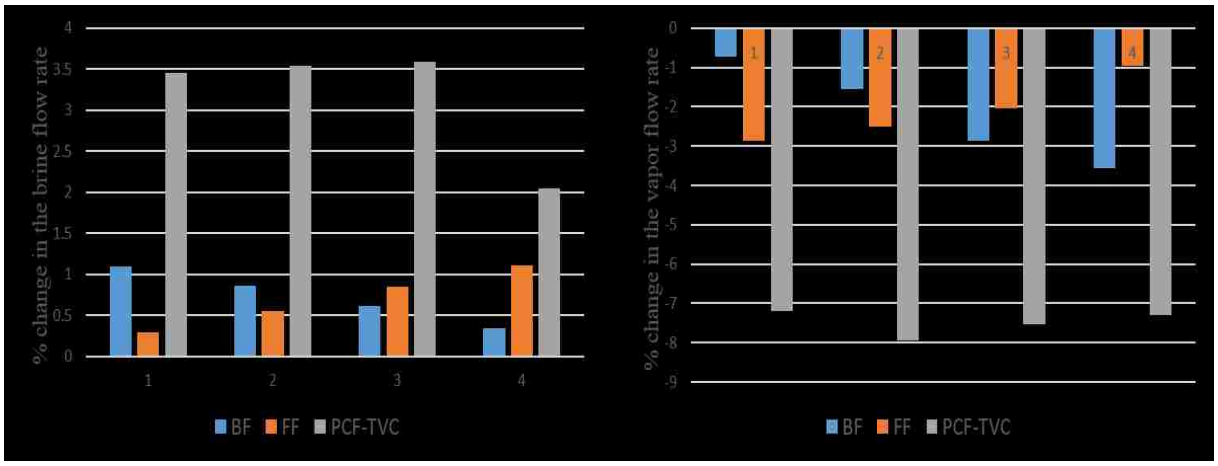

Figure 33 Percentage change in brine and vapor flow rate with 10% reduction in the cooling seawater temperature.

5.5.3. MED- Processes Performance

The effects of the previously applied disturbances on the performance of the different MED flow arrangements are presented in Figure 36 as percentage change from steady-state values of the plant GOR. In general, the MED-TVC performance is most sensitive to all disturbances. The reductions in heat source flow rate and in cooling seawater temperature in the case of MED-TVC cause the highest decrease in GOR (8%). For a reduction in the seawater cooling flow rate, MED-TVC experiences an increase in the GOR by ~ 2% due to an increase in the vapor flow rate that reaches ~ 2:4 folds than the stand-alone PCF configuration. The PF and PCF configurations are least affected by the reduction in cooling seawater temperature. Though the PCF process integrated with a TVC unit can be significantly affected by the applied disturbances, it gives multiple benefits compared to the other types of configurations. These interests include the highest production rate, lowest product cost, lowest condenser area, lowest cooling seawater flow rate and lowest specific heat consumption. All these benefits allow the MED-TVC to capture a significant share of fresh water production on a commercial scale using thermal desalination. The sensitivity issues of these

plants need further investigation by studying the intensity and sensitivity of these applied disturbances to find out the critical values which may cause plant shutdown due to flooding or drying in the effects as reported in [193]. Also, it is worthwhile to mention that the average times required to return to steady state operation after turning off the applied disturbances are 7500, 10000, 6000, 5000 and 4600 s for the BF, FF, PF, PCF and MED-TVC configurations, respectively.

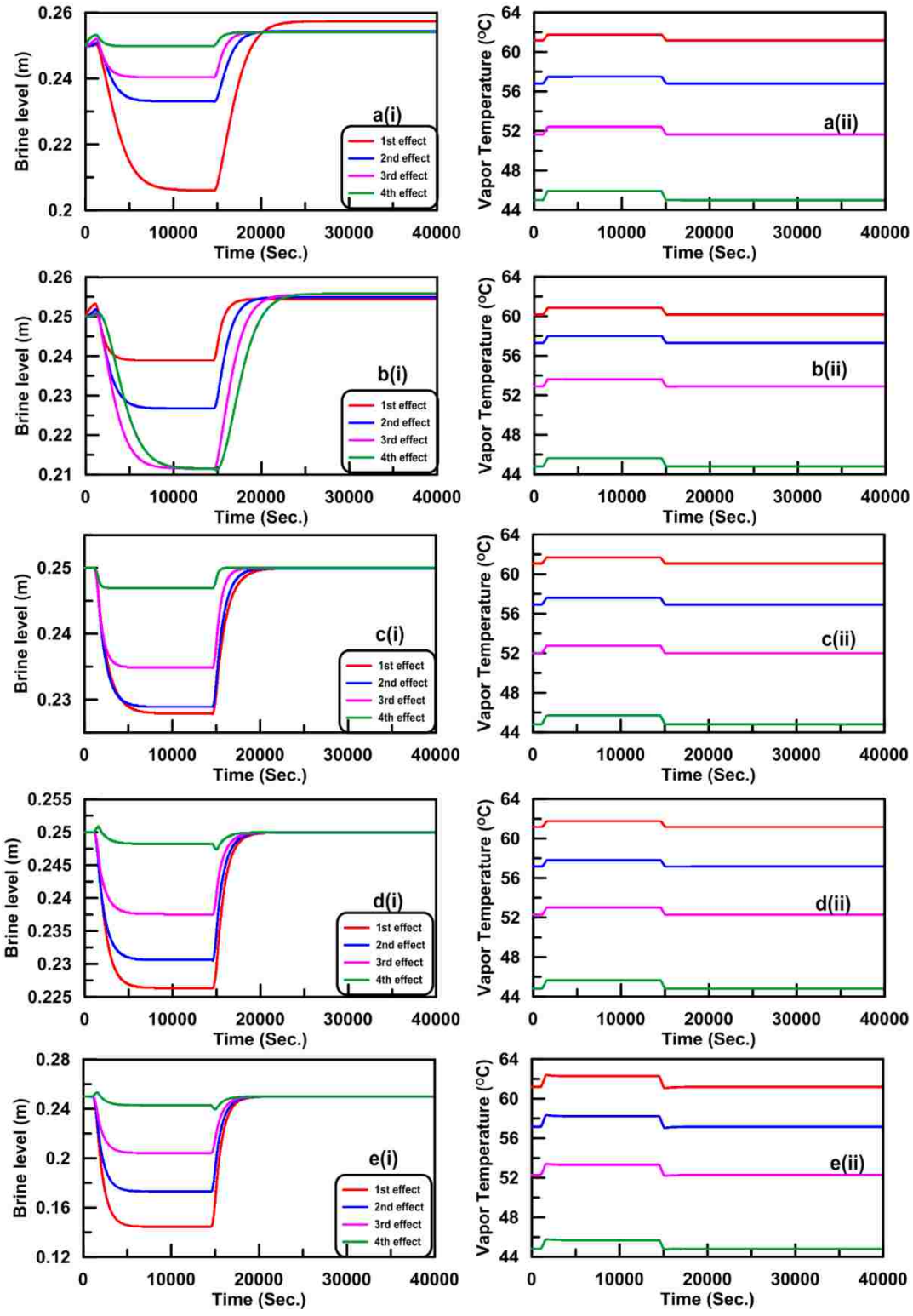

Figure 34 Variation for brine level and vapor temperature for different feed configurations and reduction in cooling seawater flowrate. (a)BF, (b) FF, (c) PF, (d) PCF, (e) PCF-TVC.

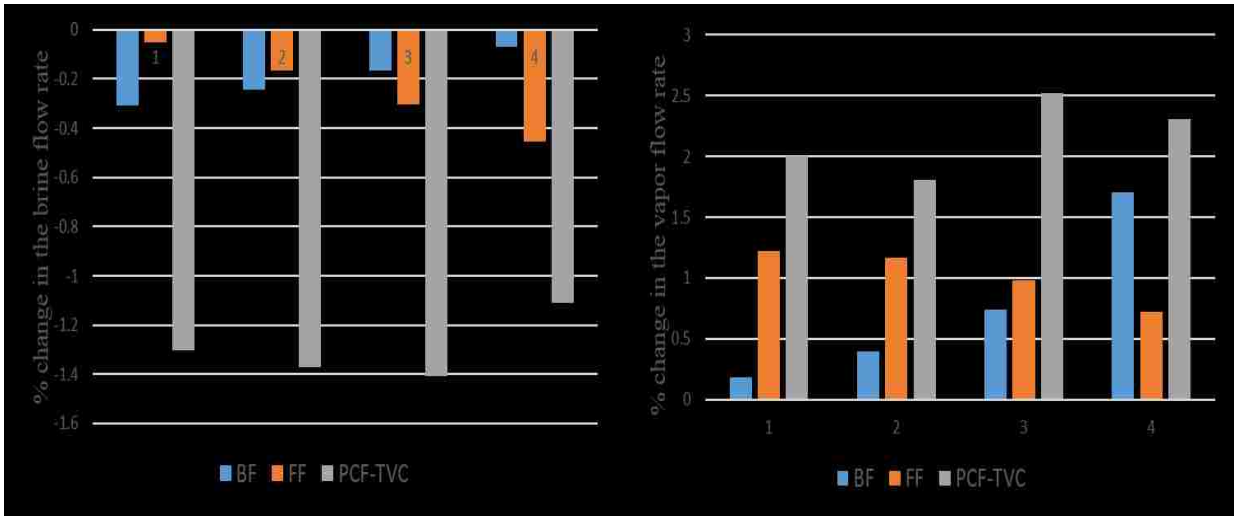

Figure 35 Percentage change in brine and vapor flow rate with 10% reduction in the cooling seawater flow rate.

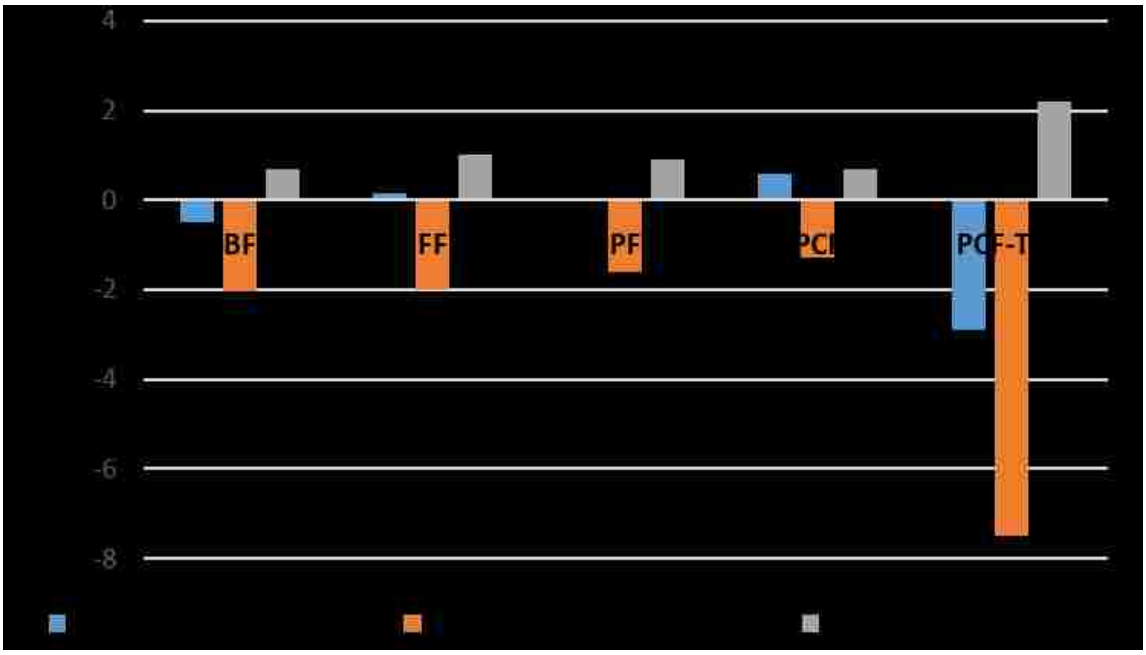

Figure 36 Percentage change in the GOR for all feed configurations under different disturbances types.

5.6 Conclusions

Steady-state and dynamic models are developed for the four different feed configurations of MED and MED-TVC as well. The results show that, with a fixed number of effects and TBT, the parallel/cross (PCF) configuration has the best performance in terms of the total production of fresh water, GOR, specific heat transfer area, and specific heat consumption. However, it requires a relatively higher cooling flow rate compared to the other configurations. Integrating TVC to the last effect of the PCF configuration lowers the cooling seawater requirements and the specific heat consumption. Also, the total water price is reduced from 2.51 $/m^3 to 2.08 $/m^3, and GOR is boosted from 3.88 to 6.34. On the other hand, the FF configuration has the highest TWP of 2.77 $/m^3 and the lowest GOR of 3.5 among the different feed configurations.

Detailed dynamic modeling of different feed configurations reveals that the MED-TVC has the fastest response compared to other types of feed configurations and the FF requires a longer time to reach steady state condition. In the case of the heat source disturbance, the backward feed has the highest increase in the brine level followed by MED-TVC, while PF and PCF show only a moderate increase in the brine level. For the MED-TVC process, the vapor flow rate is highly reduced compared to the other configurations for the case of a reduction in the heat source flow rate. For the heat sink disturbance, MED-TVC process is the most sensitive among the configurations, and this could be attributed to the smaller size of the condenser compared to the PCF or other configurations. However, for the cooling seawater temperature disturbance, BF has the highest increase in the brine level that is progressively transmitted from the last effect.

The maximum increase in the pressure of the first effect for the BF configuration due to a 10 % reduction in the steam supplied is 9 kPa. For the three types of applied disturbances, the average times required to return to steady state operation after turning off the applied disturbances are

7500, 10000, 6000, 5000 and 4600 s for the BF, FF, PF, PCF and MED-TVC configurations, respectively. Also, the MED-TVC is the most sensitive of all configurations, where the reductions in heat source flow rate and cooling seawater temperature may lead to a high reduction of ~ 8% in GOR. The PF and PCF configurations are least affected by the decrease in cooling seawater temperature. For a reduction in the seawater cooling flow rate, MED-TVC experiences an increase in the GOR by ~ 2%. This is due to an increase in the vapor flow rate that reaches ~ 2 to 4 times that in the stand-alone PCF configuration. However, without a reliable control system, the MED-TVC configuration is the configuration most susceptible to a plant drying condition.

CHAPTER 6 EFFECT OF DISTURBANCES ON MED-TVC PLANT CHARACTERISTICS, DYNAMIC MODELING AND SIMULATION[**]

Abstract

The current study describes a detailed steady-state analysis and transient operation of a multi-effect desalination plant with a thermal vapor compressor unit (MED-TVC). The model developed is based on solving the basic conservation equations of mass, energy, and salt. It can predict steady-state operation and transient behavior when the plant is subject to abrupt changes in the main input parameters including motive steam flow rate (m_{ms}), cooling seawater flow rate (m_{cw}) and cooling seawater temperature (T_{cw}). These sudden changes simulate the conditions a MED-TVC plant may be exposed to. Both the steady-state and dynamic aspects of the model are validated against published experimental data. Monitoring the variation of four state variables (vapor temperature, brine level, brine and vapor flow rates) in each effect shows that disturbances in the motive steam flow rate and the cooling seawater temperature have a significant effect on the plant performance. On the other hand, the disturbance in the cooling seawater mass flow rate has only a moderate effect. For all applied disturbances, the change in the brine level is the slowest compared to the changes in vapor temperature, and brine and vapor flow rates. Furthermore, the effect of changing seawater salinity shows a slight effect on the total distillate production and the specific heat transfer area.

[**] **Mohamed L. Elsayed**, Osama Mesalhy, Ramy H. Mohammed, Louis C. Chow, "Effect of disturbances on MED-TVC plant characteristics: Dynamic modeling and simulation." Desalination, volume 443, October 2018, Pages 99-109.

Introduction

Desalination of seawater is a well-studied means of supplying fresh water in many countries, especially in the Gulf countries (GC) and in the Middle East and North Africa (MENA) regions. Desalination is economically and technically practicable to recover fresh water with excellent quality and in huge quantities. Desalination can be accomplished using several techniques which can be categorized as thermal-based and membrane-based. An example of the thermal process is multi-effect-desalination (MED) which reuses the latent heat vaporization multiple times to vaporize the seawater by utilizing falling-film horizontal tube evaporator/condensers [73]. To minimize scale formation and corrosion, MED operates with a relatively low top brine temperature (TBT), typically lower than 75°C [31]. MED is an attractive approach for desalination because of the combination of low economic costs and low energy consumption, together with plant durability due to low-temperature operation. With MED, there are little requirements for comprehensive seawater pretreatment as in Reverse Osmosis (RO) [34]. Comparing with multi-stage-flash (MSF) desalination, regarding energy/electricity utilization, MED is more efficient and economical than MSF due to the use of lower pressure steam [162]. Also, it is easier to utilize solar energy as an energy source with MED than with MSF desalination.

Thermal or mechanical vapor compression (VC) improves the overall efficiency of thermal desalination, especially when it is combined with a MED system [32]. In VC desalination, the low-temperature vapor is recovered from certain locations of the thermal desalination system and converted to vapor with high temperature [108]. Also, adding VC to the thermal desalination system requires less cooling seawater and lower electricity consumption. Basic types of vapor compression include thermal vapor compressor (TVC) and mechanical vapor compressor (MVC). The mechanical compressor in MVC is used to compress vapor from the last effect to deliver high-

temperature steam to the first effect. MVC is an effective technique for small-scale desalination where electrical power is available. It is, therefore, suitable for remote regions with a small population and access to power grid lines due to simplicity and compactness [41]. Also, it is considered a practical alternative to the RO systems as it has a much simpler pretreatment system and limited operational problems related to fouling and scaling [38]. On the other hand, due to the advantages of lower corrosion/scaling rates, lower capital cost, longer operation life and less pumping power consumption, TVC-MED units are commonly used in industrial desalination plants of different sizes [70]. The TVC compressor uses high-pressure motive steam to drive a portion of the last effect vapor back to the first effect.

Dynamic modeling of MED is used to establish advanced control strategies, test operating scenarios, address potential problems related to unexpected transient events, and produce a relatively constant output during the production period. Also, it helps engineers to understand better, maintain, develop optimal control strategies, prevent significant damages caused by malfunction, and troubleshoot the causes of disorders. Applications of dynamic modeling include off-line or on-line modeling to investigate the transient behavior of the system and execute control strategies [169]. Though there are very few published papers in the literature on transient modeling for MED, modeling of steady-state operation of single and MED has been made by various researchers and solved by using different solution techniques [73]. El-Dessouky et al. [170] designed steady-state models to investigate the single/multi-effect TVC process. They concluded that the parallel/cross flow configuration had excellent performance and gained output ratio (GOR), which is defined as the ratio of distillate output to the consumed steam. Decreasing the TBT while increasing the number of effects would increase the specific heat transfer area. For parallel configuration MED-TVC, Darwish and El-Dessouky [194] developed a simplified steady-

state model and they found that the heat transfer area was much less than that of an MSF system with the same input of heat energy. Also, they obtained the same GOR for a four-effect MED-TVC compared to an eleven-effect MED or a 24-stage MSF. Kouhikamali and Sharifi [195] adopted an optimization design scheme for a MED-TVC system including the usage of pre-heaters between effects and concluded that, for the same temperature difference between inlet and outlet of the pre-heaters and between effects, energy consumption is decreased to a minimum. Thermodynamic analysis of different MED systems feeds water arrangements were presented by Darwish and Abdulrahim [196]. For each arrangement, the steady state mathematical equations were written. The GOR, heat transfer area and cooling seawater flow rate were compared, and the rationale for choosing these configurations was provided.

A dynamic model for a 17-effect MED system was developed and solved simultaneously for the state variables at the end of each time step using the Newton-Raphson method in [189]. Later on, results for a dynamic model for 10-effect MED showed fair agreement while compared with experimental data from a 150 m^3/day pilot MED in Israel [197]. El-Nashar and Qamhiyeh [180] used a lumped model to investigate the dynamic behavior of Multi-Effect-Stack (MES) evaporators. Conservation equations of mass and energy were written and solved simultaneously for each effect. The model yields reasonable agreement with actual data taken from an operating desalination plant at Abu Dhabi during plant start-up. The dynamic behavior of four-effect MED systems was introduced by Aly and Marwan [179] that allowed predicting the changes in the system variables under transient operating conditions. They used a lumped model for time-dependent mass, energy, and salt balance equations, but there was no validation provided. A dynamic simulator was proposed for a MED-MVC unit [141] without providing results that show the dynamic behavior and system response due to a load change. Roca et al. [181] investigated a

solar assisted-MED unit experimentally and compared it with a simplified dynamic model based on the work developed in [179]. Mazini et al. [183] developed a lumped dynamic model and validated it with actual data of an operating plant. Although disturbances in feed flow rate and seawater temperature were considered, the physics of the system response was not clearly illustrated. Cipollina et al. [185] developed a dynamic MED-TVC model based on available data from the Trapani plant using the equation-based process simulator gPROMS®. However, the developed dynamic model was not validated with real dynamic operation of the Trapani plant. In addition, a steady-state model for the condenser unit was considered despite the important role of the condenser unit in the MED system. Furthermore, the general thermodynamic model for the TVC unit developed by El-Dessouky et al. [73] was adopted which simplifies the mixing process and affects the simulation accuracy [198]. Recently, Elsayed et al. [90] presented a comprehensive model to investigate the transient behavior of four different feed configurations of MED systems and MED-TVC. Their results showed that MED-TVC with parallel/cross feed has the fastest response while backward feed and forward feed have slower response to the applied disturbances. Also, they concluded that the MED-TVC is more susceptible to the heat sink disturbances compared to the other traditional MED configurations.

The physics behind the transient behavior of a MED-TVC system subject to external disturbances has not received adequate attention in the open literature. Generally, adding a TVC unit to the MED improves the performance through decreasing the required amount of thermal energy input. However, the MED-TVC systems are sensitive to the applied disturbances and fluctuations in the input parameters compared to stand alone MED. Therefore, the present work aims to further improve and apply the dynamic model developed in [90] to study the behavior of a parallel/cross feed of MED-TVC system. A robust dynamic model for the condenser is developed to predict the

dynamic variation of the condenser pressure, condenser liquid level and the feed temperature. The MED-TVC system transient behavior under different input conditions (disturbances) from the nominal steady-state values of input parameters is obtained. Three disturbances namely, motive steam flow rate, cooling seawater flow rate and cooling seawater temperature are considered. Also, the effect of change in feed seawater salinity on plant operation was also investigated.

MED-TVC configuration

The configuration of combining the MED-TVC system is accomplished by using conventional rows of effects, each placed into a circular/rectangular vessel along with a condenser. A thermo-compressor is integrated with the last effect to form the MED-TVC system as shown in Figure 37. Preheated feed seawater from the condenser is distributed to a sequence of successively lower pressure vessels, called effects. A major portion of the seawater that enters the condenser is directed back to the sea. Feed is sprayed into each evaporation effect and flows down as a thin liquid film along the outside wall of the horizontally installed tubes. Hot compressed steam (supply steam) from the TVC flows into the tube inside the 1st effect. The vapor generated in the last effect of MED system $m_{v,n}$ is divided into two streams at the pressure P_n. The first stream D_{ev} is pulled by the TVC and the remaining steam $m_{v,n} - D_{ev}$ is used to preheat the cooling seawater in the condenser. A stream of motive steam m_{ms} at a relatively high motive pressure P_S enters the TVC unit. The motive steam is usually supplied from the boiler or steam turbine of a power plant. The entrained vapor, compressed by the TVC, is combined with the motive steam and directed to first effect with a mass flow rate of $m_{ms} + D_{ev}$ and discharge pressure of P_d. The fraction of the mass flow rate of the motive steam to the entrained vapor is called the entrainment ratio (R_a).

The steam stream delivered from TVC unit, through condensation inside the tubes of the first effect, raises the temperature of the feed seawater to its boiling temperature which is also known as the TBT. A fraction of the feed seawater in the first effect evaporates and the vapor flows into the second effect which is at a lower pressure and temperature than the first effect. This vapor acts as a heat source for the evaporation of a part of the feed seawater in the second effect. This process repeats and continues to the last effect. The unevaporated brine from the first effect enters the second effect to utilize its energy by flashing at a lower pressure. The brine flow process also continues to the last effect. This manner of feed water and brine flow is shown in Figure 37 and is known as the parallel/cross configuration. The vapor inside the second to the last effect is generated by both evaporation and flashing. The fresh water and concentrated brine are cascaded to the last effect where they are drawn out by pumps.

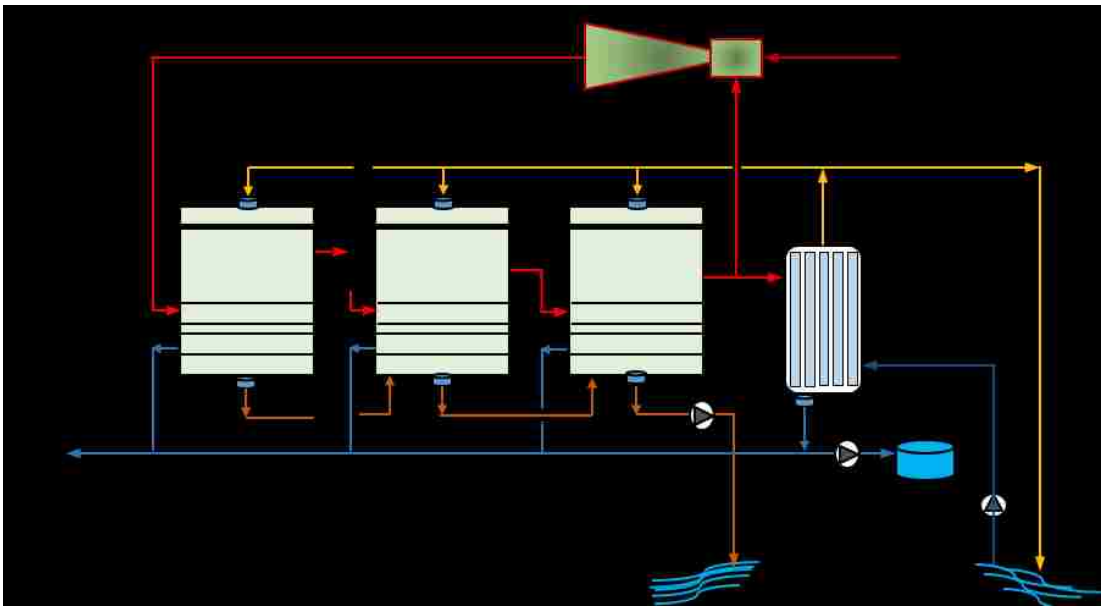

Figure 37 Schematic diagram of a MED system with four effects and thermo-compressor unit.

Models development

6.4.1. Steady state model

The steady-state conservation equations of mass, energy, and salt are solved to obtain the steady-state conditions of all the parameters in the plant using the following assumptions:

19. Non-condensable gases (NCG) are properly deaerated and vented out to avoid accumulation inside the MED system, so its effect on effect performance is not considered.
20. The brine stream from the *i-1* effect is assumed to flash adiabatically upon entering the i effect.
21. Thermophysical properties for the brine and vapor are considered to be temperature and salinity dependent. Appropriate correlations are selected from [73].
22. Thermodynamic penalty representing the temperature difference between the brine pool and the vapor generated in the effect is taken as the Boiling Point Elevation (BPE).

$$T_{v,i} = T_{b,i} - BPE\left(T_{v,i}, X_{b,i}\right) \tag{50}$$

The steady state solution is carried out iteratively to adjust the temperature drop across the effects to yield the same evaporator area for all the effects. Using the above assumptions, the steady-state mass, energy and salt balance equations for MED-TVC system are presented in Table 26. In the steady state solution, the vapor/brine temperature, feed flow rate, brine flow rate, vapor flow rate and salinity at each effect are calculated in addition to the heat transfer surface areas in the effects. The motive steam flow rate, compression ratio and expansion ratio determine the entrainment ratio which in turn defines the amount of vapor entrained to the TVC unit.

Table 26 Steady-state conservation equations for a MED-TVC system.

Equations	1st effect	2 to n (last effect)	F	B	D
Mass	$B_1 = F_1 - D_1$	$B_i = F_i - D_i + B_{i-1} - d_i$	$\sum_{i=1}^{n} F_i$	B_n	$\sum_{i=1}^{n} D_i + d_i$
Salt	$F_1.X_f = B_1.X_1$	$B_i.X_i = B_{i-1}.X_{i-1} + F_i.X_f$			
Energy	$D_1 = \frac{S.\lambda_s - F_1(h_1 - h_f)}{\lambda_1}$, $d_1 = 0$	$D_i = \frac{(D_{i-1} + d_{i-1}).\lambda_{i-1}}{\lambda_i} - \frac{F_i(h_i - h_f)}{\lambda_i}$, $d_i = \frac{B_{i-1}(h_{i-1} - h_i)}{\lambda_i}$			
Overall mass balance $F = B + D$ Overall salt balance $F.X_f = B.X_n$					
d_i , represents the amount of vapor generated from hot brine flashing when exposed to lower pressure. S, supplied steam flow rate D, Total distillate flow rate F, Total feed flow rate B, Total brine flow rate.					

6.4.2. Dynamic model

The solution of the steady-state model is considered as the initial condition for the dynamic model. For the developed dynamic model, each evaporator is divided into three lumps: brine, vapor, and tube lump. For each lump, energy, mass, and salt balance are written. The accumulation of mass and energy in the evaporator tubes is taken to be negligible compared to the accumulation of mass and energy in the brine pool inside an effect. Figure 38 shows schematic diagrams for the first and ith effect evaporators and the condenser. Based on the assumptions stated above, the mass, energy, and salt balance equations for the ith effect evaporator are presented. The evaporator is assumed to have a cross-sectional area $A_{ce,i}$ and a total height H_E. The brine pool height $L_{b,i}$ and vapor height $H_E - L_{b,i}$ are shown in Figure 38b. Brine flow rate between effects is represented by $m_{b,i} = C_{b,i}\sqrt{\Delta P_{b,i}}$ where $\Delta P_{b,i} = P_{i-1} - P_i + \rho_b g(L_{b,i} - L_{b,i-1})$ and the vapor flow from an effect to the next is calculated from $m_{v,i} = C_{vi}\sqrt{\Delta P_{vi}}$ where $\Delta P_{vi} = P_i - P_{i-1}$. Equation 33 represents the matrix form of the derived combined lumps mass, energy and salt balances for *ith* evaporator effect.

$$\begin{bmatrix} C_{11} & C_{12} & C_{13} \\ C_{21} & C_{22} & C_{23} \\ C_{31} & C_{32} & C_{33} \end{bmatrix} \begin{bmatrix} dL_{b,i}/dt \\ dT_{v,i}/dt \\ dX_{b,i}/dt \end{bmatrix} = \begin{bmatrix} C_{14} \\ C_{24} \\ C_{34} \end{bmatrix} \tag{51}$$

where:

C_{11}	C_{12}	C_{13}	C_{14}
$A_{ce,i}(\rho_{b,i} - \rho_{v,i})$	$\left[A_{ce,i}L_{b,i}\frac{d\rho_{b,i}}{dT_{b,i}}\left(1+\frac{\partial BPE}{\partial T_{v,i}}\right) + (H_E - L_{b,i})A_{ce,i}\frac{d\rho_{v,i}}{dT_{v,i}}\right]$	$\left[A_{ce,i}L_{b,i}\frac{d\rho_{b,i}}{dT_{b,i}}\frac{\partial BPE}{\partial X_{b,i}} + A_{ce,i}L_{b,i}\frac{d\rho_{b,i}}{dX}\right]$	$m_{f,i} + m_{b,i-1} - m_{b,i} - m_{v,i}$
C_{21}	C_{22}	C_{23}	C_{24}
$A_{ce,i}(\rho_{b,i}h_{b,i} - \rho_{v,i}h_{vi})$	$\left[A_{ce,i}L_{b,i}\rho_{b,i}\frac{dh_{b,i}}{dT_{b,i}}\left(1+\frac{\partial BPE}{\partial T_{v,i}}\right) + A_{ce,i}L_{b,i}h_{b,i}\frac{d\rho_{b,i}}{dT_{b,i}}\left(1+\frac{\partial BPE}{\partial T_{v,i}}\right) + \rho_{v,i}(H-L_{b,i})A_{ce,i}\frac{dh_{v,i}}{dT_{v,i}} + h_{v,i}(H-L_{b,i})A_{ce,i}\frac{d\rho_{v,i}}{dT_{v,i}}\right]$	$\left[A_{ce,i}L_{b,i}h_{b,i}\frac{d\rho_{b,i}}{dT_{b,i}}\frac{\partial BPE}{\partial X_{b,i}} + A_{ce,i}L_{b,i}\rho_{b,i}\frac{dh_{b,i}}{dT_{b,i}}\frac{\partial BPE}{\partial X_{b,i}} + A_{ce,i}L_{b,i}h_{b,i}\frac{d\rho_{b,i}}{dX}\right]$	$m_{f,i}h_{f,i} + m_{b,i-1}h_{b,i-1} - m_{b,i}h_{b,i} + Q_{E,i}$
C_{31}	C_{32}	C_{33}	C_{34}
$A_{ce,i}\rho_{b,i}X_{b,i}$	$\left[A_{ce,i}L_{b,i}X_{b,i}\frac{d\rho_{b,i}}{dT_{b,i}}\left(1+\frac{\partial BPE}{\partial T_{v,i}}\right)\right]$	$\left[A_{ce,i}L_{b,i}X_{b,i}\frac{d\rho_{b,i}}{dT_{b,i}}\frac{\partial BPE}{\partial X_{b,i}} + A_{ce,i}L_{b,i}\rho_{b,i} + A_{ce,i}L_{b,i}X_{b,i}\frac{d\rho_{b,i}}{dX}\right]$	$m_{f,i}X_{f,i} + m_{b,i-1}X_{b,i-1} - m_{b,i}X_{b,i}$

As mentioned in MED-TVC process description, some of the vapor generated in the last effect is entrained by the TVC and the remaining portion is directed to the condenser to raise the feed temperature and eventually this vapor is completely condensed. In the present study, a detailed model for the condenser is developed which can predict the dynamic variation of condenser pressure, condenser liquid level, and the feed temperature with time. The condenser is treated similarly to the evaporator of the effects. It is sectioned into three lumps; condensate liquid, vapor, and tube as shown in Figure 38c. As shown the condenser assumed to have a cross-sectional area A_{cc} and a total height of H_{con} while the condensate pool height is L_{con} and vapor height

is $H_{con} - L_{con}$. Combined mass, and energy for vapor and condensate lumps in the condenser are given by equation 34. Mass balance of the liquid and vapor lumps can be written as:

$$\begin{bmatrix} D_{11} & D_{12} \\ D_{21} & D_{22} \end{bmatrix} \begin{bmatrix} dL_{con}/dt \\ dT_{con}/dt \end{bmatrix} = \begin{bmatrix} D_{13} \\ D_{23} \end{bmatrix} \tag{52}$$

where:

$\boldsymbol{D_{11}}$	$\boldsymbol{D_{12}}$	$\boldsymbol{D_{13}}$
$A_{cc}(\rho_{L,con} - \rho_{v,con})$	$\left[A_{cc}L_{con}\frac{d\rho_{L,con}}{dT} + (H_{con} - L_{con})A_{cc}\frac{d\rho_{v,cin}}{dT}\right]$	$(m_{v,n} - D_{ev}) - m_{con,O}$
$\boldsymbol{D_{21}}$	$\boldsymbol{D_{22}}$	$\boldsymbol{D_{23}}$
$A_{cc}(\rho_{L,con}h_{con} - \rho_{v,con}h_v)$	$\left[A_{cc}L_{con}h_{con}\frac{d\rho_{L,con}}{dT} + (H_{con} - L_{con})h_vA_{cc}\frac{d\rho_{v,con}}{dT} + A_{cc}L_{con}\rho_{L,con}\frac{dh_{con}}{dT} + (H_{con} - L_{con})\rho_{L,con}A_{cc}\frac{dh_v}{dT}\right]$	$(m_{v,n} - D_{ev})h_{v,n} - m_{con,O}h_{con,O} - Q_{con}$

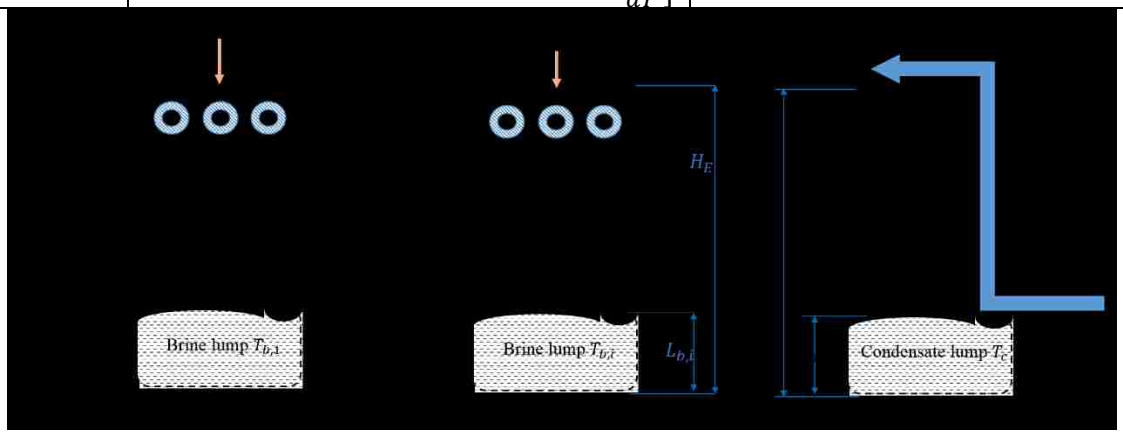

Figure 38 Control volume with different terms for (a) first effect, (b) i[th] effect and (c) condenser.

In order to obtain the transient nature of feed seawater temperature, condenser tube enthalpy is assumed to be the average enthalpy of the feed and cooling seawater as $h_{T,con} = \frac{h_f + h_{cw}}{2}$. The rate of change of feed water temperature with time can be written as,

$$\frac{dT_{feed}}{dt} = \frac{2\left(Q_{con} + m_{cw}h_{cw} - m_{cw}h_f\right)}{\rho_{tube,c}\forall_{tube,c}\frac{dh_f}{dT}} \tag{53}$$

$$Q_{con} = U_{con}A_{con}\frac{(T_{v,n-}T_f) - (T_{con-}T_{cw})}{ln\left[\frac{T_{v,n-}T_f}{T_{con-}T_{cw}}\right]} \quad (54)$$

6.4.3. TVC unit model

An accurate prediction of the TVC performance is needed to ensure the reliability of the overall MED-TVC process. Enhancement of the TVC entrainment efficiency promotes the performance of MED significantly and therefore the entrainment ratio is the most critical parameter in the modeling of the MED-TVC system. Due to the rapid dynamic response of ejector unit to changes in input parameters compared to other MED components, the TVC is considered to be in a quasi-steady state situation and therefore, no dynamic equations are needed [183]. However, to estimate the performance of TVC, an accurate quasi-steady equation for the entrainment ratio that relates the different input and output parameters of the ejector is required. Several approaches are available in the literature to evaluate entrainment ratios. Most of these methods need tedious and lengthy mathematical, computational procedures and use many correction factors [73]. The entrainment ratio R_a depends on the expansion ratio $E_r = \frac{P_s}{P_n}$ and the compression ratio $C_r = \frac{P_d}{P_n}$ as given in the Power's graphical data chart used to relate the amount of motive steam and entrained vapor [32, 91]. El-Dessouky and Ettouney [73] proposed a semi–empirical correlation for entrainment ratio by introducing motive steam pressure correction factor (PCF) and entrained vapor temperature correction factor (TCF). Bin Amer [188] eliminated these correction factors used in [73] for simplicity and his results were tested and compared with those obtained by the Power's chart for validity in the range of motive pressure 3000 $\geq P_s \geq$ 2000 kPa. Hassan and Darwish [92] used the Power's chart and correlated the entrainment ratio R_a as a function of E_r and C_r as presented in Table 27. The results from these correlations were compared with the Power's chart and with the two semi-empirical correlations mentioned in [73, 188]. These R_a

correlations agree with the Power's charts. However, the two semi-empirical equations give inaccurate estimates which could be 50% lower than the values from the Power's chart under certain conditions. In this regard, the correlations by Hassan and Darwish [92] are used to obtain R_a for the TVC unit in the present study.

Table 27 Correlated data equation for the Power's curves [92]

$-1.93 + 2.15C_r + 113.49/E_r - 0.52{C_r}^2 - 14735.97/{E_r}^2 - 31.85\,C_r/E_r + 0.048{C_r}^3 + 900786.04/{E_r}^3 - 495.58\,C_r/{E_r}^2 + 10.025\,{C_r}^2/E_r$	$E_r \geq 100$
$-3.21 + 3.93C_r + 27.24/E_r - 1.19{C_r}^2 - 141.42/{E_r}^2 - 22.54\,C_r/E_r + 0.13{C_r}^3 + 348.5/{E_r}^3 - 41.79\,C_r/{E_r}^2 + 6.44\,{C_r}^2/E_r$	$100 \geq E_r \geq 10$
$-1.61 + 11.03\ln C_r + 13.53/E_r - 14.93\ln {C_r}^2 - 34.44/{E_r}^2 - 48.48\ln C_r/E_r + 6.46\ln {C_r}^3 + 29.97/{E_r}^3 - 70.81\ln C_r/{E_r}^2 + 46.96\ln {C_r}^2/E_r$	$10 \geq E_r \geq 2$

6.4.4. Model Limitations

The current dynamic model should be used only when the assumptions stated are valid. However, it should be noted that these limitations do not usually apply in most applications. First, the effect of non-condensable gases (NCG) is not considered in the model. The presence of NCG dissolved in the supplied seawater can have a significant effect on the evaporation and condensation processes inside the evaporator and condenser which may in turn deteriorate the performance of these units [199]. However, in an actual operation, the feed seawater is always properly deaerated and vented physically to avoid the accumulation of NCG to guarantee normal operation of the plant. Otherwise, these NCG can be released in the flashing chambers and transferred to the MED effects through the injection lines. This will decrease the heat transfer coefficients in the heat exchanger surfaces and significantly degrade the thermal performance of the MED plant [200]. Second, the dynamic model must have a reliable prediction for the TVC component. The empirical correlations used to describe the TVC unit are valid and accurate within 20% over the range of compression ratios up to 5, expansion ratios up to 1000, and entrainment ratios from 0.25 to 5 [92].

The ranges are fairly broad and cover most MED-TVC operations. Finally, the cross-sectional areas of the effects and condenser are assumed to be constant in the model. However, to include other designs such as horizontal cylindrical shell and tube effects, a geometrical equation that relates the brine height with the cross-section area of the effect can be easily implemented.

6.4.5. Numerical solution

The first-order nonlinear ODEs derived above for the condenser and evaporators are solved simultaneously using the Runge-Kutta fourth order method through a FORTRAN code. The solution procedure starts by obtaining the steady-state solution for the MED-TVC system. In the steady state solution, the temperature, feed flow rate, brine flow rate, vapor flow rate and salinity at each effect are calculated in addition to the evaporators and condenser surface areas. The steady-state solution is carried out iteratively to adjust the temperature drop across the effects to obtain equal heat transfer areas for the evaporators as shown in Figure 39. The maximum difference in heat transfer areas is calculated and an error criterion $\varepsilon = 0.01$ m^2 is used. If the error criterion is not satisfied, a new iteration sequence is initiated. The new iteration starts with the calculations of the new heat transfer areas. A new profile for the temperature drop across the effects is then calculated. A new iteration is then taken, which starts with temperature profiles and continues until the error criterion is met. After the steady-state solution is obtained, it is used as the initial condition for the dynamic response calculations as presented in Figure 39. At each time step, the temperature, liquid level, and salinity are calculated in each effect. The condenser temperature, condenser distillate level and feed temperature are also calculated. The brine and vapor flow rates among the effects are calculated based on the liquid level and the saturation pressure in each effect. The entrainment ratio of the thermal-compressor is updated at every time step using the correlations given in [92] and the values of the pressure at the last effect and the pressure of the motive steam.

A time step was chosen to be 0.1 s to eliminate numerical instability [179]. Any parameter can be changed (or disturbed) from its steady state value for a specified time period. The MED operating condition is expected to deviate from the steady state condition upon the introduction of disturbances. If the MED is stable, it should return to steady state operation when the disturbances are removed.

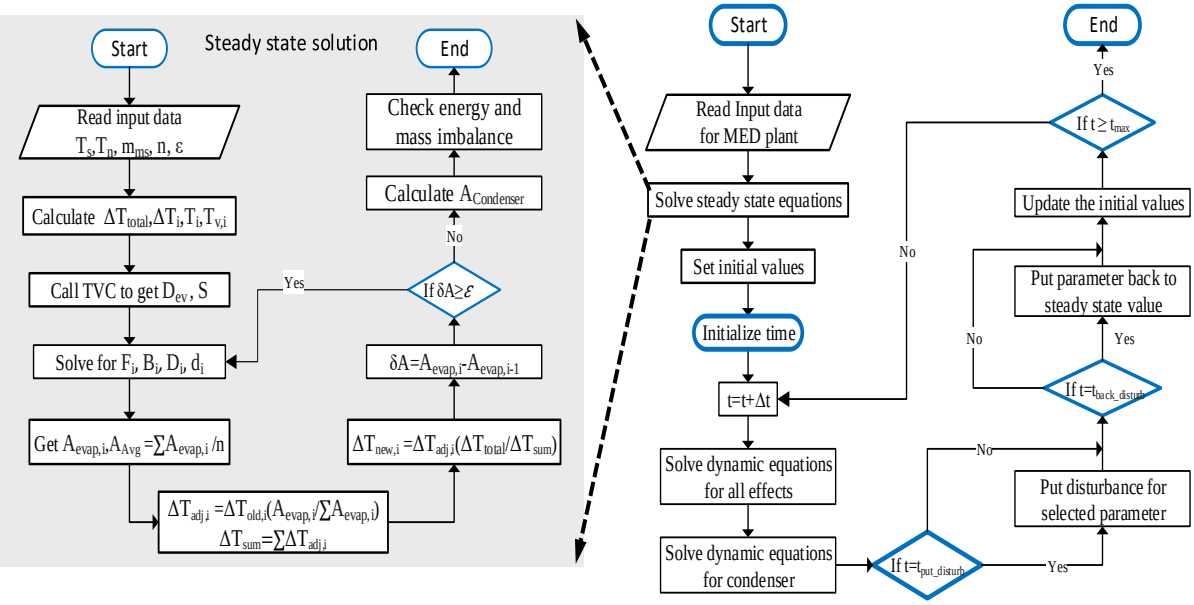

Figure 39 Block diagram of an MED-TVC system steady-state and dynamic models.

Models validation

6.5.1. Validation of steady-state calculations

The results from the developed steady-state model are checked against actual data from several commercial MED-TVC plants in Trapani, Tripoli, Sidem (western area of UAE) and Kish Iceland [72, 100, 201, 202]. The comparison between the calculated and actual performance parameters shows good agreement as shown in Table 28. The percentage error in the GOR ranges from 2.55 to 8.29%.

Table 28 Validation of MED–TVC model results against data from commercial plants.

	Input data for the MED–TVC model							
	Trapani [201]		Tripoli [72]		Sidem [202]		Kish Iceland [100]	
Number of effects	12		4		4		5	
Motive steam pressure, kPa	4500		2300		2400		1000	
Motive steam flow rate, kg/s	6.67		8.89		6.361		2.89	
Top brine temperature T_1, °C	62.2		60.1		59		68	
last brine temperature T_n, °C	37		45.4		47		54	
Temperature drop / effect, °C	2.3		4.9		4		3.5	
Feed temperature T_f, °C	35		41.5		44		44	
Seawater temperature Tcw, °C	22		31.5		33		33	
Feed content, g/kg	40		35		47		45[a]	
Brine content, g/kg	60		53		71.5		70[a]	
System performance								
	Model	Actual	Model	Actual	Model	Actual	Model	Actual
Gain output ratio (GOR)	15.41	15.617	6.342	6.508	7.588	8.275	7.72	8
Distillate production kg/s	98.69	104.167	56.38	57.861	48.27	52.64	22.311	23.148
Brine flow rate, kg/s	200.56	209.72	106.783	109.21	97.129	106.25	51.326	54.629
Feed flow rate, kg/s	299.25	313.889	163.163	167	145.398	158.88	73.637	77.778
Steam flow rate to 1st effect	11.98	NA	14.72	14.44	12.853	NA	5.31	NA
Entrained flow from last effect	5.31	NA	5.83	5.55	6.492	NA	2.42	NA
Entrainment Ratio for TVC	1.256	NA	1.525	1.601	0.98	NA	1.194	NA
%Error GOR	5.26		2.55		8.29		3.5	
a, Assumed values								

6.5.2. Dynamic response validation

There is a dearth of published dynamic response data for the actual MED and MSF desalination plants. Manufacturers of MED and MSF plants, perhaps due to competition reason, are not revealing their plant data especially the plant dynamic response with actual disturbances that the

unit may be exposed to. So the dynamic model results are compared with a lab-controlled three-effect MED plant of shell and tube evaporators with a total freshwater production of 3 m^3/day [191]. The heat source used in this plant is a hot water stream that is introduced to the first effect. The vapor produced in the first effect is used to heat the second effect and so on. The vapor temperature in each effect is measured when the hot water heat source is shut off for a certain time interval. To investigate the validity of the dynamic model under experimentally similar conditions, the heat supplied to the first effect is set as the disturbance in the numerical model. Its value is set to zero at the time of hot water shutdown and is returned to its steady-state value at the end of the disturbance period. A comparison between the vapor temperature in each effect obtained from the dynamic model simulation and the data provided in [191] is shown in Figure 40. The average absolute error between the actual and simulated data for each effect is 2% which indicates good agreement between the simulation and the measured experimental data.

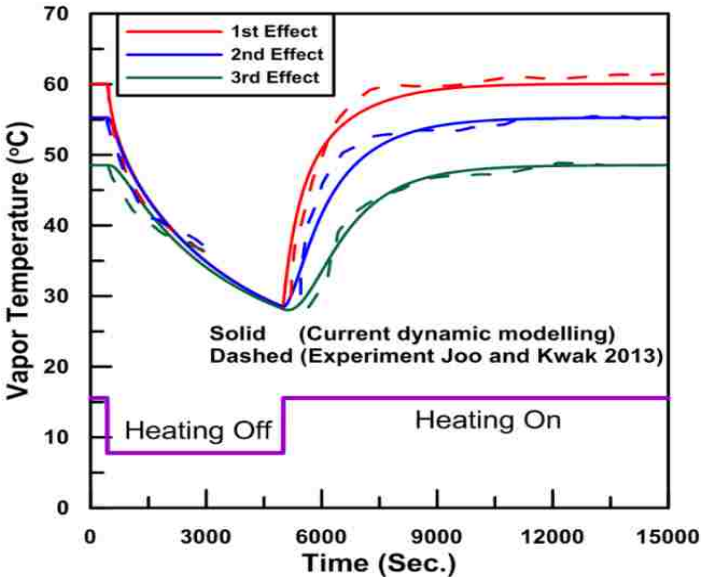

Figure 40. The Vapor temperature of the evaporators for simulated model and experiment [191].

Results and discussion

In order to study the dynamic response of MED-TVC desalination plants, the developed model is applied to a plant in the western area of Abu Dhabi plant [202]. All the available data for this plant are considered. The initial brine/condenser liquid level was assumed to be 0.25 m based on the actual effects and condenser dimensions. The dynamic response of the plant is studied when four stepwise changes (disturbances) in operational parameters from the nominal steady-state values are allowed. These disturbed parameters include motive steam flow rate, cooling seawater flow rate and cooling seawater temperature which are denoted as 1st, 2nd and 3rd disturbances, respectively, plus the change in feed seawater salinity. It is assumed that the disturbances are applied for a certain time interval and returned back to its steady state operational values.

The 1st disturbance is considered to be a 10% stepwise reduction in the steady-state value of the motive steam flow rate (6.36 kg/sec) at 1000 s, and this reduction lasts for 9000 s. This disturbance may be attributed to a decrease in the supplied power to the boiler. At the beginning of the 1st disturbance, the thermal energy delivered to the first effect drops due to the sudden decrease in the motive steam. This leads to a reduction in vapor temperature (Figure 41b) and evaporation rate. Consequently, an increase in the brine level for effects 1 to 3 is experienced as shown in Figure 41a. The rate of increase in the brine level in each effect is lower than that of the previous one. It is interesting to notice that when the disturbance is applied with a fixed motive steam pressure, the steam ejector sucks a lower amount of entrained vapor from the last effect which causes a small sudden increase in vapor temperature in the last effect as shown in Figure 41b. This slight increase in last effect pressure plus the drop in the brine flow rate from the upstream effects is the reason for the decrease in brine level in the last effect as shown in Figure 41a. Similarly, in a reverse

manner, when the disturbance ends at 10000 s, the ejector sucks in more vapor leading to a sudden drop in the last effect vapor temperature and a rise in the brine level.

The response of the vapor lump in each effect is much faster than the response of the liquid lump. So, the vapor pressure response is faster than the hydrostatic brine level response. As soon as the 1^{st} disturbance starts the brine lump is subjected to a lower saturation pressure due to the decrease in the effect temperature. This decreases the brine mass flow rate as shown in Figure 41c. After some time, the brine flow rate increases gradually due to the buildup of the hydrostatic pressure as the brine accumulates and its level increases. Conversely, at the end of the disturbance, the motive steam increases again and causes an increase in the temperature and pressure of each effect, which increases the brine mass flow rate. Figure 41d shows the vapor flow rate from each effect and the steam flow rate to the first effect. It is clear that at the beginning of the disturbance, the instantaneous decrease in the steam supplied to 1^{st} effect is sensed rapidly in the form of a sudden drop in the vapor mass flow rate from the subsequent effects. However, the system is slower to return to steady state vapor flow rate values when the disturbance ends. To reach steady state values after the disturbance is off, it takes about 5000 seconds for the brine level and brine flow rate and 3000 seconds for vapor temperature and vapor mass flow rate.

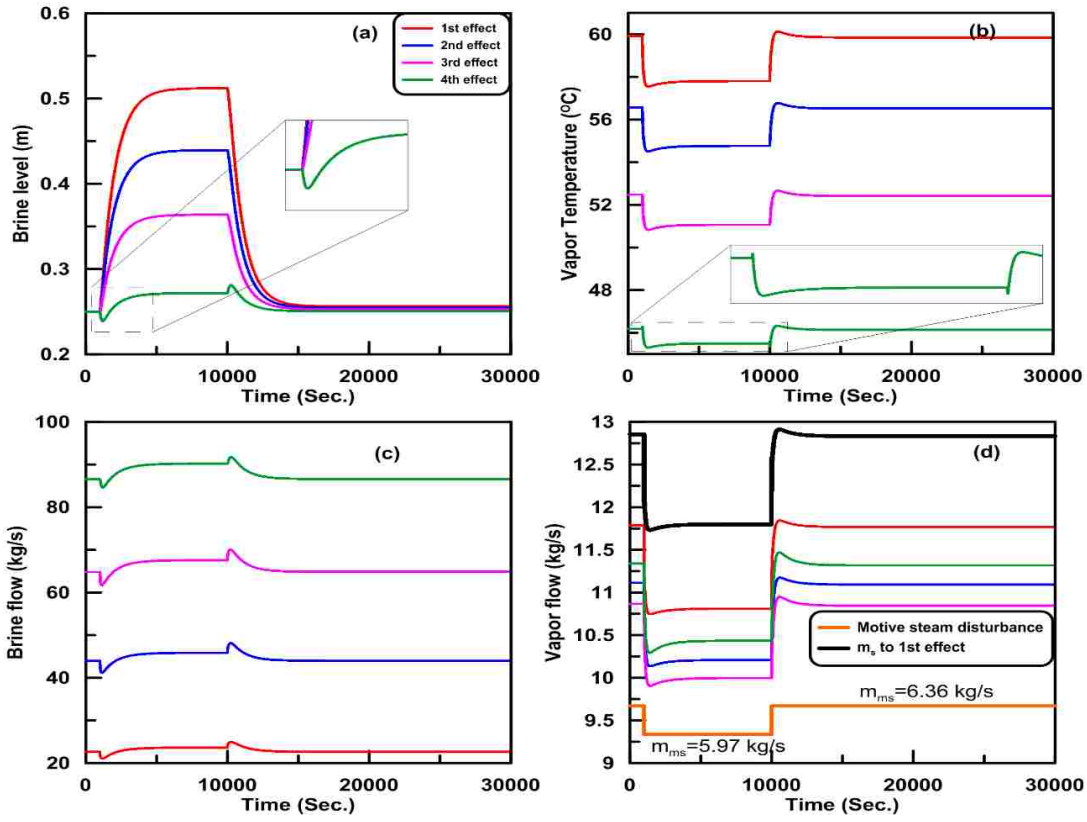

Figure 41 Variation for different parameters with 1st disturbance.

The 2nd disturbance is a 5% stepwise reduction applied to the steady-state value of the cooling seawater mass flow rate (253 kg/sec) at 1000 s, and this reduction lasts for 9000 s. This reduction in mass flow rate could be attributed to a reduction in pump efficiency. Reducing the mass flow rate of the cooling seawater directly increases the feed water temperature and condenser pressure. Figure 42 shows the variation of the parameters under investigations as soon as the 2nd disturbance is applied. The brine levels for all effects decrease due to the increase in feed temperature which enhances evaporation. After the disturbance is off, it takes approximately 5000 seconds for the MED to return to steady-state operation. During the disturbance period, the vapor temperature and mass flow rate increase due to the increase in feed temperature as shown in Figure 42 (b,d). The brine mass flow rate is driven by vapor pressure and the hydrostatic pressure of the brine. Since

the vapor pressure response is faster compared to the response of the brine level, the brine flow rate increases in all effects at the beginning of the disturbance due to the increase in vapor temperature and pressure. As the brine level decreases due to enhanced evaporation, the brine hydrostatic pressure decreases which in turn reduces the brine flow rate as shown in Figure 42c. Reducing the cooling seawater mass flow rate results in an increase in the condenser pressure. This creates a small sudden decrease in the vapor mass flow rate from the last effect as shown in Figure 42d. Increasing the brine flow rate from the upstream effects at the beginning of the 2nd disturbance produces a jump in brine level in the last effect but it gradually decreases as the vapor temperature increases due to the enhanced evaporation as shown in Figure 42a. At the end of the 2nd disturbance, the reverse behavior occurs.

The 3rd disturbance is a 10% stepwise reduction applied to the steady-state value of the cooling seawater temperature (33^{o}C) at 1000 s, and this reduction lasts for 9000 sec. It may be dictated by the weather and ambient condition as an external uncontrollable parameter that affects seawater temperature [203]. As the cooling seawater temperature decreases, the feed temperature decreases for all effects at the same time. This leads to a reduction in the evaporation rate and in vapor temperature which in turn produces an increase in the brine level in all effects as shown in Figure 43(a,b). Similar to the previous scenarios of 1st disturbance, the brine flow rate decreases as soon as the 3rd disturbance is applied due to the rapid decrease in the pressure in the effects, it then increases gradually as the hydrostatic pressure due to the brine level increases as shown in Figure 43c. At the end of the disturbance, it is expected that the vapor flow rate will follow the reverse behavior. However, the outcome from the vapor flow rate is interesting: immediately after returning cooling seawater temperature to its steady state original value, vapor flow rate is drastically decreased to lower values and this effect is more significant in the 3rd and 4th effect.

This can be attributed to the sudden increase in the condenser pressure due to the increase in the cooling seawater temperature. The effect of condenser back pressure travels backward to the 4th and 3rd effects, as shown in Figure 43d, with a minimal impact on the 1st effect.

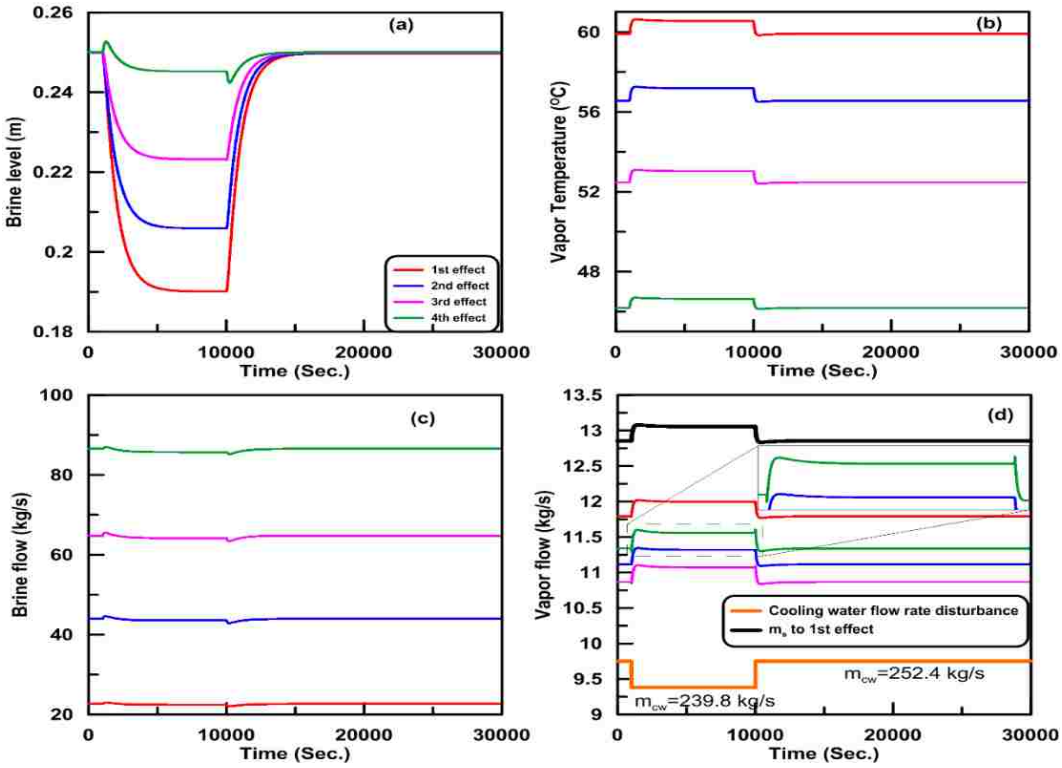

Figure 42 Variation for different parameters with 2nd disturbance.

The change of MED unit installation region may cause a change in seawater salinity, i.e., it is a parameter of site location condition. A reduction is applied to steady-state value of the seawater feed salinity from 47 g/kg to 35 g/kg to investigate the effect of different salinity values on the plant steady-state characteristics. One of the advantages of the developed dynamic model is that it can predict the steady state solution if the program is allowed to run for a relatively long-time interval. Reducing the feed salinity leads to a lower BPE which reduces the difference between brine and vapor temperature in effects. As seen in Figure 44, the vapor temperature and vapor flow rate increase in all effects upon applying the salinity change. This increase in the vapor rate

increases the total freshwater production from 48.3 to 49.7 kg/s. In addition to that, the specific heat transfer area which represents the total area of the effects per unit mass of the distilled water production decreases from 35.1 to 34.9 m^2-s/kg. Compared to the other previous three disturbances, changing the seawater salinity seems to have minimal effect on the MED performance. This shows that unlike RO desalination technique, the MED-TVC plants can handle high salinity sea water without a considerable drop in performance.

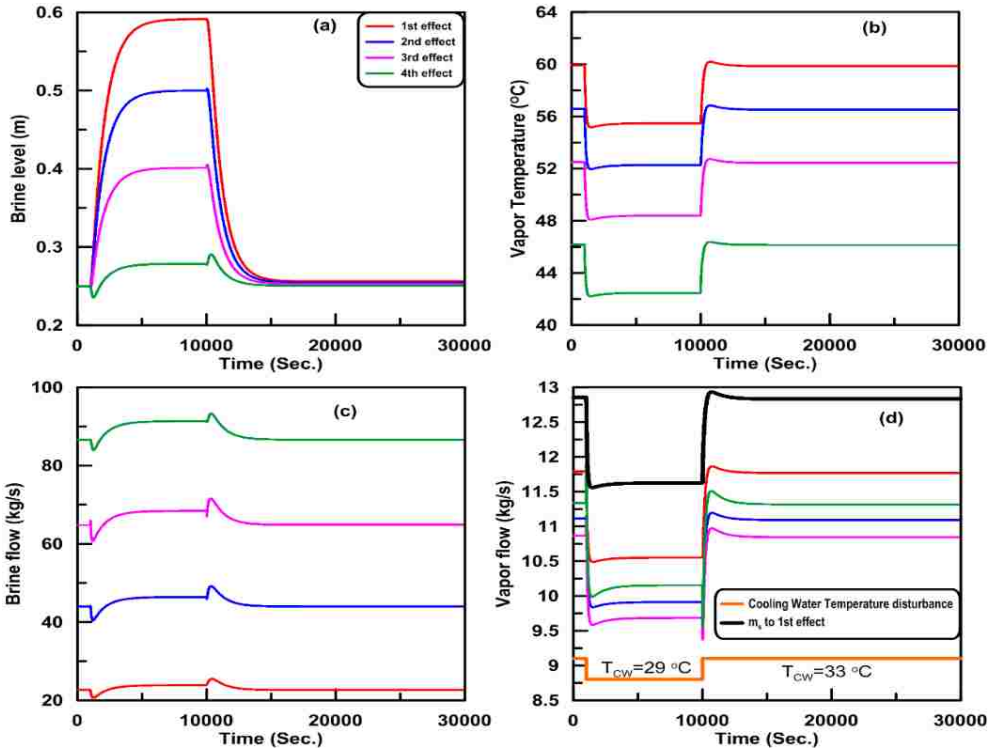

Figure 43 Variation for different parameters with 3rd disturbance.

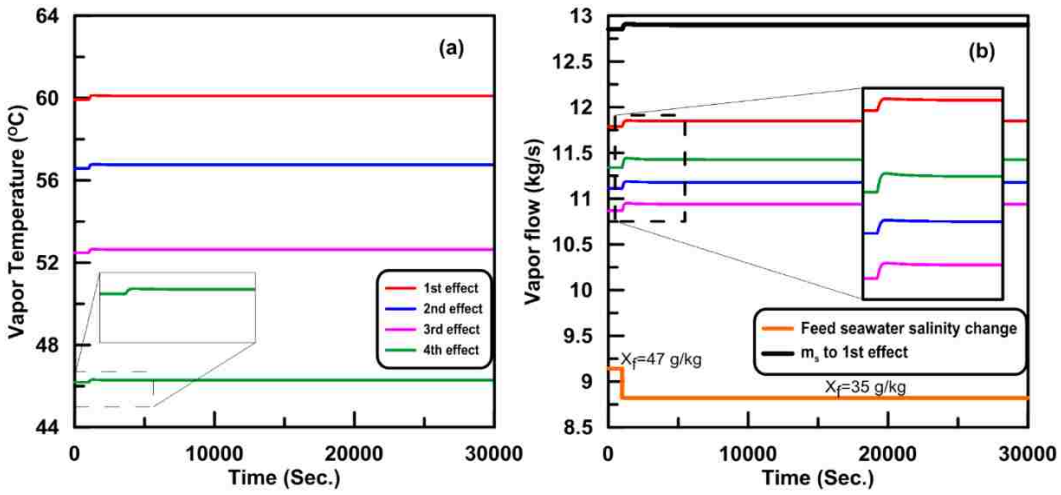

Figure 44 Variation for vapor temperature and flow rate with feed seawater salinity change.

Conclusions

In the current work, a steady/dynamic model for a MED-TVC desalination plant with a parallel/cross flow configuration is developed and validated against available steady-state data from a commercial plant and experimental data available in the literature. The model has some limitations such as the effect of non-condensable gases is not considered. The model is used to investigate the system behavior under different disturbances that simulate the real conditions that the plant may be exposed to. The simulation results reveal that the disturbances in motive steam flow rate and in cooling seawater temperature have the largest effect on the plant performance while a disturbance in the cooling seawater mass flow rate has only a moderate effect. Changing seawater salinity shows a slight effect on the total distillate and the specific heat transfer area. The dynamic simulation results reveal that the vapor temperature response is quick and is affected mainly by disturbances in the motive steam flow rate and cooling seawater temperature. For all applied disturbances, the change in the brine level is the slowest compared to the changes in vapor temperature, and brine and vapor flow rates.

CHAPTER 7 EFFECT OF INPUT PARAMETERS INTENSITY AND DURATION ON DYNAMIC PERFORMANCE OF MED-TVC PLANT[**]

Abstract

Multi-Effect-Desalination (MED) may be exposed to fluctuations (disturbances) in input parameters during operation. Therefore, there is a requirement to analyze the transient behavior of such MED systems. In this work, a dynamic model is developed and used to examine the effect of abrupt and ramp changes in the main operational parameters on the plant behavior and performance. The results show that the disturbance intensity variation has a major role in the desalination plant behavior. For the current MED-TVC configuration, it is recommended to limit the reduction in the seawater cooling flow rate to under 12% of the designed steady-state value to avoid dry out in the evaporators. A reduction in the motive steam flow rate and cooling seawater temperature of more than 20% and 35% of the nominal operating values, respectively, may lead to flooding in the evaporators and a complete plant shutdown. On the other hand, the disturbance period has a minimal effect on plant performance if it avoids the critical values of the disturbance intensity that can cause plant shutdown. Simultaneous combinations of two different disturbances with opposing effects result in a modest effect on the plant operation and they can be used to control and mitigate the flooding/drying effects of the disturbances. For simultaneous combinations of disturbances with similar effect, the plant needs an accurate control system to avoid an operational shutdown.

[**] **Mohamed L. Elsayed**, Osama Mesalhy, Ramy H. Mohammed, Louis C. Chow, "Effect of Input Parameters Intensity and Duration on Dynamic Performance of MED-TVC Plant." Applied Thermal Engineering, volume 139, July 2018, pages 210-221.

Introduction

Much research has been done to compare the merits of various desalination processes integrated with renewable energy systems [63, 160, 162], including Multi-effect-desalination (MED), multistage flash (MSF) and reverse osmosis (RO) [65, 163, 164]. Significant advantages have been demonstrated in several scenarios for RO over MED and MSF; however, there has been rapidly increasing interest to use MED in the countries near the Persian Gulf and the Arabian Sea, where ambient conditions are challenging with seasonal high seawater temperatures and saline concentrations [204] and the resources of solar energy is abundant [166]. MED process requires less comprehensive seawater pretreatment as in RO. Also, MED is considered to be an attractive approach for desalination because of the combination of low economic costs and low energy consumption, especially when MED is combined with electricity cogeneration using solar or waste heat. Furthermore, MED showed better performance compared to RO or MSF processes using the newly proposed figure of merit, called the universal performance ratio (UPR) which represents the ratio of evaporative energy to the primary energies not the deriving energies. The reported values of UPR for RO, MED and MSF were 102.3, 131.0 and 60.3, respectively [64]. Adding thermal or mechanical vapor compression (TVC, MVC) to thermal desalination system improves the overall efficiency as it requires less cooling seawater and lowers electricity consumption [32, 39, 117, 205]. In VC desalination, low-temperature vapor is recovered from certain locations of the thermal desalination system and converted to vapor with high temperature. A significant amount of research in detailed and simplified modeling of steady-state operation of MED has been made by various researchers using different solution techniques to determine various MED features and product cost [170, 196, 206-209]. The main conclusions of these contributions include the following, for all MED configurations, increasing the number of effects at a constant production rate increases the Gained Output Ratio (GOR) which represents the distillate product per amount

of heat source supplied. Also, at a constant number of effects and brine blow down the temperature, an increase in the top brine temperature (TBT) improves the system GOR and reduces the required specific heat transfer area as a result of an increase in the temperature drop and the overall heat transfer coefficient.

Multi-effect evaporation systems may be generally exposed to fluctuations (disturbances) in input parameters during operation. These disturbances could be changes due to the environment such as cooling water swings with the weather or the time of day and heating source swings. Another type of disturbances is called "turndown" which represents the changes in gross plant throughput and this is done intentionally to handle for example power demand swings [168]. Therefore, it is important to analyze the transient behavior of MED output based on the changes of the input with time to get a better understanding of the desalination process performance and behavior. Dynamic simulation predicts the system behavior from start up to shut down and can be used to establish advanced control strategies, test operating scenarios, address potential problems related to unexpected transient events, and produce a comparatively stable output during the production period. Also, it helps engineers to better understand and develop optimal control strategies, prevent significant damages caused by malfunction, and troubleshoot disorders [169, 210]. Applications of dynamic modeling include off-line or on-line modeling to investigate the transient behavior of the system and execute control strategies [211].

Burdett and Hollanu [189] developed the first dynamic model for a 17-effect MED. The state variables at the end of each time step were obtained using the Newton-Raphson method. Later on, results for a dynamic model for a 10-effect MED were obtained by using the Euler method to integrate the time derivatives of the state variables. The analytical results of a step change in the heating steam temperature show a fair agreement compared to the experimental data from 150

m^3/day pilot MED in Israel [197]. Their experimental results show that for small overall ΔT and consequently inter-effect ΔP, plant performance drops. Cadet et al. [212] formulated a detailed evaporator model based on energy and mass balance incorporating semi-empirical equilibrium formulas for a sugar plant industry. Miranda and Simpson [176] described a steady and dynamic lumped model of multi-effect evaporators (MEE) using data collected in a tomato concentrate industrial plant. Their model assumes the total mass in each effect is not accumulated due to concentrate level control. Tonelli et al. [177] presented an open-loop dynamic response of triple effect evaporators for apple juice concentrators with the backward arrangement and preheating. A series of dynamic blocks corresponding to each stage are linked together to yield the complete dynamic model that includes the possibility of simulating dead-time lag between effects. Considerable disturbances in the inlet steam pressure and feed flow rate were applied and the results compared well with experimental response results from an actual unit located in Unipektin, Zurich. The dynamic behavior of four effect MED systems was introduced by Aly and Marwan [179] which allowed the study of system start-up, shutdown and load changes using time-dependent conservation equations of mass, energy, and salt. The overall heat transfer coefficient was assumed to change linearly with temperature but no industrial or actual data for validation was used. Kumar et al. [178] modeled transient behavior of a sextuple tubular falling film evaporator system with mixed feed in the paper industry by means of energy and material balance equations following the work in [179]. Dynamic disturbance of ±10% was applied to the liquor feed concentration, flow rate, steam and feed temperatures to predict the response in effects temperature and product concentration. Their results show that the effect temperature reaches steady state faster compared to the liquor concentration. Medhat Bojnourd et al. [184] presented lumped and distributed models for four-MEEs to concentrate whole milk, following the work conducted in

[213, 214] but with some modification. The transient behavior due to disturbances in input variables was investigated and compared with real data for an actual industrial unit. A slightly better prediction of the distributed model against the lumped model was obtained, especially in predicting the effect temperature, though the lumped model is simpler and requires less simulation time compared to the distributed model.

El-Nashar and Qamhiyeh [180] presented a lumped model to estimate the dynamic behavior of Multi-Effect-Stack (MES) evaporators. Conservation equations of mass and energy were derived and solved simultaneously for each effect. The numerical results showed a reasonable agreement with real data taken from an operating desalination plant at Abu Dhabi throughout plant start-up. A dynamic simulator was proposed for a MED-VC unit as work-in-progress for steady state and the dynamic behaviors [141] by using the same equations in [179] but no system response due to load change was shown. Roca, et al. [181] experimentally tested a solar assisted-MED unit and compared their results with a simplified dynamic model based on the work developed in [179]. Mazini [183] used the same approach of [179] and modeled the distillate level of the condenser and a thermo-compressor. In addition, their model was validated by using actual data from an operating plant in Kish Island in Iran. At CIEMAT-Plataforma Solar de Almerı´a (PSA), a study described the dynamic nature and performance of a 14 forward-MED unit in a vertical arrangement. The object-oriented Modelica language was used to develop the non-linear first principles model [182]. Furthermore, this model was divided into sub-models that encapsulated and covered the dynamics of each one of the sub-processes that took place in the system in order to study the plant performance in different scenarios and design operating strategies to improve its efficiency [215]. Shahzad et al. [56, 67] presented a simulation model for predicting the transient behavior of an advanced hybrid MED and adsorption cycle (AD) desalination pilot plant installed

in Singapore. The simulation model used the actual characteristics of the adsorbent/adsorbate. Conservation equations of mass and energy were applied to the subcomponent of the advanced cycle. The advanced MEDAD cycle offers a 2.5~3 fold increase in freshwater production compared to the traditional MEDs for the same TBT by allowing some of MED effects to operate below ambient temperature. Cipollina et al. [185] developed a dynamic model for a 12-effect MED-TVC based on available data from the Trapani plant in Italy using the equation-based process simulator gPROMS®. Specific disturbances on the main input parameters were implemented to investigate the system behavior. Negligible variations were predicted for the increase in the seawater temperature, while a slight reduction in the plant GOR was shown when the seawater temperature was reduced.

In the current study, a dynamic model for a parallel/cross flow MED-TVC system including four effects, an end condenser, and a steam jet ejector is considered. Three nonlinear ODEs are obtained for three state variables, namely the brine level, brine salinity and vapor temperature, to represent the dynamic behavior of each evaporator effect. In addition, a detailed model for the condenser is developed which can predict the dynamic variation of the condenser pressure, condenser liquid level and the feed temperature with time. Also, an accurate model for steam jet ejectors is used in order to evaluate the performance of the TVC unit. Eventually, the set of equations are linked, combined and solved simultaneously using the Runge-Kutta fourth order method through a FORTRAN code to obtain the system dynamic behavior. The steady state solution is used as the initial input for the dynamic response calculations. The dynamic model investigates the plant behavior and performance under various intensity and duration of disturbances introduced in the main operational parameters that include the motive steam flow rate, motive steam pressure, cooling seawater flow rate and cooling seawater temperature. A constraint on the brine level inside

the effects is assigned to define the critical limits for the fluctuations of the input parameters to avoid plant shutdown due to flooding or dry out. After studying the effects of individual disturbances on the MED-TVC behavior and performance, the effects of simultaneous combinations of two different disturbances in assisting and opposing effects direction are studied as well.

MED-TVC combination arrangement

Multi-effect-desalination operates in three common configurations: forward-feed FF, backward feed BF, and parallel feed PF. A thermal vapor compressor (TVC) is integrated with the last effect to form a typical MED-TVC system which consists of a train of effects, thermal vapor compressor, condenser, a boiler which supplies the motive steam, and pumps, along with an operating control system as shown in Figure 45. Seawater is preheated to the feed water temperature by passing through the condenser. The major portion of the seawater is directed back to sea, while the remaining preheated feed seawater is distributed to a sequence of successively lower pressure vessels, called effects. Feed is sprayed into each evaporation effect and flows down as a thin liquid film along the outside walls of the horizontally installed tubes inside each effect. Motive steam m_{ms} extracted from a boiler or a power plant steam turbine at a relatively high motive pressure P_S enters through the TVC. The motive steam entrains a portion $D_{ev}$of the vapor $m_{v,n}$generated in the last effect of the MED system at pressure P_n. The remaining vapor $m_{v,n} - D_{ev}$ is used to preheat the seawater in the condenser. The ratio of the motive steam to the entrained vapor flow rate is called the entrainment ratio (R_a).

The TVC unit improves the GOR and decreases the cost of input energy by recompressing the entrained vapor with the motive steam to form hot compressed steam [188]. For a MED-TVC

system, the GOR is defined as the ratio of the rate of total distillate produced to the flow rate of motive steam supplied to TVC unit. Steam from the TVC flows inside the tubes of the 1st effect with a mass flow rate of $m_{ms} + D_{ev}$ and discharge pressure of P_d. The thermal compression process is not an efficient one. However, it can increase the performance of the MED system significantly and reduce the specific energy consumption [216]. The supply steam to the 1st effect raises the temperature of the thin film of feed seawater around the tubes to its boiling temperature which is also known as the top brine temperature (TBT). A fraction of the feed in the first effect evaporates and the vapor flows as a heat source into the second effect which is at a lower pressure and temperature than the first effect. Simultaneous vapor condensation inside the tubes and seawater film evaporation outside the tubes occurs in all the effects. Also, unevaporated seawater brine from the first effect enters the second effect to harness its energy by flashing at a lower pressure. The brine flow process also continues through all effects to the last effect. This manner of feed water and brine flow is shown in Figure 45 and is known as the parallel/cross configuration. The vapor inside the second to the last effect is generated by both evaporation and flashing. The fresh water and concentrated brine are cascaded to the last effect where they are drawn out by pumps.

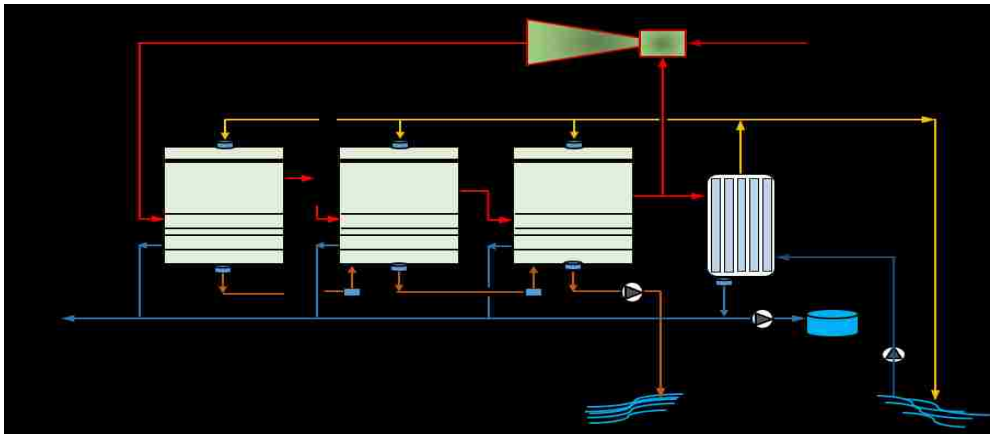

Figure 45 Schematic diagram of a MED-TVC system with a thermo-compressor.

In order to estimate the performance of TVC, a quasi-steady equation for the entrainment ratio that relates the different input and output parameters of the ejector is required. Several approaches are available in the literature to calculate entrainment ratios. Most of these methods need tedious and lengthy mathematical computational procedures and use many correction factors [73]. The entrainment ratio R_a depends on the expansion ratio $E_r = \frac{P_s}{P_n}$ and the compression ratio $C_r = \frac{P_d}{P_n}$ as given in the Power's graphical data chart used to relate the amount of motive steam and entrained vapor [32, 91]. For the TVC model, the correlations of R_a as a function of E_r and C_r obtained by Hassan and Darwish [92], which are suitable for the range of typical MED operation conditions, are used in the current model. The results from these correlations were compared with the Power's chart and with the two semi-empirical correlations mentioned in [73, 188]. These R_a correlations agree with the Power's charts. However, the two semi-empirical equations gave inaccurate estimation which could be 50% lower than the values from the Power's chart under certain conditions.

Dynamic Model Development

In order to predict changes in the MED-TVC system variables under the transient operating condition, a dynamic model of four-effect with a parallel/cross flow configuration is considered. Each evaporator is divided into three lumps: brine, vapor, and tube lump. For each lump, energy, mass, and salt balance are written. The assumptions used in generating the MED-TVC system dynamic model are listed as follows [179, 189]:

23. The accumulation of mass and energy in the evaporator tubes is taken to be negligible compared to the accumulation of mass and energy in the brine pool inside an effect.
24. Non-condensable gases effect on evaporator operation is taken to be insignificant.

25. The brine stream from the *i-1* effect is assumed to flash adiabatically upon entering the i effect.
26. Thermophysical properties for the brine and vapor are considered to be temperature and salinity dependent. Appropriate correlations are selected from [73].
27. Thermodynamic penalty representing the temperature difference between the brine pool and the vapor generated in an effect is taken as the Boiling Point Elevation (BPE).
28. The thermo-compressor has quick dynamic response compared to other components [183]. It is considered to be in a quasi-steady state condition and modeled by the correlations from [92].
29. The vapor and distillate are salt-free.

Prior to solving the dynamic model, the steady state conservation equations of mass, energy, and salt are solved to obtain the steady-state values of all the parameters in the plant. The solution is carried out iteratively to adjust the temperature drop across the effects to yield the same evaporator area for all the effects. The details of the steady state solution model are similar to [73] and are not mentioned here. The solution of the steady-state model is considered as the initial condition for the dynamic model. Figure 46 shows schematic diagrams for the first and ith effect evaporators and the condenser. Based on the work in [179, 183] and the assumptions stated above, the mass, energy, and salt balance equations for the ith effect evaporator are presented. The evaporator is assumed to have a cross-sectional area $A_{ce,i}$ and a total height H_E. The brine pool height $L_{b,i}$ and vapor height $H_E - L_{b,i}$ are shown in Figure 46 b. Brine pool to pool flow between effects is represented by $m_{b,i} = C_{b,i}\sqrt{\Delta P_{b,i}}$ where $\Delta P_{b,i} = P_{i-1} - P_i + \rho_b g\left(L_{b,i-1} - L_{b,i}\right)$ and the vapor flow from an effect to the next is calculated from $m_{v,i} = C_{vi}\sqrt{\Delta P_{vi}}$ where $\Delta P_{vi} = P_{i-1} - P_i$. Combined lumps mass, energy and salt balances for *ith* evaporator effect are given by equations 1, 2 and 3 respectively [179, 183]:

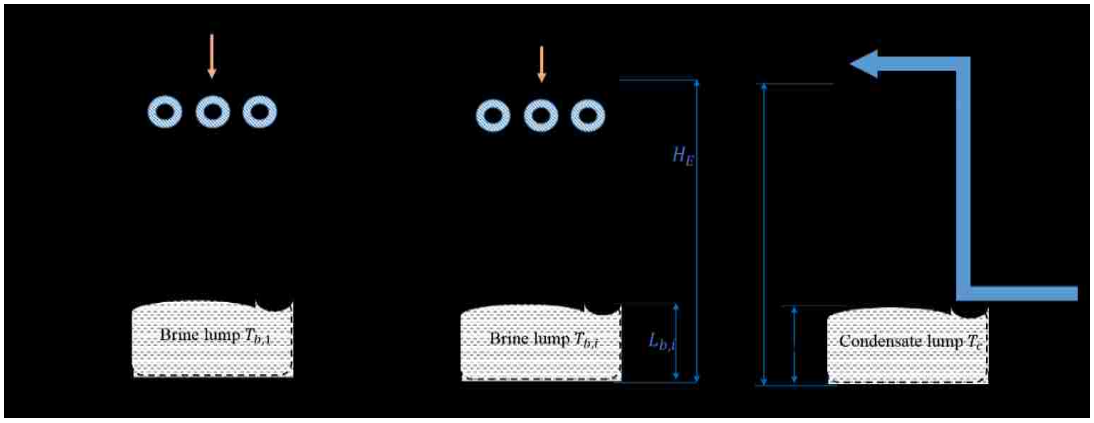

Figure 46 Control volume with different terms for (a) first effect, (b) i[th] effect and (c) condenser.

$$A_{ce,i}(\rho_{b,i}-\rho_{v,i})\frac{dL_{b,i}}{dt} + \left[A_{ce,i}L_{b,i}\frac{d\rho_{b,i}}{dT_{b,i}}\left(1+\frac{\partial BPE}{\partial T_{v,i}}\right)+(H_E-L_{b,i})A_{ce,i}\frac{d\rho_{v,i}}{dT_{v,i}}\right]\frac{dT_{v,i}}{dt} + \left[A_{ce,i}L_{b,i}\frac{d\rho_{b,i}}{dT_{b,i}}\frac{\partial BPE}{\partial X_{b,i}}+A_{ce,i}L_{b,i}\frac{d\rho_{b,i}}{dX}\right]\frac{\partial X_{b,i}}{\partial t} = m_{f,i}+m_{b,i-1}-m_{b,i}-m_{v,i} \quad (55)$$

$$A_{ce,i}(\rho_{b,i}h_{b,i}-\rho_{v,i}h_{vi})\frac{dL_{b,i}}{dt}+\left[A_{ce,i}L_{b,i}\rho_{b,i}\frac{dh_{b,i}}{dT_{b,i}}\left(1+\frac{\partial BPE}{\partial T_{v,i}}\right)+ A_{ce,i}L_{b,i}h_{b,i}\frac{d\rho_{b,i}}{dT_{b,i}}\left(1+\frac{\partial BPE}{\partial T_{v,i}}\right)+\rho_{v,i}(H_E-L_{b,i})A_{ce,i}\frac{dh_{v,i}}{dT_{v,i}}+h_{v,i}(H_E- L_{b,i})A_{ce,i}\frac{d\rho_{v,i}}{dT_{v,i}}\right]\frac{dT_{v,i}}{dt}+\left[A_{ce,i}L_{b,i}h_{b,i}\frac{d\rho_{b,i}}{dT_{b,i}}\frac{\partial BPE}{\partial X_{b,i}}+A_{ce,i}L_{b,i}\rho_{b,i}\frac{dh_{b,i}}{dT_{b,i}}\frac{\partial BPE}{\partial X_{b,i}}+ A_{ce,i}L_{b,i}h_{b,i}\frac{d\rho_{b,i}}{dX}\right]\frac{\partial X_{b,i}}{\partial t}=m_{f,i}h_{f,i}+m_{b,i-1}h_{b,i-1}-m_{b,i}h_{b,i}+Q_{E,i} \quad (56)$$

$$A_{ce,i}\rho_{b,i}X_{b,i}\frac{dL_{b,i}}{dt}+\left[A_{ce,i}L_{b,i}X_{b,i}\frac{d\rho_{b,i}}{dT_{b,i}}\left(1+\frac{\partial BPE}{\partial T_{v,i}}\right)\right]\frac{dT_{v,i}}{dt} + \left[A_{ce,i}L_{b,i}X_{b,i}\frac{d\rho_{b,i}}{dT_{b,i}}\frac{\partial BPE}{\partial X_{b,i}}+A_{ce,i}L_{b,i}\rho_{b,i} + A_{ce,i}L_{b,i}X_{b,i}\frac{d\rho_{b,i}}{dX}\right]\frac{\partial X_{b,i}}{\partial t}=m_{f,i}X_{f,i}+m_{b,i-1}X_{b,i-1}-m_{b,i}X_{b,i} \quad (57)$$

In the current study, a detailed model for the condenser is developed in order to predict accurately the dynamic variation of condenser pressure, condenser liquid level, and the feed temperature with

time. The condenser has a major role in the MED-TVC plant operation as it is used to condense the fraction of the vapor generated in the last effect which is not entrained by the TVC. The condensation process raises the cooling seawater to the required feed temperature. The condenser is sectioned into three lumps; condensate liquid, vapor, and tube as shown in Figure 46c. Combined mass balance for liquid and vapor lumps is written as:

$$\frac{dM_{con}}{dt} = \left(m_{v,n} - D_{ev}\right) - \frac{dM_v}{dt} - m_{con,O} \tag{58}$$

The terms $\frac{dM_{con}}{dt}, \frac{dM_v}{dt}$ can be written in terms of the rate of change of vapor temperature, and condensate level. By assuming the condenser has a cross sectional area A_{cc} and a total height of H_{con} while the condensate pool height is L_{con} and vapor height is $H_{con} - L_{con}$, the final mass balance equation in the condenser takes the following form.

$$A_{cc}\left(\rho_{L,con} - \rho_{v,con}\right)\frac{dL_{con}}{dt} + \left[A_{cc}L_{con}\frac{d\rho_{L,con}}{dT} + \left(H_{con} - L_{con}\right)A_{cc}\frac{d\rho_{v,con}}{dT}\right]\frac{dT_{con}}{dt} \tag{59}$$
$$= \left(m_{v,n} - D_{ev}\right) - m_{con,O}$$

Energy balances for condensate liquid, vapor and tube lumps are given as follow:

$$\frac{dM_{con}h_{con}}{dt} = m_{con}h_{con} - m_{con,O}h_{con,O} = M_{con}\frac{dh_{con}}{dT_{con}}\frac{dT_{con}}{dt} + h_{cond}\frac{dM_{con}}{dt} \tag{60}$$

$$\frac{dM_v h_v}{dt} = \left(m_{v,n} - D_{ev}\right)h_{v,n} - m_{con}h_{con} - Q_{con} = M_v\frac{dh_v}{dT_{con}}\frac{dT_{con}}{dt} + h_v\frac{dM_v}{dt} \tag{61}$$

$$M_{T,con}\frac{dh_{T,con}}{dt} = m_{cw}h_{cw} - m_{cw}h_f + Q_{con} \quad , \quad M_{T,con} = \rho_{T,con}\forall_{T,con} \tag{62}$$

By combining Eqs. (43) and (44), the following equation is obtained:

$$A_{cc}\left(\rho_{L,con}h_{con}-\rho_{v,con}h_{v}\right)\frac{dL_{con}}{dt} \tag{63}$$

$$+\left[A_{cc}L_{con}h_{con}\frac{d\rho_{L,con}}{dT}+\left(H_{con}-L_{con}\right)h_{v}A_{cc}\frac{d\rho_{v,con}}{dT}+A_{cc}L_{con}\rho_{L,con}\frac{dh_{con}}{dT}\right.$$

$$\left.+\left(H_{con}-L_{con}\right)\rho_{L,con}A_{cc}\frac{dh_{v}}{dT}\right]\frac{dT_{con}}{dt}=\left(m_{v,n}-D_{ev}\right)h_{v,n}-m_{con,O}h_{con,O}-Q_{con}$$

Equations 41 and 45, representing mass and energy balance for condenser lumps, can be simplified to the following equations,

$$D_{11}\frac{dL_{con}}{dt}+D_{12}\frac{dT_{con}}{dt}=D_{13} \tag{64}$$

$$D_{21}\frac{dL_{con}}{dt}+D_{22}\frac{dT_{con}}{dt}=D_{23} \tag{65}$$

where $D_{1(1,2,3)}$ and $D_{2(1,2,3)}$ are the coefficients for mass and energy balance equations in the condenser, respectively. Finally, the derivatives of the distillate level and condenser temperature can be calculated from,

$$\frac{dL_{con}}{dt}=\frac{\boldsymbol{D_{22}D_{13}-D_{12}D_{23}}}{\boldsymbol{D_{11}D_{22}-D_{12}D_{21}}} \tag{66}$$

$$\frac{dT_{c,con}}{dt}=\frac{\boldsymbol{D_{11}D_{23}-D_{21}D_{13}}}{\boldsymbol{D_{11}D_{22}-D_{12}D_{21}}} \tag{67}$$

In order to obtain the transient nature of feed seawater temperature, the condenser tube enthalpy is assumed to be the average of the feed and cooling seawater enthalpies and is given as $h_{T,con}=\frac{h_f+h_{cw}}{2}$. Substituting this into Eq. (43), the rate of change of feed water temperature with time can be written as,

$$\frac{dT_{feed}}{dt}=\frac{2\left(Q_{con}+m_{cw}h_{cw}-m_{cw}h_{f}\right)}{\rho_{tube,c}\forall_{tube,c}\frac{dh_{f}}{dT}} \tag{68}$$

$$\text{where}Q_{con}=U_{con}A_{con}\frac{\left(T_{v,n}-T_{f}\right)-\left(T_{con}-T_{cw}\right)}{ln\left[\frac{T_{v,n}-T_{f}}{T_{con}-T_{cw}}\right]} \tag{69}$$

By solving Eqs. (47-55), the condenser liquid level, condenser vapor temperature, and feed temperature can be calculated at each time step. The condenser pressure is assumed to be equal to the saturation temperature at the condenser temperature.

A FORTRAN code is developed in order to simultaneously solve the first-order nonlinear ODEs for the condenser and evaporators using the Runge-Kutta fourth order method. In the beginning, the steady-state solution for the MED-TVC system is obtained. This solution is then used as the initial conditions for the dynamic response calculations. In the steady state solution, the temperature, feed flow rate, brine flow rate, vapor flow rate and salinity at each effect are calculated in addition to the evaporators and condenser surface areas. At each time step, the temperature, liquid level, and salinity are calculated in each effect. The condenser temperature, condenser distillate level and feed temperature are also calculated. The brine and vapor flow rates among the effects are calculated based on the liquid level and the saturation pressure in each effect. The entrainment ratio of the thermal-compressor is updated at every time step using the correlations given in [92] and the values of the pressure at the last effect and the pressure of the motive steam. A time step was chosen to be 0.1 s to eliminate the instability in the solution [179].

The model solution flow is presented in Figure 47. Any parameter can be changed (or disturbed) with various intensity from its steady state value abruptly or in a ramp form for a specified time period. The MED-TVC operating condition is expected to deviate from the steady state condition upon the introduction of disturbances. If the MED-TVC is stable, it should return to its original steady state operation when the disturbances are removed. Behavior indicator parameters such as brine level, effect temperature and vapor flow between effects are obtained in addition to the performance indicator parameters such as GOR as a function of time while the disturbances are applied or removed from the dynamic model solution.

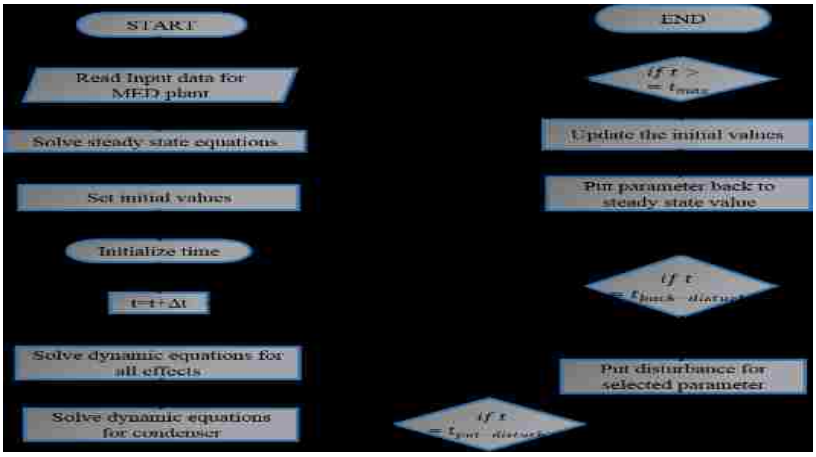

Figure 47 Flow chart for the solution procedure of the dynamic model disturbance.

Model validation

7.5.1. Validation of steady-state calculations

To verify the results of the present steady-state model, a comparison with actual data from the literature for several commercial MED-TVC plants is made. For this purpose, the following values available in real plants with different installation capacities such as Sidem (western area of UAE), Trapani and Tripoli [72, 201, 202] are introduced in Table 29. A comparison between the results calculated by the present model and the corresponding values of actual data from commercial plants is shown in Table 29. The percentage error in the GOR ranges from 2.55 to 8.29%.

Table 29 Validation of MED–TVC model results against data from commercial plants.

MED–TVC model Input data	Sidem [202]	Trapani [201]	Tripoli [72]
Number of effects	4	12	4
Motive steam pressure, kPa	2400	4500	2300
Motive steam flow rate, kg/s	6.361	6.67	8.89
Top brine temperature T1, °C	59	62.2	60.1
last brine temperature Tn, °C	47	37	45.4
Temperature drop / effect, °C	4	2.3	4.9

Feed temperature Tf, °C	44		35		41.5	
Seawater temperature Tcw, °C	33		22		31.5	
Feed content, g/kg	47		40		35	
Brine content, g/kg	71.5		60		53	
System performance						
	Model	Actual	Model	Actual	Model	Actual
Gain output ratio (GOR)	7.588	8.275	15.41	15.617	6.342	6.508
Distillate production kg/s	48.269	52.6388	98.69	104.167	56.38	57.861
Brine flow kg/s	97.129	106.25	200.56	209.72	106.783	109.21
Feed flow kg/s	145.398	158.88	299.25	313.889	163.163	167
Steam flow rate to 1st effect	12.853	NA	11.98	NA	14.72	14.44
Entrained flow from last effect	6.492	NA	5.31	NA	5.83	5.55
Entrainment Ratio for TVC	0.98	NA	1.256	NA	1.525	1.601
% Error GOR	8.29		5.26		2.55	

7.5.2. Dynamic response validation

Published real transient data or curves that characterize the behavior or performance of actual MED and MSF desalination plants are scarce, especially during startup or shutdown. Manufacturers of MED and MSF plants, perhaps due to competition reason, are not revealing their plant data especially the plant dynamic response with actual disturbances that the unit may be exposed to. So, the dynamic model results are compared with a lab-controlled three-effect MED plant of shell and tube evaporators with a total freshwater production of 3 m^3/day. This MED plant operational and design parameters are available in [191]. The heat source used in this plant is a hot water stream that is introduced to the first effect. The vapor generated in the first effect is used to heat the second effect and so on. The vapor temperature in each effect is measured when the hot water heat source is shut off for a certain time interval (disturbance).

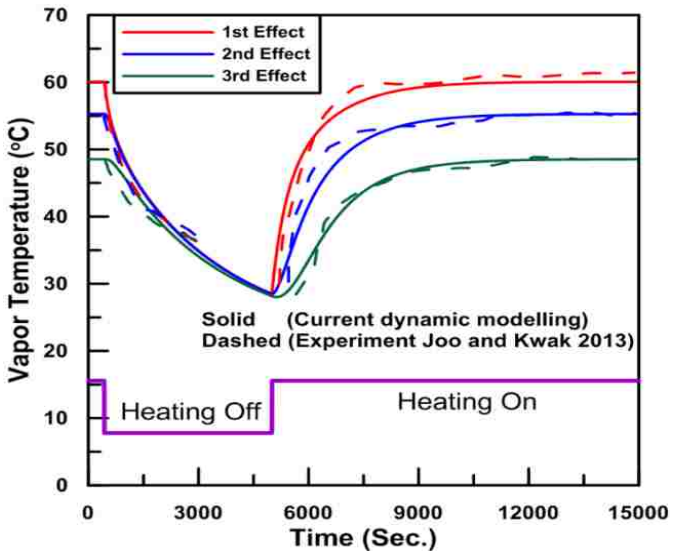

Figure 48. Temperature profiles of the vapor in each evaporator for the current simulation and the experiment in [191].

In order to investigate the validity of the dynamic model under experimentally similar conditions, the heat supplied to the first effect is set as the disturbance in the numerical model. Its value is set to zero at the time of hot water shutdown and is returned to its steady-state value at the end of the disturbance period. Figure 48 shows a comparison between the transient representation of vapor temperature in each effect obtained from the present dynamic model and the data published in [191]. The average absolute error between the actual and simulated data for each effect is 2% which indicates good agreement between the simulation and the published experimental data.

Results and Discussion

The steady and dynamic models in this study are applied to a plant in Western Abu Dhabi when it is subjected to perturbations from the design steady-state values of the main input parameters both in duration and intensity. For this plant operating at steady state, the specific thermal and electrical power consumption are 72.6 and 1.88 kWh/m^3, respectively [202]. Using the energy conversion

factors given in [64] , the value of UPR at steady state operation can be determined to be 95.5, which is consistent with the results for thermal desalination units found in the literature [64, 65]. In real operation, the operating parameters may not be maintained constant due to the changes in weather conditions and fluctuations in power supplied to the plant. The deviations of the operating parameters away from the design steady state values may: i) lead the plant to reach another steady state condition with different performance or, ii) disrupt the plant operation due to the drying or flooding of one or more of the effects. Whether these situations occur depends on the intensity and the time duration of the imposed disturbances. Three disturbances are selected as a step increase/decrease from the steady state values of the operational parameters. These disturbed parameters include cooling seawater flow rate, cooling seawater temperature, and motive steam flow rate which is denoted as a, b, and c disturbances, respectively. The amplitude and duration of each disturbance are changed to study the effect of the disturbance intensity and duration on the plant performance. In addition to that, a 10% reduction in motive steam pressure at constant entrainment ratio is considered to determine the effect of motive steam pressure on the plant behavior and performance indicators. The initial brine/condenser liquid level was assigned to 0.25 m. Based on the actual effect dimensions, two constraints are imposed on the brine level, L_b<1.0 m and L_b>0.1 m, to avoid flooding or dry out conditions, respectively.

7.6.1. Effect of disturbance intensity

The dynamic responses of the brine level, vapor temperature, and vapor mass flow rate in the first and last effects are shown in Figure 49 for disturbances a, b, and c. All disturbances last for 10,000 s while their intensities are changed. In disturbance a, the reduction in cooling seawater mass flow rate ranges from 2-12% of the steady-state value. It can be seen from Figure 49a(i) that the brine level for all effects decreases gradually due to enhanced evaporation accompanied by the reduction

in mass flow rate of the cooling seawater. This disturbance directly increases the feed water temperature which enhances the vapor flow rate and vapor temperature in all effects. For the current MED-TVC configuration and dimensions, it is found that a 12% reduction in cooling seawater flow rate causes the brine level of the first effect to reach to the assigned constraint for dry out. So, the further decrease is not permissible because the vapor in the first effect may blow through the second effect. This will disrupt the flashing and evaporation process and the plant will subject to operational failure [217]. Although this disturbance may offer enhancement in the evaporation process inside the evaporators it may cause rapid shutdown of the plant due to dry out in the first effect. Also, decreasing cooling seawater mass flow rate is accompanied by an increase in condenser pressure and temperature. The rapid response of the vapor lump of the condenser causes a sudden drop in vapor mass flow rate from the last effect due to the increase in the condenser pressure (back pressure of the last effect) as shown in Figure 49a(iii). Increasing the temperature of the feed due to the reduction in cooling seawater mass flow rate enhances the evaporation and increases the vapor pressure. This helps in pushing more brine to flow to the last effect which results in an increase in its brine level at the beginning of applying disturbance at the last effect. The brine level gradually decreases due to the enhanced evaporation. At the end of the disturbance, the reverse behavior occurs. A 12% reduction in cooling seawater results in about a 6% increase in vapor flow rate from the first and last effect. Evaporator dry out and a relatively small enhancement in the vapor produced inside the effects are the main outcome of the reduction in seawater flow rate [185].

Figure 49b(i) shows that the disturbance due to a reduction in the seawater temperature causes a rapid increase in the brine level in all effects. This rise in brine level is due to the reduction in evaporation rate and vapor temperature in each effect. Brine flow rate increases gradually with the

hydrostatic level of the brine level. A back pressure is experienced in the condenser due to the increase in seawater temperature that decreases the vapor flow rate to a minimum value at the end of applied disturbance as shown in Figure 49b(iii). Further decrease in the cooling seawater temperature up to 35% of the original value results in a continuous increase and decrease in the hydrostatic pressure of brine level and vapor temperature, respectively. Reduction in cooling seawater temperature causes a decrease in the plant performance and the plant may be exposed to operation malfunction [218] because the vapor temperature inside an effect can drop and increase significantly at the start and end of the disturbance.

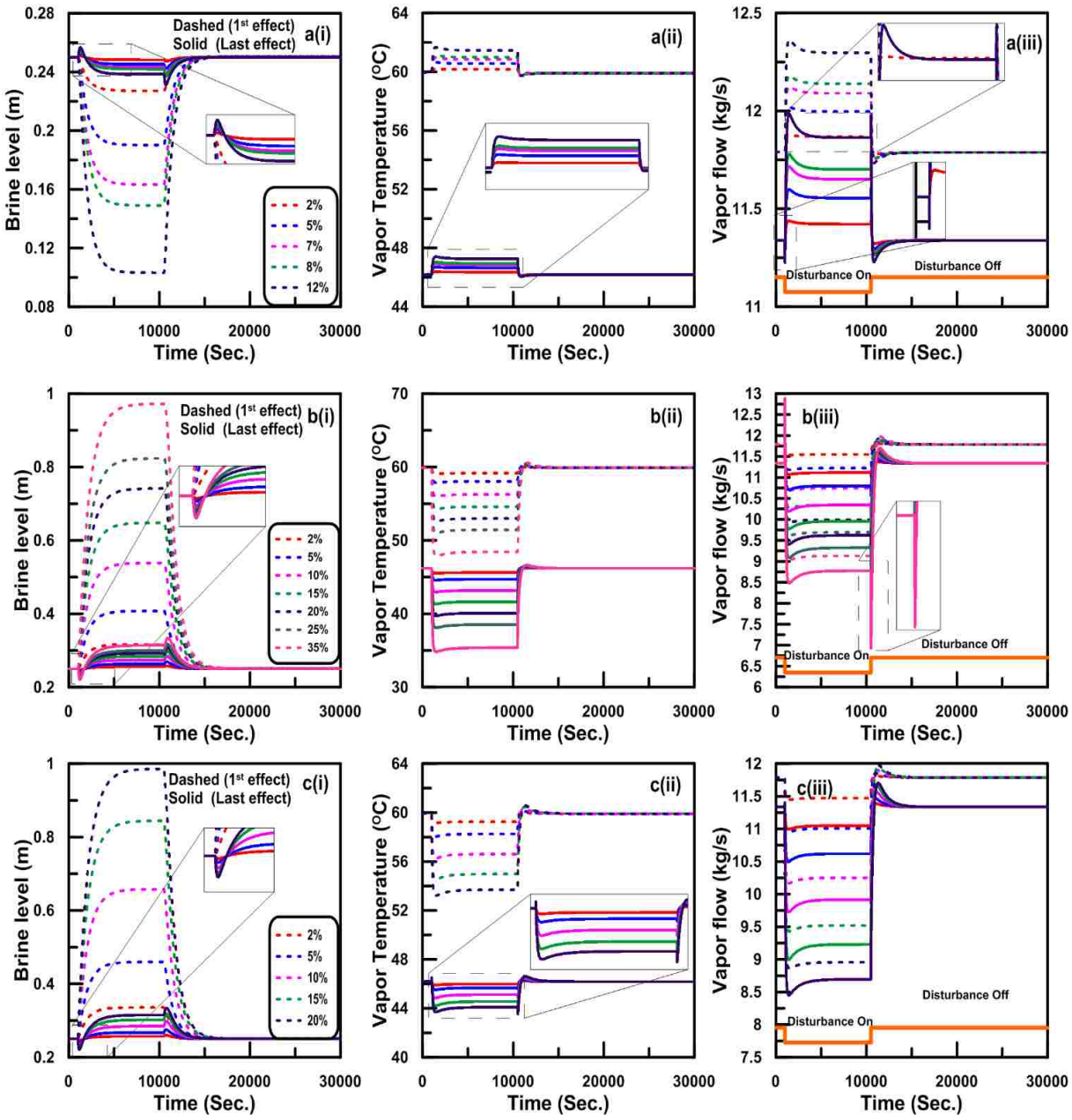

Figure 49 Variation of different parameters with the intensity of the disturbances a, b, and c.

For the third disturbance, reducing the supplied motive steam flow rate to the TVC unit results in a rapid decrease in the vapor temperature and flow rate in the first and last effects as shown in Figure 49c(ii and iii). Due to the reduction in the evaporation process in all effects, the hydrostatic pressure of the brine level increases gradually and thus the brine mass flow rate. A reduction of the motive steam flow rate up to 20% of the steady-state value causes a higher increase in the

amount of brine level and flow rate as shown in Figure 49c(i). Disturbance in motive steam flow rate is linked to a change or a swing in the supplied power to the boiler or the pressure of the steam extracted from the power plant turbine, which is considered random unrelated plant operations. Reduction in motive steam flow rate is considered critical as it causes a decrease in the desalination plant performance and may lead to filling up the entire vapor space below the demister and cause evaporator flooding. This clearly is not acceptable during operation and will lead to a plant shutdown. It is recommended for the current plant design to avoid working with motive steam with 20% reduction of the steady-state designed value as shown in Figure 49c(ii). In order to keep a steady course operation and maintain relevant parameters in the plant under control throughout the whole plant operation with disturbances, knowledgeable control-room operators and field operators must be particularly skilled [168]. It is also recommended to smoothen out the dangerous behavior such as a fast change in temperature that the plant may be exposed to due to the increase in the intensity of disturbances. This could be done by implementing a specified startup procedure that fits these disturbances [218].

In actual practice, a change in motive steam pressure is associated with a proportional change in the motive steam mass flow rate [91, 104]. But to study the separate effect of changing the motive steam pressure, a 10% increase in motive steam pressure is allowed while the steam mass flow rate is kept constant. It is found that increasing the motive steam pressure results in a negligible change in the total steam discharged from TVC unit which means that the change in the motive steam pressure will have a negligible change to the plant behavior and performance indicators. This could be attributed to the nature of the relationship between expansion ratio E_r, compression ratio C_r and entrainment ratio R_a plotted on Power's chart [91] at constant entrainment ratio, where the slope dC_r/dE_r is very small (~0.00135 for $R_a = 1.0$). The change in expansion ratio due to

the 10% increase in the motive steam pressure results a negligible variation in C_r and inlet steam temperature to the 1st effect, so changing the motive steam pressure intensity was not considered further in the current study.

7.6.2. Effect of disturbance applied duration

In addition to evaluating the system behavior due to the change in disturbance intensity, it is important to investigate the effect of disturbance applied duration on the desalination plant characteristics. So, a stepwise increase in the applied disturbance duration is allowed while the intensity is fixed at 8% reduction in the cooling seawater flow rate. Figure 50a shows the variation of brine level, vapor temperature, and vapor mass flow rate for the first and last effect. In terms of dynamic characteristics of the investigated system indicators, the vapor temperature has the fastest response while the brine level has the slowest response. Successive increase in the applied duration of the disturbance over 9000 s causes the system to reach a complete steady state condition during the application of the disturbance. Duration of the disturbance has a minimal effect on plant performance if the critical values of the disturbance intensity that can cause plant shutdown are avoided. For a 8% reduction in cooling water flow rate in the current plant design, disturbance duration is not considered critical since the brine level in the first effect will never reach the dry out condition.

In case of applying an intensity higher than the critical limits assigned in the last section, there is a need to determine the controlling period in which plant shutdown can be avoided. Figure 50b (i, ii and iii) show the brine level dynamic response for 13, 40 and 25 % reduction of the cooling seawater flow rate, cooling seawater temperature, and motive steam flow rate, respectively. When the brine level reaches the values assigned for effect for flooding or dry out, the simulation stops.

For the aforementioned intensities, it is found that the time required for the plant to avoid a shutdown is as follow: (i) the 1500s for a reduction in cooling seawater flow rate, (ii) 4500s for a reduction in cooling water temperature and motive steam flow rate.

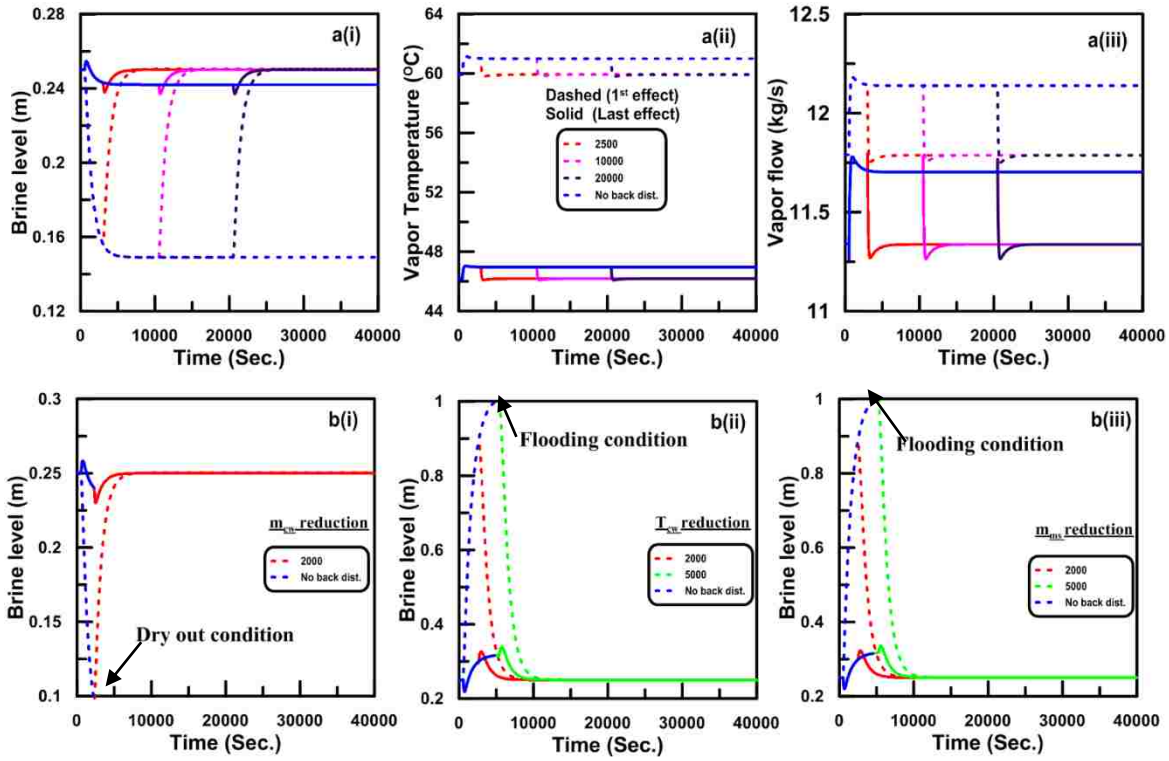

Figure 50 (a) Variation of different parameters with applied disturbance duration of cooling water flow rate. (b) Brine level for different applied disturbance duration.

7.6.3. Effect of combined disturbances

In some occasions, two or more types of variation in the main input parameters may occur simultaneously during the plant operation. These disturbances may have co-effect (enhancing effect) or opposing-effect on the plant operation when applied simultaneously. In order to investigate the simultaneous disturbances in opposing directions, two sets are considered. The first reduction set is a combination of (10% m_{cw}+10% m_{ms}) and the second reduction set is a combination of (10% m_{cw}+10% T_{cw}). Figure 51a shows the effect of these disturbances applied simultaneously or individually for a duration of 15000 s on the brine level of the 1st and last effects.

As discussed earlier, a reduction in motive steam flow rate and cooling water temperature increases the brine level in the first effect towards the flooding limit while reducing the cooling water flow rate has the opposing effect. Applying these combinations of the simultaneous reductions would result in a more modest effect on the plant operation as shown in Figure 51a(i,ii). So, it is possible to intentionally control the cooling water and motive steam flow rates to mitigate the flooding/drying effects of the disturbances in other parameters.

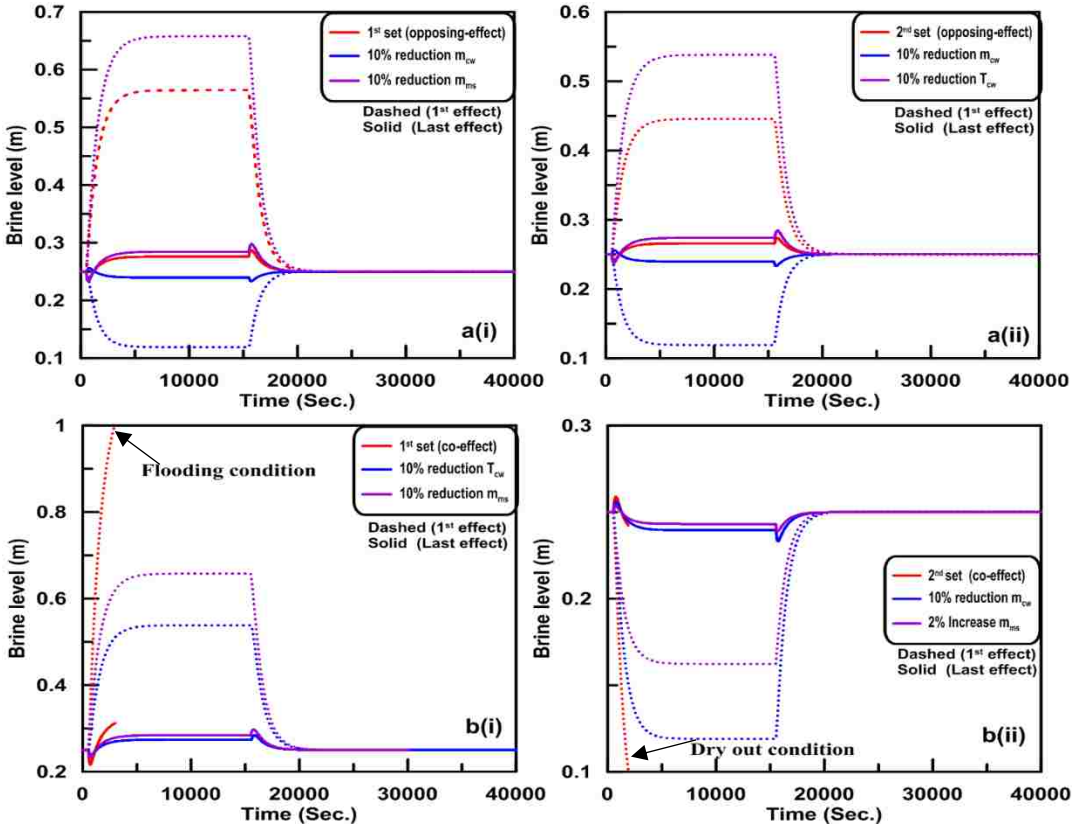

Figure 51 Variation of brine level for separate and simultaneous applied disturbances.

Another two combination sets of simultaneous disturbances in co-effect direction are investigated. The first set is a combination of 10% reduction in T_{cw} and 10% reduction in m_{ms} while the second set represents 10% reduction in m_{cw} and a 2% increase in m_{ms}. Indeed, the individual disturbances

in the first and second sets increase and decrease the brine level in the 1st effect, respectively as shown in Figure 51b. But it is still under the assigned value for evaporator flooding or dry out conditions. In the case of applying the first set, it results in a significant change in the plant and the condition of evaporator flooding is reached. Similarly, with the second set, the brine level in the 1st effect reaches the assigned condition for evaporator drying with only 2% increase in the motive steam flow rate and 10% reduction in cooling water mass flow rate after a relatively small time. This indicates that the plant needs an accurate control system to avoid these types of co-effect simultaneous disturbances that they may lead to an operational shutdown. The overall influences of the applied simultaneous disturbances on the total product and the GOR of the plant compared to the original steady state operating condition are presented quantitatively in Table 30 for the opposing-effect combination sets and the individual disturbances. It can be noted that the GOR and the total product of the plant are more sensitive to the reduction in the cooling water temperature and the motive steam mass flow rate, respectively.

Table 30 Variation of MED-TVC performance indicators for individual and simultaneous disturbances.

				Opposing-effect sets	
Variable	10% m_{cw}	10% m_{ms}	10% T_{cw}	1st set	2nd set
% change in total production	3.69 %	-12.33 %	-8.016 %	-9.456 %	-5.24 %
% change in GOR	3.68 %	-2.585 %	-8.06 %	0.586 %	-5.25 %

7.6.4. Effect on Plant Performance

As shown in Figure 52a, a decrease in cooling seawater flow rate (lower than the design value) boosts the amount of condensate in each effect. This, in turn, increases the plant total production of fresh water and GOR [198]. On the other hand, there is a chance that the plant may be exposed

to a shut down due to dry out in the effects if the cooling seawater flow reduction exceeds a certain limit. In actual start-up process of MED plant, if the cooling water flow rate is lower than the steady state condition a higher system GOR is obtained but this leads to a longer start-up time [219]. In contrast, a reduction in cooling seawater temperature or motive steam flow rate results in a decrease in the production of fresh water and GOR. The reason behind these behaviors is that the decrease in seawater temperature or motive steam decreases the top brine temperature. This results in a decrease in the flashing and evaporation rates in all effects which in turn generates less vapor and increases the brine level in all the effects. The total productions of the fresh water are 52.2, 39.3 and 37.9 kg/s (designed value=49 kg/s) at the maximum (critical) applied disturbances: 12% reduction in cooling seawater flow rate, 35% reduction in cooling seawater temperature and 20% reduction in motive steam flow rate reduction, respectively.

At the start and end of all the disturbances, the value of GOR shows over and undershoots in its value. The over or undershoots due to the reduction in cooling water mass flow rate and cooling water temperature is attributed to the rapid response of the vapor pressure in the effects to the disturbances as shown in Figure 52 (b,c). This generates a favorable or adverse pressure gradient for the vapor flow among the effects which results in a sudden increase or decrease in the freshwater production. However, the over or undershoots in GOR due to the disturbance in motive steam flow rate are more prominent as shown in Figure 52c. This is attributed to the change in the denominator of GOR definition. At the beginning of reducing the motive steam flow rate, the GOR value shoots up due to the decrease in motive steam in the denominator of GOR definition and the late response of the plant to the abrupt change. On the contrary, at the end of this disturbance, a sudden drop in GOR value occurs.

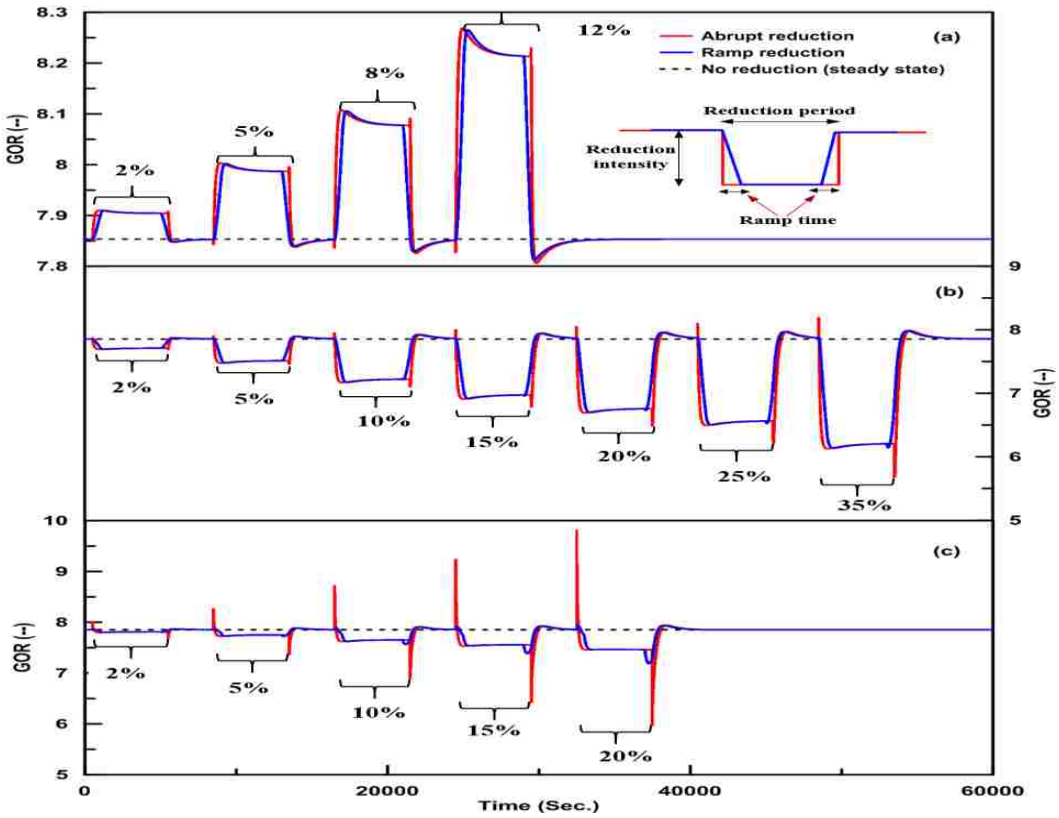

Figure 52 Transient response of GOR for step (abrupt and ramp) reduction in disturbances.

Abrupt reduction in the main input parameters in the desalination plant is considered the worst-case scenario the plant would be exposed to during normal operation. So, a ramp disturbance with a linear variation in the main input parameters is investigated to figure out the difference between both (abrupt and ramp) types on the plant characteristics and performance. The magnitude of reduction and applied duration of the ramp and abrupt disturbances are fixed. However, in the case of ramp reduction, a ramp time of 500 s is considered. Ramp time represents the time that the designed value of input parameter takes to reach the value of the reduction at the beginning of disturbance application. On the other hand, before the end of the disturbance, ramp time represents the time needed to reach the designed values of input parameter as shown in the insert of Figure 52a. Ramp time smoothens the transition in the reduction of input parameters and in turn removes the overshoots and undershoots in GOR as shown in Figure 52. However, both types of disturbance

application (abrupt or ramp) lead to similar conclusions regarding the increase or decrease in GOR for the plant upon exposing to a disturbance.

Conclusions

A detailed model for transient modeling of parallel/crossflow configurations MED-TVC system has been developed and validated with experimental data available in the literature. The model is then used to investigate the effect of the fluctuations in magnitude and duration of the main operational parameters on the plant behavior and performance. The operational parameters included are: motive steam flow rate, motive steam pressure, cooling seawater flow rate and cooling seawater temperature. The results show that the disturbance intensity variation plays a major role in the desalination plant behavior. For the current MED-TVC configuration and dimensions, it is recommended to limit the reduction in the seawater cooling flow rate to under 12% of the designed steady-state value to avoid dry out in the evaporators. Also, a reduction in the motive steam flow rate and cooling seawater temperature of more than 20% and 35% of the nominal operating values may lead to flooding in the evaporators and complete plant shutdown. It is also shown that a change in the motive steam pressure at constant entrainment ratio has a negligible effect on the plant performance and behavior. On the other hand, the disturbance period has a minimal effect on plant performance if it avoids the critical values of the disturbance intensity that can cause plant shutdown. Simultaneous combinations of two different disturbances with opposing effects result in a modest effect on the plant operation and the combinations can be used to control and mitigate the flooding/drying effects of the disturbances. For co-effect combinations, the plant needs an accurate control system to avoid an operational shutdown. A ramp type disturbance mitigates the changes in input parameter disturbances and eliminates the over/under-shoots in the GOR observed when disturbances are applied and removed in an abrupt manner.

CHAPTER 8 TRANSIENT AND THERMO-ECONOMIC ANALYSIS OF MED-MVC DESALINATION PROCESS[**]

Abstract

An exergo-economic model is used to assess the performance of a multi-effect desalination plant integrated to a mechanical vapor compressor unit (MED-MVC) with a water production capacity of 1500 m^3/day. The results show that the second law efficiency (η_{II}) is 2.8%. The MVC and evaporator units are responsible for about 39 and 52% of the total exergy destruction, respectively. The total water price (TWP) is 1.70 \$/m^3 when calculated using a simple conventional economic model and 1.63 \$/m^3 when calculated using an exergy-based cost model. Increasing the number of effects from 1 to 6 results in a 39% reduction in the specific power consumption (SPC), a 70% increase in η_{II} and a 24% decrease in TWP. A dynamic model is developed to investigate the effect of fluctuations of compressor work ($\dot{W}_c$) and inlet seawater temperature (T_{sw}) on the plant behavior and performance. The dynamic model results show that the disturbance in $\dot{W}_c$ has a significant effect on the plant transient behavior and may cause the plant to cease operation while a disturbance in T_{sw} has only a moderate impact. Increasing T_{sw} above a certain value of the steady-state condition without proper control on the plant response could lead to evaporator dry out. In term of performance, a reduction in $\dot{W}_c$ causes a decrease in the plant production capacity and SPC, while it increases the plant performance ratio (PR). On the other hand, a reduction in the inlet T_{sw} causes a reduction in the plant production capacity and PR and an increase in SPC for the same compressor work. Furthermore, a comparison between a MED-MVC system and a MED

[**] **Mohamed L. Elsayed**, Osama Mesalhy, Ramy H. Mohammed, Louis C. Chow, "Transient and thermo-economic analysis of MED-MVC desalination system" Energy volume 167, January 2019, pages 283-269.

integrated to a thermal vapor compressor system (MED-TVC) reveals that the latter system is rather sensitive to the reduction in T_{sw} due to the presence of the condenser unit in the MED-TVC. The response of the MED-MVC system is slower than the MED-TVC which is due to the high thermal capacity of the preheaters for the feed in the MED-MVC.

Introduction

Seawater desalination is considered a viable solution for drinking water shortage besides other integrated solutions such as water management, reclamation and better water conservation. There are two primary desalination techniques: membrane (non-thermal) and evaporation (thermal) processes. Membrane techniques such as reverse osmosis (RO) are characterized by low energy consumption but also low water product quality associated with residuals of borides, chlorides and bromides, as well as high maintenance cost and short membrane lifespan [220]. Thermally-driven processes such as Multi-Effect Desalination (MED), Multi-Stage Flash Desalination (MSF), Mechanical and Thermal Vapor Compression (MVC and TVC) are usually used in countries such as Gulf co-operation countries (GCC) where the supplied feed seawater is exhibited to changes in feed quality arising from fine sand, silt, harmful algae blooms (HABs) and water salinity fluctuation [56]. Recovering the latent heat of condensation in the product vapor was proposed through heat pump concepts such as TVC and MVC units to allow further evaporation of seawater when the temperature level of the produced vapor is too low for stable evaporation. The MVC evaporation system has been widely studied and frequently applied as a solution for medium-scale (100-4000 m^3/day) water reclamation desalination and solution concentration for high-salinity wastewater treatment (salt recovery) [105]. The advantages associated with MVC systems are high-quality water recovered that need little or no treatment, compact equipment, low operating cost, stable operation and simple integration with renewable energy systems [106]. The low

capacity of available vapor compressors, low volumetric flow and low-pressure head limit the production capacity of MED-MVC systems to 5000 m^3/day [108].

Various studies for MVC systems are available in the literature and include steady-state mathematical model development, simplified design methods, experimental research and performance prediction. For instance, Helal and Al-Malek [125] presented a hybrid diesel/solar photovoltaic (PV) assisted MVC desalination system. The system was to supply small communities in remote areas with drinkable water at a production capacity of 120 m^3/day. A diesel engine was used to overcome the uncertainty in the availability of solar energy. Henderson et al. [126] proposed a wind/diesel hybrid driven MVC desalination system for off electric grid locations in the USA. Optimization of a similar plant driven by wind/PV hybrid was carried out by Zejli et al. [127] for a water production capacity of 120 m^3/day. An energy storage system was used to store the extra power generated to address the intermittent nature of the renewable energy used.

Exergy analysis is known as a powerful tool to analyze the performance of mechanical and thermal systems. Using such method to analyze seawater desalination systems is a practical approach to identify the components with high thermodynamic irreversibilities [77]. Such information is useful to show which components in the system have room for improvement to increase the overall exergy efficiency and to optimize designs [78]. Alasfour and Abdulrahim [129] applied a steady-state model using the second law of thermodynamics to a single-effect MVC unit. The results indicated that an increase in the temperature drop across the effect causes an increase in exergy destruction. Nafey et al. [38] analyzed a MED-MVC system with a two-effect forward-feed configuration plant and showed that the specific power consumption (SPC), second law exergetic efficiency (η_{II}) and the unit product cost are 9.4 kWh/m^3, 5.7% and 1.7 \$/ m^3, respectively. Ahmadi et al. [111] compared a single- and two-effect mechanical vapor recompression (MVR) and

showed that energy saving can be achieved by using the two-effect MVR rather than the single-effect one. Also, the reduction in heat transfer area was 5.6 m^2 for the two-effect system compared to the single-effect one.

Recently, MED-MVC systems have been used as brine concentrators before sending the brine to crystallizers or evaporation ponds. These system combinations are called Zero liquid discharge (ZLD) systems [221]. Typically, the crystallizers have a constant evaporation capacity. Thus the evaporator rejected brine mass or content should be controlled to maintain the optimum operational conditions, leading to energy savings and prevention of scale formation. Therefore, the system transient behavior needs to be predicted to conduct control strategies, examine different scenarios of operation, handle the possibility of unexpected transient conditions, and guarantee a relatively stable output through the production duration [169].

Thermal desalination systems may be exposed to unexpected fluctuations (disturbances) in input parameters throughout their operation periods that include environmental changes such as swings in the feed seawater temperature due to varying weather condition and swings in the supplied heat source. The second type of fluctuations is called “turndown” that represents the possible change in total plant output. This type of disturbance is carried out by design to address a swing in the power requirement [168]. Dynamic simulation can predict the system behavior from start up to shut down and can be used to establish advanced control strategies and test operating scenarios. It can also address potential problems related to unexpected transient events, and produce a comparatively stable output during the production period [210]. Several efforts were made to study the dynamic characteristics of conventional thermal desalination MED [181, 182, 215, 222] and MED-TVC systems [90, 179, 183, 185]. For instance, at CIEMAT-Plataforma Solar de Almerı´a (PSA), a transient operation model of the MED plant in a vertical arrangement was developed and

solved using the object-oriented Modelica language [182]. The model was divided into sub-models that encapsulated and covered the dynamics of each one of the sub-processes that took place in the system in order to study the plant performance in different scenarios and design operating strategies to improve its efficiency [215]. Furthermore, Roca et al. [222] developed a dynamic model using Modelica for MED systems and the results were validated using data from the PSA facility. Two first-order models for the distillate production and outlet MED temperature as a function of inlet MED temperature were obtained by linearizing the dynamic model in [215] and good agreement was obtained for a wide operation range. For MED-TVC systems, Mazini et al. [183] developed a lumped dynamic model and validated it with actual data from a MED-TVC operating plant. Although disturbances in feed flow rate and seawater temperature were considered, the physics of the system response was not clearly illustrated. Cipollina et al. [185] used the gPROMS® dynamic simulator to predict the transient behavior of a MED-TVC based on available data from the Trapani plant in Italy. The dynamic operation was obtained by applying changes to specific disturbances on the main input parameters. Negligible variations were predicted with an increase in the seawater temperature, while a slight reduction in the plant gain output ratio (GOR= distillate to steam supplied ratio) was shown when the seawater temperature was reduced. Recently, a comprehensive model was developed by Elsayed et al. [90] to study the dynamic characteristics of different feed configurations of MED systems and MED-TVC as well. The simulation results revealed that MED-TVC with parallel/cross feed has the fastest response compared to slower response associated with backward and forward feed for the same applied disturbances. Furthermore, the MED-TVC is more susceptible to the heat sink disturbances compared to the other traditional MED configurations.

There have been very few efforts to model the dynamic nature of the MVC evaporation systems. For instance, El-Khatib et al. [223] proposed a transient model through control of multiple inputs and outputs to an MVC single-effect desalination unit. The model is limited to the dynamic representation of the vapor temperature inside the effect without considering the level of the brine pool or the brine salinity. Two changes were applied to the MVC unit, namely a variation in the production of distillate flow rate and the inlet feed flow rate of ±20 %. The model results were not validated by experimental or actual operating data. Kishore et al. [141] proposed a dynamic simulator for the MED-MVC system as work-in-progress for steady state and the dynamic behaviors. However, no system response due to load change was shown. Another contribution in dynamic simulation and control for a single-effect MVC to investigate the acceptable level of parameter disturbances in the dairy industry was made by Winchester and Marsh [224]. It is essential to study the dynamic behavior of a MED-MVC system subject to changes in the input operating parameters to improve the understanding of the process behavior and performance. In the present study, a dynamic model to study the transient behavior of a parallel/cross feed MED-MVC desalination system is developed based on the work on MED-TVC reported by Elsayed et al. [90] by adding features that are in the MED-MVC but not in the MED-TVC. The present model is also modified and customized with equations that dynamically track the behavior of four effects, two preheaters and a mechanical compressor unit. Three nonlinear ordinary differential equations are derived for three state variables, namely the vapor temperature, brine salinity and brine level, to simulate the dynamics of the evaporator effect. Also, a dynamic model for the brine and distillate preheaters is developed to obtain the transient variation of the inlet and outlet stream temperatures. Finally, the entire set of equations is solved simultaneously using the Runge-Kutta fourth-order. The dynamic model yields the plant behavior and performance under various fluctuations in the

main input operating conditions that include the compressor work and inlet seawater temperature. Furthermore, the exergo-economic analysis is used to assess the MED-MVC system performance and to obtain the total water price compared to the simple conventional economic method.

MED-MVC process description

A parallel/cross feed (PCF) multi-effect-desalination integrated with a mechanical vapor compression unit is considered in the present study. A schematic diagram of MED-MVC is shown in Figure 53. A typical MED-MVC system contains major elements such as a train of horizontal falling film evaporators, MVC unit, pre-heaters for intake seawater, a boiler which supplies the external steam, pumps for brine and product, a venting system to remove non-condensable gases, along with an operating control system [225]. Each evaporator consists of a shell that houses tube bundles of horizontal falling film tubes, spray nozzles, demister and space for the vapor and brine pool. Vapor compression is a cyclic process [110], so the entire vapor generated in the last effect is routed through a wire mesh mist eliminator (demister) to separate water droplets from the vapor before entering the compressor. The vapor is compressed to the desired target temperature and pressure before directing it as supply steam to the inside of the 1st effect tube bundles. The supply steam from the MVC unit condenses inside the tube bundles by rejecting its latent heat to the continuously sprayed thin film of the seawater feed on the exterior wall of the tube bundles. The temperature of the feed seawater around the tubes in the 1st effect is raised to its saturation temperature that is known as top brine temperature (TBT). Part of the supplied seawater feed to the 1st effect vaporizes, and the vapor flows into the 2nd effect which is at a lower pressure and temperature than the first effect. The evaporated portion of the feed in each effect works as a heat source for the following effect. In all effects, condensation and evaporation occur simultaneously inside and outside the tubes for vapor and thin sprayed seawater film, respectively. The

unevaporated portion of the supplied seawater feed (brine) from the first effect flows into the second effect to utilize its energy by flashing due to the abrupt decrease in pressure when the brine leaves the first effect and enters the second effect. The brine continues to flow through all effects until it finally reaches the last effect as shown in Figure 53. The vapor inside the 2nd to the last effect is produced by both evaporation and flashing. The concentrated brine and fresh water produced are drawn to the preheaters by pumps at a temperature above the ambient temperature.

In the MED-MVC system, there is no need for a condenser as in conventional MED systems, but two multi-flow plate-type heat exchangers (pre-heaters) are needed to recuperate the heat from both the product and brine blowdown streams. The feed seawater is split into two streams, and its temperature is elevated by passing through the pre-heaters. The supplied feed seawater is divided and directed into a series of consecutively lower pressure effects. The supplied feed is atomized and directed to the outside walls of the horizontally installed tubes forming a thin liquid film. Industrial MED-MVC desalination plants operate at temperatures between about 50-70°C. At such low temperature, the conditions favoring the deposition of insoluble sulfates and carbonates do not exist [226], and the risk of material corrosion is minimal.

Electricity is the only required source to operate the MED-MVC system. However, for start-up purpose and maintaining normal operating conditions without compressor surge, external steam (make-up steam) obtained from a steam boiler or extracted from a steam turbine may be needed to raise the 1st effect temperature to the TBT [36, 113]. The mechanical energy required for a MED-MVC desalination system can be provided through the energy produced by a steam power plant (mechanically shaft driven). Also, electricity-driven MVC can be used by drawing electrical power from the electricity grid or a renewable energy source, or electrical energy generator if electricity services are not available. It has been demonstrated that the use of a MED-MVC system coupled

with an electrical power generator is suitable for use in remote locations where water transport is expensive [127]. Energy is needed to activate the MVC unit, pumps, vacuum system and other control components. It is worth noting that the MVC unit represents the main power consuming component in MED-MVC system [129]. This power required depends on the vapor compression ratio, the thermodynamic efficiency of the polytropic process and the efficiency of the electric motor if one is used. For the MED-MVC system, the SPC (kWh/m^3) is represented in terms of the enthalpy difference of the compressed vapor (supply steam) and the inlet vapor from the last effect.

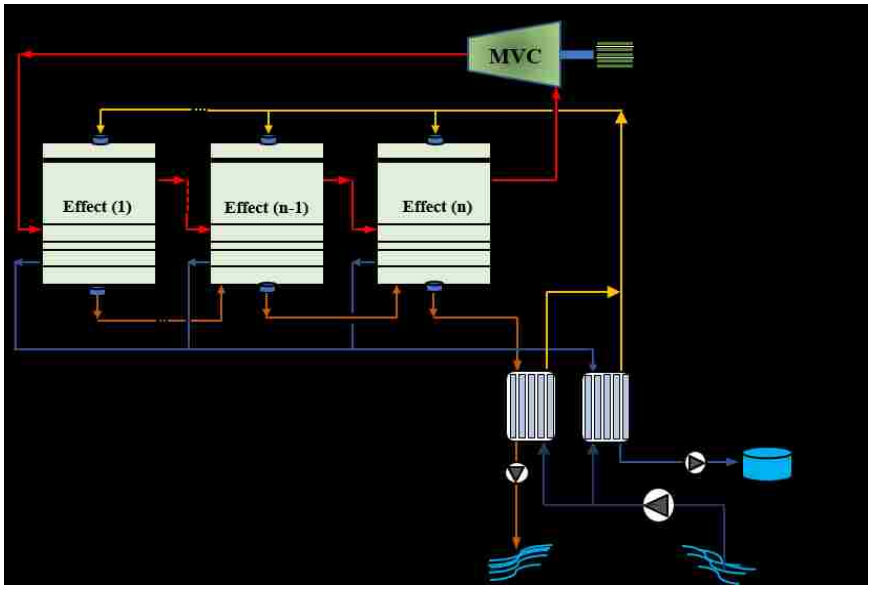

Figure 53 MED-MVC desalination system diagram.

Models development

8.4.1. Steady-state model

The steady-state conservation equations of mass, energy, and salt are solved to obtain the steady-state values of all the parameters in the plant. The assumptions used in the steady-state model for a MED-MVC system are listed as follows:

30. Since the presence of non-condensable gases is normally vented out of the MED system whenever needed, the effect of non-condensable gases on evaporator performance is not considered.
31. Properties of the seawater brine and water vapor depend on temperature and salt content [73].
32. The temperature difference between the brine pool and vapor generated in an effect is due to the following reasons; (i) boiling point elevation (BPE), and (ii) non-equilibrium allowance (NEA).
33. The vapor and produced freshwater are salt-free.

Using the above assumptions, the steady-state mass, energy and salt balance equations for a MED-MVC system are obtained and presented in Table 31.

Table 31 Conservation equations for a MED-MVC system.

Equations	First effect	Second to last effect (n)	F	B	D
Mass	$B_1 = F_1 - D_1$	$B_i = F_i - D_i + B_{i-1} - d_i$	$\sum_{i=1}^{n} F_i$	B_n	$\sum_{i=1}^{n} D_i + d_i$
Salt	$F_1.X_f = B_1.X_1$	$B_i.X_i = B_{i-1}.X_{i-1} + F_i.X_f$			
Energy	$D_1 = \frac{Q_{s,1} - F_1(h_1 - h_f)}{\lambda_1}$, $d_1 = 0$	$D_i = \frac{(D_{i-1} + d_{i-1}).\lambda_{i-1}}{\lambda_i} - \frac{F_i(h_i - h_f)}{\lambda_i}$, $d_i = \frac{B_{i-1}(h_{i-1} - h_i)}{\lambda_i}$			
Total mass balance $F = B + D$ Total salt balance $F.X_f = B.X_n$					
d_i , Vapor produced by brine flashing. D, Total distillate flow rate. F, Total feed flow rate. B, Total brine flow rate.					

The isentropic work of the MVC unit is calculated from:

$$\dot{W}_{i,c} = \dot{m}_s \frac{\gamma . P_n . v_n}{(\gamma - 1)} \left(\left(\frac{P_s}{P_n} \right)^{\frac{\gamma - 1}{\gamma}} - 1 \right) \tag{70}$$

where γ is the specific heats ratio, P_s is the pressure at the compressor outlet which is the saturation pressure at the steam inlet temperature T_s, P_n is the pressure at the compressor inlet, and v_n is the specific volume of the vapor from the last effect.

The energy supplied to the first effect as shown in Figure 54 is defined as:

$$Q_{s,1} = \dot{m}_s.\lambda_s + E_{SH} \quad ; \quad E_{SH} = \dot{m}_s\left(h_{v,\acute{T}_s} - h_{v,T_s}\right) \tag{71}$$

where $\dot{m}_s.\lambda_s$ represents the heat of condensation at T_s of the vapor produced in the last effect and E_{SH} represents the rate of energy gained by compression above the saturation condition, $h_{v,\acute{T}_s}$ is the enthalpy of the superheated vapor at the compressor exit, and h_{v,T_s} is the saturation enthalpy of the compressed vapor.

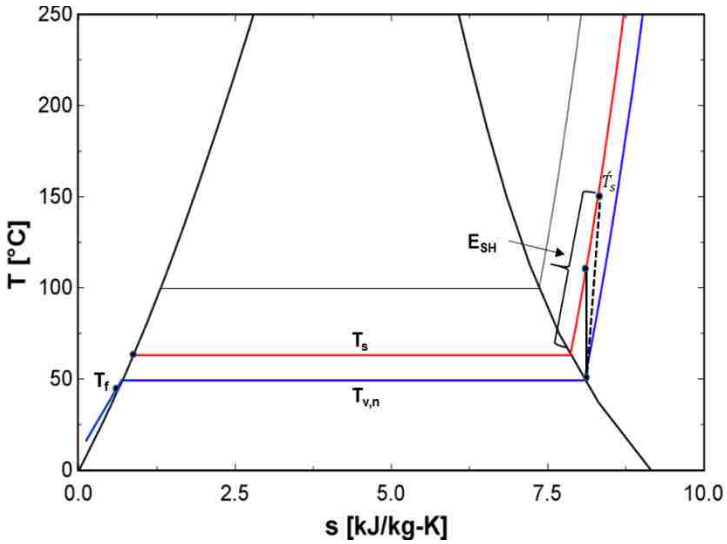

Figure 54 Temperature-Entropy (T-S) diagram for a MED-MVC system operation.

The actual compressor work can be calculated from:

$$\dot{W}_c = \dot{m}_s.\left(h_{v,\acute{T}_s} - h_{v,T}\ \right) \tag{72}$$

where h_{v,T_n} is the saturated vapor enthalpy at the compressor inlet.

The primary contributor to the SPC in a MED-MVC system is the compressor work which depends on the compressor efficiency, compression ratio and inlet vapor specific volume. The secondary consumptions are due to vacuum pumps and starting up the boiler [112]. The SPC is calculated by:

$$\mathrm{SPC}(kWh/\mathrm{m}^3) = \frac{\dot{\mathrm{W}}_{\mathrm{compressor}} + \sum \dot{\mathrm{W}}_{\mathrm{pumps}}}{\mathrm{D}\ (\mathrm{m}^3/h)} \tag{73}$$

The performance ratio (PR) is calculated by the following relation as suggested by Nafey [38] which is modified to accommodate the actual work converted to the primary fuel energy. For conventional fossil fuel-based power plant, Shahzad et al. suggested a thermal to work conversion factor less than 0.45 [65].

$$\mathrm{PR} = \frac{D\lambda_d}{\dot{m}_s.\lambda_s + \frac{\dot{\mathrm{W}}_{\mathrm{c}}}{\eta_{thermal}=0.35}} \tag{74}$$

Different modeling methods exist for the modeling of (chevron) plate heat exchangers. For design purposes, the thermal effectiveness method and the log-mean-temperature-difference (LMTD) method are often used to model the steady-state performance of a plate heat exchanger. In this regard, two multi-flow direction plate type heat exchangers with an effectiveness of 0.8 are used in the current simulation to preheat the seawater inlet feed. The total feed is divided into two portions: one portion flows into the brine heat exchanger and the second portion flows into the distillate heat exchanger. The heat transfer areas for both heat exchangers are calculated based on the log mean temperature differences and the estimated overall heat transfer coefficients for the plate type heat exchangers (U_B and U_D) using the following equations:

$$A_{b,HEx} = \frac{\dot{m}_B\left(h_{b,n} - h_{o,b}\right)}{U_B.LMTD_{b,HEx}} \quad , \quad A_{d,HEx} = \frac{\dot{m}_D\left(h_{hin,d} - h_{o,d}\right)}{U_D.LMTD_{d,HEx}} \tag{75}$$

The log mean temperature differences in the brine and distillate preheaters $LMTD_{HEx(B,D)}$ are calculated using the following equations:

$$LMTD_{b,HEx} = \frac{(T_{b,n}-T_{F,b})-(T_{o,b}-T_{cw})}{ln\left[\frac{T_{b,n}-T_{F,b}}{T_{o,b}-T_{sw}}\right]},\ LMTD_{d,HEx} = \frac{(T_{hin,d}-T_{F,d})-(T_{o,d}-T_{cw})}{ln\left[\frac{T_{hin,d}-T_{F,d}}{T_{o,d}-T_{sw}}\right]} \quad (76)$$

The mixing temperature of the distillate from the plant ($T_{hin,d}$) is calculated by:

$$T_{hin,d} = \frac{\sum_{i=1}^{n-1} D_i\, c_{P[T_{v,i}]} T_{v,i} + D_n c_{P[T_s]} T_s}{D c_{P[T_{hin,d}]}} \quad (77)$$

The total heat transfer coefficient for the plate type heat exchangers is calculated using:

$$U_{B,D} = \left[\frac{1}{h_o} + \frac{1}{h_o} + R_{f,o} + R_{f,o} + \frac{\delta_{plate}}{k_{wall}}\right]^{-1} \quad (78)$$

where k_{wall} is the thermal conductivity of the stainless steel plates, and the inner/outer convective heat transfer coefficients (h_i, h_o) are obtained using the following correlation [227]:

$$h_{o,i} = 0.2536 Re^{0.65} Pr^{0.4} \left(\frac{k_{wall}}{D_{eq}}\right),\ Re = \frac{\rho V D_{eq}}{\mu},\ D_{eq} = \frac{4(W.t_{plate})}{2(w+t_{plate})} \sim 2t_{plate} \quad (79)$$

where w is the plate width, δ_{plate} is the plate thickness and t_{plate} is the plate spacing. The velocity of each stream is V (m/s) and Re is the stream flow Reynolds number. The previous equation is valid for water in the following ranges: $Re > 400$, $1.5 < Pr < 5.0$ [227].

The second law exergetic efficiency for a MED-MVC system is the ratio of the exergy employed to change the salinity of the products (the minimum work of separation) to the total exergy consumed [228] and is calculated by:

$$\eta_{II} = 1 - \frac{\dot{E}_{D,total}}{\dot{E}_{in,total}} = \frac{\dot{W}_{min}}{\dot{E}_{in,total}} \quad (80)$$

where, $\dot{E}_{in,total}$ is the sum of the exergies at the various inlet fluid streams in addition to the exergies supplied to the compressor and pumps. $\dot{E}_{D,total}$ is the exergy consumption and can be expressed as

the sum of the subsystem exergy destructions. $\dot{W}_{min}$ is the minimum work input for the salt separation for a certain amount of seawater feed from a state of 25°C, 1 atm and a salinity of 36 ppt to fresh water with zero salinity, while rejecting the saline water at the same temperature and pressure. For a steady flow adiabatic process this work is equal to the difference between the stream exergies at the outlets and inlet [78].

$$\dot{W}_{min} = \dot{E}_{o,b} + \dot{E}_{o,d} - \dot{E}_{sw} \quad (81)$$

where, $\dot{E}_{o,b}$ and $\dot{E}_{o,d}$ represent the exergy of the outlet brine and distillate, respectively, while $\dot{E}_{sw}$ represents the exergy of the inlet feed water stream.

8.4.2. Simple cost model

The production cost is divided into direct/indirect costs and annual operating cost. The direct capital costs (DCCs) represent the costs that are directly associated with the desalination plant construction and the process components purchase [93]. Table 32 presents the equations used to estimate the price of the MED-MVC system components. The other direct costs (land, well construction, auxiliary equipment and building construction) are estimated to be ~80K $ following the approach given in [95] for a fixed production capacity (1500 m^3/day). The total DCC is equal to the summation of the purchased equipment for the MED-MVC system in Table 32 plus the other remaining costs. Also, the indirect capital cost IDCC (freight, insurance, construction overhead, owner's costs and contingency costs) is expressed as a percentage of the total direct capital cost and is estimated by IDCC = 0.15*DCC [95].

Table 32 Purchased cost equations for MED-MVC system components.

Component	Purchase cost (Z_k) ($)	Comments	Ref.
Preheater (heat exchanger)	$\mathbf{Z_{preheater} = 1000(12.82 + A_{Hex}^{0.8})}$	S for shell side and t for tube side, dp (kPa), A (m^2), U $(kW/m^2.k)$	[74]
MED effect (evaporator)	$\mathbf{Z_{effect} = 250.26 \times UA_{evaporator} dp_t^{-0.01} dp_s^{-0.1}}$		[94]
Water pump	$\mathbf{Z_{pump} = 13.92 \times \dot{m}_{water}^{0.55} \Delta P^{0.55} \left(\frac{\eta_p}{1-\eta_p}\right)^{1.05}}$	$\eta_p = 0.9$, ΔP (kPa)	
Compressor (MVC)	$\mathbf{Z_{MVC} = 794.68 \times \dot{W}_{compressor} + 66.11}$	$\dot{W}_{compressor}$ (Watt)	[95]
Other direct costs	$\mathbf{Z_{rest} = 21635.4 \times D^{0.1773}}$	D (m^3/day)	

The operating costs include all expenses afforded after plant commissioning and during real operation and are classified as variable and fixed costs. The variable operating costs are those related to the price of electrical power, heat source, chemicals for pre/post-treatments and other requirements that depend on the plant production capacity and standards. The fixed operating costs are used for the plant operation and are related to the plant capacity or taken as a factor of the direct capital cost (DCC). A cost index from Marshall and Swift equipment chemical engineering plant cost index (PCI) is used to accommodate the equipment price change and to fit the current time calculations (year 2018) [229]. Since the compressor cost often presents the most considerable part of the MVC direct costs, a linearly dependent compressor cost of the compressor work is assumed based on the work done by Lukic et al. [95]. Both variable and fixed operating costs are obtained based on published data from the literature [73]. Also, maintenance costs are taken as a portion of the fixed operating cost. Investment and operating costs analyses are performed for each configuration using an interest rate of 5%. The costs associated with owning and plant operation depend on the financing type, the capital requirement and the components expected life. The annualized cost method is used to estimate the annual capital cost of system components in this

study for 20 years plant lifetime and plant maintenance factor (ϕ) of 1.06. Table 33 presents the equations used to obtain the annual capital and operating costs using the amortization cost.

Table 33 Simple cost model equation for MED-MVC system.

Parameter	Equation	Comments	Ref.
Capital recovery factor, 1/y	$\boldsymbol{CRF = \frac{i.(1+i)^{nt}}{(1+i)^{nt}-1}}$	i is the interest rate 5%, nt (20 year)	[73]
Annual fixed costs, \$/y	$\boldsymbol{AFC = (1.38 \times DCC) \times CRF}$		
Annual electric power cost, \$/y	$\boldsymbol{AEPC = C_e.SPC.D/\phi}$	Specific electricity cost $\boldsymbol{C_e = 0.08\ \frac{\$}{kWh}}$	
Annual chemical cost, \$/y	$\boldsymbol{ACC = SCC\ .D/\phi}$	Specific chemical cost $\boldsymbol{SCC = 0.025\ \frac{\$}{m^3}}$	
Annual labor cost, \$/y	$\boldsymbol{ALC = SLC\ .D/\phi}$	Specific labor cost $\boldsymbol{SLC = 0.1\ \frac{\$}{m^3}}$	
Operating and maintenance annual costs, \$	$\boldsymbol{OMC = 0.02 \times CRF \times DCC}$		
Total annual cost, \$/y	$\boldsymbol{TAC = AFC + AEPC + ACC + ALC + OMC}$		
Total water price \$/m^3	$\boldsymbol{TWP_{simple} = \frac{TAC.\phi}{D}}$	D ($\frac{m^3}{year}$)	

8.4.3. Exergy-economic model

Levelized annual cost values for all components are used in the evaluation and cost optimization. The hourly capital investment (CI) cost for each component based on the actual annual number of operating hours (N) is calculated as:

$$\dot{Z}^{CI}_{component}(\$/h) = \frac{Z_{component}.CRF.\phi}{N} \quad (82)$$

The exergo-economic analysis is used to estimate the cost rate of the product streams of the system. The cost balance expresses the variable $\dot{C}$ that denotes a cost rate associated with an exergy stream: stream of matter, power, or heat transfer. According to the conservative nature of costs [97], the

cost rate associated with the system product $\dot{C}_P \left(\frac{\$}{h}\right)$ is equal to the total rate of expenditure used to generate this product in a component, namely the fuel cost resulting from the cost associated with the exergy flows $\dot{C}_F \left(\frac{\$}{h}\right)$ and the cost rates of the capital investment (CI) and operating and maintenance (OM):

$$\dot{C}_P = \sum \dot{C}_F + \dot{Z}_k^{CI} + \dot{Z}_k^{O\&M} \tag{83}$$

The above cost balance equation is applied to the MED-MVC system components to obtain the product stream cost. Typically, the number of unknown cost parameters is higher than the number of cost balance equations for the component, so additional auxiliary thermodynamic equations are used to accommodate this difference. Usually, the auxiliary equations represent the equality of the average cost of the inlet and exit for the same stream, and they are formulated based on different principles (exergy extraction, multiple outputs, and external assessment) [98]. To include the labor and chemical cost (non-exergy related costs) in the exergo-economic analysis, inlet feed stream to the feed pump was considered as $\dot{C}_o(\$/h) = (SLC + SCC)(\$/m^3) \times D(m^3/h)$. The total water price ($\mathrm{TWP}_{exerg-economic}$) $(\$/m^3)$ from the exergo-economic analysis is calculated by dividing the cost rates of all the outlet streams (distillate and brine) $(\$/h)$ from the MED-MVC unit by the total production rate of the plant (m^3/h).

8.4.4. Dynamic model

Following the steady-state solution, a generic dynamic model for a four-effect MED with an MVC unit and two preheaters is developed. Each evaporator effect consists of three lumps: vapor, brine, and tube lump. It is assumed that the accumulation of mass and energy in the evaporator tubes is negligible compared to the accumulation of mass and energy in the brine pool inside an effect

[189]. The dynamic model equations of the i^{th} evaporator effect combined lumps mass, energy and salt balances are given by equations (15), (16) and (17), respectively [90]. Each effect is assumed to have a cross-sectional area $A_{ce,i}$ and a total height H_E. The brine pool height $L_{b,i}$ and vapor height $H_E - L_{b,i}$ are shown in Figure 55 for the i[th] effect. The brine pool to pool flow between effects is represented by $m_{b,i} = C_{b,i}\sqrt{\Delta P_{b,i}}$ where $\Delta P_{b,i} = P_{i-1} - P_i + \rho_b g\left(L_{b,i-1} - L_{b,i}\right)$ and the vapor flow from one effect to the next is calculated from $m_{v,i} = C_{vi}\sqrt{\Delta P_{vi}}$ and $\Delta P_{vi} = P_{i-1} - P_i$.

$$C_{11}\frac{dL_{b,i}}{dt} + C_{12}\frac{dT_{v,i}}{dt} + C_{13}\frac{\partial X_{b,i}}{\partial t} = C_{14} \quad (84)$$

$$C_{21}\frac{dL_{b,i}}{dt} + C_{22}\frac{dT_{v,i}}{dt} + C_{23}\frac{\partial X_{b,i}}{\partial t} = C_{24} \quad (85)$$

$$C_{31}\frac{dL_{b,i}}{dt} + C_{32}\frac{dT_{v,i}}{dt} + C_{33}\frac{\partial X_{b,i}}{\partial t} = C_{34} \quad (86)$$

where the coefficients ($C_{11}, \ldots \ldots C_{34}$) are shown in Table 34.

Table 34 Rate coefficients of the i[th] effect dynamic equations for a MED-MVC system.

C_{11}	C_{12}	C_{13}	C_{14}
$A_{ce,i}(\rho_{b,i} - \rho_{v,i})$	$\left[A_{ce,i}L_{b,i}\frac{d\rho_{b,i}}{dT_{b,i}}\left(1+\frac{\partial BPE}{\partial T_{v,i}}\right) + (H_E - L_{b,i})A_{ce,i}\frac{d\rho_{v,i}}{dT_{v,i}}\right]$	$\left[A_{ce,i}L_{b,i}\left\{\frac{d\rho_{b,i}}{dT_{b,i}}\frac{\partial BPE}{\partial X_{b,i}} + \frac{d\rho_{b,i}}{dX}\right\}\right]$	$m_{f,i} + m_{b,i-1} - m_{b,i} - m_{v,i}$
C_{21}	C_{22}	C_{23}	C_{24}
$A_{ce,i}(\rho_{b,i}h_{b,i} - \rho_{v,i}h_{vi})$	$\left[A_{ce,i}L_{b,i}\left\{\rho_{b,i}\frac{dh_{b,i}}{dT_{b,i}} + h_{b,i}\frac{d\rho_{b,i}}{dT_{b,i}}\right\}\left(1+\frac{\partial BPE}{\partial T_{v,i}}\right) + (H_E - L_{b,i})A_{ce,i}\left\{\rho_{v,i}\frac{dh_{v,i}}{dT_{v,i}} + h_{v,i}\frac{d\rho_{v,i}}{dT_{v,i}}\right\}\right]$	$\left[A_{ce,i}L_{b,i}h_{b,i}\left(\frac{d\rho_{b,i}}{dT_{b,i}}\frac{\partial BPE}{\partial X_{b,i}} + \frac{d\rho_{b,i}}{dX}\right) + A_{ce,i}L_{b,i}\rho_{b,i}\frac{dh_{b,i}}{dT_{b,i}}\frac{\partial BPE}{\partial X_{b,i}}\right]$	$m_{f,i}h_{f,i} + m_{b,i-1}h_{b,i-1} - m_{b,i}h_{b,i} + Q_{s,1}$
C_{31}	C_{32}	C_{33}	C_{34}
$A_{ce,i}\rho_{b,i}X_{b,i}$	$\left[A_{ce,i}L_{b,i}X_{b,i}\frac{d\rho_{b,i}}{dT_{b,i}}\left(1+\frac{\partial BPE}{\partial T_{v,i}}\right)\right]$	$\left[A_{ce,i}L_{b,i}\left\{X_{b,i}\frac{d\rho_{b,i}}{dT_{b,i}}\frac{\partial BPE}{\partial X_{b,i}} + \rho_{b,i} + X_{b,i}\frac{d\rho_{b,i}}{dX}\right\}\right]$	$m_{f,i}X_{f,i} + m_{b,i-1}X_{b,i-1} - m_{b,i}X_{b,i}$

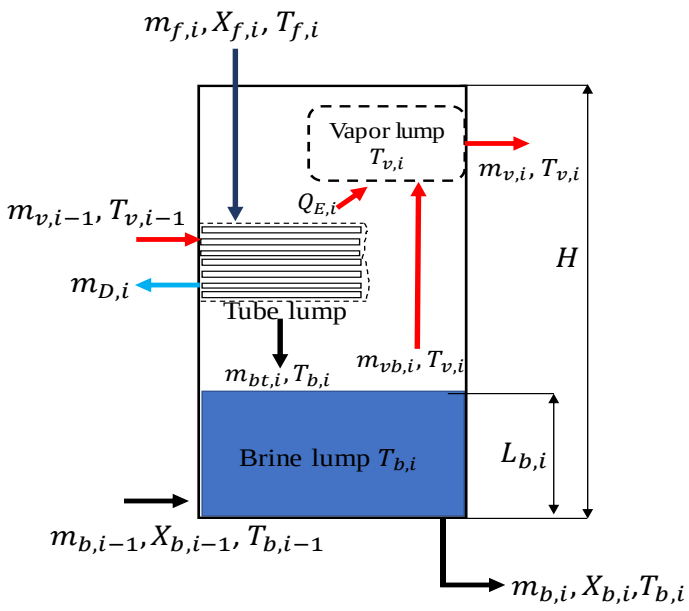

Figure 55 Schematic diagram of the three lumps for the i[th] effect.

The detailed transient characteristics of heat exchangers (HExs) described by partial differential equations are complicated and are not suitable for practical use [230]. Therefore, a lumped model is used to estimate the preheaters outlet temperature variation with time. Both preheaters are considered as counter-flow plate heat exchangers as shown in Figure 56. The cold stream of seawater feed is heated by circulating the hot fluid (brine and distillate) through the other side of the plate wall. The last effect brine temperature and distillate mixing temperature represent the hot fluid stream temperatures in the brine and distillate preheaters, respectively. The following assumptions are made in developing the mathematical model for both preheaters [230] where spatial temperature distributions are not considered:

i) Heat losses to the environment are negligible

ii) The heat capacity of fluids is significantly higher than that of the metallic walls.

iii) Mass accumulation inside the pre-heaters is not considered.

Based on the assumptions above, the energy balance equations for the preheaters are presented as:

Brine preheater

$$\frac{\boldsymbol{dT_{F,b}}}{\boldsymbol{dt}} = 2\frac{U_b A_{b,HEx} LMTD_{b,HEx} - \dot{m}_{F,b}\left[T_{F,b}c_{P[T_{F,b},X_f]} - T_{sw}c_{P[T_{sw},X_f]}\right]}{\rho_{[T_{m,F},X_f]}c_{P[T_{m,F},X_f]}\forall_{HEx,channels}} \quad (87)$$

$$\frac{\boldsymbol{dT_{o,b}}}{\boldsymbol{dt}} = 2\frac{\dot{m}_B\left[T_{b,n}c_{P[T_{b,n},X_b]} - T_{o,b}c_{P[T_{o,b},X_b]}\right] - U_b A_{b,HEx} LMTD_{b,HEx}}{\rho_{[T_{m,b},X_b]}c_{P[T_{m,b},X_b]}\forall_{HEx,channels}} \quad (88)$$

Distillate preheater

$$\frac{\boldsymbol{dT_{F,d}}}{\boldsymbol{dt}} = 2\frac{U_d A_{d,HEx} LMTD_{d,HEx} - \dot{m}_{F,d}\left[T_{F,d}c_{P[T_{F,d},X_f]} - T_{sw}c_{P[T_{sw},X_f]}\right]}{\rho_{[T_{m,F},X_f]}c_{P[T_{m,F},X_f]}\forall_{HEx,channels}} \quad (89)$$

$$\frac{\boldsymbol{dT_{o,d}}}{\boldsymbol{dt}} = 2\frac{\dot{m}_D\left[T_{hin,d}c_{P[T_{hind,d}]} - T_{o,d}c_{P[T_{o,b}]}\right] - U_d A_{d,HEx} LMTD_{d,HEx}}{\rho_{[T_{m,d}]}c_{P[T_{m,d}]}\forall_{HEx,channels}} \quad (90)$$

where $\dot{m}$ represents flow rate of the streams of cold and hot fluids (kg/s), c_p is the streams heat capacities (kJ/kg.K), ρ is fluid density (kg/m^3), U is the total heat transfer coefficient (in kW/m^2.K), A is the heat transfer area (m^2) for both preheaters, $\forall$ is the effective volume (m^3) of the preheaters channels, and $LMTD$ is the logarithmic mean temperature difference in the brine and distillate preheaters.

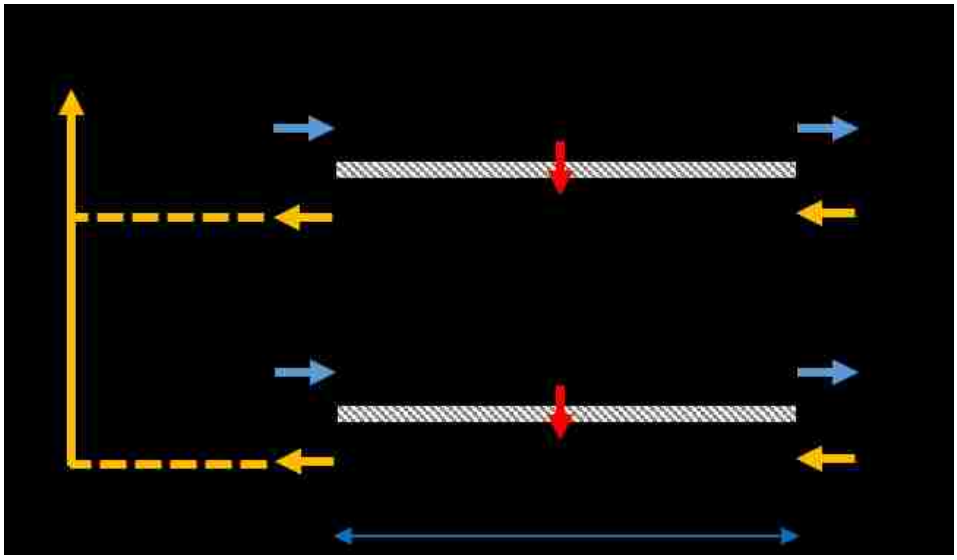

Figure 56 Control volume for preheaters of (a) distillate and (b) brine.

The MVC unit is considered to be in a quasi-steady-state condition since the mechanical vapor compressor has a rapid dynamic response compared to the other heat transfer components. The compressor efficiency η_c is determined by comparing the steady-state isentropic and actual compressor work and is used as an input to the dynamic model. Both the isentropic work and the compressor isentropic efficiency are used to obtain the instantaneous compression ratio of the MVC unit. From the compression ratio, the inlet steam temperature can be determined. The main differences and commonalities between the present dynamic model for the MED-MVC and the dynamic model for the MED-TVC described in [90] are: (i) the core of the MED which is the evaporator unit is treated the same way using the lumped model developed in [90]; (ii) there is no dynamic model for the condenser unit needed in the MED-MVC, a compressor model is included instead; (iii) two preheater units are dynamically simulated in the MED-MVC; (iv) The MED-TVC system operates on thermal energy from an external source such as a steam power plant or boiler, while the MED-MVC system uses a compressor unit to recycle the vapor from the last effect to the first effect.

As shown in Figure 57, the steady-state solution procedure for MED-MVC system starts by assuming the brine temperature in all effects and the energy supplied to the first effect. Then, the steady-state conservation equations in Table 31 are solved to obtain the feed and brine flow rates as well as the vapor generated in each effect. The mass flow rate imbalance between the vapor produced in the last effect and the required steam for the first effect is minimized iteratively by modifying the term E_{SH}. This calculation continues until a specified error criterion is achieved (ε=10^{-4}). This value for error criterion is determined to be small enough so that the solution obtained is independent of it. The mixing temperature of the distillate is used to calculate the actual

feed temperature by solving the equations of the brine and distillate feed preheaters. The entire calculations are repeated until the specified feed temperature is reached. From the steady-state solution, parameters such as the vapor and brine temperature, the vapor and brine flow rate and salinity at each effect are used as initial input for the dynamic model calculations. A FORTRAN code is developed to solve both the steady-state and dynamic models. The system of ordinary differential equations is solved by using the fourth-order Runge-Kutta method. By solving Eqs. (84)-(90), the vapor temperature, brine level, effect salinity, preheaters outlet temperatures and supplied feed temperature are obtained at each time step. The brine and vapor flow rates between effects are adjusted based on the vapor pressure calculated in the effects. In the dynamic model, the compressor work and seawater temperature can be disturbed with different intensities from the steady-state condition for a pre-specified duration. Indicator parameters such as the effect temperature, brine level and vapor flow across effects are calculated with time. The performance indicator parameters such as PR and SPC are obtained as well.

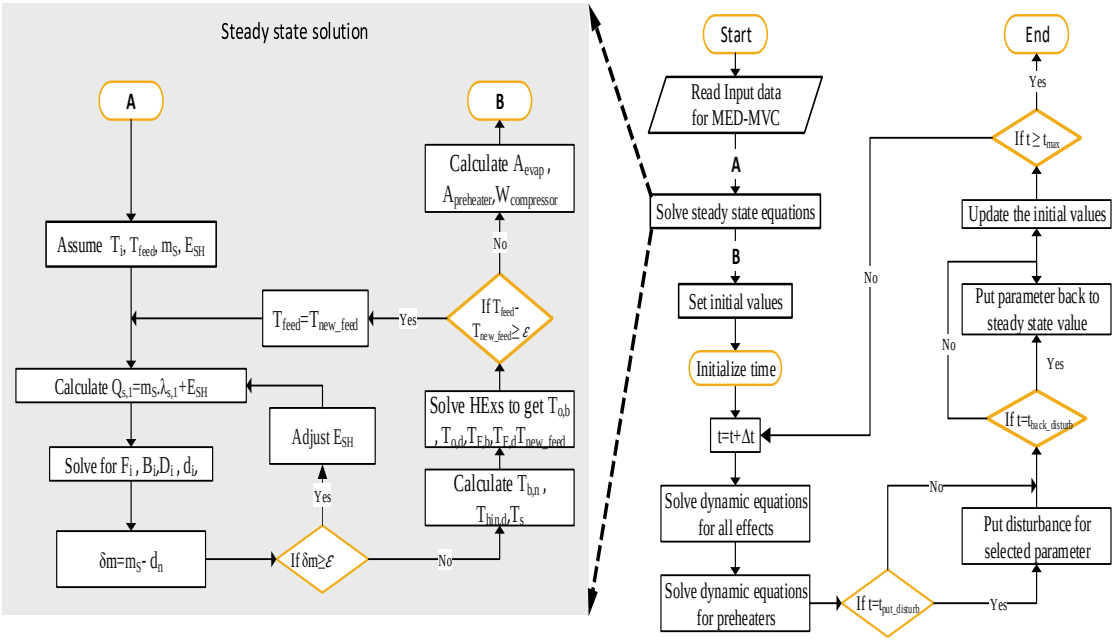

Figure 57 Procedures of the MED-MVC steady-state and dynamic models solution method.

Results and discussion

8.5.1. Steady-state operation and exergo-economic analysis

The focus of this study is to present a generic steady-state and dynamic model which can be easily modified to describe any number of effects for MED-MVC systems and two independent preheaters for the inlet seawater. The steady-state model is validated using the actual operational parameters of MED-MVC plant located in Flamanville, France [113], which operates with four effects in s parallel/cross feed configuration integrated with a MVC unit. Table 35 shows the currently steady-state model resulting values for the process variables which show excellent agreement compared with the data reported in [113]. Exergy analysis overcomes the shortcomings of energy analysis by identifying the causes, locations and actual magnitudes of waste due to thermodynamic inefficiencies [78]. The minimum work of separation $\dot{W}_{min}$ for the separation of 39.44 kg/s of seawater into 17.6 kg/s of fresh water and 21.84 kg/s of brine with a salinity of 65 ppt at the same temperature and pressure can be determined independently by using the relation developed by Cerci [153]. For a recovery ratio of ~40%, the relation gives 28.16 kW, which is sufficiently close to the result obtained from equation (81).

There are two causes of exergy destruction in the MED systems. The first is due to the heat transfer across the temperature difference between hot and cold streams in each evaporator effect and the preheaters. Also, exergy destructions in the pump and compressor are due to irreversibilities in the pump and compression processes. The exergy destruction (kW) for the main components of MED-MVC are presented in Figure 58. A significant source of exergy destruction occurs in MVC unit (39%) and evaporators (52.6%). This can be attributed to the thermodynamic inefficiency of the MVC unit and the heat transfer in the effects that are associated with phase change processes. The high exergy destructions in the evaporators indicate that the evaporation process itself is highly

inefficient. Therefore, modifications and improvements to the process must be considered. This can be reduced by increasing the number of effects, though the number is limited by the operating compression ratio of MVC units currently available. Also, the economic consideration due to increasing the heat transfer surface needed to achieve evaporation and condensation processes should be accounted. Other components such as brine and distillate feed heaters introduce exergy destructions that nearly equal to 7.0%. Moreover, Figure 58 indicates that the highest exergetic efficiencies belong to pumps. It should be noted that the exergetic efficiency of the MED-MVC plant is quite low (2.82%), which reveals its high irreversibilities that is close to the values presented in the reported literature [38, 154].

Table 35 Operational steady-state conditions for MED-MVC system.

Configuration	Model	Flamanville [113]	% error
Inlet seawater temperature, °C	25		--
Feed content in, g/kg	36		--
Brine content out, g/kg	65		--
Steam temperature T_s, °C	62.5		--
last effect brine temperature T_n, °C	50.3		--
Pressure ratio	1.85	1.86	0.5
Distillate production (D), m^3/h	64.0	62.5	2.4
Feed flow (F), m^3/h	141.45	140	1
Brine flow (B), m^3/h	78.34	77.5	1
Feed temperature T_f, °C	48.03	49	1.9
Compressor actual work ($\dot{W}_{comp}$), kW	690	650	6.1
Performance ratio PR	3.44	--	--

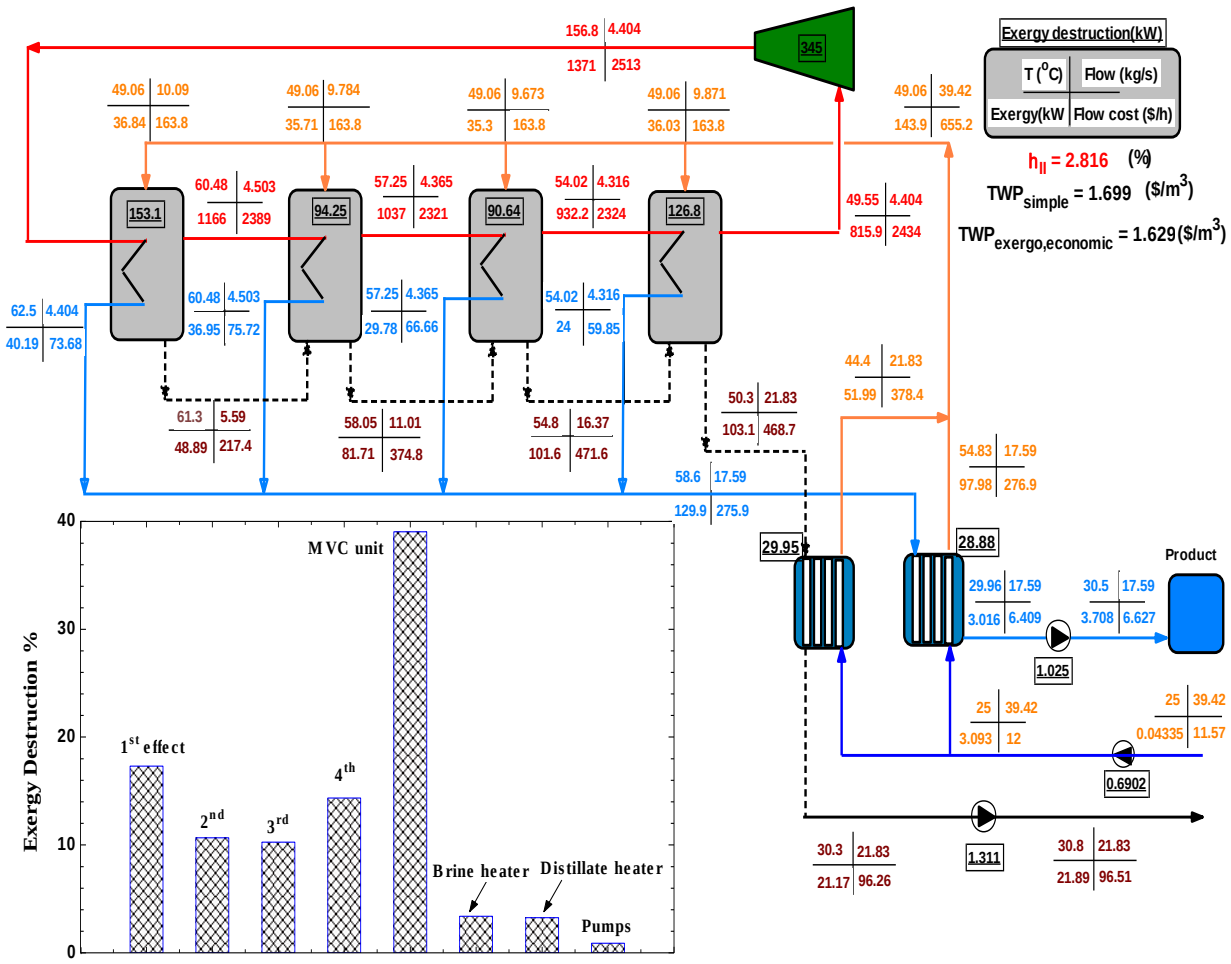

Figure 58 Cost flow diagram with exergy destruction for main component of MED-MVC systems.

A simple conventional economic model treating the MED-MVC plant as a whole unit is used to calculate the annualized cost of the plant and to estimate the total water price for a MED-MVC system. The total levelized fixed cost associated with CI&IM of the components per hour basis is 19.98 $/h. The most expensive components are the evaporators (~10.13 $/h) while the cheapest are the pumps (~0.3 $/h). The costs for the MVC unit and the preheaters are 7.3 and 1.3 $/h, respectively. However, to indicate the contribution of each flow stream and each component in the final product cost, an exergo-economic analysis is applied to all MED-MVC components and flow streams. When conducting a thermoeconomic analysis for the current MED-MVC system, a cost

balance equation is used to correlate the exergy instead of the energy of the flow stream with the pricing value of the component. The exergy-cost unit analysis is more reasonably distributed and is meaningful than the energy-based ones. The non-exergy related costs represented by chemical cost and labor cost are added to the exergo-economic model as input stream in the feed seawater. Further, it should be mentioned that there is no additional information to appropriately apportion the value of other cost and indirect cost between the product streams (distillate and brine) in the cost exergy equations. The other costs (80K $) and indirect capital costs (0.15 DCC) are calculated on a per hour basis, and a value of 3.65 $/h is obtained. For simplicity, these costs are divided equally between distillate and brine streams. Solving the exergy-cost balance equations, the cost rates for various streams at different locations in the MED-MVC plant are obtained. The cost rate pricing for all flow streams through the MED-MVC system of 1500 m^3/day production capacity is shown as a diagram in Figure 58 with the estimated production cost of 1.70 and 1.63 $/$m^3$ using simple conventional economic model and exergy-based cost model, respectively. Both methods results are consistent with the results for MED-MVC desalination system and similar systems found in the literature [38, 95, 157, 231]. Besides showing the cost flow rate at each stream point, the figure shows flow exergy, temperature and stream flow rate as well. To some extent, both methods (simple economical method and the exergo-economic method) have a similar estimation for the final product price (freshwater). However, the exergo-economic method slightly underestimates the water price, and this is directly attributed to the assumptions used in the auxiliary equations and the uncertainty associated with the cost due to round-off [98].

The primary contributor to the SPC in a MED-MVC system is the power required for the MVC unit which depends on the compressor efficiency, compression ratio and inlet vapor specific volume. The operation cost can be reduced by increasing the performance ratio (PR) or decreasing

the SPC. Therefore, efforts are made to reduce the cost associated with the MVC. This can be done by reducing the vapor flow rate through the MVC unit by installing more effects N while keeping the same overall temperature difference. On the other hand, capital cost can be reduced by reducing the required specific heat transfer area (S_A) for the evaporators and pre-heaters units. For the MED-MVC, to decrease the S_A, the TBT must be increased. The increase in TBT may require specific chemical pre-treatments and add cost for better tube material and higher maintenance. Increasing N has its limits as this increases the required S_A for evaporation due to the decrease in the temperature difference between the effects. Consequently, capital cost savings should be considered along with the increase in operating cost. It is essential to determine the optimal balance between the design parameters of N and TBT that achieves the best economic operation. The decrease in the SPC with increasing the number of effects N has its limit as shown in Figure 59. A single-effect MVC has the highest SPC due to the amount of vapor flow (displacement volume) through the MVC unit, leading to the highest TWP. Adding a second effect increases the η_{II} and reduces the SPC as shown in Figure 59. Although this increases the S_A, the TWP reduces to ~ 1.6 \$/m^3 due to a reduction in the operating cost of the MVC unit. Further increase in the number of effects from 2 to 6 brings little increase in the η_{II} and little change in the SPC. On the other hand, the TWP keeps increasing with the increase in N which is due to the continuous increase in S_A (capital cost). Increasing N beyond 6 leads to an increase in the SPC and a decrease in η_{II} for a fixed production capacity. This is attributed to the large decrease in the volumetric vapor flow rate through the MVC unit which may not be sufficient to generate the required amount of vapor in the first effect. Increasing the number of effects from 2 to 10 causes an increase in the TWP by 16% approximately. The main reason for not using multiple effects beyond 6 in MVC systems is the practical limitation of the displacement volume of the commercially available compressors [159].

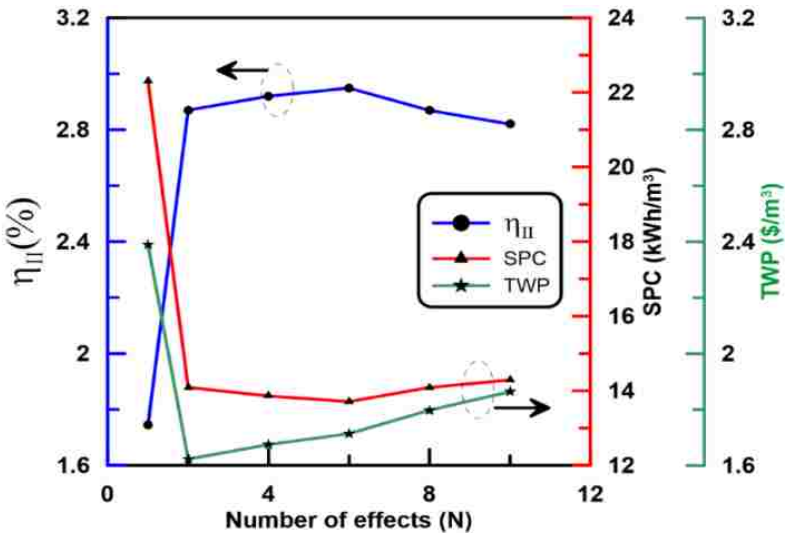

Figure 59 Effect of the number of effects on SPC, η_{II} and TWP.

8.5.2. Dynamic analysis

First, the dynamic model results are justified with a three-effects lab-scale MED plant with a total production capacity of 3 m^3/day. The detailed description of the steady-state operating conditions of the 3-effect plant and the results of the dynamic model validation are presented in [90]. In a real application, the operational conditions may not be kept constant due to the changes in climate conditions and the rate of the designed heat source flow rate or electrical power to the plant. These fluctuations from the design steady-state values may i) cause the plant to approach a new steady-state condition; ii) agitate the plant performance thus causing production capacity changes; or iii) in some occasions, lead the plant to reach dry out or flooding. Thus, the model describes the relationships between the disturbance input parameters (compressor work and inlet seawater temperature) and the output process variables (effects temperature, brine level, brine flowrate and vapor flow rate). A linear change in the main input parameters is considered that form a ramped type disturbance with the pre-specified magnitude of change and applied duration. Based on the actual evaporator configuration dimensions, the initialized brine level was chosen as 0.25 m [232].

Two limitations are assigned on the brine level, $L_b < 1.0$ m and $L_b > 0.1$ m to avoid flooding or dry out conditions, respectively.

In some situations, a disturbance (or fluctuation) is applied to the work supplied to the MVC unit to change total plant output. If intentional, this change is called “turndown“ and is carried out to address the power demand swings [168]. This turndown ratio may reach 50%, meaning the minimum flow is half of the maximum design flow. The system variables namely: brine level, vapor temperature, supplied steam temperature, brine flow rate and vapor flow rate are calculated to assess the impact of a 10% ramp reduction in the supplied compressor work on the system variables as shown in Figure 60. The applied ramp reduction starts at the time of 5,000 s with a ramp time of 1,000 s. The system is allowed to run with this reduced compressor work until it reaches another steady-state condition. The reduction in the supplied energy to the MVC unit causes a decrease in the compression ratio and the temperature of the supplied steam to the first effect. The response of the vapor lump in each effect is much faster than the response of the liquid lump (brine level) due to the higher thermal capacity of the liquid compared to that of the vapor. Consequently, a reduction in the vapor temperature and pressure in all effects is experienced at the beginning of the disturbance. This leads to a gradual decrease in the brine and condensed vapor flow rates in the preheaters, which in turn decreases the feed temperature to the effects. Furthermore, the steam temperature decreases due to the reduction in the vapor temperature in the last effect. The reduction in both vapor and feed temperatures eventually results in more accumulation of the brine in the effects and increases the brine level as shown in Figure 60. The build-up in the brine level causes the hydrostatic pressure for the brine lump to increase, pushing the hot brine to flow from one effect to the next and to cause the feed temperature to rise. This

increase in the feed temperature enhances the vapor temperature and slightly reduces the brine level to attain a new steady-state operating condition.

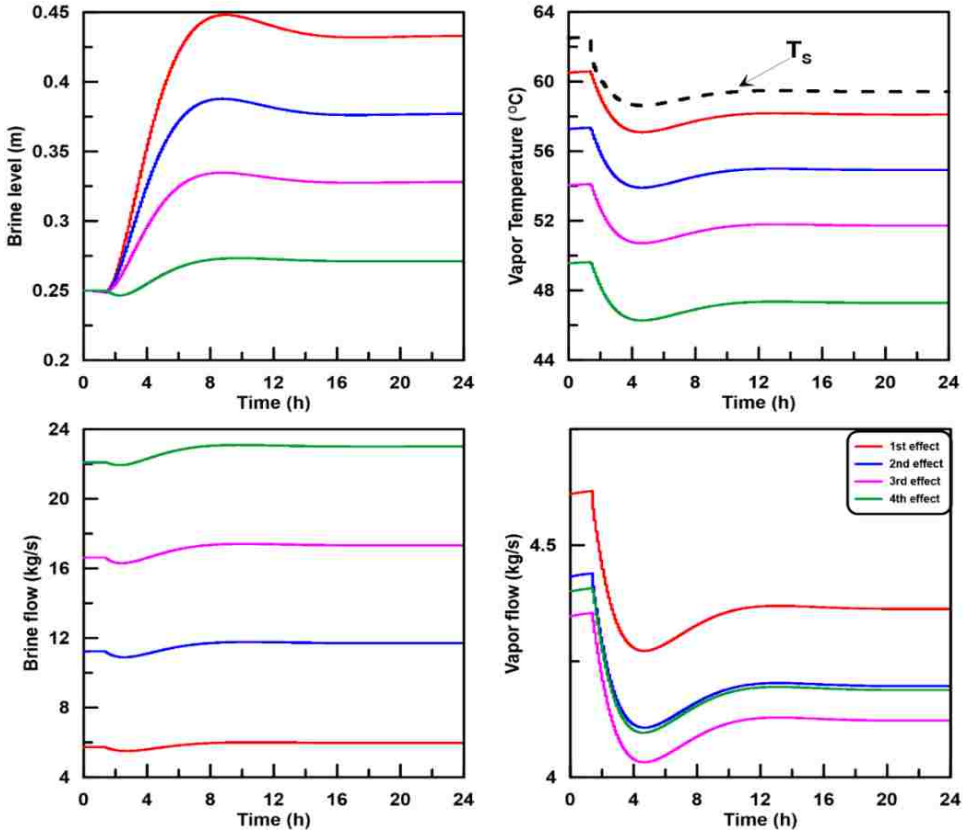

Figure 60 Brine level, vapor temperature, brine and vapor flow for a 10% reduction in compressor work.

Figure 61 shows the effect of the application of a 10% increase in the inlet seawater temperature (2.5°C) on the plant process variables. At the beginning of the disturbance, the feed temperature to all effects increases at the same time. This improves the evaporation rate and increases the vapor temperature in all the effects and the increase in vapor pressure inside the effects increases the brine flow rate. However, the reduction in the brine level causes a gradual decrease in the brine flow rate as shown in Figure 61. The dynamic response of the feed preheaters to the variations in brine and distillate flow rates causes the vapor temperature and vapor flow rate to go up before they reach their steady-state values as shown in Figure 61.

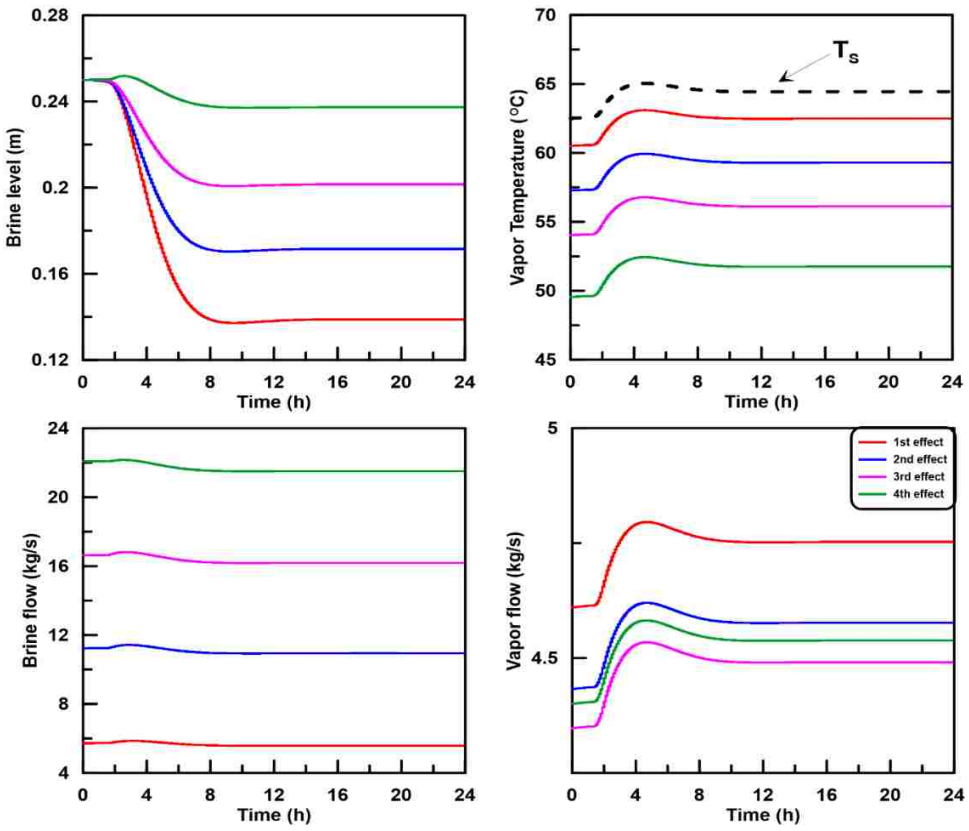

Figure 61 Brine level, vapor temperature, brine and vapor flow for a 10% increase in inlet seawater temperature.

The economics, steady-state performance and transient behavior of a MED–MVC system are compared to those of a MED-TVC system with a similar production capacity. The MED-TVC system, operating with four effects and a bottom condenser, is investigated using the model developed by Elsayed et al. [90] under the same constraints for the freshwater production rate (17.6 kg/s) and rejected brine salinity (65 ppt). The calculated values of the GOR and TWP for a fresh water production rate of 1500 m^3/d are 3.99 and 1.6 \$/m^3, respectively for the MED–MVC, and 6.4 and 2.6 \$/m^3, respectively for the MED-TVC. Dynamic simulations for both systems under a 15% reduction in the inlet seawater temperature (3.75°C) are performed. As shown in Figure 62, the MED-TVC is rather sensitive to the decrease in seawater temperature which affects the condenser unit as mentioned in Elsayed et al. [90]. This sensitivity causes a significant increase

and decrease in the brine level and production capacity, respectively in the MED-TVC system compared to the MED-MVC system. The MED-MVC system has a slower response due to the high thermal capacity of the brine/distillate feed preheaters compared to the low thermal capacity of the condenser's vapor lump in the MED-TVC system.

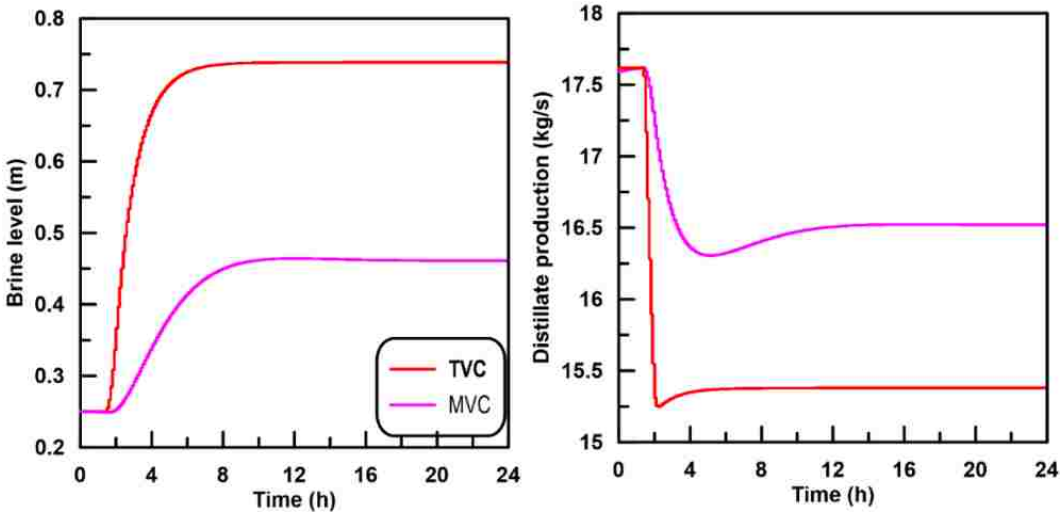

Figure 62 First effect brine level and plant total distillate production with a 15% decrease in the inlet seawater temperature for MED-TVC and MED-MVC systems.

Next, the effect of the intensity of the applied disturbances on the vapor temperature and brine level of the first effect is shown in Figure 63. The compressor work and seawater temperature have been reduced by up to 30% and 25% of the steady-state values, respectively. For the current MED-MVC configuration and dimensions, it is noted that a significant reduction in compressor work could lead to a substantial decrease in the temperature difference between the first effect brine and the steam at compressor exit. For instance, the steam temperature supplied by the MVC unit approaches the brine pool temperature for a 30% reduction in the compressor work. In this case, although the evaporation can still occur between the sprayed feed and the steam temperature inside the tubes, the hot brine pool temperature will drop with time, and the brine level in the 1st effect will reach the flooding condition. In addition to approaching the flooding condition, operating the

MED-MVC evaporator unit at higher brine levels than designed may lead to salt deposition and light scaling at the bottom of the tubes [233]. The reduction in the inlet seawater temperature reduces the feed temperature causing the brine level to increase, but it does not affect the temperature difference between the steam supplied and the first effect temperature brine. However, as shown in Figure 61, increasing the seawater temperature above 10% of the steady-state condition would lead to dry out in the first effect evaporator. A dry out condition means the vapor generated in the 1st effect may storm through the 2nd effect. This blowout of the vapor through the brine pipes will perturb the brine flashing and feed evaporation processes where the plant may be exposed to operational failure.

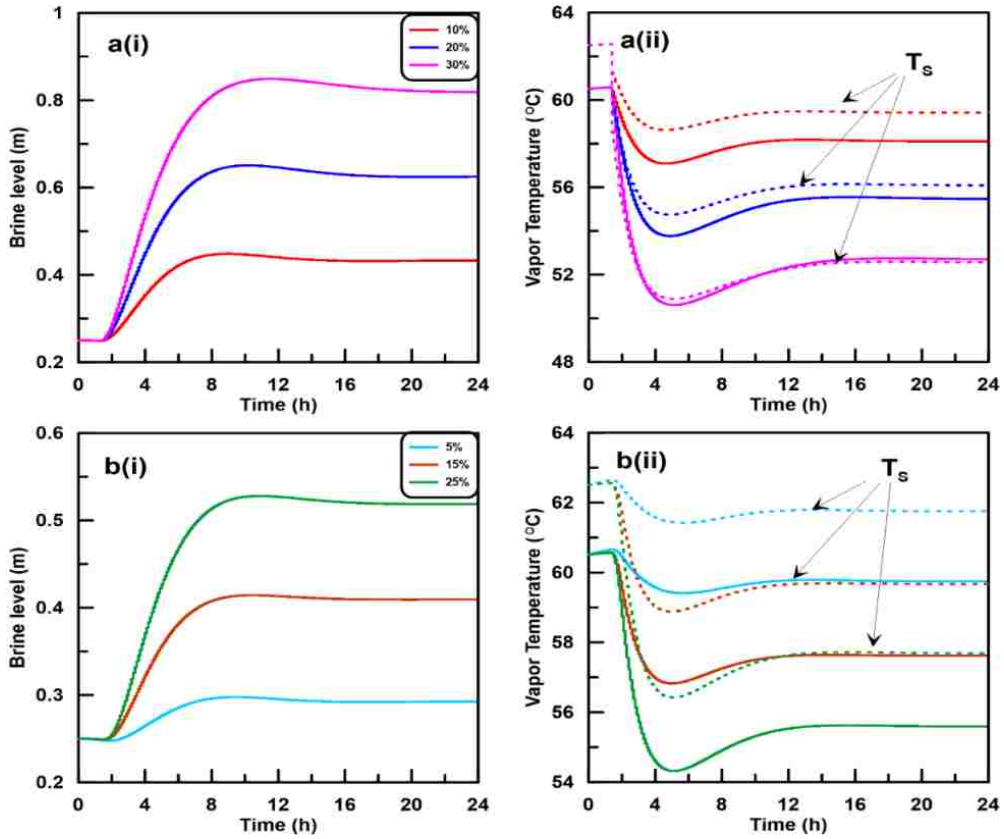

Figure 63 First effect brine level, and vapor temperature with intensity of reduction in: (a) compressor work, (b) inlet seawater temperature.

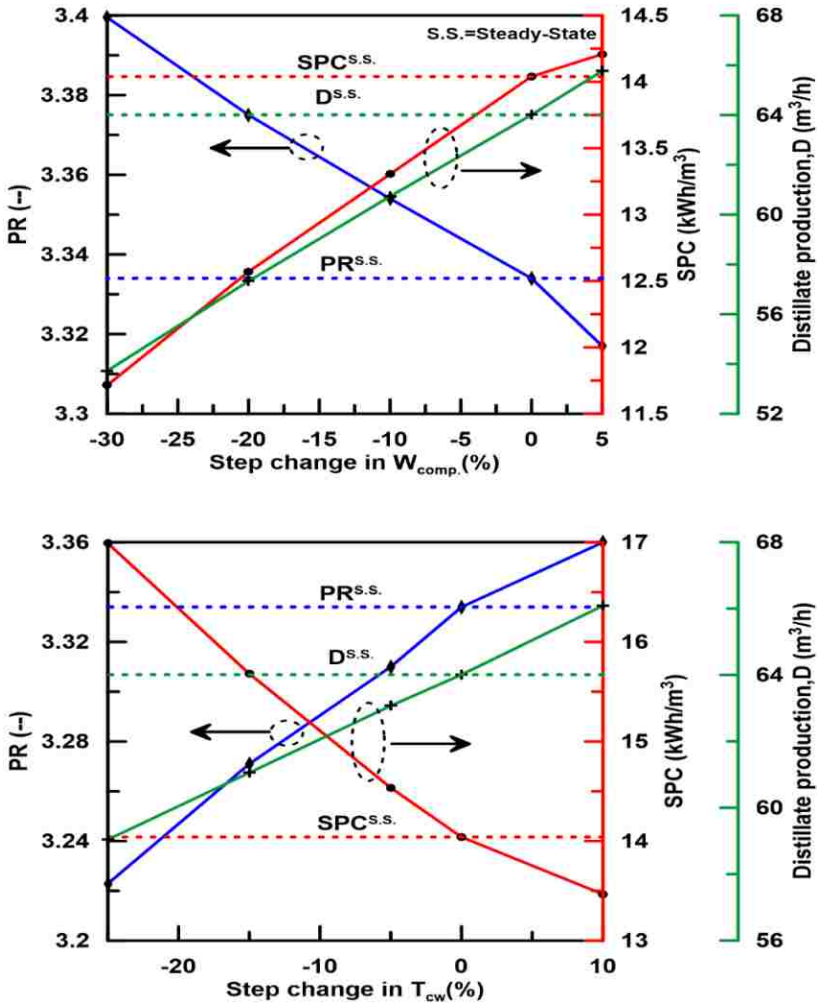

Figure 64 Effect of step changes of compressor work and seawater temperature on the MED-MVC total distillate production, PR and SPC.

A plot of the variations of the PR, SPC and total distillate production with step changes in the compressor work and inlet seawater temperature is shown in Figure 64. The dependence of PR and SPC on $\dot{W}_c$ and T_{sw} is approximately linear. As shown in Figure 64a, a decrease in the compressor work below the steady-state designed condition decreases the condensation rate (distillate) in each effect. But since the magnitude of the decrease in the total distillate production rate is less than the reduction in compressor work, PR increases and SPC decreases. A reduction in inlet seawater temperature results in a decrease in the production of fresh water, brine blowdown temperature and PR which in turn causes an increase in SPC for the same supplied compressor

work [73]. The reduction in the supplied seawater temperature decreases the TBT which leads to a decrease in the brine flashing and seawater evaporation rates in all effects as shown in Figure 64b. This results in less vapor generation and higher brine level increase in all the effects.

Conclusions

Within the current work, a new formulation for the steady-state thermodynamic model of MED-MVC desalination systems operating in parallel/cross configuration has been presented. The steady-state solution reveals that the η_{II} is 2.82%. The exergy destructions in the MVC unit and evaporators combine to approximately 90% of the total exergy destruction in the system. The most expensive components are the evaporator units with a cost of ~10.13 $/h compared to 7.3, 1.3 and 0.3 $/h for MVC unit, preheaters and pumps, respectively. The TWP for the MED-MVC with a 1500 m^3/day production capacity is 1.70 and 1.63 $/$m^3$ using a simple conventional economic model and a specific exergy cost model, respectively. Sensitivity analysis shows that a two-effect MVC system is superior to the single-effect MVC system, but the number of effects N that can be implemented is limited. Increasing N from 2 to 6 results in little change in the SPC or η_{II} . On the other hand, the value of TWP increases by approximately 16% as N increases from 2 to 10.

The dynamic model results show that the disturbances in compressor work have a significant effect on the plant transient behavior while a disturbance in the inlet seawater temperature has only a moderate impact. A reduction in compressor work leads to a reduction in the steam temperature that causes an increase in the effects brine level. For instance, the steam temperature supplied by the MVC unit approaches the brine pool temperature when a 30% reduction in the compressor work occurs. So, any further decrease in compressor work may lead to flooding in the effects and the plant may cease to operate. A decrease in the inlet seawater temperature reduces the feed

temperature causing the brine level to increase, but this does not affect the temperature difference between the steam supplied and the first effect temperature. On the other hand, increasing the seawater temperature above 10% of the steady-state condition without proper control on the plant response could lead to dry out in the effects. Thermo-economic and dynamic response comparisons between the MED-MVC and MED-TVC systems reveal that: (i) the TWP for the MED-TVC is higher than the MED-MVC; (ii) the MED-TVC is more sensitive to the reduction in the seawater temperature than the MED-MVC; (iii) the MED-MVC is slower in response compared to the MED-TVC. In term of performance, a reduction in compressor work causes a decrease in the plant total distillate production capacity, but an increase in PR and a decrease in SPC. On the other hand, a reduction in the inlet seawater temperature decreases the TBT, which causes a decrease in brine flashing and feed evaporation rates with an increase in the brine levels in the effects. This leads to a reduction in the production of fresh water, a decrease in PR and an increase in the SPC for the same supplied compressor work.

CHAPTER 9 GENERAL DISCUSSION AND CONCLUSIONS

The aim of the research reported here was to investigate the impact of operational and design parameters on the performance of multi-effect desalination (MED) by developing robust mathematical models under various conditions and validating them with available designed experimental data in the literature. The detailed objectives of this dissertation were to:

1 Develop a validated steady-state thermodynamic cycle model that allows rapid estimation of performance for MED operating with the different configuration as a function of the process heat source temperatures flow rate, feed concentration, and flow rate.
2 Develop a validated dynamic model that allows performance prediction of different types and configuration of MED as a function of process conditions, including operating times and location installation.
3 Use of the models developed above to elucidate the effect of input process parameters on the performance of MED and draw conclusions on the range of conditions where MED is likely to be economically viable.

9.1 Research findings

An extensive amount of research outcome has been accomplished since the beginning of this study. Furthermore, the objectives were achieved, and the principle findings of the research were reported through 6 papers listed in Chapters 3-8, which can be summarized as:

9.1.1. *Exergy and thermo-economic analysis for MED-TVC systems (Ch.3)*

- The 1st law analysis for MED-TVC system show that, the PCF configuration has the lowest specific heat consumption (SHC) and the lowest total power consumption (TPC) compared to the other feed configurations, but it has a high specific cooling water flow rate. On the other hand, the BF configuration has a smaller specific cooling seawater flow rate. The electric power consumption is higher for the FF configuration due to the required high pumping power. Also, the study reveals that the exergy destruction in the TVC unit and evaporator units, represent the highest share of the total exergy destruction in the system. The 2nd law efficiency is the highest for PCF, while the PF has the lowest value.
- A detailed thermo-economic analysis of the BF and PCF configurations of MED-TVC system show that the most expensive (highest investment cost) components are the evaporator units. The lower value of the exergo-economic factor (f_k) for the TVC unit shows that the cost associated with the TVC unit is dominated by the exergy destruction while the remaining part is determined by the hourly capital investment ($\dot{Z}_k$) value of the component. Reducing the exergy destruction in the TVC unit could be cost effective for the entire system even if this would increase the capital investment costs associated with this component. Part of the exergy destruction in the TVC unit can be avoided by reducing the motive steam pressure without affecting the flow rate of the motive steam. So, TVC motive steam pressure is a key design variable because it affects the exergy associated with the inlet stream as well as the performance and investment cost of the TVC unit. Changes in cost index, interest rate and electricity cost have a minimal effect on the total water price. On the other hand, changing the specific steam cost has a significant effect on the TWP, especially for the FF configuration.

9.1.2. Process performance modeling for MED-MVC systems: Exergy and thermo-economic analysis approach (Ch.4)

- A new formulation for the steady-state thermodynamic model of MED-MVC desalination systems operating in different feed configurations has been developed. Of the four configurations, the FF configuration yields the lowest SPC, followed by the PCF configuration. The study reveals that the exergy destructions in the MVC unit and evaporator units represent the highest share of the total exergy destruction in the system. Other components, such as the brine and distillate feed heaters, have much lower shares in the exergy destruction. The second law efficiency is the highest for the PCF configuration, while the BF has the lowest value. The most expensive (highest investment cost) components are the evaporator units. For the PF and FF configurations, the low values of the variable f_k for the MVC unit, evaporator units and the two preheaters show that the costs associated with these components are dominated by exergy destruction with the remaining costs determined by the $\dot{Z}_k$value. Reducing the exergy destruction in these units could be cost effective for the entire system even if this would increase the associated capital investment costs. Sensitivity analysis show that the MED-MVC system is superior to the single-effect MVC system, but there is a limit on the number of effects N that can be implemented. Increasing the number of effects from 2 to 6 results in no significant increase in the SPC or η_{II} for both the PF and FF configurations. On the contrary, the value of TWP increases by 15 and 63% as the number of effects increases from 2 to 10 for the FF and PCF configurations, respectively. Also, lowering the steam temperature supplied by the MVC unit from 110 to 55^{o}C results in 100% increase in the η_{II} , and 20 and 40 % decrease in the SPC and TWP, respectively. By using average values for the economic parameters, different cost models are used to estimate the average total water price for the BF, FF, PF

and PCF configurations as 3.0, 1.69, 2.4 and 1.7 $/m^3, respectively. Changes in the cost index and interest rate have a minimal effect on the total water price. On the other hand, changing the electricity cost has a significant effect on the TWP. The TWP for the PCF configuration could reach 0.92 $/m^3 if the electricity cost is 0.03 $/kWh.

9.1.3. Transient Performance of MED/MED-TVC systems with Different Feed Configurations (Ch.5)

- Detailed dynamic modeling of different feed configurations reveals that the MED-TVC has the fastest response compared to other types of feed configurations and the FF requires a longer time to reach steady state condition. In the case of the heat source disturbance, the backward feed has the highest increase in the brine level followed by MED-TVC, while PF and PCF show only a moderate increase in the brine level. For the MED-TVC process, the vapor flow rate is highly reduced compared to the other configurations for the case of a reduction in the heat source flow rate. For the heat sink disturbance, MED-TVC process is the most sensitive among the configurations, and this could be attributed to the smaller size of the condenser compared to the PCF or other configurations. However, for the cooling seawater temperature disturbance, BF has the highest increase in the brine level that is progressively transmitted from the last effect.

9.1.4. Effect of disturbances on MED-TVC plant characteristics: Dynamic modeling and simulation (Ch.6)

- The dynamic developed model for MED-TVC system has some limitations such as the effect of non-condensable gases is not considered. The model is used to investigate the system behavior under different disturbances that simulate the real conditions that the plant may be exposed to. The simulation results reveal that the disturbances in motive steam flow rate and in cooling seawater temperature have the largest effect on the plant

performance while a disturbance in the cooling seawater mass flow rate has only a moderate effect. Changing seawater salinity shows a slight effect on the total distillate and the specific heat transfer area. For all applied disturbances, the change in the brine level is the slowest compared to the changes in vapor temperature, and brine and vapor flow rates.

9.1.5. Effect of Input Parameters Intensity and Duration on Dynamic Performance of MED-TVC Plant (Ch.7)

- The developed model is used to investigate the effect of the fluctuations in magnitude and duration of the main operational parameters. The results show that the disturbance intensity variation plays a major role in the desalination plant behavior. For the current MED-TVC configuration and dimensions, it is recommended to limit the reduction in the seawater cooling flow rate to under 12% of the designed steady-state value to avoid dry out in the evaporators. Also, a reduction in the motive steam flow rate and cooling seawater temperature of more than 20% and 35% of the nominal operating values may lead to flooding in the evaporators and complete plant shutdown. It is also shown that a change in the motive steam pressure at constant entrainment ratio has a negligible effect on the plant performance and behavior. On the other hand, the disturbance period has a minimal effect on plant performance if it avoids the critical values of the disturbance intensity that can cause plant shutdown. Simultaneous combinations of two different disturbances with opposing effects result in a modest effect on the plant operation and the combinations can be used to control and mitigate the flooding/drying effects of the disturbances. For co-effect combinations, the plant needs an accurate control system to avoid an operational shutdown. A ramp type disturbance mitigates the changes in input parameter disturbances and eliminates the over/under-shoots in the GOR observed when disturbances are applied and removed in an abrupt manner.

9.1.6. Transient and Thermo-Economic Analysis of MED-MVC Desalination Process (Ch.8)

- The MED-MVC system dynamic model results show that the disturbances in compressor work have a significant effect on the plant transient behavior while a disturbance in the inlet seawater temperature has only a moderate impact. A reduction in compressor work leads to a reduction in the steam temperature that causes an increase in the effects brine level. For instance, the steam temperature supplied by the MVC unit approaches the brine pool temperature when a 30% reduction in the compressor work occurs. So, any further decrease in compressor work may lead to flooding in the effects and the plant may cease to operate. A decrease in the inlet seawater temperature reduces the feed temperature causing the brine level to increase, but this does not affect the temperature difference between the steam supplied and the first effect temperature. On the other hand, increasing the seawater temperature above 10% of the steady-state condition without proper control on the plant response could lead to dry out in the effects.
- Thermo-economic and dynamic response comparisons between the MED-MVC and MED-TVC systems reveal that: (i) the TWP for the MED-TVC is higher than the MED-MVC; (ii) the MED-TVC is more sensitive to the reduction in the seawater temperature than the MED-MVC; (iii) the MED-MVC is slower in response compared to the MED-TVC. In term of performance, a reduction in compressor work causes a decrease in the plant total distillate production capacity, but an increase in PR and a decrease in SPC. On the other hand, a reduction in the inlet seawater temperature decreases the TBT, which causes a decrease in brine flashing and feed evaporation rates with an increase in the brine levels in the effects. This leads to a reduction in the production of fresh water, a decrease in PR and an increase in the SPC for the same supplied compressor work.

9.2 Recommendation for Future Research

In the current dissertation, a comprehensive simulation has been conducted and new steady state and dynamic models formulations has been developed for predicting energy, exergy, thermo-economic and dynamic performance for MED, MED-TVC and MED-MVC desalination systems. Nevertheless, there are several more research aspects recommended for the future research. Here are some suggested topics:

1- **System comparison**. The developed dynamic models for MED, MED-TVC and MED-MVC systems need to be further tested to simulate the transient performance when these systems exposed to equal changes in input parameters.

2- **Renewable energy sources**. The potential use of renewable energy such as geothermal or solar energy integration to MED systems need to be addressed in term of dynamic performance. System integration is not limited to water production and could be extended to cooling, heating and electricity production. Therefore, there is an opportunity to maximize the utilization factor of thermal energy produced through these renewable energy resources during different operating periods.

3- **Water-power integration**. A key performance parameter is the thermal/electrical energy required per unit mass of water produced. We have assumed that this energy for the various configurations is supplied through the grid in this study. Future integration between power (upper) cycle with the thermal desalination method may focus on the transient operation of the system integration in order to obtain a realistic system operational.

4- **Developed model implementation**. The advantages of the current developed models are in their applicability to different industrial applications where multi-effect evaporation (MEE) systems are used such as food processing and dairy, petroleum, petrochemical,

pharmaceuticals, pulp and paper, sugar and desalination of water. Therefore, using these heuristic models to improve the design and operating conditions of MEE would be of great use for future research.

APPENDIX: RESEARCH PAPERS AND PRESENTATIONS

The international journals published are all closely related to the field of the research of this work.

The dissertation is based on the following publications:

1. **Mohamed L. Elsayed**, Osama Mesalhy, Ramy H. Mohammed, Louis C. Chow, “Transient Performance of MED Processes with Different Feed Configurations.” Desalination, volume 438, July 2018, Pages 37-53.
2. **Mohamed L. Elsayed**, Osama Mesalhy, Ramy H. Mohammed, Louis C. Chow, “Effect of disturbances on MED-TVC plant characteristics: Dynamic modeling and simulation.” Desalination, volume 443, October 2018, Pages 99-109.
3. **Mohamed L. Elsayed**, Osama Mesalhy, Ramy H. Mohammed, Louis C. Chow, “Effect of Input Parameters Intensity and Duration on Dynamic Performance of MED-TVC Plant.” Applied Thermal Engineering, volume 139, July 2018, pages 210-221.
4. **Mohamed L. Elsayed**, Osama Mesalhy, Ramy H. Mohammed, Louis C. Chow, “Exergy and thermo-economic analysis for MED-TVC systems.” Desalination, volume 447, December 2018, Pages 29-42.
5. **Mohamed L. Elsayed**, Osama Mesalhy, Ramy H. Mohammed, Louis C. Chow, “Transient and thermo-economic analysis of MED-MVC desalination system” Energy volume 167, January 2019, pages 283-269.
6. **Mohamed L. Elsayed**, Osama Mesalhy, Ramy H. Mohammed, Louis C. Chow, “Performance modeling of MED-MVC systems: Exergy and thermo-economic analysis” Energy volume 166, January 2019, pages 552-568.

The following conference papers are of close relevance to the present work:

1. Mohamed L. Elsayed, Osama Mesalhy, Ramy H. Mohammed, Louis C. Chow, “Effect of Changes in Input Parameters on the Operation of a MED-TVC Plant.” 3rd Thermal and Fluids Engineering Conference (TFEC) March 4–7, 2018, Fort Lauderdale, FL, USA.
2. **Mohamed L. Elsayed**, “Thermal/Hydrodynamic Study of Novel Solar Powered Thermal Desalination” Poster presented at Renewable Energy Systems and Sustainability ConferenceJuly31–Aug.1,2017, Lakeland, FL, Florida Polytechnic University.
3. **Mohamed L. Elsayed**, Osama Mesalhy, Ramy H. Mohammed, Louis C. Chow, “MED-MVC systems: Exergy and thermo-economic analysis approach.” IMECE 2018, Nov. 9-15, 2018, Pittsburgh, PA, USA.

The following under-preparation journal publications were also the results of this research candidature, but not included in this dissertation.

1. **Mohamed L. Elsayed**, Sattam Alharbi , Ramy H. Mohammed, Osama Mesalhy, Louis C. Chow, “Exergy, economic performance of cogeneration system for power, cooling and water production.” Under preparation.
2. **Mohamed L. Elsayed**, Osama Mesalhy , Ramy H. Mohammed, Louis C. Chow, “Steady, dynamic and control models of multi-effect evaporators: A comprehensive review.” Under preparation.

LIST OF REFERENCES

[1] U. Nation, The Millennium Development Goals Report, (2015).

[2] K. Zotalis, E.G. Dialynas, N. Mamassis, A.N. Angelakis, Desalination technologies: Hellenic experience, Water, 6 (2014) 1134-1150. https://doi.org/10.3390/w6051134.

[3] S.A. Kalogirou, Seawater desalination using renewable energy sources, Progress in energy and combustion science, 31 (2005) 242-281. https://doi.org/10.1016/j.pecs.2005.03.001.

[4] DesalData, DesalData, in, 2016.

[5] S. Shafiee, E. Topal, When will fossil fuel reserves be diminished?, Energy policy, 37 (2009) 181-189. https://doi.org/10.1016/j.enpol.2008.08.016.

[6] N. Gronewold, One-quarter of world's population lacks electricity, Scientific American, 24 (2009).

[7] K. Spiegler, Y. El-Sayed, A Desalination Primer: Introductory Book for Students and Newcomers to Desalination, 1994.

[8] K.H. Mistry, J.H. Lienhard, Generalized least energy of separation for desalination and other chemical separation processes, Entropy, 15 (2013) 2046-2080. http://dx.doi.org/10.3390/e15062046.

[9] M. Elimelech, W.A. Phillip, The future of seawater desalination: energy, technology, and the environment, science, 333 (2011) 712-717. https://doi.org/10.1126/science.1200488.

[10] G. Kronenberg, F. Lokiec, Low-temperature distillation processes in single-and dual-purpose plants, Desalination, 136 (2001) 189-197. https://doi.org/10.1016/S0011-9164(01)00181-3.

[11] W.H. Organization, Guidelines for drinking-water quality: recommendations, World Health Organization, 2004.

[12] M.B. Amor, P. Lesage, P.-O. Pineau, R. Samson, Can distributed generation offer substantial benefits in a Northeastern American context? A case study of small-scale renewable technologies using a life cycle methodology, Renewable and Sustainable Energy Reviews, 14 (2010) 2885-2895. https://doi.org/10.1016/j.rser.2010.08.001.

[13] J. Twidell, T. Weir, Renewable energy resources, Routledge, 2015.

[14] G. Resch, A. Held, T. Faber, C. Panzer, F. Toro, R. Haas, Potentials and prospects for renewable energies at global scale, Energy Policy, 36 (2008) 4048-4056. https://doi.org/10.1016/j.enpol.2008.06.029.

[15] M. Hoogwijk, A. Faaij, R. Van Den Broek, G. Berndes, D. Gielen, W. Turkenburg, Exploration of the ranges of the global potential of biomass for energy, Biomass and bioenergy, 25 (2003) 119-133. https://doi.org/10.1016/S0961-9534(02)00191-5.

[16] R. Rayegan, Y. Tao, A procedure to select working fluids for Solar Organic Rankine Cycles (ORCs), Renewable Energy, 36 (2011) 659-670. https://doi.org/10.1016/j.renene.2010.07.010.

[17] J. Wang, Y. Dai, L. Gao, Exergy analyses and parametric optimizations for different cogeneration power plants in cement industry, Applied Energy, 86 (2009) 941-948. https://doi.org/10.1016/j.apenergy.2008.09.001.

[18] T. Engin, V. Ari, Energy auditing and recovery for dry type cement rotary kiln systems—A case study, Energy conversion and management, 46 (2005) 551-562. https://doi.org/10.1016/j.enconman.2004.04.007.

[19] N. Ghaffour, J. Bundschuh, H. Mahmoudi, M.F. Goosen, Renewable energy-driven desalination technologies: A comprehensive review on challenges and potential applications of integrated systems, Desalination, 356 (2015) 94-114. https://doi.org/10.1016/j.desal.2014.10.024.

[20] W.D. Childs, A.E. Dabiri, H.A. Al-Hinai, H.A. Abdullah, VARI-RO solar-powered desalting technology Desalination, 125 (1999) 155-166. https://doi.org/10.1016/S0011-9164(99)00134-4.

[21] A. Nafey, M. Sharaf, Combined solar organic Rankine cycle with reverse osmosis desalination process: Energy, exergy, and cost evaluations, Renewable Energy, 35 (2010) 2571-2580. https://doi.org/10.1016/j.renene.2010.03.034.

[22] G. Kosmadakis, D. Manolakos, S. Kyritsis, G. Papadakis, Design of a two stage Organic Rankine Cycle system for reverse osmosis desalination supplied from a steady thermal source, Desalination, 250 (2010) 323-328. https://doi.org/10.1016/j.desal.2009.09.050.

[23] A.M. Delgado-Torres, L. García-Rodríguez, Preliminary design of seawater and brackish water reverse osmosis desalination systems driven by low-temperature solar organic Rankine cycles (ORC), Energy Conversion and Management, 51 (2010) 2913-2920. https://doi.org/10.1016/j.enconman.2010.06.032.

[24] B. Tchanche, G. Lambrinos, A. Frangoudakis, G. Papadakis, Exergy analysis of micro-organic Rankine power cycles for a small scale solar driven reverse osmosis desalination system, Applied Energy, 87 (2010) 1295-1306. https://doi.org/10.1016/j.apenergy.2009.07.011.

[25] S. Mussati, P. Aguirre, N.J. Scenna, Optimal MSF plant design, Desalination, 138 (2001) 341-347. https://doi.org/10.1016/S0011-9164(01)00283-1.

[26] E. Cardona, A. Piacentino, Optimal design of cogeneration plants for seawater desalination, Desalination, 166 (2004) 411-426. https://doi.org/10.1016/j.desal.2004.06.096.

[27] J. De Gunzbourg, D. Larger, Cogeneration applied to very high efficiency thermal seawater desalination plants, Desalination, 125 (1999) 203-208. https://doi.org/10.1016/S0011-9164(99)00139-3.

[28] M. Darwish, A. Alsairafi, Technical comparison between TVC/MEB and MSF, Desalination, 170 (2004) 223-239. https://doi.org/10.1016/j.desal.2004.01.006.

[29] S. Kalogirou, Survey of solar desalination systems and system selection, energy, 22 (1997) 69-81. https://doi.org/10.1016/S0360-5442(96)00100-4.

[30] V. Slesarenko, Comparison of the efficiency of MSF and thin-film desalination plants, Desalination, 158 (2003) 295-302. https://doi.org/10.1016/S0011-9164(03)80028-0.

[31] G. Kronenberg, Cogeneration with the LT-MED desalination process, Desalination, 108 (1997) 287-294. https://doi.org/10.1016/S0011-9164(97)00038-6.

[32] F. Al-Juwayhel, H. El-Dessouky, H. Ettouney, Analysis of single-effect evaporator desalination systems combined with vapor compression heat pumps, Desalination, 114 (1997) 253-275. https://doi.org/10.1016/S0011-9164(98)00017-4.

[33] D.C. Alarcón-Padilla, L. García-Rodríguez, J. Blanco-Gálvez, Experimental assessment of connection of an absorption heat pump to a multi-effect distillation unit, Desalination, 250 (2010) 500-505. https://doi.org/10.1016/j.desal.2009.06.056.

[34] A. Ophir, F. Lokiec, Advanced MED process for most economical sea water desalination, Desalination, 182 (2005) 187-198. https://doi.org/10.1016/j.desal.2005.02.026.

[35] C. Sommarva, Utilisation of power plant waste heat steams to enhance efficiency in thermal desalination, Desalination, 222 (2008) 592-595. https://doi.org/10.1016/j.desal.2007.01.122.

[36] N.H. Aly, A.K. El-Figi, Mechanical vapor compression desalination systems—a case study, Desalination, 158 (2003) 143-150. https://doi.org/10.1016/S0011-9164(03)00444-2.

[37] J. Siqueiros, F. Holland, Water desalination using heat pumps, Energy, 25 (2000) 717-729. https://doi.org/10.1016/S0360-5442(00)00012-8.

[38] A. Nafey, H. Fath, A. Mabrouk, Thermoeconomic design of a multi-effect evaporation mechanical vapor compression (MEE–MVC) desalination process, Desalination, 230 (2008) 1-15. https://doi.org/10.1016/j.desal.2007.08.021.

[39] R. Kouhikamali, M. Sanaei, M. Mehdizadeh, Process investigation of different locations of thermo-compressor suction in MED–TVC plants, Desalination, 280 (2011) 134-138. https://doi.org/10.1016/j.desal.2011.06.070.

[40] K. Ansari, H. Sayyaadi, M. Amidpour, A comprehensive approach in optimization of a dual nuclear power and desalination system, Desalination, 269 (2011) 25-34. https://doi.org/10.1016/j.desal.2010.12.035.

[41] H. Ettouney, Design of single-effect mechanical vapor compression, Desalination, 190 (2006) 1-15. https://doi.org/10.1016/j.desal.2005.08.003.

[42] R. Bahar, M.N.A. Hawlader, L.S. Woei, Performance evaluation of a mechanical vapor compression desalination system, Desalination, 166 (2004) 123-127. https://doi.org/10.1016/j.desal.2004.06.066.

[43] M.L. Elsayed, O. Mesalhy, R.H. Mohammed, L.C. Chow, Transient and thermo-economic analysis of MED-MVC desalination system, Energy, 167 (2019) 283-296. https://doi.org/10.1016/j.energy.2018.10.145.

[44] F. Mandani, H. Ettouney, H. El-Dessouky, LiBr.H2O absorption heat pump for single-effect evaporation desalination process, Desalination, 128 (2000) 161-176. https://doi.org/10.1016/S0011-9164(00)00031-X.

[45] R. Gomri, Thermal seawater desalination: possibilities of using single effect and double effect absorption heat transformer systems, Desalination, 253 (2010) 112-118. https://doi.org/10.1016/j.desal.2009.11.023.

[46] A. Al-Ansari, H. Ettouney, H. El-Dessouky, Water–zeolite adsorption heat pump combined with single effect evaporation desalination process, Renewable Energy, 24 (2001) 91-111. https://doi.org/10.1016/S0960-1481(00)00192-0.

[47] X. Wang, K.C. Ng, Experimental investigation of an adsorption desalination plant using low-temperature waste heat, Applied Thermal Engineering, 25 (2005) 2780-2789. https://doi.org/10.1016/j.applthermaleng.2005.02.011.

[48] R.H. Mohammed, O. Mesalhy, M.L. Elsayed, L.C. Chow, Assessment of numerical models in the evaluation of adsorption cooling system performance, International Journal of Refrigeration, 99 (2019) 166-175. https://doi.org/10.1016/j.ijrefrig.2018.12.017.

[49] R.H. Mohammed, O. Mesalhy, M.L. Elsayed, L.C. Chow, Experimental and numerical investigation of a new silica-gel/water packed bed for adsorption cooling applications, ASTFE Digital Library, (2018) 1535-1546. https://doi.org/10.1615/TFEC2018.prm.021615.

[50] R.H. Mohammed, O. Mesalhy, M.L. Elsayed, L.C. Chow, Performance evaluation of a new modular packed bed for adsorption cooling systems, Applied Thermal Engineering, 136 (2018) 293-300. https://doi.org/10.1016/j.applthermaleng.2018.02.103.

[51] P. Youssef, R. Al-Dadah, S. Mahmoud, Comparative analysis of desalination technologies, Energy Procedia, 61 (2014) 2604-2607. https://doi.org/10.1016/j.egypro.2014.12.258.

[52] R.H. Mohammed, O. Mesalhy, M.L. Elsayed, M. Su, L.C. Chow, Revisiting the adsorption equilibrium equations of silica-gel/water for adsorption cooling applications, International Journal of Refrigeration, 86 (2018) 40-47. https://doi.org/10.1016/j.ijrefrig.2017.10.038.

[53] R.H. Mohammed, O. Mesalhy, M.L. Elsayed, S. Hou, M. Su, L.C. Chow, Physical properties and adsorption kinetics of silica-gel/water for adsorption chillers, Applied Thermal Engineering, 137 (2018) 368-376. https://doi.org/10.1016/j.applthermaleng.2018.03.088.

[54] R.H. Mohammed, O. Mesalhy, M.L. Elsayed, L.C. Chow, Scaling analysis of heat and mass transfer processes in an adsorption packed bed, International Journal of Thermal Sciences, 133 (2018) 82-89. https://doi.org/10.1016/j.ijthermalsci.2018.07.017.

[55] R.H. Mohammed, O. Mesalhy, M.L. Elsayed, L.C. Chow, Novel compact bed design for adsorption cooling systems: parametric numerical study, International Journal of Refrigeration, 80 (2017) 238-251. https://doi.org/10.1016/j.ijrefrig.2017.04.028.

[56] M.W. Shahzad, K.C. Ng, K. Thu, B.B. Saha, W.G. Chun, Multi effect desalination and adsorption desalination (MEDAD): A hybrid desalination method, Applied Thermal Engineering, 72 (2014) 289-297. https://doi.org/10.1016/j.applthermaleng.2014.03.064.

[57] R.H. Mohammed, O. Mesalhy, M.L. Elsayed, L.C. Chow, Adsorption cooling cycle using silica-gel packed in open-cell aluminum foams, International Journal of Refrigeration, (2019). https://doi.org/10.1016/j.ijrefrig.2019.03.013.

[58] F. Trieb, H. Müller-Steinhagen, Concentrating solar power for seawater desalination in the Middle East and North Africa, Desalination, 220 (2008) 165-183. https://doi.org/10.1016/j.desal.2007.01.030.

[59] M. Al-Shammiri, M. Al-Dawas, Maximum recovery from seawater reverse osmosis plants in Kuwait, Desalination, 110 (1997) 37-48. https://doi.org/10.1016/S0011-9164(97)00082-9.

[60] S. Lattemann, M.D. Kennedy, J.C. Schippers, G. Amy, Global Desalination Situation, Chapter 2, Sustainability Science and Engineering, 2 (2010) 7-39. https://doi.org/10.1016/S1871-2711(09)00202-5.

[61] N. Ghaffour, T.M. Missimer, G.L. Amy, Combined desalination, water reuse, and aquifer storage and recovery to meet water supply demands in the GCC/MENA region, Desalination and Water Treatment, 51 (2013) 38-43. https://doi.org/10.1080/19443994.2012.700034.

[62] A. Alkaisi, R. Mossad, A. Sharifian-Barforoush, A Review of the Water Desalination Systems Integrated with Renewable Energy, Energy Procedia, 110 (2017) 268-274. https://doi.org/10.1016/j.egypro.2017.03.138.

[63] M.W. Shahzad, M. Burhan, L. Ang, K.C. Ng, Energy-water-environment nexus underpinning future desalination sustainability, Desalination, 413 (2017) 52-64. https://doi.org/10.1016/j.desal.2017.03.009.

[64] K.C. Ng, M.W. Shahzad, H.S. Son, O.A. Hamed, An exergy approach to efficiency evaluation of desalination, Applied Physics Letters, 110 (2017) 184101. https://doi.org/10.1063/1.4982628.

[65] M.W. Shahzad, M. Burhan, H.S. Son, S.J. Oh, K.C. Ng, Desalination processes evaluation at common platform: A universal performance ratio (UPR) method, Applied Thermal Engineering, 134 (2018) 62-67. https://doi.org/10.1016/j.applthermaleng.2018.01.098.

[66] M.W. Shahzad, M. Burhan, K.C. Ng, Pushing desalination recovery to the maximum limit: Membrane and thermal processes integration, Desalination, 416 (2017) 54-64. https://doi.org/10.1016/j.desal.2017.04.024.

[67] M.W. Shahzad, K. Thu, Y.-d. Kim, K.C. Ng, An experimental investigation on MEDAD hybrid desalination cycle, Applied Energy, 148 (2015) 273-281. 10.1016/j.apenergy.2015.03.062.

[68] M.W. Shahzad, K.C. Ng, K. Thu, Future sustainable desalination using waste heat: kudos to thermodynamic synergy, Environmental Science: Water Research & Technology, 2 (2016) 206-212. https://doi.org/10.1039/C5EW00217F.

[69] K.C. Ng, K. Thu, S.J. Oh, L. Ang, M.W. Shahzad, A.B. Ismail, Recent developments in thermally-driven seawater desalination: Energy efficiency improvement by hybridization of the MED and AD cycles, Desalination, 356 (2015) 255-270. https://doi.org/10.1016/j.desal.2014.10.025.

[70] I.S. Al-Mutaz, I. Wazeer, Current status and future directions of MED-TVC desalination technology, Desalination and Water Treatment, 55 (2015) 1-9. https://doi.org/10.1080/19443994.2014.910841.

[71] I.S. Al-Mutaz, I. Wazeer, Development of a steady-state mathematical model for MEE-TVC desalination plants, Desalination, 351 (2014) 9-18. https://doi.org/10.1016/j.desal.2014.07.018.

[72] M.M. Ashour, Steady state analysis of the Tripoli West LT-HT-MED plant, Desalination, 152 (2003) 191-194. https://doi.org/10.1016/S0011-9164(02)01062-7.

[73] H.T. El-Dessouky, H.M. Ettouney, Fundamentals of salt water desalination, Elsevier, 2002.

[74] W. El-Mudir, M. El-Bousiffi, S. Al-Hengari, Performance evaluation of a small size TVC desalination plant, Desalination, 165 (2004) 269-279. https://doi.org/10.1016/j.desal.2004.06.031.

[75] R. Kamali, A. Abbassi, S.S. Vanini, M.S. Avval, Thermodynamic design and parametric study of MED-TVC, Desalination, 222 (2008) 596-604. https://doi.org/10.1016/j.desal.2007.01.120.

[76] A. Binamer, Second law and sensitivity analysis of large ME-TVC desalination units, Desalination and Water Treatment, 53 (2015) 1234-1245. https://doi.org/10.1080/19443994.2013.852481.

[77] M.H. Sharqawy, S.M. Zubair, On exergy calculations of seawater with applications in desalination systems, International Journal of Thermal Sciences, 50 (2011) 187-196. https://doi.org/10.1016/j.ijthermalsci.2010.09.013.

[78] N. Kahraman, Y.A. Cengel, Exergy analysis of a MSF distillation plant, Energy Conversion and Management, 46 (2005) 2625-2636. https://doi.org/10.1016/j.enconman.2004.11.009.

[79] F. Alasfour, M. Darwish, A.B. Amer, Thermal analysis of ME—TVC+ MEE desalination systems, Desalination, 174 (2005) 39-61. https://doi.org/10.1016/j.desal.2004.08.039.

[80] H.-S. Choi, T.-J. Lee, Y.-G. Kim, S.-L. Song, Performance improvement of multiple-effect distiller with thermal vapor compression system by exergy analysis, Desalination, 182 (2005) 239-249. https://doi.org/10.1016/j.desal.2005.03.018.

[81] N.M. Al-Najem, M. Darwish, F. Youssef, Thermovapor compression desalters: energy and availability—analysis of single-and multi-effect systems, Desalination, 110 (1997) 223-238. https://doi.org/10.1016/S0011-9164(97)00101-X.

[82] B. Han, Z. Liu, H. Wu, Y. Li, Experimental study on a new method for improving the performance of thermal vapor compressors for multi-effect distillation desalination systems, Desalination, 344 (2014) 391-395. https://doi.org/10.1016/j.desal.2014.03.038.

[83] H. Sayyaadi, A. Saffari, Thermoeconomic optimization of multi effect distillation desalination systems, Applied Energy, 87 (2010) 1122-1133. https://doi.org/10.1016/j.apenergy.2009.05.023.

[84] M.A. Sharaf, A. Nafey, L. García-Rodríguez, Exergy and thermo-economic analyses of a combined solar organic cycle with multi effect distillation (MED) desalination process, Desalination, 272 (2011) 135-147.

[85] I.J. Esfahani, A. Ataei, V. Shetty, T. Oh, J.H. Park, C. Yoo, Modeling and genetic algorithm-based multi-objective optimization of the MED-TVC desalination system, Desalination, 292 (2012) 87-104. https://doi.org/10.1016/j.desal.2012.02.012.

[86] S.E. Shakib, M. Amidpour, C. Aghanajafi, Simulation and optimization of multi effect desalination coupled to a gas turbine plant with HRSG consideration, Desalination, 285 (2012) 366-376. https://doi.org/10.1016/j.desal.2011.10.028.

[87] P. Catrini, A. Cipollina, G. Micale, A. Piacentino, A. Tamburini, Exergy analysis and thermoeconomic cost accounting of a Combined Heat and Power steam cycle integrated with a Multi Effect Distillation-Thermal Vapour Compression desalination plant, Energy Conversion and Management, (2017). https://doi.org/10.1016/j.enconman.2017.04.032.

[88] I.B. Askari, M. Ameri, F. Calise, Energy, exergy and exergo-economic analysis of different water desalination technologies powered by Linear Fresnel solar field, Desalination, 425 (2018) 37-67. https://doi.org/10.1016/j.desal.2017.10.008.

[89] M. Salimi, M. Amidpour, Modeling, simulation, parametric study and economic assessment of reciprocating internal combustion engine integrated with multi-effect desalination unit, Energy Conversion and Management, 138 (2017) 299-311. https://doi.org/10.1016/j.enconman.2017.01.080.

[90] M.L. Elsayed, O. Mesalhy, R.H. Mohammed, L.C. Chow, Transient performance of MED processes with different feed configurations, Desalination, 438 (2018) 37-53. https://doi.org/10.1016/j.desal.2018.03.016.

[91] R.B. Power, Steam jet ejectors for the process industries, McGraw-Hill, New York, 1994.

[92] A.S. Hassan, M.A. Darwish, Performance of thermal vapor compression, Desalination, 335 (2014) 41-46. https://doi.org/10.1016/j.desal.2013.12.004.

[93] M.M. El-Halwagi, Sustainable design through process integration: fundamentals and applications to industrial pollution prevention, resource conservation, and profitability enhancement, Butterworth-Heinemann, 2017.

[94] Y. El-Sayed, Designing desalination systems for higher productivity, Desalination, 134 (2001) 129-158. https://doi.org/10.1016/S0011-9164(01)00122-9.

[95] N. Lukic, L. Diezel, A. Fröba, A. Leipertz, Economical aspects of the improvement of a mechanical vapour compression desalination plant by dropwise condensation, Desalination, 264 (2010) 173-178. https://doi.org/10.1016/j.desal.2010.07.023.

[96] A. Lazzaretto, G. Tsatsaronis, SPECO: a systematic and general methodology for calculating efficiencies and costs in thermal systems, Energy, 31 (2006) 1257-1289. https://doi.org/10.1016/j.energy.2005.03.011.

[97] S. Usón, A. Valero, A. Agudelo, Thermoeconomics and industrial symbiosis. Effect of by-product integration in cost assessment, Energy, 45 (2012) 43-51. https://doi.org/10.1016/j.energy.2012.04.016.

[98] A. Bejan, G. Tsatsaronis, Thermal design and optimization, John Wiley & Sons, 1996.

[99] Y. Wang, N. Lior, Thermoeconomic analysis of a low-temperature multi-effect thermal desalination system coupled with an absorption heat pump, Energy, 36 (2011) 3878-3887. https://doi.org/10.1016/j.energy.2010.09.028.

[100] R. Kouhikamali, Thermodynamic analysis of feed water pre-heaters in multiple effect distillation systems, Applied Thermal Engineering, 50 (2013) 1157-1163. https://doi.org/10.1016/j.applthermaleng.2012.08.055.

[101] M.A. Darwish, F. Al-Juwayhel, H.K. Abdulraheim, Multi-effect boiling systems from an energy viewpoint, Desalination, 194 (2006) 22-39. https://doi.org/10.1016/j.desal.2005.08.029.

[102] A. Almutairi, P. Pilidis, N. Al-Mutawa, M. Al-Weshahi, Energetic and exergetic analysis of cogeneration power combined cycle and ME-TVC-MED water desalination plant: Part-1 operation and performance, Applied Thermal Engineering, 103 (2016) 77-91. https://doi.org/10.1016/j.applthermaleng.2016.02.121.

[103] N.H. Aly, A. Karameldin, M. Shamloul, Modelling and simulation of steam jet ejectors, desalination, 123 (1999) 1-8. https://doi.org/10.1016/S0011-9164(99)00053-3.

[104] E.E. Ludwig, Applied process design for chemical and petrochemical plants, Gulf Professional Publishing, 1997.

[105] H. Lu, J. Wang, T. Wang, N. Wang, Y. Bao, H. Hao, Crystallization techniques in wastewater treatment: An overview of applications, Chemosphere, 173 (2017) 474-484. https://doi.org/10.1016/j.chemosphere.2017.01.070.

[106] L. Weimer, T. Fosberg, L. Musil, Maximizing water recovery/reuse via mechanical vapor-recompression (MVR) evaporation, Environmental Progress & Sustainable Energy, 2 (1983) 246-250. https://doi.org/10.1002/ep.670020410.

[107] Z. Zimerman, Development of large capacity high efficiency mechanical vapor compression (MVC) units, Desalination, 96 (1994) 51-58. https://doi.org/10.1016/0011-9164(94)85156-5.

[108] M. Sharaf, A. Nafey, L. García-Rodríguez, Thermo-economic analysis of solar thermal power cycles assisted MED-VC (multi effect distillation-vapor compression) desalination processes, Energy, 36 (2011) 2753-2764. https://doi.org/10.1016/j.energy.2011.02.015.

[109] Y.M. El-Sayed, Thermoeconomics of some options of large mechanical vapor-compression units, Desalination, 125 (1999) 251-257. https://doi.org/10.1016/S0011-9164(99)00146-0.

[110] V.C. Onishi, A. Carrero-Parreño, J.A. Reyes-Labarta, R. Ruiz-Femenia, R. Salcedo-Díaz, E.S. Fraga, J.A. Caballero, Shale gas flowback water desalination: Single vs multiple-effect

evaporation with vapor recompression cycle and thermal integration, Desalination, 404 (2017) 230-248. https://doi.org/10.1016/j.desal.2016.11.003.

[111] M. Ahmadi, E. Baniasadi, H. Ahmadikia, Process modeling and performance analysis of a productive water recovery system, Applied Thermal Engineering, 112 (2017) 100-110. https://doi.org/10.1016/j.applthermaleng.2016.10.067.

[112] J. Veza, Mechanical vapour compression desalination plants—A case study, Desalination, 101 (1995) 1-10. https://doi.org/10.1016/0011-9164(95)00002-J.

[113] M. Lucas, B. Tabourier, The mechanical vapour compression process applied to seawater desalination: a 1,500 ton/day unit installed in the nuclear power plant of Flamanville, France, Desalination, 52 (1985) 123-133. https://doi.org/10.1016/0011-9164(85)85003-7.

[114] U. Plantikow, Wind-powered MVC seawater desalination—operational results, Desalination, 122 (1999) 291-299. https://doi.org/10.1016/S0011-9164(99)00049-1.

[115] D.L. Shaffer, L.H. Arias Chavez, M. Ben-Sasson, S. Romero-Vargas Castrillón, N.Y. Yip, M. Elimelech, Desalination and reuse of high-salinity shale gas produced water: drivers, technologies, and future directions, Environmental science & technology, 47 (2013) 9569-9583. https://doi.org/10.1021/es401966e.

[116] A. Koren, N. Nadav, Mechanical vapour compression to treat oil field produced water, Desalination, 98 (1994) 41-48. https://doi.org/10.1016/0011-9164(94)00130-8.

[117] D. Han, W. He, C. Yue, W. Pu, Study on desalination of zero-emission system based on mechanical vapor compression, Applied Energy, 185 (2017) 1490-1496. https://doi.org/10.1016/j.apenergy.2015.12.061.

[118] H. Wu, Y. Li, J. Chen, Research on an evaporator-condenser-separated mechanical vapor compression system, Desalination, 324 (2013) 65-71. https://doi.org/10.1016/j.desal.2013.06.004.

[119] J. Shen, Z. Xing, K. Zhang, Z. He, X. Wang, Development of a water-injected twin-screw compressor for mechanical vapor compression desalination systems, Applied Thermal Engineering, 95 (2016) 125-135. https://doi.org/10.1016/j.applthermaleng.2015.11.057.

[120] J. Shen, Z. Xing, X. Wang, Z. He, Analysis of a single-effect mechanical vapor compression desalination system using water injected twin screw compressors, Desalination, 333 (2014) 146-153. https://doi.org/10.1016/j.desal.2013.10.014.

[121] H.S. Aybar, Analysis of a mechanical vapor compression desalination system, Desalination, 142 (2002) 181-186. https://doi.org/10.1016/S0011-9164(01)00437-4.

[122] D. Aussenac, M. Enjalbert, S. Domenech, Mathematical model of a mechanical-vapor compression evaporator. Application to the production of freshwater by seawater desalination: Part II—Numerical exploitation, Desalination, 49 (1984) 111-139. https://doi.org/10.1016/0011-9164(84)85026-2.

[123] G. Aly, Computer simulations of multiple-effect FFE-VC systems for water desalination, Desalination, 45 (1983) 119-131. https://doi.org/10.1016/0011-9164(83)87209-9.

[124] C. Fernández-López, A. Viedma, R. Herrero, A. Kaiser, Seawater integrated desalination plant without brine discharge and powered by renewable energy systems, Desalination, 235 (2009) 179-198. https://doi.org/10.1016/j.desal.2007.10.041.

[125] A. Helal, S. Al-Malek, Design of a solar-assisted mechanical vapor compression (MVC) desalination unit for remote areas in the UAE, Desalination, 197 (2006) 273-300. https://doi.org/10.1016/j.desal.2006.01.021.

[126] C.R. Henderson, J.F. Manwell, J.G. McGowan, A wind/diesel hybrid system with desalination for Star Island, NH: feasibility study results, Desalination, 237 (2009) 318-329. https://doi.org/10.1016/j.desal.2005.07.054.

[127] D. Zejli, A. Ouammi, R. Sacile, H. Dagdougui, A. Elmidaoui, An optimization model for a mechanical vapor compression desalination plant driven by a wind/PV hybrid system, Applied energy, 88 (2011) 4042-4054. https://doi.org/10.1016/j.apenergy.2011.04.031.

[128] S.H. Mounir, M. Feidt, C. Vasse, Thermoeconomic study of a system for pollutant concentration with mechanical vapour compression, Applied thermal engineering, 25 (2005) 473-484. https://doi.org/10.1016/j.applthermaleng.2004.05.011.

[129] F.N. Alasfour, H.K. Abdulrahim, The effect of stage temperature drop on MVC thermal performance, Desalination, 265 (2011) 213-221. https://doi.org/10.1016/j.desal.2010.07.054.

[130] M.A. Jamil, S.M. Zubair, Design and analysis of a forward feed multi-effect mechanical vapor compression desalination system: An exergo-economic approach, Energy, 140 (2017) 1107-1120. https://doi.org/10.1016/j.energy.2017.08.053.

[131] K.H. Mistry, R.K. McGovern, G.P. Thiel, E.K. Summers, S.M. Zubair, J.H. Lienhard, Entropy generation analysis of desalination technologies, Entropy, 13 (2011) 1829-1864. https://doi.org/10.3390/e13101829.

[132] H. Wu, Y. Li, J. Chen, Analysis of an evaporator-condenser-separated mechanical vapor compression system, Journal of Thermal Science, 22 (2013) 152-158. https://doi.org/10.1007/s11630-013-0606-1.

[133] R. Matz, U. Fisher, A comparison of the relative economics of sea water desalination by vapour compression and reverse osmosis for small to medium capacity plants, Desalination, 36 (1981) 137-151. https://doi.org/10.1016/S0011-9164(00)88637-3.

[134] H.T. El-Dessouky, H.M. Ettouney, Plastic/compact heat exchangers for single-effect desalination systems, Desalination, 122 (1999) 271-289. https://doi.org/10.1016/S0011-9164(99)00048-X.

[135] J. Carta, J. Gonzalez, V. Subiela, The SDAWES project: an ambitious R&D prototype for wind-powered desalination, Desalination, 161 (2004) 33-48. https://doi.org/10.1016/S0011-9164(04)90038-0.

[136] L. Liang, D. Han, R. Ma, T. Peng, Treatment of high-concentration wastewater using double-effect mechanical vapor recompression, Desalination, 314 (2013) 139-146. https://doi.org/10.1016/j.desal.2013.01.016.

[137] L. Rizzuti, H.M. Ettouney, A. Cipollina, Solar desalination for the 21st century: a review of modern technologies and researches on desalination coupled to renewable energies, Springer Science & Business Media, 2007.

[138] Y. Li, H. Wu, X. Liang, C. Rong, H. Chen, Experimental study of waste concentration by mechanical vapor compression technology, Desalination, 361 (2015) 46-52. https://doi.org/10.1016/j.desal.2015.01.036.

[139] M. Darwish, M.A. Jawad, G. Aly, Comparison between small capacity mechanical vapor compression (MVC) and reverse osmosis (RO) desalting plants, Desalination, 78 (1990) 313-326. https://doi.org/10.1016/0011-9164(90)80052-D.

[140] B.G. Andrade, V.T. Andrade, B.R. Costa, J.C. Campos, M. Dezotti, Distillation of oil field produced water for reuse on irrigation water: evaluation of pollutants removal and ecotoxicity, Journal of Water Reuse and Desalination, 1 (2011) 224-236. https://doi.org/10.2166/wrd.2011.044.

[141] G. Kishore, S. Nisan, S. Dardou, A. Adak, V. Srivastava, P. Tewari, Development of a dynamic simulator (INFMED) for the MED/VC plant, Desalination and Water Treatment, 21 (2010) 364-374. https://doi.org/10.5004/dwt.2010.1752.

[142] N.-E. Clausen, Development of a plate evaporator/condenser for the mechanical vapour compression process, Desalination, 81 (1991) 399-406. https://doi.org/10.1016/0011-9164(91)85072-3.

[143] W.K. Pang, L.W. Yang, Z.T. Zhang, Operation Characteristic of a Mechanical Vapor Recompression Heat Pump Driven by a Centrifugal Fan, Advanced Materials Research, 732 (2013) 165-171. https://doi.org/10.4028/www.scientific.net/AMR.732-733.165.

[144] J. Yang, C. Zhang, Z. Zhang, L. Yang, W. Lin, Study on mechanical vapor recompression system with wet compression single screw compressor, Applied Thermal Engineering, 103 (2016) 205-211. https://doi.org/10.1016/j.applthermaleng.2016.04.053.

[145] W. Bulang, Desalination by vapor compression, Desalination, 38 (1981) 85-97. https://doi.org/10.1016/S0011-9164(00)86051-8.

[146] V.G. Gude, Energy storage for desalination processes powered by renewable energy and waste heat sources, Applied Energy, 137 (2015) 877-898. https://doi.org/10.1016/j.apenergy.2014.06.061.

[147] S. Mussati, N. Scenna, E. Tarifa, S. Franco, J. Hernandez, Optimization of the mechanical vapor compression (MVC) desalination process using mathematical programming, Desalination and Water Treatment, 5 (2009) 124-131. https://doi.org/10.5004/dwt.2009.572.

[148] M.L. Elsayed, O. Mesalhy, R.H. Mohammed, L.C. Chow, Effect of disturbances on MED-TVC plant characteristics: Dynamic modeling and simulation, Desalination, 443 (2018) 99-109. https://doi.org/10.1016/j.desal.2018.05.021.

[149] M.L. Elsayed, O. Mesalhy, R.H. Mohammed, L.C. Chow, Effect of input parameters intensity and duration on dynamic performance of MED-TVC plant, Applied Thermal Engineering, 137 (2018) 475-486. https://doi.org/10.1016/j.applthermaleng.2018.03.106.

[150] R. Buonopane, R. Troupe, J. Morgan, Heat transfer design method for plate heat exchangers, Chemical Engineering Progress, 59 (1963) 57-61.

[151] K. Ansari, H. Sayyaadi, M. Amidpour, Thermoeconomic optimization of a hybrid pressurized water reactor (PWR) power plant coupled to a multi effect distillation desalination system with thermo-vapor compressor (MED-TVC), Energy, 35 (2010) 1981-1996. https://doi.org/10.1016/j.energy.2010.01.013.

[152] A. Malek, M. Hawlader, J. Ho, Design and economics of RO seawater desalination, Desalination, 105 (1996) 245-261. https://doi.org/10.1016/0011-9164(96)00081-1.

[153] Y. Cerci, The minimum work requirement for distillation processes, Exergy, An International Journal, 2 (2002) 15-23. https://doi.org/10.1016/S1164-0235(01)00036-X.

[154] F. Hafdhi, T. Khir, A.B. Yahia, A.B. Brahim, Exergoeconomic optimization of a double effect desalination unit used in an industrial steam power plant, Desalination, 438 (2018) 63-82. https://doi.org/10.1016/j.desal.2018.03.020.

[155] A.A. Mabrouk, A. Nafey, H. Fath, Thermoeconomic analysis of some existing desalination processes, Desalination, 205 (2007) 354-373. https://doi.org/10.1016/j.desal.2006.02.059.

[156] M.L. Elsayed, O. Mesalhy, R.H. Mohammed, L.C. Chow, Exergy and thermo-economic analysis for MED-TVC desalination systems, Desalination, 447 (2018) 29-42. https://doi.org/10.1016/j.desal.2018.06.008.

[157] S. Frioui, R. Oumeddour, Investment and production costs of desalination plants by semi-empirical method, Desalination, 223 (2008) 457-463. https://doi.org/10.1016/j.desal.2007.01.180.

[158] S. Alharbi, M.L. Elsayed, L. Chow, Thermo-Economic Analysis of an Integrated Supercritical CO2 Brayton Cycle and Multiple Effect Desalination Systems, ASME 2018 International Mechanical Engineering Congress and Exposition, (2018) V06BT08A011-V006BT008A011. https://doi.org/10.1115/IMECE2018-88409.

[159] M. Darwish, Thermal analysis of vapor compression desalination system, Desalination, 69 (1988) 275-295. https://doi.org/10.1016/0011-9164(88)80030-4.

[160] N. Ghaffour, S. Lattemann, T. Missimer, K.C. Ng, S. Sinha, G. Amy, Renewable energy-driven innovative energy-efficient desalination technologies, Applied Energy, 136 (2014) 1155-1165. https://doi.org/10.1016/j.apenergy.2014.03.033.

[161] K.C. Ng, M.W. Shahzad, Sustainable desalination using ocean thermocline energy, Renewable and Sustainable Energy Reviews, 82 (2018) 240-246. https://doi.org/10.1016/j.rser.2017.08.087.

[162] A. Al-Karaghouli, L.L. Kazmerski, Energy consumption and water production cost of conventional and renewable-energy-powered desalination processes, Renewable and Sustainable Energy Reviews, 24 (2013) 343-356. https://doi.org/10.1016/j.rser.2012.12.064.

[163] M.A. Sharaf, Thermo-economic comparisons of different types of solar desalination processes, Journal of Solar Energy Engineering, 134 (2012) 031001. https://doi.org/10.1115/1.4005752.

[164] X. Wang, A. Christ, K. Regenauer-Lieb, K. Hooman, H.T. Chua, Low grade heat driven multi-effect distillation technology, International Journal of Heat and Mass Transfer, 54 (2011) 5497-5503. https://doi.org/10.1016/j.ijheatmasstransfer.2011.07.041.

[165] C. Li, S. Besarati, Y. Goswami, E. Stefanakos, H. Chen, Reverse osmosis desalination driven by low temperature supercritical organic Rankine cycle, Applied energy, 102 (2013) 1071-1080. https://doi.org/10.1016/j.apenergy.2012.06.028.

[166] M. Nair, D. Kumar, Water desalination and challenges: The Middle East perspective: a review, Desalination and Water Treatment, 51 (2013) 2030-2040. https://doi.org/10.1080/19443994.2013.734483.

[167] B. Milow, E. Zarza, Advanced MED solar desalination plants. Configurations, costs, future—seven years of experience at the Plataforma Solar de Almeria (Spain), Desalination, 108 (1997) 51-58. https://doi.org/10.1016/S0011-9164(97)00008-8.

[168] D. Dietrich, Enhanced Digital Control of a Mechanical Recompression Evaporator in a Modern Fructose Refinery, Starch - Stärke, 37 (1985) 149-154. https://doi.org/10.1002/star.19850370502.

[169] A. Husain, A. Hassan, D.M. Al-Gobaisi, A. Al-Radif, A. Woldai, C. Sommariva, Modelling, simulation, optimization and control of multistage flashing (MSF) desalination plants Part I: Modelling and simulation, Desalination, 92 (1993) 21-41. https://doi.org/10.1016/0011-9164(93)80074-W.

[170] H.T. El-Dessouky, H.M. Ettouney, F. Mandani, Performance of parallel feed multiple effect evaporation system for seawater desalination, Applied Thermal Engineering, 20 (2000) 1679-1706. https://doi.org/10.1016/S1359-4311(99)00098-8.

[171] I.S. Al-Mutaz, I. Wazeer, Comparative performance evaluation of conventional multi-effect evaporation desalination processes, Applied Thermal Engineering, 73 (2014) 1194-1203. https://doi.org/10.1016/j.applthermaleng.2014.09.025.

[172] P. Sharan, S. Bandyopadhyay, Energy optimization in parallel/cross feed multiple-effect evaporator based desalination system, Energy, 111 (2016) 756-767. https://doi.org/10.1016/j.energy.2016.05.107.

[173] K.H. Mistry, M.A. Antar, J.H. Lienhard V, An improved model for multiple effect distillation, Desalination and Water Treatment, 51 (2013) 807-821. https://doi.org/10.1080/19443994.2012.703383.

[174] P. Palenzuela, D. Alarcon, G. Zaragoza, J. Blanco, M. Ibarra, Parametric equations for the variables of a steady-state model of a multi-effect desalination plant, Desalination and Water Treatment, 51 (2013) 1229-1241. https://doi.org/10.1080/19443994.2012.704718.

[175] F. Zhang, S. Xu, D. Feng, S. Chen, R. Du, C. Su, B. Shen, A low-temperature multi-effect desalination system powered by the cooling water of a diesel engine, Desalination, 404 (2017) 112-120. https://doi.org/10.1016/j.desal.2016.11.006.

[176] V. Miranda, R. Simpson, Modelling and simulation of an industrial multiple effect evaporator: tomato concentrate, Journal of Food Engineering, 66 (2005) 203-210. https://doi.org/10.1016/j.jfoodeng.2004.03.007.

[177] S.M. Tonelli, J. Romagnoli, J. Porras, Computer package for transient analysis of industrial multiple-effect evaporators, Journal of food engineering, 12 (1990) 267-281. https://doi.org/10.1016/0260-8774(90)90002-P.

[178] D. Kumar, V. Kumar, V. Singh, Modeling and dynamic simulation of mixed feed multi-effect evaporators in paper industry, Applied Mathematical Modelling, 37 (2013) 384-397. https://doi.org/10.1016/j.apm.2012.02.039.

[179] N.H. Aly, M. Marwan, Dynamic response of multi-effect evaporators, Desalination, 114 (1997) 189-196. https://doi.org/10.1016/S0011-9164(98)00011-3.

[180] A.M. El-Nashar, A. Qamhiyeh, Simulation of the performance of MES evaporators under unsteady state operating conditions, Desalination, 79 (1990) 65-83. https://doi.org/10.1016/0011-9164(90)80071-I.

[181] L. Roca, L.J. Yebra, M. Berenguel, D.C. Alarcón-Padilla, Modeling of a solar seawater desalination plant for automatic operation purposes, Journal of Solar Energy Engineering, 130 (2008) 041009. https://doi.org/10.1115/1.2969807.

[182] A. de la Calle, J. Bonilla, L. Roca, P. Palenzuela, Dynamic modeling and performance of the first cell of a multi-effect distillation plant, Applied Thermal Engineering, 70 (2014) 410-420. https://doi.org/10.1016/j.applthermaleng.2014.05.035.

[183] M.T. Mazini, A. Yazdizadeh, M.H. Ramezani, Dynamic modeling of multi-effect desalination with thermal vapor compressor plant, Desalination, 353 (2014) 98-108. https://doi.org/10.1016/j.desal.2014.09.014.

[184] F. Medhat Bojnourd, M.A. Fanaei, H. Zohreie, Mathematical modelling and dynamic simulation of multi-effect falling-film evaporator for milk powder production, Mathematical and

Computer Modelling of Dynamical Systems, 21 (2015) 336-358. https://doi.org/10.1080/13873954.2014.980276.

[185] A. Cipollina, M. Agnello, A. Piacentino, A. Tamburini, B. Ortega, P. Palenzuela, D. Alarcon, G. Micale, A dynamic model for MED-TVC transient operation, Desalination, 413 (2017) 234-257. https://doi.org/10.1016/j.desal.2017.03.005.

[186] E. Hernandez, C. Chen, J. Johnson, R. Carter, Viscosity changes in orange juice after ultrafiltration and evaporation, Journal of Food Engineering, 25 (1995) 387-396. https://doi.org/10.1016/0260-8774(94)00013-Y.

[187] Q. Ruan, H. Jiang, M. Nian, Z. Yan, Mathematical modeling and simulation of countercurrent multiple effect evaporation for fruit juice concentration, Journal of Food Engineering, 146 (2015) 243-251. https://doi.org/10.1016/j.jfoodeng.2014.09.015.

[188] A.B. Amer, New trend in the development of ME-TVC desalination system, Desalination, Trends and Technologies, (2011) 185. https://doi.org/10.5772/14799.

[189] J. Burdett, C. Hollanu, Dynamics of a multiple-effect evaporator system, AIChE Journal, 17 (1971) 1080-1089. https://doi.org/10.1002/aic.690170512.

[190] Y. Ammar, H. Li, C. Walsh, P. Thornley, V. Sharifi, A.P. Roskilly, Desalination using low grade heat in the process industry: challenges and perspectives, Applied Thermal Engineering, 48 (2012) 446-457. https://doi.org/10.1016/j.applthermaleng.2012.05.012.

[191] H.-J. Joo, H.-Y. Kwak, Performance evaluation of multi-effect distiller for optimized solar thermal desalination, Applied Thermal Engineering, 61 (2013) 491-499. https://doi.org/10.1016/j.applthermaleng.2013.08.006.

[192] M. Ameri, S.S. Mohammadi, M. Hosseini, M. Seifi, Effect of design parameters on multi-effect desalinationsystem specifications, Desalination, 245 (2009) 266-283. https://doi.org/10.1016/j.desal.2008.07.012.

[193] M.L. Elsayed, O. Mesalhy, R.H. Mohammed, L.C. Chow, Effect of Changes In Input Parameters on The Operation of a MED-TVC Plant, ASTFE Digital Library, (2018) 709-723. https://doi.org/10.1615/TFEC2018.ewf.021614.

[194] M. Darwish, H. El-Dessouky, The heat recovery thermal vapour-compression desalting system: A comparison with other thermal desalination processes, Applied Thermal Engineering, 16 (1996) 523-537. https://doi.org/10.1016/1359-4311(95)00034-8.

[195] R. Kouhikamali, N. Sharifi, Experience of modification of thermo-compressors in multiple effects desalination plants in Assaluyeh in IRAN, Applied Thermal Engineering, 40 (2012) 174-180. https://doi.org/10.1016/j.applthermaleng.2012.02.002.

[196] M. Darwish, H.K. Abdulrahim, Feed water arrangements in a multi-effect desalting system, Desalination, 228 (2008) 30-54. https://doi.org/10.1016/j.desal.2007.05.039.

[197] M. Schaal, F. Aschner, Dynamic behavior of thin film sea water evaporators, Desalination, 25 (1978) 233-252. https://doi.org/10.1016/S0011-9164(00)80323-9.

[198] J. Ji, R. Wang, L. Li, H. Ni, Simulation and analysis of a single-effect thermal vapor-compression desalination system at variable operation conditions, Chemical Engineering & Technology, 30 (2007) 1633-1641. https://doi.org/10.1002/ceat.200700303

[199] R. Semiat, Y. Galperin, Effect of non-condensable gases on heat transfer in the tower MED seawater desalination plant, Desalination, 140 (2001) 27-46. https://doi.org/10.1016/S0011-9164(01)00352-6.

[200] X. Wang, A. Christ, K. Regenauer-Lieb, K. Hooman, H.T. Chua, Low grade heat driven multi-effect distillation technology, International Journal of Heat and Mass Transfer, 54 (2011) 5497-5503. https://doi.org/10.1016/j.ijheatmasstransfer.2011.07.041.

[201] C. Temstet, G. Canton, J. Laborie, A. Durante, A large high-performance MED plant in Sicily, Desalination, 105 (1996) 109-114. https://doi.org/10.1016/0011-9164(96)00064-1.

[202] T. Michels, Recent achievements of low temperature multiple effect desalination in the western areas of Abu Dhabi. UAE, Desalination, 93 (1993) 111-118. https://doi.org/10.1016/0011-9164(93)80098-8.

[203] T. Tahri, M. Douani, S. Abdul-Wahab, M. Amoura, A. Bettahar, Simulation of the vapor mixture condensation in the condenser of seawater greenhouse using two models, Desalination, 317 (2013) 152-159. https://doi.org/10.1016/j.desal.2013.02.025.

[204] J. Lienhard, M.A. Antar, A. Bilton, J. Blanco, G. Zaragoza, Solar desalination, Annual review of heat transfer, 15 (2012). https://doi.org/10.1615/AnnualRevHeatTransfer.2012004659.

[205] B. Ortega-Delgado, M. Cornali, P. Palenzuela, D.C. Alarcón-Padilla, Operational analysis of the coupling between a multi-effect distillation unit with thermal vapor compression and a Rankine cycle power block using variable nozzle thermocompressors, Applied Energy, 204 (2017) 690-701. https://doi.org/10.1016/j.apenergy.2017.07.062.

[206] M. Al-Sahali, H. Ettouney, Developments in thermal desalination processes: design, energy, and costing aspects, Desalination, 214 (2007) 227-240. https://doi.org/10.1016/j.desal.2006.08.020.

[207] H. El-Dessouky, I. Alatiqi, S. Bingulac, H. Ettouney, Steady-state analysis of the multiple effect evaporation desalination process, Chemical engineering & technology, 21 (1998) 437. https://doi.org/10.1002/(SICI)1521-4125(199805)21:5.

[208] H. El-Dessouky, H. Ettouney, F. Al-Juwayhel, Multiple effect evaporation—vapour compression desalination processes, Chemical Engineering Research and Design, 78 (2000) 662-676. https://doi.org/10.1205/026387600527626.

[209] H.T. El-Dessouky, H. Ettouney, Multiple-effect evaporation desalination systems. Thermal analysis, Desalination, 125 (1999) 259-276. https://doi.org/10.1016/S0011-9164(99)00147-2.

[210] M. Mazzotti, M. Rosso, A. Beltramini, M. Morbidelli, Dynamic modeling of multistage flash desalination plants, Desalination, 127 (2000) 207-218. https://doi.org/10.1016/S0011-9164(00)00011-4.

[211] H. Al-Fulaij, A. Cipollina, D. Bogle, H. Ettouney, Steady state and dynamic models of multistage flash desalination: A review, Desalination and Water Treatment, 13 (2010) 42-52. https://doi.org/10.5004/dwt.2010.1068.

[212] C. Cadet, Y. Toure, G. Gilles, J. Chabriat, Knowledge modeling and nonlinear predictive control of evaporators in cane sugar production plants, Journal of Food Engineering, 40 (1999) 59-70. https://doi.org/10.1016/S0260-8774(99)00037-0.

[213] Z. Stefanov, K. Hoo, A distributed-parameter model of black liquor falling film evaporators. Part I. Modeling of a single plate, Industrial & engineering chemistry research, 42 (2003) 1925-1937. https://doi.org/10.1021/ie020483a.

[214] Z. Stefanov, K. Hoo, Distributed parameter model of black liquor falling-film evaporators. 2. Modeling of a multiple-effect evaporator plant, Industrial & engineering chemistry research, 43 (2004) 8117-8132. https://doi.org/10.1021/ie049611g.

[215] A. de la Calle, J. Bonilla, L. Roca, P. Palenzuela, Dynamic modeling and simulation of a solar-assisted multi-effect distillation plant, Desalination, 357 (2015) 65-76. https://doi.org/10.1016/j.desal.2014.11.008.

[216] M. Ameri, S.S. Mohammadi, M. Hosseini, M. Seifi, Effect of design parameters on multi-effect desalination system specifications, Desalination, 245 (2009) 266-283. https://doi.org/10.1016/j.desal.200.0087.12.

[217] H. Al-Fulaij, A. Cipollina, H. Ettouney, D. Bogle, Simulation of stability and dynamics of multistage flash desalination, Desalination, 281 (2011) 404-412. https://doi.org/10.1016/j.desal.2011.08.012.

[218] F. Manenti, M. Masi, G. Santucci, Start-up operations of MED desalination plants, Desalination, 329 (2013) 57-61. 10.1016/j.desal.2013.09.006.

[219] Z. Ge, X. Du, L. Yang, Y. Yang, S. Wu, Simulation on the start-up of MED seawater desalination system coupled with nuclear heating reactor, Applied Thermal Engineering, 28 (2008) 203-210. https://doi.org/10.1016/j.applthermaleng.2007.03.030.

[220] K. Thu, Y.-D. Kim, A. Myat, A. Chakraborty, K.C. Ng, Performance investigation of advanced adsorption desalination cycle with condenser–evaporator heat recovery scheme, Desalination and Water Treatment, 51 (2013) 150-163. https://doi.org/10.1080/19443994.2012.693659.

[221] T. Tong, M. Elimelech, The global rise of zero liquid discharge for wastewater management: drivers, technologies, and future directions, Environmental science & technology, 50 (2016) 6846-6855. https://doi.org/10.1021/acs.est.6b01000.

[222] L. Roca, J.A. Sánchez, F. Rodríguez, J. Bonilla, A. de la Calle, M. Berenguel, Predictive control applied to a solar desalination plant connected to a greenhouse with daily variation of irrigation water demand, Energies, 9 (2016) 194. https://doi.org/10.3390/en9030194.

[223] K. El-Khatib, A.A. El-Hamid, A. Eissa, M. Khedr, Transient model, simulation and control of a single-effect mechanical vapour compression (SEMVC) desalination system, Desalination, 166 (2004) 157-165. https://doi.org/10.1016/j.desal.2004.06.070.

[224] J. Winchester, C. Marsh, Dynamics and control of falling film evaporators with mechanical vapour recompression, Chemical Engineering Research and Design, 77 (1999) 357-371. https://doi.org/10.1205/026387699526340.

[225] H. Ettouney, Design of single-effect mechanical vapor compression, Desalination, 190 (2006) 1-15. https://doi.org/10.1016/j.desal.2005.08.003.

[226] R. Matz, Z. Zimerman, Low-temperature vapour compression and multi-effect distillation of seawater. Effects of design on operation and economics, Desalination, 52 (1985) 201-216. https://doi.org/10.1016/0011-9164(85)85009-8.

[227] Z.H. Ayub, Plate heat exchanger literature survey and new heat transfer and pressure drop correlations for refrigerant evaporators, Heat transfer engineering, 24 (2003) 3-16. https://doi.org/10.1080/01457630304056.

[228] J.A. Carballo, J. Bonilla, L. Roca, A. De la Calle, P. Palenzuela, D.C. Alarcón-Padilla, Optimal operating conditions analysis for a multi-effect distillation plant according to energetic

and exergetic criteria, Desalination, 435 (2018) 70-76. https://doi.org/10.1016/j.desal.2017.12.013.

[229] H. Ozcan, I. Dincer, Exergoeconomic optimization of a new four-step magnesium–chlorine cycle, International Journal of Hydrogen Energy, 42 (2017) 2435-2445. https://doi.org/10.1016/j.ijhydene.2016.03.098.

[230] N. Abbasov, R. Zeinalov, O. Azizova, S. Imranova, Dynamic models of heat exchangers, Chemistry and technology of fuels and oils, 42 (2006) 25-29. http://dx.doi.org/10.1007/s10553-006-0022-2.

[231] M.L. Elsayed, O. Mesalhy, R.H. Mohammed, L.C. Chow, Performance modeling of MED-MVC systems: Exergy-economic analysis, Energy, 166 (2019) 552-568. https://doi.org/10.1016/j.energy.2018.10.080.

[232] O. Kotb, Optimum numerical approach of a MSF desalination plant to be supplied by a new specific 650 MW power plant located on the Red Sea in Egypt, Ain Shams Engineering Journal, 6 (2015) 257-265. https://doi.org/10.1016/j.asej.2014.09.001.

[233] P. Budhiraja, A.A. Fares, Studies of scale formation and optimization of antiscalant dosing in multi-effect thermal desalination units, Desalination, 220 (2008) 313-325. https://doi.org/10.1016/j.desal.2007.01.036.